UNIVERSITAT DE VALÈNCIA

DEPARTAMENT DE FÍSICA TEÒRICA

Resonancias mesónicas escalares y vectoriales en el medio nuclear.

Daniel Cabrera Urbán

Tesis Doctoral
Octubre 2004

D. Manuel J. Vicente Vacas, Profesor Titular de Física Teórica de la Universidad de Valencia,

> CERTIFICA: Que la presente Memoria *Resonancias mesónicas escalares y vectoriales en el medio nuclear* ha sido realizada bajo mi dirección en el Departamento de Física Teórica de la Universidad de Valencia por D. Daniel Cabrera Urbán como Tesis para optar al grado de Doctor en Física.

Y para que así conste presenta la referida Memoria y firma el presente certificado.

Manuel J. Vicente Vacas

A Sonia

A mi madre y hermanos

Contents

Resumen

Introducción y objetivos del trabajo

Un problema importante y de actualidad en física nuclear es la comprensión de las propiedades de los hadrones a las altas densidades bariónicas que se dan en núcleos ordinarios, colisiones de iones pesados o estrellas de neutrones. El propósito de esta tesis es el estudio de las propiedades de algunas de las resonancias mesónicas más ligeras (σ, κ, ρ, ϕ) en materia nuclear.

Un buen conocimiento de la propiedades de los mesones en el medio es necesario para describir muchos procesos físicos donde los mesones se propagan a través de un medio nuclear. La explicación actual de la dinámica de la materia nuclear depende en sí misma de las propiedades de mesones en el medio nuclear, ya que un cambio sustancial en sus características conllevaría una interacción nucleón nucleón modificada con consecuencias directas en la ecuación de estado del sistema.

En los últimos años, se han dedicado muchos esfuerzos a explorar diferentes regiones del diagrama de fases de la materia nuclear, estimulados en parte por la posible existencia de una fase deconfinada de QCD, conocida como Plasma de Quark y Gluones (QGP), que puede ocurrir a altas densidades nucleares y/o temperaturas. Las colisiones de iones pesados (HIC) se propugnan como un escenario adecuado para reproducir tales condiciones de materia nuclear a altas temperaturas y densidades. Sin embargo, cualquier intento de describir tal sistema físico y buscar indicios de dicha fase deconfinada debería proporcionar una descripción precisa de las propiedades de los mesones en la fase hadronizada aún caliente y densa que seguiría la formación de un QGP conforme la región de interacción se expande y enfría.

Otros sistemas físicos que ponen a prueba las propiedades de mesones

en un medio nuclear son los átomos piónicos y kaónicos, hipernúcleos y las reacciones de producción de mesones en núcleos. Los átomos piónicos son particularmente adecuados para estudiar el potencial óptico nuclear en onda S de niveles de piones profundamente ligados. La interpretación teórica de los datos actuales ha estimulado una discusión muy activa sobre el origen de los efectos nucleares como consecuencia de una restauración parcial de la simetría quiral en el medio nuclear o en términos de mecanismos de muchos cuerpos bien establecidos por la fenomenología pión-núcleo.

El potencial óptico nuclear del kaón también se puede estudiar experimentalmente en la producción de átomos kaónicos. La posible existencia de una fase condensada de kaones en materia densa ha estimulado una investigación intensa de la propiedades del kaón en el medio nuclear. Datos experimentales recientes de colisiones de iones pesados sobre la proporción producción de K^+/K^- respaldan la idea de un potencial de antikaón atractivo en el medio. Sin embargo, la intesidad de este potencial no puede ser discernida con los datos experimentales actuales, lo que supone un problema todavía abierto.

Se han propuesto muchas reacciones de producción de mesones que podrían ser útiles para estudiar las propiedades de los mesones a densidades finitas, como por ejemplo la producción de piones en núcleos inducida por piones o fotones. Las interacciones de estado inicial y final de las partículas involucradas se han estudiado ampliamente para tener en cuenta efectos de muchos cuerpos como interacciones elásticas y cuasielásticas y procesos de absorción. En particular, la producción de mesones ρ y ϕ está siendo actualmente investigada como una fuente limpia de información sobre las propiedades en el medio de los mesones vectoriales mediante sus desintegraciones electromagnéticas en pares de dileptones.

En este trabajo presentamos una descripción microscópica de los efectos del medio nuclear sobre las resonancias escalares (σ, κ) y vectoriales (ρ, ϕ). Desde un punto de vista fenomenológico, las propiedades espectrales de las resonancias mesónicas están ligadas a las de los mesones pseudoscalares (π, K) a los cuales se acoplan y desintegran. Por tanto, una descripción realista de las propiedades de las resonancias mesónicas exige un tratamiento cuidadoso de la renormalización de los pseudoscalares en presencia de un medio bariónico denso. En concreto, los piones y kaones experimentan una

renormalización apreciable a densidades finitas como consecuencia de sus interacciones con los nucleones, como se ha encontrado en muchos cálculos teóricos y resultados experimentales.

Como esquema general en este trabajo, el punto de partida de nuestros cálculos es un modelo dinámico fiable que describa de forma adecuada las propiedades de las resonancias que queremos estudiar en el vacío, así como sus acoplamientos a los mesones pseudoescalares. Las extensiones no perturbativas y unitarias de la Teoría Quiral de Perturbaciones (χPT) proporcionan un marco sólido para estudiar las interacciones mesón mesón y barión barión. χPT, que es la teoría de campos efectiva a bajas energías para QCD, describe con éxito la fenomenología hadrónica a energías muy bajas a partir de un desarrollo de las amplitudes de dispersión en potencias del momento de las partículas sobre una cierta escala ($\frac{p}{\Lambda_\chi}$). El poder predictivo de esta teoría está claramente limitado por el gran número de parámetros libres del Lagrangiano conforme se exploran energías más elevadas y se hace necesario incorporar términos de orden superior en la expansión perturbativa. Otra limitación obvia de χPT es la presencia de resonancias en las interacciones mesón mesón y mesón barión, que se manifiestan en forma de singularidades de las amplitudes de dispersión. Estas singularidades (polos) no se pueden generar en un esquema perturbativo en potencias del momento de las partículas. No obstante, resultaría muy útil si pudiéramos extender el dominio de aplicación de esta teoría para explorar mayores energías, ya que χPT satisface las simetrías del Lagrangiano de QCD al tiempo que utiliza los grados de libertad apropiados (mesones y bariones) para un régimen de QCD no perturbativo; y además impone importantes restricciones a bajas energías sobre las amplitudes de dispersión y otros observables físicos. Los modelos quirales no perturbativos y unitarios consiguen recuperar la estructura analítica de las amplitudes de dispersión y así son capaces de acomodar la presencia de resonancias al tiempo que satisfacen las restricciones de χPT a bajas energías, y dan lugar a descripciones muy satisfactorias de la fenomenología hadrónica en un rango muy amplio de energías mediante un número muy pequeño de parámetros. Otra ventaja adicional de estos modelos es que hay efectos del medio nuclear que se pueden incorporar muy fácilmente mediante una renormalización de los propagadores de los mesones pseudoescalares en términos de

autoenergías dependentes de la densidad nuclear. En este trabajo llevaremos a cabo la renormalización de los mesones pseudoescalares como ingrediente esencial para estudiar los efectos del medio sobre las resonancias mesónicas que vamos a tener en cuenta. Calcularemos para ello las autoenergías de los pseudoescalares mediante técnicas de muchos cuerpos, incorporando así sus interacciones con el medio nuclear, que describiremos como un mar de Fermi no interactivo. Con esta formulación del problema estaremos considerando la contribución de canales adicionales de desintegración de las resonancias que no se dan en el vacío, porque requieren la interacción con uno o más nucleones del medio. Citemos como ejemplo un canal típico de desintegración del mesón ρ en el medio, que conlleva la excitación de un nucleón del mar de Fermi por un pión virtual. Este canal automáticamente modifica el umbral de desintegración del ρ, pues resulta ser energéticamente más económico que la producción de un pión real.

Nuestra aproximación al problema de las propiedades de las resonancias mesónicas en el medio nuclear debe considerarse complementaria a otros métodos de teoría de campos que se encuentran habitualmente en la literatura, como por ejemplo el estudio de reglas de suma de QCD. Algunos cálculos basados en estos métodos respaldan en parte la idea de un descenso generalizado de las masas de los hadrones en presencia de densidades bariónicas elevadas. En particular, en algunos de estos trabajos se considera la disminución de la masa del mesón σ como indicativo de una restauración (parcial) de la simetría quiral, que podría tener lugar a densidades y/o temperaturas muy altas. En este escenario, el pión y la σ estarían degenerados en la fase quiral simétrica. Diversos tratamientos que utilizan técnicas de muchos cuerpos para calcular los efectos del medio dan lugar a un mesón sigma cuya masa y anchura de desitegración disminuyen conforme aumenta la densidad nuclear, como consecuencia del potencial muy atractivo que el pión experimenta en el medio nuclear. Por otro lado, en el caso de los mesones vectoriales se encuentra que sus masas muestran cambios muy pequeños mientras que sus anchuras de desintegración crecen notablemente. Estos resultados están por tanto en claro desacuerdo con lo que cabría esperar de un tratamiento simplificado en términos de leyes de escala para las masas. Por desgracia, los datos experimentales actuales no pueden distinguir posibles cambios en las masas

de los mesones vectoriales. Por ejemplo, los espectros de dileptones medidos en reacciones de colisión de iones pesados son consistentes a un tiempo con un descenso finito de la masa del mesón ρ y con un crecimiento de su anchura de desintegración en un medio nuclear.

Hemos organizado el trabajo de la siguiente manera. En el Capítulo 2, hemos discutido las propiedades de piones y kaones en un medio nuclear simétrico ($N = Z$) a temperatura cero. Estas propiedades ya han sido estudiadas en otros trabajos y hemos incluido en este capítulo los resultados más relevantes que utilizaremos después en el estudio de los mesones escalares y vectoriales. En particular, discutimos cómo se generan las autoenergías de piones y kaones a partir de los mecanismos más importantes de interacción con los nucleones del medio. También nos hemos concentrado en estudiar la estructura analítica de los propagadores de estos mesones, que nos serán de mucha utilidad para simplificar los cálculos posteriores de las resonancias escalares y vectoriales. La autoenergía del pión en el medio nuclear se ha estudiado durante mucho tiempo desde el punto de vista teórico y experimental. Hemos intentado proporcionar una introducción pedagógica a este tema, dando ejemplos de cálculos estándar de teoría nuclear de muchos cuerpos. Esta parte se complementa con el Apéndice A, en el que hemos discutido algunos conceptos elementales de sistemas fermiónicos de muchos cuerpos, con el objetivo de obtener el propagador del nucleón en el mar de Fermi no interactivo. Por otro lado, las propiedades del kaón en el medio nuclear se conocen bastante menos. Hemos considerado resultados teóricos recientes acerca de la autoenergía del kaón en un medio nuclear, que se basan en un modelo quiral unitario y no perturbativo de las interacciones mesón barión en el sector de extrañeza -1. Este modelo da lugar a un potencial nuclear para el kaón, dependiente de la energía, consistente con los datos actuales de átomos kaónicos.

Los capítulos siguientes (del 3 al 6) están dedicados al estudio de los mesones σ, κ, ρ y ϕ en el medio nuclear, respectivamente [1–10]. Cada uno de estos capítulos se puede leer con independencia, junto con el Capítulo 2, ya que hemos incluido una introducción específica a cada tema y una referencia a las líneas de trabajo más relevantes, y hemos comentado los principales resultados tanto teóricos como experimentales. Al final de cada capítulo

hemos resumido las conclusiones de nuestro estudio y analizado posibles estrategias para extender el trabajo realizado y comparar los resultados con el experimento.

El Capítulo 3 está dedicado a describir el mesón σ en el medio nuclear. Sus propiedades, difícilmente detectables en observables de dispersión en el vacío, podrían cambiar de forma dramática a densidades finitas, como consecuencia del potencial fuertemente atractivo que siente el pión. Los posibles cambios del mesón σ se están investigando actualmente, por ejemplo, mediante la reacción de fotoproducción de dos piones estudiada en el laboratorio Mainz Microtron (MAMI). Hemos analizado la amplitud de dispersion $\pi\pi$ escalar isoescalar, en la que el mesón σ aparece en un modelo quiral unitario de la interacción mesón mesón. Los efectos del medio, implementados en el pión, conllevan importantes modificaciones de la amplitud de dispersión. Nosotros investigamos qué relación existe entre estos efectos en las amplitudes y la evolución en densidad del polo del mesón σ [10]. Hemos incluido también mecanismos adicionales que no se habían considerado con anterioridad en este modelo en cuestión, que podrían ser importantes para la interacción $\pi\pi$ en el medio nuclear, como se ha propuesto en estudios recientes del contaje quiral en el contexto del problema de muchos cuerpos.

En el Capítulo 4, estudiamos la resonancia κ a partir de la dispersión $K\pi$ descrita por un modelo quiral unitario de acuerdo con el mismo esquema del Capítulo 3. Dadas las notables diferencias entre las interacciones de kaón y antikaón con el medio nuclear, el mesón κ podría ser una herramienta para testar los potenciales nucleares para el kaón disponibles en la literatura. Investigamos también la posibilidad de encontrar un mesón κ muy estrecho como consecuencia de los potenciales atractivos de pión y antikaón en el medio, y cómo se reflejaría esta característica en las amplitudes de dispersión $K\pi$ [9].

En el Capítulo 5 abordamos la renormalización de los mesones vectoriales en materia nuclear, y comenzamos con el mesón ρ. Los mesones vectoriales resultan particularmente interesantes para explorar la materia nuclear densa, porque se desintegran electromagnéticamente y estas desintegraciones proporcionan señales poco distorsionadas por el medio en forma de pares e^+e^- o $\mu^+\mu^-$. Varias instituciones experimentales se dedican actualmente

a estudiar las desintegraciones de los mesones vectoriales en reacciones de fotoproducción en el núcleo y mediante colisiones de iones pesados. En este trabajo llevamos a cabo un análisis detallado de los mecanismos posibles de muchos cuerpos que dan lugar a una interacción $\pi\pi$ vectorial isovectorial en materia nuclear, en los que la autoenergía del pión juega un papel fundamental. También investigamos la contribución de resonancias nucleónicas en la renormalización del ρ en el medio [1–5, 7].

El mesón ϕ es el objetivo del Capítulo 6. Este tema ha tenido un interés creciente en los últimos años debido a que las propiedades del ϕ en el medio nuclear están directamente relacionadas con las del kaón, de las que sólo se tiene información parcial tanto teórica como experimentalmente. Además, al contrario de lo que ocurre con otras resonancias, el espectro del ϕ está relativamente aislado de otras fuentes de desintegración, y esto hace que las desintegraciones del ϕ den lugar a señales experimentales más claras. Por otro lado, debido a que su anchura es muy pequeña, la mayoría de las desintegraciones del ϕ ocurren fuera del sistema nuclear. Esto tiene como consecuencia que la mayoría de experimentos disponen de estadísticas muy pobres de los sucesos que ocurren dentro del medio. Nosotros calculamos en este capítulo la autoenergía del ϕ en un modelo dinámico del ϕ como vector gauge. Incluiremos las autoenergías de los kaones como principal ingrediente de los efectos del medio nuclear que, como veremos, dan lugar a cambios sustanciales de la anchura de desintegración del ϕ [6,7]. También aplicaremos nuestros resultados a un cálculo de la probabilidad de supervivencia del ϕ en la reacción de fotoproducción en las condiciones cinemáticas del experimento que se lleva a cabo en Spring8/Osaka, actualmente en fase de análisis.

Para terminar, en el Capítulo 7 hemos recopilado las principales conclusiones de este trabajo. También hemos incluido un conjunto de apéndices al final de la tesis, previamente a la bibliografía, en los que hemos reunido algunos cálculos de mecanismos de interacción en el medio nuclear. De igual forma, hemos detallado las expresiones analíticas de las funciones de Lindhard, que hemos utilizado con frecuencia para calcular las autoenergías de piones y kaones. A modo de referencia, hemos listado los términos de orden más bajo del Lagrangiano de χPT para las interacciones mesón mesón y mesón barión.

Discusión de los resultados y conclusiones

El presente trabajo ilustra la complejidad de la física de muchos cuerpos involucrada en la renormalización de las propiedades de resonancias mesónicas en un medio nuclear. Hemos estudiado los mecanismos más relevantes, a bajas densidades nucleares, responsables de la modificación de las propiedades de la resonancias mesónicas ligeras en los sectores escalar (σ, κ) y vectorial (ρ, ϕ). Hemos seguido un principio como guía a lo largo de este trabajo. A saber, las propiedades de las resonancias mesónicas en un medio nuclear dependen mucho de los mesones pseudoscalares ligeros a los cuales se desintegran (π, K). Un cálculo apropiado, mediante teoría de muchos cuerpos, de las autoenergías de los mesones pseudoscalares en el medio es el ingrediente esencial en los modelos aquí presentados.

En el Capítulo 2 hemos discutido con algo de detalle las autoenergías del pión y del kaón en un medio nuclear. En el lenguaje de muchos cuerpos, la autoenergía del pión viene fundamentalmente dominada por la excitación de componentes ph y Δh debido a la interacción πN en onda P. También hemos considerado las correlaciones nucleares de corto alcance mediante una resumación adecuada de diagramas de segundo orden que involucran la interacción entre componentes ph y Δh, que hemos descrito en términos del parámetro de Landau-Migdal g'. Una resumación de Dyson de términos de autoenergía irreducibles lleva a la renormalizacón del propagador del pión en el medio nuclear, el cual hemos reescrito en términos de la representación de Lehman basada en la función espectral del pión. Esta representación espectral ha sido muy útil para simplificar muchos cálculos en los siguientes capítulos, habida cuenta que pone claramente de manifiesto la estructura analítica del propagador del pión. Como resultado de los mecanismos en el medio considerados, el pión experimenta un fuerte potencial atractivo ya a densidades del orden de ρ_0. Su función espectral manifiesta una estructura muy rica, ampliamente extendida en energía, en la cual puede identificarse la contribución de los modos de ph y Δh. Por completitud, también hemos discutido otras contribuciones a la autoenergía del pión que no son relevantes en el presente trabajo a las energías y bajas densidades nucleares consideradas. Éstas incluyen la autoenergía del pión en onda S, la excitación de otras reso-

nancias del nucleón con modos de desintegración πN y mecanismos de orden superior en la expansión en densidad como autoenergías de dos partículas y dos agujeros.

En lo que respecta a la autoenergía del kaón, las diferencias manifiestas entre la interacción KN y $\bar{K}N$ aconsejan un tratamiento totalmente diferente de los efectos del medio nuclear sobre el kaón y el antikaón. Mientras que normalmente la aproximación $t\rho$ es suficiente para describir la autoenergía del K, debido al suave comportamiento de la interacción KN a bajas energías, el sistema $\bar{K}N$ está fuertemente influido por la resonancia $\Lambda(1405)$, por tanto es aconsejable un cálculo no perturbativo. Hemos discutido un modelo reciente de la interacción $\bar{K}N$ basado en una extensión unitaria de χPT en canales acoplados el cual, tras un tratamiento autoconsistente de los efectos del medio nuclear, proporciona a una autoenergía en onda S del $\bar{K}$ dependiente en energía y consistente con los datos experimentales de átomos kaónicos. La interacción KN en onda P también conlleva efectos del medio relevantes en la propiedades del kaón. Se ha discutido una autoenergía en onda P a partir del acoplamiento a excitaciones Yh, proporcionando correcciones notables a la autoenegía del $\bar{K}$ y efectos prácticamente despreciables en el caso del K. Para obtener los vértices de interacción se ha utilizado el Lagrangiano quiral de mesones y bariones. En este caso, una unitarización de las amplitudes KN a nivel árbol no mejora el cálculo, ya que la interacción de onda P no proporciona la intensidad necesaria para generar un estado resonante, como se ha mostrado en otros trabajos. Como hicimos para el caso del pión, hemos discutido la representación espectral del propagador del kaón en términos de las funciones espectrales para el kaón y el antikaón.

En los Capítulos 3 y 4 hemos estudiado los mesones escalares ($L = 0$) σ y κ propagándose en un medio nuclear. Estas resonancias se acoplan a los sistemas mesónicos $\pi\pi$ y $K\pi$ en los canales de isospín 0 y 1/2, respectivamente. Hemos partido de una descripción de las amplitudes de dispersión mesón mesón en el sector escalar mediante un modelo quiral unitario en canales acoplados. El modelo se basa en la solución de la ecuación de Bethe-Salpeter que itera la interacción mesón mesón de orden inferior del Lagrangiano quiral. En el presente trabajo las resonancias escalares se generan dinámicamente, a partir de los grados de libertad pseudoscalares, y aparecen como polos en las

amplitudes de dispersión en las hojas de Riemann no físicas. Tras considerar los efectos del medio para el pión, que equivale a usar el propagador del pión renormalizado en la función del *loop* de dos mesones en amplitud de dispersión, encontramos una amplitud $\pi\pi$ fuertemente modificada que acumula una considerable cantidad de intensidad a energías alrededor y por debajo del umbral de dos piones, conforme aumenta la densidad nuclear. Hemos investigado si este comportamiento podría estar reflejando una migración del polo de la σ hacia más bajas energías. Para ello, hemos continuado la amplitud $\pi\pi$ hacia la segunda hoja de Riemann del plano de energía complejo. Esto es posible de un modo bastante sencillo, ya que la estructura analítica de la amplitud de dispersión viene proporcionada por la función del *loop* de dos mesones. Dicha función se puede evaluar para valores complejos de la energía en la hoja no física una vez se obtiene la discontinuidad en el corte analítico (eje real positivo de energía). Se ha obtenido que el polo de la σ se mueve a energías menores y se aproxima al eje real conforme se incrementa la densidad nuclear, lo que no sólo indica un reducción de masa sino también una disminución de la anchura de la σ. A densidad nuclear normal, la masa obtenida a partir de la posición del polo alcanza un valor de aproximadamente 250 MeV y encontramos un valor similar para la anchura de desintegración, a comparar con los valores en el espacio libre $M_\sigma = 500$ MeV y $\Gamma_\sigma = 400$ MeV. Este comportamiento es consecuencia del inteso potencial atractivo que siente el pión en el medio nuclear. Realmente uno esperaría incluso una mayor reducción de la anchura de la σ a densidades finitas, dado el menor espacio fásico disponible para la desintegración a 2π como consecuencia de la reducción de la masa de la σ. Sin embargo, los canales de desintegración de la σ abiertos en el medio, como por ejemplo $\sigma \to \pi\, ph$ y $\sigma \to \pi\, \Delta h$, previenen una reducción más drástica en la anchura de la σ y el efecto final es moderado.

También hemos tenido en cuenta en el presente estudio algunos nuevos mecanismos en el medio previamente no considerados en este modelo que, de acuerdo a un esquema de contaje quiral, podrían ser relevantes para la interacción $\pi\pi$ en el medio nuclear. Hemos encontrado, en un cálculo aproximado de la ecuación de dispersión, que estos mecanismos tiene poca influencia sobre la posición del polo de la σ como función de la densidad nuclear, y conllevan

resultados similares a los previamente encontrados.

Sugerimos que los efectos de densidad sobre las propiedades de la σ obtenidos y particularmente sobre la amplitud de dispersión $\pi\pi$ podrían proporcionar una señal visible en experimentos que produzcan dos piones en el estado final, que se acoplen en el canal $I = 0$. Un cálculo reciente de la reacción de fotoproducción de dos piones en núcleos, en donde las interacciones de estado final de los dos piones han sido implementadas siguiendo el modelo presentado aquí, predice efectos apreciables en la distribución isoescalar de masa invariante de dos piones para varios núcleos. Datos experiementales posteriores de la Colaboración TAPS parecen corroborar esta predicción, aunque todavía se está debatiendo una interpretación teórica de los efectos medidos.

El estudio del mesón κ en el Capítulo 4 sigue el mismo esquema que hemos comentado para el mesón σ. Ahora hay una novedad respecto al Capítulo 3, pues el propagador del kaón entra en el cálculo de la amplitud de dispersión $K\pi$. En el medio nuclear, los propagadores del K y el $\bar{K}$ se comportan de modo bastante diferente, como se ha discutido en el Capítulo 2. Esto implica que la propiedades de la κ, que obtenemos de la amplitud $K\pi$, diferirán de las de la anti-κ, que es generada en la dispersión $\bar{K}\pi$. La fuerte atracción experimentada por el pión en el medio nuclear sugiere que similares efectos de reducción de masa y anchura de desintegración, como se ha obtenido para el mesón σ, podrían tener lugar para el mesón κ a densidades finitas. Si esto sucede, dado que el antikaón también es atraído en el medio, uno podría esperar una disminución dramática de la masa de la κ que podría dar lugar a una resonancia κ muy estrecha, si la masa se reduce por debajo del umbral de $K\pi$ conforme aumenta de la densidad nuclear. También hemos sugerido que las diferencias entre las propiedades en el medio de la κ y la anti-κ podrían ser útiles para poner a prueba los muchos modelos diferentes existentes para el potencial antikaón núcleo, que sin embargo reproducen consitentemente los datos de átomos kaónicos.

Los efectos del medio se han introducido dentro de los propagadores del pión y del kaón, como se ha discutido en el Capítulo 2. Para buscar el polo de la κ a densidades nucleares finitas, hemos extendido la amplitud de dispersión a la segunda hoja de Riemann, siguiendo un procedimiento simi-

lar al realizado para el mesón σ, por medio de la representación espectral (Lehmann) de los propagadores del pión y del kaón. Conforme se incrementa la densidad, vemos que el polo de la κ se mueve a energías menores, fuertemente dominado por el efecto de la autoenergía del pión, como puede verse comparando las trayectorias del polo para la κ y la anti-κ. En efecto, las diferencias globales entre las dos ramas son moderadas. En particular, para el modo de la anti-κ encontramos una reducción de anchura apreciable, pero no suficiente para proporcionar una clara señal susceptible de ser observada experimentalmente. Como ocurría en el caso de la σ en la dispersión $\pi\pi$, los canales de desintegración abiertos disponibles en el medio nuclear compensan en parte la reducción de masa y la anchura de la κ no disminuye tan drásticamente. Las amplitudes de dispersión $K\pi$ manifiestan modificaciones apreciables reflejando los efectos del medio en los pseudosclaraes y en el comportamiento del polo de la κ. Por ejemplo, la parte imaginaria de la amplitud $\bar{K}\pi$ se incrementa por debajo y alrededor del umbral $K\pi$, a consecuencia de los canales en el medio que están abiertos a energías mucho menor que $m_K + m_\pi$. En particular, para el modo $K\pi$, donde el potencial $\bar{K}$ tiene poca influencia, hemos encontrado una acumulación de intensidad a energías por encima del umbral $K\pi$, similar a lo que se observa para el mesón σ en la dispersión $\pi\pi$. Sería de gran utilidad proponer estrategias experimentales para investigar estos efectos en la amplitud $K\pi$, en reacciones en que se produjera un par $K\pi$ correlacionado en el estado final.

En los Capítulos 5 y 6 hemos llevado a cabo la renormalización en el medio nuclear de las resonancias mesónicas vectoriales ρ y ϕ. Estos mesones son considerados como herramientas adecuadas para explorar materia nuclear a altas densidades. Tanto el mesón ϕ como el ρ se acoplan fuertemente a pares de dileptones, que apenas son distorsionados en su camino de salida desde las regiones de alta densidad que tienen lugar en colisiones de iones pesados o incluso en núcleos ordinarios. Esto proporciona una sonda limpia de las propiedades en el medio del ρ y el ϕ, dado que el espectro de masa de los dileptones debería reflejar la forma espectral de los mesones vectoriales desintegrándose en un medio nuclear. Por otro lado, el estudio de las desintegraciones del mesón ϕ podría proporcionar señales visibles de efectos del medio sobre los mesones vectoriales, habida cuenta que no se solapa con

otras resonancias ligeras en el espectro de masas. Además, como se afirma en algunos cálculos teóricos, los cambios en algunas de las propiedades del ϕ a densidades finitas son comparativamente mayores que las del ρ. Por tanto, la observación experimental de estas propiedades podría ser en principio más fácil, como por ejemplo midiendo el espectro K^+K^- proveniente de la desintegración del ϕ en núcleos. El estudio de las propiedades del mesón ϕ en el medio nuclear es también útil para poner a prueba los potenciales nucleares de kaón actualemnte discutidos en la literatura. Desafortunadamente, los experimentos actuales no son lo suficientemente precisos como para proporcionar una interpretación clara de los datos en términos de cambios en la masa y/o anchura de mesones vectoriales. Futuros experimentos (HADES @ GSI) en los que se exploran las desintegraciones de mesones vectoriales en colisiones de iones pesados podrían proporcionar una mejor estadística y resolución en masa. Recientemente, también se han propuesto (Spring8/Osaka, CLAS @ Jefferson Lab) métodos alternativos para evaluar posibles señales de efectos en el medio en reacciones nucleares de fotoproducción de mesones vectoriales.

El mesón ρ se estudia en el Capítulo 5, partiendo de un modelo quiral unitario de la dispersión $\pi\pi$ en $L = 1$. Los potenciales básicos de interacción mesón mesón vienen dados por el Lagrangiano quiral de orden inferior con acoplamiento explícito de resonancias desnudas. La unitarización de las amplitudes a nivel árbol se consigue siguiendo el método N/D en canales acoplados, que determina las amplitudes de dispersión en términos de las amplitudes a nivel árbol sobre la capa másica y la función de *loop* de dos mesones, ya utilizada en el Capítulo 3. El modelo no tiene parámetros libres una vez se imponen las restricciones quirales de bajas energías, salvo un parámetro de regularización que se ajusta para optimizar la posición física del pico de la resonancia en las amplitudes de dispersión. El modelo se ha probado frente a datos experimentales de factores de forma electromagnéticos de pión y kaón y defasajes de dispersión mesón-mesón, con una reproducción muy precisa de los datos en un amplio rango de energías. Hemos explorado el canal $\pi\pi$ en $I = 1$, donde el mesón ρ se manifiesta. De estudios teóricos previos del ρ en un medio nuclear, encontramos que un modo muy conveniente de describir las modificaciones en el medio del mesón vectorial es obtener la autoenergía

del ρ en una representación de campo vectorial de *gauge*. Hemos mostrado que ambos formalismos producen resultados similares para la amplitud $\pi\pi$ en vacío, que puede escribirse en términos de un propagador del ρ 'vestido' con un término de autoenergía que considera el acoplamiento del ρ a dos piones. Se encuentra que esta autoenergía, responsable de la desintegración del mesón ρ en vacío, es equivalente en ambos formalismos a nivel de un *loop*. Nuestro estudio de los efectos del medio en el mesón ρ y la amplitud de dispersón $\pi\pi$ isovectorial nos lleva a evaluar todos los posibles mecanismos que contribuyen a la autoenergía del ρ a densidades finitas. El ingrediente esencial es, de nuevo, la autoenergía del pión en onda P de Capítulo 2. Sin embargo, el principio de *gauge* proporciona para este problema acoplamientos del ρ a piones, nucleones y Δ's que generan muchas otras topologías de autoenergía que deben ser consideradas para satisfacer la invariancia *gauge* y obtener un tensor de autoenergía del ρ transverso. Hemos discutido en detalle la mayoría de estas topologías. Algunos de los cálculos han sido introducidos en los apéndices.

Conforme se incrementa la densidad nuclear, la distribución del ρ se ensancha apreciablemente, dado que se abren nuevos canales de desintegración en el medio, provenientes de la excitación de componentes de ph y Δh. Pese al fuertemente atractivo potencial del pión, la masa del ρ apenas se modifica, manifestando un pequeño corrimiento hacia energías mayores, que depende moderadamente de las incertidumbres del modelo de autoenergía del pión. Entre otras contribuciones, considerar la anchura de desintegración de la Δ tiene importantes consecuencias en la función espectral del ρ, particularmente a bajas energías. La inclusión explícita de la anchura de desintegración de la Δ introduce pequeñas violaciones de la invariancia *gauge*, que es un problema abierto en la literatura.

Se ha encontrado que la contribución de excitaciones N^*h aumenta considerablemente la intesidad espectral del ρ a bajas energías. A densidad nuclear normal la función espectral del ρ manifiesta dos estructuras claramente diferenciadas, una correspondiente al ρ, con una anchura alrededor de 200 MeV, y una segunda a energías menores debida al modo N^*h. Hemos discutido sobre la necesidad de un tratamiento autoconsistente de los efectos del medio, que podrían ser importantes para explorar densidades mayores a

las estudiadas en este trabajo. Una cálculo apropiado de los efectos del medio en los modos de desintegración de la N^* en $\pi\Delta$ y ρN proporcionaría una evaluación autoconsistente de la autoenergía del ρ y una mejor determinación de su función espectral.

En el Capítulo 6, hemos calculado la autoenergía del mesón ϕ en un medio nuclear, siguiendo un esquema similar al de la autoenergía del ρ en el Capítulo 5. Podríamos haber partido también de la amplitud de dispersión mesón mesón en un modelo quiral unitario para el canal $(L = 1, I = 0)$, donde el ϕ se manifiesta. Aquí hemos optado por obtener la masa del ϕ y la anchura de desintegración en el medio directamente de la autoenergía del ϕ, siguiendo una aproximación de Lagrangiano de vector de *gauge*. Este modelo había sido previamente utilizado para obtener la anchura del ϕ en un medio nuclear. Hemos mejorado el modelo para poder calcular tanto la masa del ϕ como la anchura a densidades finitas. La renormalización de los propagadores del kaón en el medio nuclear es uno de los elementos más importantes del cálculo. La representación espectral de los propagadores del kaón nos ha sido muy útil para simplificar muchos cálculos analíticos, proporcionando evaluaciones numéricas más sencillas. Hemos prestado especial atención a estimar posibles fuentes de pequeñas violaciones de invariancia *gauge* provenientes de aproximaciones no relativistas en el modelo, justificando la elección de una cierta familia de diagramas y despreciando otras contribuciones en la autoenergía del ϕ. Para un ϕ en reposo respecto del medio nuclear, hemos obtenido contribuciones importantes a la anchura de desintegración de los canales abiertos en el medio $\phi \to K\pi\Lambda h$ and $\phi \to K\pi\Sigma h$, relacionados con la autoenergía del kaón en onda S, y $\phi \to K\Lambda h$ y $\phi \to K\Sigma^* h$ relacionados con la autoenergía del kaón en onda P. La anchura final del ϕ a densidad nuclear normal es aproximadamente 7 veces la anchura de desintegración libre. A pesar de ese efecto apreciable, el ϕ todavía permanece como una resonancia estrecha. La parte real del potencial del ϕ da lugar un corrimiento de la masa muy pequeño, de unos pocos MeV a densidades del orden de ρ_0. Datos experimentales recientes del espectro de K^+K^- en la reacción pA parecen ser consistentes con este resultado aunque una interpretación fiable de estos datos requeriría un estudio teórico detallado de esta reacción.

También hemos extendido nuestro modelo a momento finito del ϕ para

poder estudiar una propuesta experimental reciente (Spring8/Osaka) de la reacción de fotoproducción del ϕ en núcleos. Hemos estudiado la probabilidad de supervivencia de los ϕ's emitidos, que depende directamente de la parte imaginaria de la autoenergía del ϕ, y manifiesta una particular dependencia con el número másico nuclear. Hemos encontrado probabilidades de supervivencia que se desvían significativamente de la unidad para varios núcleos, que en principio se podría medir experimentalemente. Hemos estudiado también posibles configuraciones experimentales para evitar la contribución de la fotoproducción coherente del ϕ, que no está incluída en nuestros cálculos. Hemos proporcionado estimaciones de cotas superiores para el cociente de la sección eficaz coherente sobre la incoherente, basadas en un estudio de la estructura de espín de la amplitud de producción elemental y un cálculo del factor de forma nuclear.

En este trabajo hemos mostrado ampliamente que la renormalización de resonancias mesónicas en un medio nuclear no es una tarea sencilla, y hay que considerar un análisis detallado de posibles mecanismos de interacción con el medio nuclear para proporcionar una descripción fiable de las propiedades mesónicas a densidades nucleares finitas. Además, no se puede ignorar el acoplamiento de resonancias mesónicas a los mesones pseudoscalares ligeros, dado que se producen cambios sustanciales como consecuencia de los potenciales que experimentan estos mesones en el medio. Hemos demostrado que el uso de la Teoría Quiral de Perturbaciones para imponer restricciones en las amplitudes de dispersion mesón mesón a bajas energías; junto con el uso de modelos no perturbativos en canales acoplados, capaces de describir resonancias mesónicas, constituyen un marco de trabajo adecuado para estudiar la renormalización de los mesones en el medio nuclear; que hemos llevado a cabo empleando técnicas estándar de Teoría Cuántica de muchos cuerpos.

Chapter 1

Introduction

An important problem in nuclear physics is the understanding of the properties of hadrons at the high baryonic densities that occur in ordinary nuclei, heavy ion collisions or neutron stars. The study of the properties of some of the lightest meson resonances (σ, κ, ρ, ϕ) in nuclear matter is the purpose of this thesis.

A good knowledge of the in-medium properties of mesons is necessary to describe many physical processes in which mesons propagate through a nuclear medium. The current explanation of nuclear matter dynamics depends itself on the properties of mesons in the nuclear medium, since a substantial change in their characteristics would lead to a modified nucleon nucleon interaction with direct consequences on the equation of state of the system.

In the last years, many experimental efforts have been directed to explore different regions of the phase diagram of nuclear matter, partly stimulated by the possible existence of a deconfined phase of QCD, known as Quark Gluon Plasma (QGP), which may occur at high nuclear densities and/or temperatures. Heavy ion collisions (HIC) are advocated as a suitable scenario to reproduce such conditions of nuclear matter at high temperatures and densities. However, any attempt to describe such a physical system and search for traces of the predicted deconfined phase should account for a precise description of the properties of mesons in the still hot and dense hadronized phase which would follow the formation of a QGP as the interacting region expands and cools down.

Other physical systems which put under the test the properties of mesons

in a nuclear medium are pionic and kaonic atoms, hypernuclei and meson production reactions in nuclei. Pionic atoms are particularly suitable to study the $S-$wave nuclear optical potential of pions in deeply bound levels. The theoretical interpretation of present data has lead to a very active discussion regarding the origin of nuclear effects as a consequence of a partial restoration of chiral symmetry in the nuclear medium or in terms well established many body mechanisms of the pion nucleus phenomenology.

The kaon nuclear optical potential can be also studied experimentally from the production of kaonic atoms. The possibility of existence of a kaon condensed phase in dense matter has stimulated an intense research on the kaon properties in the nuclear medium. Recent experimental data from heavy ion collisions regarding the K^+/K^- yield ratio support the idea of an attractive antikaon potential in the medium. However, the strength of this potential cannot be resolved with the present experimental data and it is still an open problem.

Many meson production reactions have been proposed which could be useful to study meson properties at finite densities, as for instance pion production in nuclei induced by pions or photons. The initial and final state interactions of the particles involved have been thoroughly studied to account for many body effects as elastic and quasielastic interactions and absorption processes. Particularly the production of ρ and ϕ mesons in nuclei is currently investigated as a clean source of information on the in-medium properties of vector mesons, from their electromagnetic decays into dilepton pairs.

We present in this work a microscopical many body description of nuclear medium effects on the scalar (σ, κ) and vector (ρ, ϕ) meson resonances. From a phenomenological point of view, the spectral properties of meson resonances are tied to those of the pseudoscalar mesons (π, K) to which they couple and decay. Therefore a realistic description of the meson resonance properties demands a careful treatment of the renormalization of the pseudoscalars in the presence of a baryonic medium. Particularly, pions and kaons experience a sizable renormalization at finite densities as a consequence of their interactions with the nucleons, as it has been found in many theoretical calculations and experimental results.

As a general scheme in this work, we shall start from a well established dynamical model which describes adequately the properties of several meson resonances in vacuum and their coupling to pseudoscalar mesons. Non-perturbative, unitary extensions of Chiral Perturbation Theory (χPT) provide a solid framework to study meson meson and meson baryon interactions. χPT, which is the low energy effective field theory of QCD, describes the hadronic phenomenology at very low energies in terms of an expansion of the scattering amplitudes in powers of the momentum of the interacting particles over a certain scale ($\frac{p}{\Lambda_\chi}$). The predictive power of the theory is clearly limited by the increasing number of free parameters in the Lagrangian as long as one explores higher energies and more terms beyond the leading order in the perturbative expansion are required. Another obvious limitation of χPT is the presence of resonances in meson meson and meson baryon interactions, which manifest as singularities in the scattering amplitudes. These singularities cannot be generated in a perturbative scheme in terms of powers of momentum. Nevertheless, it is worth to extend the applicability of such a theory to higher energies, since χPT fulfills the symmetries of the QCD Lagrangian and uses the appropriate degrees of freedom (mesons and baryons) for a non-perturbative energy regime of QCD; and puts important low energy constraints on the scattering amplitudes and other physical observables. Non-perturbative chiral unitary models help recover the analytical structure of the scattering amplitudes accommodating the appearance of resonances and satisfying the low energy constraints of χPT, and provide a satisfactory description of the hadronic phenomenology over a wide range of energies with a very small number of parameters. Another advantage of this models is that nuclear medium effects can be easily incorporated by a suitable modification of the pseudoscalar meson propagators, which can be done in terms of appropriate density dependent selfenergies. We shall carry out the renormalization of the pseudoscalar mesons, by means of a many body calculation of the meson selfenergies accounting for their interactions with the nuclear medium which we shall describe as an uncorrelated Fermi sea. With the present formulation of the problem we shall be considering the presence of additional resonance decay channels which do not exist in vacuum, since they require an interaction with one or more nucleons in the medium. As an example, a

typical in-medium channel in ρ meson decay involves the excitation of a nucleon in the Fermi sea by a virtual pion. This channel automatically modifies the ρ meson decay threshold, since it is rather less energy demanding than the production of a real pion.

Our approach to the problem of meson resonance properties in the nuclear medium should be considered as complementary to other field theoretical methods currently found in the literature, such as QCD sum rules. Some calculations based in these methods partially support the idea of a generalized decrease of hadron masses in the presence of high baryonic densities. Particularly, in some works, a decrease of the σ and ρ meson masses is advocated as a positive signature of a partial restoration of chiral symmetry which may occur at high baryonic densities or temperatures. In such scenario, the pion and the σ mesons would become degenerate in the unbroken symmetry phase. Several approaches using many body techniques to calculate medium effects lead to a σ meson with reduced mass and decay width as the nuclear density is increased, as a consequence of the strongly attractive interaction experienced by the pion on the nuclear medium. However, this is not usually found in the case vector mesons (ρ, ϕ), for which small changes in their masses and a sizable enhancement in their decay widths are usually found in literature. This findings are in clear contrast to what is expected from naive scaling arguments. Unfortunately, the present experimental data cannot resolve the possible mass changes of vector mesons. For instance, dilepton spectra from heavy ion collisions are consistent both with a finite decrease of the ρ meson mass and/or an enhancement of its decay width in a nuclear medium.

This work is organized as follows. In Chapter 2 we discuss the properties of pions and kaons in a cold, symmetrical nuclear medium. This has been studied elsewhere and we quote in this chapter the most important results which we shall use later in the study of scalar and vector meson resonances. Particularly we discuss how the pion and kaon selfenergies arise from the most relevant mechanisms of interaction with the nucleons in the medium. We also concentrate on the analytical structure of the meson propagators which will be very useful in eventual calculations for the scalar and vector meson resonances. The pion selfenergy in the medium has been studied for

a long time both theoretically and experimentally. We try to provide a pedagogical introduction to this topic, giving examples of standard selfenergy calculations in nuclear many body physics. This introductory part is further complemented in Appendix A, where some elements of many body fermion systems are discussed in order to obtain the nucleon propagator in the uncorrelated Fermi sea. On the other hand, the properties of kaons in the nuclear medium are much less known. We have considered recent theoretical results on the kaon selfenergy in a nuclear medium, based on a non-perturbative chiral unitary model of meson baryon interactions in the $S = -1$ sector. This model leads to an energy dependent kaon nuclear potential consistent with the present data from kaonic atoms.

The following chapters (3 - 6) are devoted to the study of the σ, κ, ρ and ϕ mesons in a nuclear medium, respectively [1–10]. Each of these chapters can be read independently together with Chapter 2, since we have included a particular introduction to the subject and an outline of the most relevant lines of work, commenting on the main results both theoretical and experimental. At the end of each chapter we have summarized the conclusions of our study and included an outlook of possible further extensions of the work done and its comparison with experimental data.

The σ meson in a nuclear medium is described in Chapter 3. Its properties, which are hardly visible in scattering observables in vacuum, could dramatically change at finite densities, as a consequence of the strongly attractive potential felt by the pion. The possible changes of the σ properties are subject of current experimental research, for instance, in the 2π photoproduction reaction studied at the Mainz Microtron facility (MAMI). We have analyzed the scalar isoscalar $\pi\pi$ scattering amplitude, where the σ shows up in a chiral unitary model of meson meson interaction. The inclusion of medium effects on the pion leads to important modifications of the scattering amplitude. We investigate the relation between these effects and the evolution of the σ pole with the nuclear density [10]. We have included additional mechanisms, not considered before in this approach, which could be important for the $\pi\pi$ interaction in a nuclear medium, as recently proposed in a study of chiral power counting in the many body problem.

In Chapter 4, the κ resonance is studied from $K\pi$ scattering in a chiral

unitary model following the same scheme as in Chapter 3. The remarkable differences between the kaon and antikaon interactions with the nuclear medium make the κ a possible probe for the kaon nuclear potentials available in the literature. We also investigate the possibility of finding a very narrow κ meson as a consequence of the pion and antikaon attractive potentials in the medium, and its effect on the $K\pi$ scattering amplitudes [9].

In Chapter 5 we face the renormalization of vector mesons in the medium, starting by the ρ meson. Vector mesons are particularly relevant to explore dense nuclear matter since they decay electromagnetically, which provides undistorted signals from e^+e^- or $\mu^+\mu^-$ pairs. Several experimental facilities are currently studying the vector meson decays from photoproduction reactions in nuclei and heavy ion collisions. We make a detailed analysis of the possible many body mechanisms which lead to a modified isovector $\pi\pi$ interaction in the medium, in which the pion selfenergy plays a central role. We also investigate the participation of nucleon resonances in the renormalization of the ρ in nuclear matter [1–5, 7].

The ϕ meson at finite densities is the subject of Chapter 6. This a topic of growing interest since the ϕ properties in a nuclear medium are tied to those of the kaons. Moreover, unlike other resonances, the ϕ spectrum is isolated from additional decay sources, leading to more clear signals of ϕ decays in a nuclear medium. On the other hand, due to its small width, the ϕ mostly decays out from the nuclear system, and as a consequence most of experiments have poor statistics from in-medium decay events. We calculate here the ϕ selfenergy in a gauge vector model and account for the kaon selfenergies as the main input of medium effects, leading to sizable effects on the ϕ decay width [6, 7]. We apply our results to obtain the ϕ survival probability in the ϕ photoproduction reactions at the kinematical conditions of the ongoing experiment at Spring8/Osaka [8].

In Chapter 7 we summarize the global conclusions of this work. We have also included a set of appendices at the end of the thesis, prior to the Bibliography, in which we have gathered some detailed calculations of in-medium mechanisms studied in this work. We have also collected analytical expressions of Lindhard functions, extensively used in the calculation of the π and K selfenergies in the medium. For reference, we have also quoted the

lowest order Lagrangian terms of χPT for meson meson and meson baryon interactions.

Chapter 2

π and K meson properties in nuclear matter.

The understanding of meson resonances in chiral unitary models has important consequences for their interaction with a nuclear medium, since their selfenergy will be directly related to those of the mesons to which they couple. We study in these chapter the properties of pions and kaons propagating in a symmetrical nuclear medium. Their interactions with the nucleons in the medium can be considered in terms of selfenergy contributions that will modify the meson propagators. We shall also focus on the analytical structure of the meson propagators and state the spectral (Lehmann) representations that we shall use later in some of the calculations in this work.

2.1 Pions in nuclear matter

The interaction of pions with the nuclear medium has been thoroughly studied for many years both from the theoretical and experimental points of view. This section intends to be, at the same time, an introduction to the subject and a compilation of results that we shall use throughout this work. Most of the topics discussed here can be found in the book of T. E. O. Ericson and W. Weise [11], as well as in Refs. [12, 13].

When a pion propagates in a nuclear medium it may scatter with the surrounding nucleons and virtual mesons. We shall use the Fermi sea as an approximate model for nuclear matter and we just consider the pion as an external particle propagating through the nuclear environment.

We want to study the medium effects on the pion propagator in a pertur-

bative way. The in-medium Green's function for the pion field is defined as in free space, but the vacuum state is substituted by the ground state of the nucleon many-body system, $|\phi_0\rangle$ (see Appendix A for notation). We have to specify the πNN interaction, which we take from the lowest order Chiral Lagrangian that describes the coupling of the pseudoscalar meson octet to the $1/2^+$ baryon octet [14]. We use a nonrelativistic reduction ($\gamma^\mu\gamma_5 p_\mu \to -\vec{\sigma}\vec{p}$) that leads to the Feynman rule $\pm\frac{D+F}{2f}\vec{\sigma}\vec{q}$ for each πNN vertex in momentum space, where $\vec{q}$ is the momentum of the incoming/outgoing pion. A similar result is obtained from the effective Yukawa Hamiltonian in a nonrelativistic form,

$$\begin{aligned} H_{\pi NN} &= ig\bar{\Psi}_N(x)\gamma_5\vec{\tau}\vec{\phi}(x)\Psi_N(x) \\ &\simeq \frac{f_N}{m_\pi}\sigma_i\partial_i\phi^\lambda(x)\tau^\lambda \ , \end{aligned} \tag{2.1}$$

where Ψ_N is the iso-doublet nucleon field, ϕ^λ is the cartesian pion field component, $\vec{\tau}(\vec{\sigma})$ is the isospin (spin) matrix and $\frac{f_N}{m_\pi} = \frac{g}{2M_N}$. From Eq. (2.1) it follows a factor $\frac{f_N}{m_\pi}\vec{\sigma}\vec{q}\tau^\lambda$ for each πNN vertex. The coupling constant $\frac{f_N}{m_\pi}$ reads as $\frac{D+F}{2f}$ in the language of the chiral effective theory, and we shall use this latter notation from now on. We have included the meson baryon chiral Lagrangian in Appendix C for reference. The same πNN vertex as above can be derived from this Lagrangian in a non-relativistic approximation.

We can use the Wick expansion to find which diagrams contribute at a given order. As it is explained in Appendix A, only those terms with all the nucleon field operators contracted survive. It follows that the only diagram to be computed at lowest order in the perturbative expansion is the one shown in Fig. 2.1 (which corresponds to second order in the interaction since the πNN vertex appears twice).

Translational invariance makes the pion Green's function depend on $\Delta x = x - x'$, and this makes useful to work in momentum space where the perturbative expansion of the pion propagator, up to the order under discussion, reads

$$iD(q) = iD_0(q) + iD_0(q)(-i)\Pi_0(q)iD_0(q) + ... \tag{2.2}$$

The first term in the previous expression is just the bare pion propagator, and the next one corresponds to the first medium correction. This term is shown

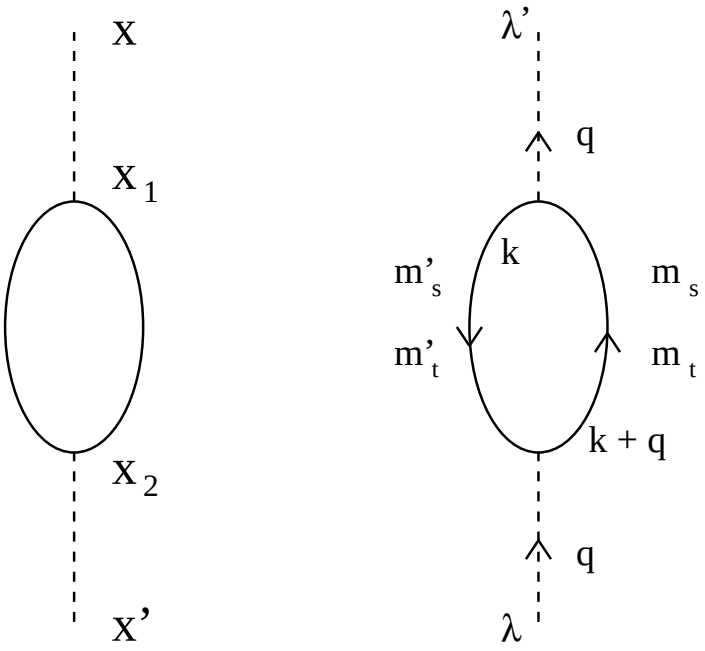

Figure 2.1: Connected first order diagram contributing to the pion propagator in nuclear matter. Left: coordinate space; Right: momentum space. Solid lines represent nucleons and dashed lines stand for pions.

diagrammatically in Fig. 2.1(right). $\Pi_0(q)$ is the first order pion selfenergy. Following the Feynman rules we can calculate $\Pi_0(q)$, which reads

$$-i\Pi_0^{\lambda\lambda'}(q) = (-1)\int \frac{d^4k}{(2\pi)^4}\left(\frac{D+F}{2f}\right)^2 \vec{\sigma}(-\vec{q})\,\vec{\sigma}\vec{q}\,\tau^\lambda\,\tau^{\lambda'} iG^0(k)\,iG^0(k+q)\ , \tag{2.3}$$

with G^0 the in-medium nucleon propagator given in Appendix A. A sum over intermediate spin and isospin states must be understood. The sum over protons and neutrons gives a factor $2\delta^{\lambda\lambda'}$, while for the spin sum we use the property

$$\sum_{m_s,m_s'} \langle m_s|\sigma_i q_i|m_s'\rangle\langle m_s'|\sigma_j q_j|m_s\rangle = 2\delta_{ij}q_iq_j = 2\vec{q}^{\,2}. \tag{2.4}$$

Explicitly substituting the nucleon propagators from Eq. (A.20) we have

$$\begin{aligned}\Pi_0^{\lambda\lambda'}(q) \ &\equiv\ \delta^{\lambda\lambda'}\,\Pi_0(q) = -i\,\delta^{\lambda\lambda'}\,4\left(\frac{D+F}{2f}\right)^2\vec{q}^{\,2}\,\times \\ &\times\int\frac{d^4k}{(2\pi)^4}\Big\{\frac{[1-n(\vec{k})]}{k^0-\varepsilon(\vec{k})+i\eta}+\frac{n(\vec{k})}{k^0-\varepsilon(\vec{k})-i\eta}\Big\}\times \\ &\times\Big\{\frac{[1-n(\vec{k}+\vec{q})]}{k^0+q^0-\varepsilon(\vec{k}+\vec{q})+i\eta}+\frac{n(\vec{k}+\vec{q})}{k^0+q^0-\varepsilon(\vec{k}+\vec{q})-i\eta}\Big\}\ . \end{aligned}\tag{2.5}$$

The k^0 integration can be done analytically. The pole structure of the in medium nucleon propagators is such that only the crossed products of terms from the first and second braces in Eq. (2.5) contribute. Then one is left with

$$\Pi_0(q) = \left(\frac{D+F}{2f}\right)^2\vec{q}^{\,2}U_N(q), \tag{2.6}$$

where $U_N(q)$ is the Lindhard function for the particle-hole (ph) excitation, given by

$$\begin{aligned}U_N(q) \equiv 4\int\frac{d^3k}{(2\pi)^3}\Big\{&\frac{n(\vec{k})[1-n(\vec{k}+\vec{q})]}{q^0-\varepsilon(\vec{k}+\vec{q})+\varepsilon(\vec{k})+i\eta}+ \\ &\frac{n(\vec{k}+\vec{q})[1-n(\vec{k})]}{-q^0-\varepsilon(\vec{k})+\varepsilon(\vec{k}+\vec{q})+i\eta}\Big\}\ . \end{aligned}\tag{2.7}$$

The integrals in Eq. (2.7) can be solved analytically and we refer to Appendix B where explicit expressions are quoted. See also [12, 13, 15] for more details of the calculation and asymptotic limits of U_N.

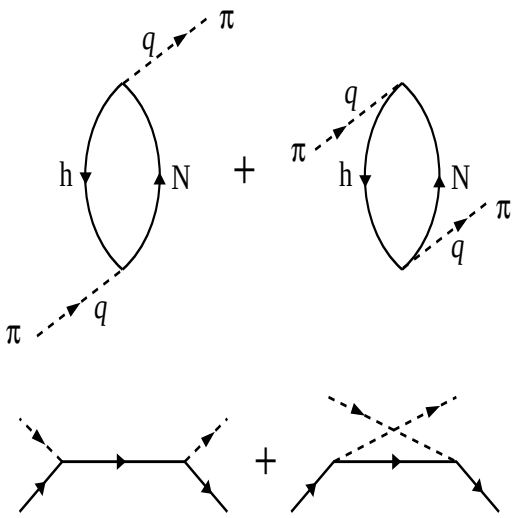

Figure 2.2: Up: direct and cross particle-hole excitation diagrams. Down: corresponding πN scattering diagrams.

An interesting fact derives from the last two equations. The final result for $\Pi_0(q)$ can be quoted as the contribution of the two time-ordered diagrams shown in Fig. 2.2 (up), which are called respectively direct and crossed terms or forward and backward propagating bubbles. In these diagrams, as it can be inferred from the surviving terms in Eq. (2.5), one of the nucleon lines corresponds to the particle piece of the nucleon propagator in the medium, while the other stands for the hole part. The arrows now indicate the particle or hole character of each nucleonic line. We shall use the following convention: 'up' arrow for particles and 'down' arrow for holes.

As it could be expected, the basic first order response to the propagation of the pionic field in a non-interacting fermion system at zero temperature manifests as an excitation of a particle-hole pair; and it corresponds to the first genuine medium correction in the perturbative expansion of the pion propagator in nuclear matter. It is interesting to note that if we open the hole lines in Fig. 2.2 (up), we find the two diagrams that contribute to πN scattering, as shown in Fig. 2.2 (down). The pion selfenergy arises from considering the pion-nucleon scattering process and summing up its associated scattering matrix over the occupied states of the Fermi sea.

2.1.1 The role of the $\Delta(1232)$ isobar.

In the region of intermediate energies ($T_\pi = 0 - 300$ MeV) the excitation of the internal degrees of freedom of the nucleon gives rise to delta excitations ($\Delta(1232)P_{33}$, $I(J^P) = \frac{3}{2}(\frac{3}{2}^+)$, $M_\Delta = 1232$ MeV). The Δ resonance accounts for most of the πN scattering amplitude around $T_\pi = 170 - 200$ MeV [12] so we must include it as an additional medium correction mechanism to the bare pion propagator.

The $\pi N\Delta$ interaction vertex can be obtained, in a non-relativistic approximation, from the effective Hamiltonian [1]

$$H_{\pi N\Delta} = \frac{f^*_\Delta}{m_\pi} S_i \partial_i \phi^\lambda(x) T^\lambda + h.c. \tag{2.8}$$

where S_i, T^λ are the $\frac{1}{2} \to \frac{3}{2}$ spin, isospin transition operators defined as

$$\langle \frac{3}{2} M_s | S^\dagger_\nu | \frac{1}{2} m_s \rangle = C(\frac{1}{2}, 1, \frac{3}{2}; m_s, \nu, M_s) \, \langle \frac{3}{2} || S^\dagger || \frac{1}{2} \rangle \ , \tag{2.9}$$

where the normalization is such that the reduced matrix element is equal to unity, and the S_ν stands for the operator in spherical base. An analogous relation holds for T^λ. The coupling constant f^*_Δ is taken from the fit to scattering data to be $\frac{f^*_\Delta}{f_N} = 2.13$. Eventually by performing the substitution

$$\sigma_i \tau^\lambda \to \frac{f^*_\Delta}{f_N} S^\dagger_i \, T^{\dagger\lambda} \tag{2.10}$$

in the Feynman rule of the πNN vertex one is lead to the Feynman rule for the $\pi N\Delta$ vertex.

Proceeding in a similar way as in the nucleon case, we find that the contribution to the pion selfenergy from delta-hole excitations is driven by the two diagrams in Fig. 2.3 up. Note, however, that in this case we always have the product of a free Δ propagator and an in-medium nucleon propagator, from which only the contribution of the hole piece survives. In analogy to the nucleonic case, we also find a direct and a crossed contribution, accounting for the two time orderings in the πN scattering amplitude with the excitation of an intermediate Δ resonance.

[1] The $\pi N\Delta$ interaction can be also described in an effective chiral Lagrangian approach by considering the coupling to the baryon decuplet [16].

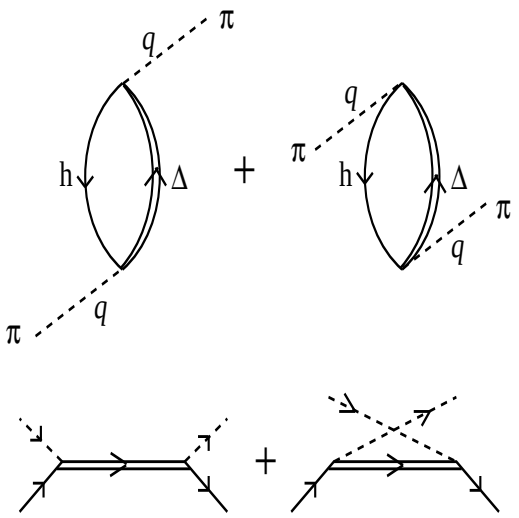

Figure 2.3: Up: direct and cross delta-hole excitation diagrams. Down: corresponding πN scattering diagrams, with a Δ intermediate state.

To perform the sums over intermediate spin and isospin states we make use of the following relation

$$\sum_{M_s} S_i|M_s\rangle\langle M_s|S_j^\dagger = \frac{2}{3}\delta_{ij} - \frac{1}{3} i\,\varepsilon_{ijk}\sigma_k \ , \tag{2.11}$$

and for the Δ propagator we use the standard non-relativistic reduction from the Rarita-Schwinger spin$-\frac{3}{2}$ field [11, 13],

$$G_{\Delta\,ij}(p) = \frac{\sum_{M_s} S_i|M_s\rangle\langle M_s|S_j^\dagger}{\sqrt{s_\Delta} - M_\Delta + \frac{i}{2}\Gamma_\Delta(p)} \ , \tag{2.12}$$

with $s_\Delta = p^2$, and Γ_Δ the Δ decay width. Provided the S_i, $S_j^\dagger$ operators are considered in the phenomenological $\pi N\Delta$ vertices we can omit them from Eq. (2.12) and use $G_\Delta(p) = [\sqrt{s_\Delta} - M_\Delta + \frac{i}{2}\Gamma_\Delta(p)]^{-1}$ as the Δ propagator. For the πN decay channel, which accounts for more than 99 % of the total decay width according to the PDG [117], the Δ width reads

$$\Gamma_\Delta(s_\Delta) = \frac{1}{3}\frac{1}{4\pi}\left(\frac{f_\Delta^*}{m_\pi}\right)^2 \frac{q^3}{\sqrt{s_\Delta}}(M_N + \sqrt{M_N^2+q^2})\Theta(\sqrt{s_\Delta} - M_N - m_\pi), \tag{2.13}$$

with $q = \lambda^{1/2}(s_\Delta, M_N^2, m_\pi^2)$ in the center of mass frame.

The result of the Δh contribution to the pion selfenergy can be written as

$$\Pi_0^{\Delta}(q) = \left(\frac{D+F}{2f}\right)^2 \vec{q}^{\,2} U_{\Delta}(q), \tag{2.14}$$

where the coupling f_{Δ}^{*} has been included in the definition of $U_{\Delta}(q)$, the Lindhard function for the Δh excitation (see Appendix B for analytical expressions, and Refs. [12, 13, 15] for details of the calculation).

For a shorter notation we shall collect both N and Δ contributions to the pion selfenergy in a single expression and redefine $\Pi_0(q)$ as follows:

$$\Pi_0(q) = \left(\frac{D+F}{2f}\right)^2 \vec{q}^{\,2} U(q), \tag{2.15}$$

with $U(q) \equiv U_N(q) + U_{\Delta}(q)$.

2.1.2 Spin-Isospin short range correlations

We have obtained a pion selfenergy from ph and Δh components which contributes to the first order perturbative calculation of the pion propagator in a nuclear medium (see Fig. 2.1 and Eq. (2.2)). This selfenergy is *irreducible* by construction, since diagrammatically it cannot be split into other valid selfenergy diagrams by cutting a single internal pion line. In terms of an irreducible pion selfenergy we can obtain a non-perturbative result for the pion propagator. The strategy is to sum up the whole series of diagrams generated by successively iterating the excitation of selfenergy bubbles - generically the irreducible selfenergy - by a propagating pion (Fig. 2.4), and we shall do that in the next section. There are many other irreducible pieces that can be considered [13], and we focus on a relevant subset of them which have a strong influence in the eventual spectral shape of the pion in the medium.

In Fig. 2.5 we show a series of diagrams in which the ph bubbles interact among themselves as a result of the nuclear forces. This means to include the effect of nuclear correlations in our model of the pion selfenergy. The way the bubbles interact includes any possible mechanisms in nucleon-nucleon interaction in accordance to the exchanged quantum numbers. This includes one pion exchange, which we do not consider because it would render a reducible selfenergy piece and it will be yet included in the non-perturbative

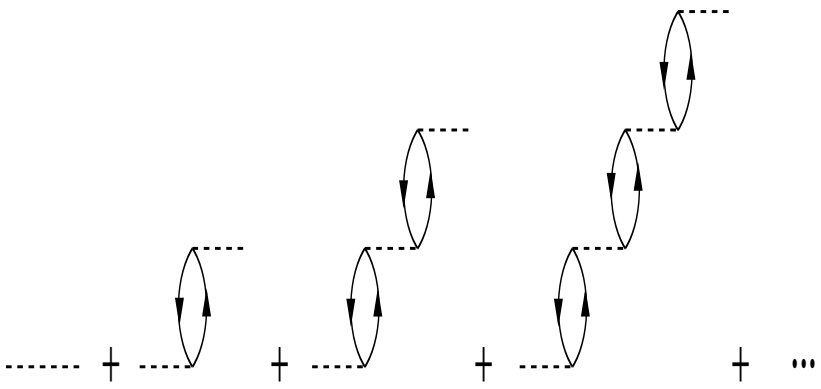

Figure 2.4: Iteration of the irreducible pion selfenergy.

sum of diagrams to be discussed in the next section. At shorter distances other meson exchange mechanisms as correlated and uncorrelated two-pion exchange and exchange of heavier resonances like the ω become important. We shall include them in an effective way, by means of a local interaction among ph excitations, given by

$$V_{ph-ph} = \left(\frac{D+F}{2f}\right)^2 g' \vec{\sigma_1}\vec{\sigma_2}\vec{\tau_1}\vec{\tau_2} \ . \tag{2.16}$$

In the frame of NN interaction, the g' coupling (Landau-Migdal parameter) takes a minimal value of $1/3$ to exactly cancel the singular term arising in the static OPE potential, but in general it could be a smoothly momentum dependent function. Commonly accepted values of g' stand in the range $[0.5, 0.8]$, as it results from the analysis of magnetic nuclear properties [11,13].

The pion selfenergy is recalculated including the contribution of short range correlations. A particle-hole bubble can interact with another one by means of a g'-like interaction, in addition to the exchange of a pion. As mentioned before do not consider here the latter mechanism, which would render that graph as a reducible contribution. Then we have the diagrams in Fig. 2.5, in which a nucleon in a ph successively interacts with other ph bubbles, contributing to the irreducible pion selfenergy since only the first and last vertices are connected to a pion line. In the same fashion one can introduce short range correlations to account for the repulsive part of the ΔN interaction ($\Delta N - NN$ and $\Delta N - \Delta N$). Assuming a universal value of

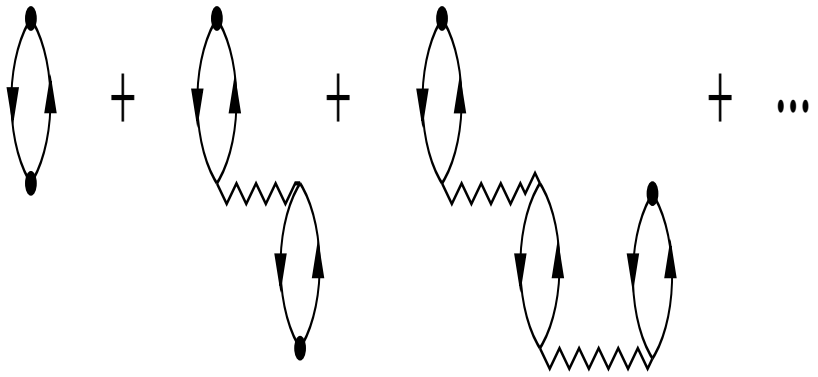

Figure 2.5: Short range correlation diagrams contributing to the pion selfenergy. The g' interactions are represented by zig-zag lines.

g' for nucleons and Δ's [2] the diagrammatic series in Fig. 2.5 can be summed up as a geometric progression and the result is

$$\left(\frac{D+F}{2f}\right)^2 \vec{q}^2\,[U(q)+U(q)\,\left(\frac{D+F}{2f}\right)^2 g'\,U(q)+...] = \left(\frac{D+F}{2f}\right)^2 \vec{q}^2 \frac{U(q)}{1-\left(\frac{D+F}{2f}\right)^2 g'U(q)}\ . \tag{2.17}$$

Thus our final expression for the pion selfenergy reads

$$\Pi_\pi(q) = \left(\frac{D+F}{2f}\right)^2 f(\vec{q}^2)^2\vec{q}^2 \frac{U(q)}{1-\left(\frac{D+F}{2f}\right)^2 g'U(q)}\ . \tag{2.18}$$

We shall study the effect of the g' interaction on the spectral behaviour of the pion in the next section. Unless explicitly mentioned, we shall use $g' = 0.7$ all throughout this work. We have explicitly shown in Eq. (2.18) the use of a monopole form factor, $f(\vec{q}^2) = \frac{\Lambda^2}{\Lambda^2+\vec{q}^2}$, for the πNN and $\pi N\Delta$ vertices with the cut-off parameter set to $\Lambda = 1$ GeV.

[2] This condition can be relaxed by introducing different couplings g'_{NN}, $g'_{N\Delta}$ and $g'_{\Delta\Delta}$ as done in [135]. However, there is no agreement in the interpretation of the experimental information on $g'_{\Delta\Delta}$ and the off-diagonal coupling, and we choose to set a single value for all the channels.

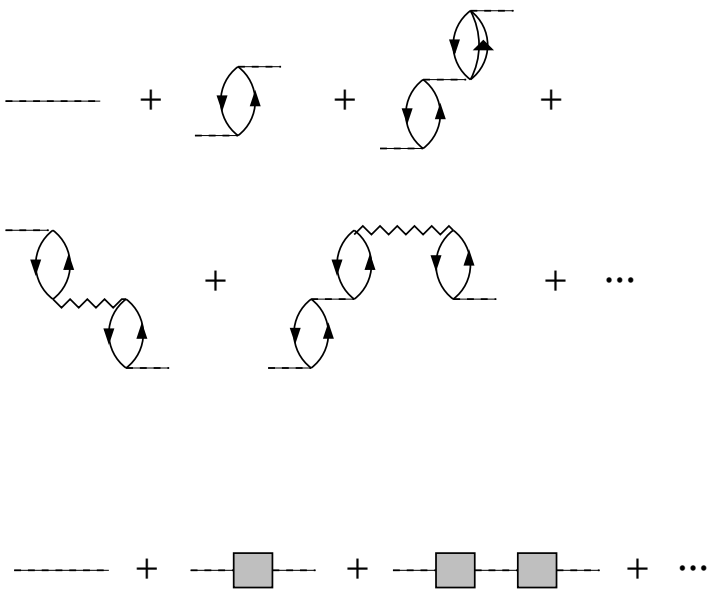

Figure 2.6: Up: Several contributions to the dressed pion propagator. Down: The Dyson series summing up irreducible pion selfenergy (represented by a box).

2.1.3 The pion propagator in the medium

The series of diagrams in Fig. 2.4 has to include the terms in which the ph and the Δh interact (Fig. 2.6up), so as to consider the effect of the short range correlations between the nucleons. The sum of terms can be reorganized in terms of successive insertions of the irreducible pion selfenergy, which already performs the RPA sum discussed in the previous section.

Then the pion propagator satisfies the following equation, corresponding to the diagrammatic series of Fig. 2.6down,

$$\begin{aligned} iD(q) &= iD_0(q) + iD_0(q)(-i)\Pi_\pi(q)iD_0(q) + \\ &\quad iD_0(q)(-i)\Pi_\pi(q)iD_0(q)(-i)\Pi_\pi(q)iD_0(q) + ... \\ &= iD_0(q) + iD_0(q)(-i)\Pi_\pi(q) \times \\ &\quad \times [iD_0(q) + iD_0(q)(-i)\Pi_\pi(q)iD_0(q) + ...]. \end{aligned} \tag{2.19}$$

Thus, the full pion propagator satisfies a selfconsistent equation, namely

$$D(q) = D_0(q) + D_0(q)\Pi_\pi(q)D(q), \tag{2.20}$$

Figure 2.7: Diagrammatic representation of the Dyson equation.

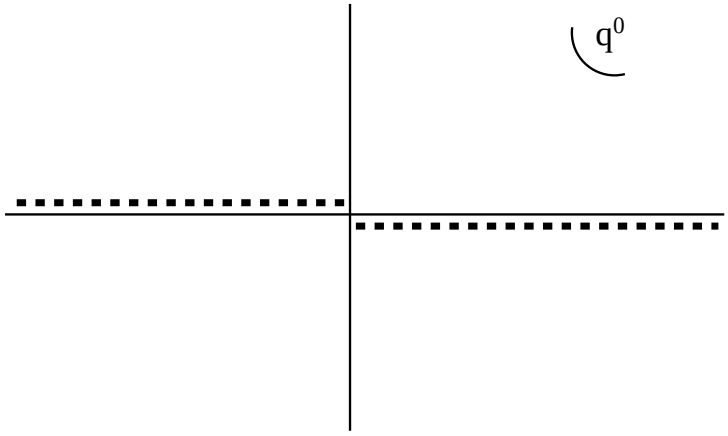

Figure 2.8: Cuts of the pion selfenergy in the complex energy plane.

which is known as the Dyson-Schwinger equation. It is shown diagrammatically in Fig 2.7. In coordinate space it becomes an integral equation and could require iterative solution. In momentum space, though, the solution is algebraic and provides the fully dressed pion propagator in nuclear matter,

$$D(q) = \frac{1}{q^2 - m_\pi^2 - \Pi_\pi(q)} \quad . \tag{2.21}$$

A first interesting result from the previous discussion is that the pole structure of the pion propagator has changed in nuclear matter. While in the vacuum the pion poles lie on the real axis, now they will appear in general as poles in the complex plane of q^0, since $\Pi_\pi(q) \in \mathbb{C}$.

As deduced from the analytical structure of the Lindhard function, Eq. (2.7), the pion selfenergy presents analytical cuts below the positive real axis and above the negative real axis in the complex energy plane (see Fig. 2.8), and the same analytical structure is inherited by the pion propagator in Eq. (2.21), via the Dyson-Schwinger equation. It is possible to write a spectral (Lehmann) representation in terms of the imaginary part of $D(q^0, \vec{q})$,

$$D(q^0, \vec{q}) \;\; = \;\; \int_{-\infty}^{0} d\omega \, \frac{S(\omega, \vec{q})}{q^0 - \omega - i\eta} + \int_{0}^{\infty} \frac{S(\omega, \vec{q})}{q^0 - \omega + i\eta}$$

$$= \int_0^\infty d\omega \, 2\,\omega \, \frac{S(\omega,\vec{q})}{(q^0)^2-\omega^2+i\epsilon} \ , \tag{2.22}$$

with $S(\omega,\vec{q}) = -\frac{1}{\pi}\mathrm{Im}\, D(\omega,\vec{q})$ the spectral function of the pion. This representation is a general property of the pion Green's function [17], independently of the model used to build the medium corrections, and restricts the analytical structure of the pion propagator in the presence of a nuclear medium. In Eq. (2.22), the integrand presents a continuum set of single poles in $q^0 = \pm\omega \mp i\eta$ what leads to analytical cuts in $D(q^0,\vec{q})$ as shown in Fig. 2.8. Thus, the present model for the $P-$wave pion selfenergy implements the correct analytical properties of the pion propagator. We shall use this representation in the next chapter. Note that the pion selfenergy in Eq. (2.18) is an even function of the energy, what implies that both the particle and the antiparticle share the same selfenergy in the medium. This is manifestly seen in the second equation of Eq. (2.22), in which the energy dependence of $D(q^0,\vec{q})$ is in $(q^0)^2$. This is a particular result for pions in symmetric nuclear matter.

In Fig. 2.9 we show the real and imaginary parts of $D(q)$, for a given momentum ($|\vec{q}| = 500$ MeV), as a function of the pion energy q^0. The calculation has been done for normal nuclear matter density $\rho = \rho_0$. The imaginary part clearly exhibits a low energy structure arising from the particle-hole excitations, as well as a resonant structure around 550 MeV corresponding to the excitation of Δ isobars. In addition, as a consequence of the attractive P-wave selfenergy, we find that the quasi-elastic pion peak appears at around 330 MeV. Therefore it has been shifted to lower energies compared to the free pion pole, whose position is marked in the plot with an arrow for reference.

We have also displayed in Fig. 2.9 the result when the short range correlations are not included in the model, just by setting $g' = 0$. The structures commented before appear now somehow more pronounced and narrow than in the previous case. In addition, the pion feels more attraction and the quasielastic peak shows up even at lower energies.

These results can be understood if we think that the net effect of the g' interactions is to soften the interaction of the pion with the surrounding nucleons. Having into account that the real part of the Lindhard function is negative in a wide range of values of q^0 and $\vec{q}$, from Eq. (2.18) it follows

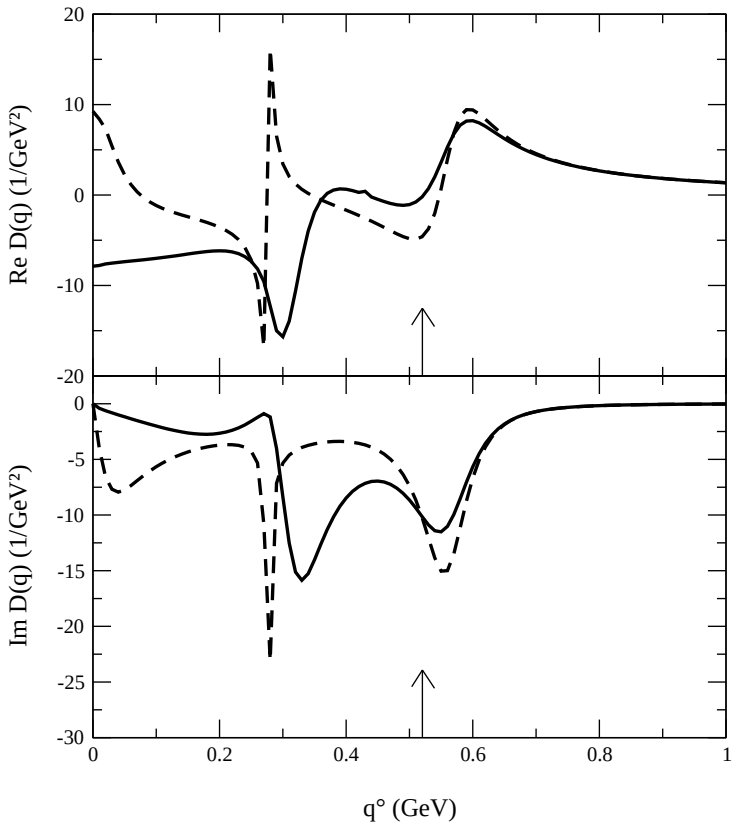

Figure 2.9: Real and imaginary parts of $D(q)$ vs energy for $|\vec{q}| = 500$ MeV and $\rho = \rho_0$. The solid lines include the contribution of short range correlations, for $g' = 0.7$. Dashed lines are the result for $g' = 0$. The arrows indicate the position of the pion pole in free space.

that the g' term in the denominator reduces the size of the pion selfenergy, leading to a smaller pion attraction.

The strongly attractive character of the $P-$wave selfenergy could lead, yet at relatively low densities ($\simeq \rho_0$), to the appearance of a pion mode with $q^0 = 0$ but $\vec{q} \neq \vec{0}$ which would be spontaneously created in the process $N \rightarrow N\pi$ with no energy cost. These pions would then condensate, since they are bosons, giving rise to a new state of matter with nucleons and pions in mutual equilibrium. This collective mode has not been observed at densities far beyond ρ_0. The inclusion of the short range correlations between the nucleons prevents this phenomenum to happen at densities of the order of ρ_0, and one would have to go to much higher densities, where many other higher order mechanisms - not included here - and a proper selfconsistent calculation become important [12].

2.1.4 Further contributions to the pion selfenergy

• *S-wave pion selfenergy*

We have considered so far $P-$wave πN interactions to build up the pion selfenergy, which we have improved by including the effect of short range correlations. Pions can also interact with nucleons in $S-$wave, although this contribution to the selfenergy is in general much smaller than the $P-$wave part, except for very low pion momenta, when the P-wave selfenergy is not so important. This is the case of pionic atoms [25]. We shall neglect the $S-$wave selfenergy for most of this work. The pion momentum regime of interest for the study of meson resonances is up to a few hundred MeV, and in this region the $P-$wave selfenergy dominates, mainly due to the coupling to $\Delta - h$ excitations. We shall provide here a brief outline of how the $S-$wave selfenergy arises and refer to the literature for details.

The $S-$wave πN interaction can be described in terms of an isoscalar and an isovector exchange which can be described in terms of an effective Lagrangian (see Ref. [13]). The couplings, λ_1 and λ_2 respectively, can be fit to reproduce the experimental scattering lengths, a_1 and a_3, of the πN scattering amplitudes in isospin 1/2 and 3/2, respectively. The isoscalar coupling is found to be about one order of magnitude smaller than the isovector

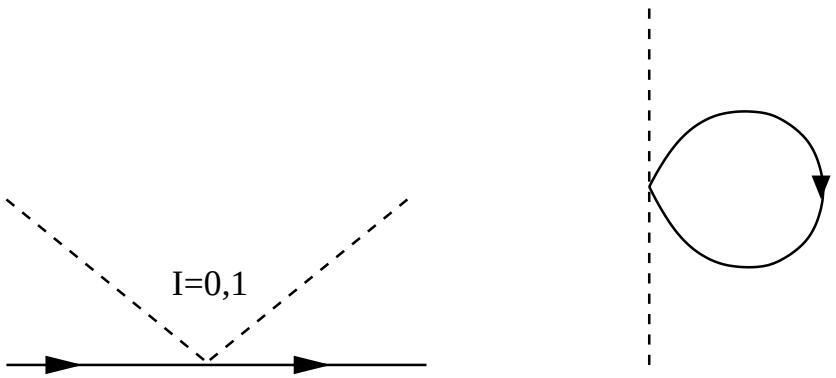

Figure 2.10: Left: Diagrammatic representation of $S-$wave πN interaction. Right: Resulting pion selfenergy diagram in a nuclear medium.

coupling, for small momentum transfers. The many-body contribution to the pion selfenergy comes, at lowest order, from the Hartree-like diagram in Fig. 2.10. The calculation of this diagram requires the isospin averaged πN amplitude, which only keeps record of the isoscalar part, since the isovector amplitude is proportional to $N - Z$ and therefore vanishes in symmetric nuclear matter. The $S-$wave pion selfenergy leads to a repulsive optical potential for the pion of a few MeV at normal nuclear density [13].

The $S-$wave πN interaction has also been studied in the context of χPT [19–21]. Recently, the πN interaction has been studied in a chiral unitary model of meson-baryon scattering in the strangeness $S = 0$ sector to extend the low energy results of χPT to the region of the $N^*(1535)$ resonance [23]. The $S-$wave pion selfenergy was evaluated in [24] from this model in a $t\rho$ approximation.

- *Excitation of other resonances with πN decay modes*

The $P-$wave selfenergy can be also improved to include the excitation of other resonances in addition to the $\Delta(1232)$. The closest candidate in energy with a πN decay mode is the $N^*(1440)$ Roper resonance. Its relevance in the πN dynamics has been studied elsewhere [18]. In the many-body formalism, it contributes at first order as a N^*h excitation, and the resulting selfenergy term can be written in total analogy to the Δh contribution, Eq. B.4 in appendix B. One has to substitute the coupling, mass, isospin factor and decay width in the Lindhard function of Eq. B.4 by the corresponding

magnitudes of the $N^*(1440)$.

The coupling to πN, which can be taken from Ref. [22], is $f_{\pi NN^*}/f_{\pi NN} = 0.48$ as compared to $f_{\pi N\Delta}/f_{\pi NN} = 2.13$. The N^*h contribution is thus expected to be much smaller than that of the Δ, and it is indeed the case as can be seen in Fig. 4 from Ref. [24], where the pion selfenergy is shown as a function of the energy for a pion momentum of 500 MeV.

- *Higher orders in density: $2p2h$ excitations*

So far we have studied the pion selfenergy at the lowest order in a perturbative expansion which approximately corresponds to a series in powers of the nuclear density. We basically focus our attention on medium effects at the lowest order in density throughout this work[3], but for the sake of completeness we also mention here some contributions at the next order in density which become important to describe some features of the pion nucleus phenomenology, and give references for further details. At second order in density the pion selfenergy accounts for processes in which two different nucleons in the medium are involved. An important class of these processes is the two particle two hole excitation mechanism ($2p2h$), an example of which is depicted in Fig. 2.11 as a many body diagram contributing to the pion selfenergy. The $2p2h$ selfenergy is particularly relevant to describe pion absorption by nuclei, a process which requires the participation of two nucleons and therefore is a contribution of order $\mathcal{O}(\rho^2)$. In Ref. [11] the pion optical potential is studied at order $\mathcal{O}(\rho^2)$ from a phenomenological point of view, and data on pion nucleus scattering is used obtain the phenomenological parameters of the potential. The $2p2h$ pion selfenergy has also been studied from a microscopical many body approach at low [25] and intermediate energies [26], and contrasted to experimental data on the pion nucleus optical potential from pionic atoms and pion nucleus scattering.

[3] We considered already in this chapter a second order effect in the pion selfenergy, the spin-isospin short range correlations, which are found to modify appreciably the spectral function of the pion at normal nuclear density.

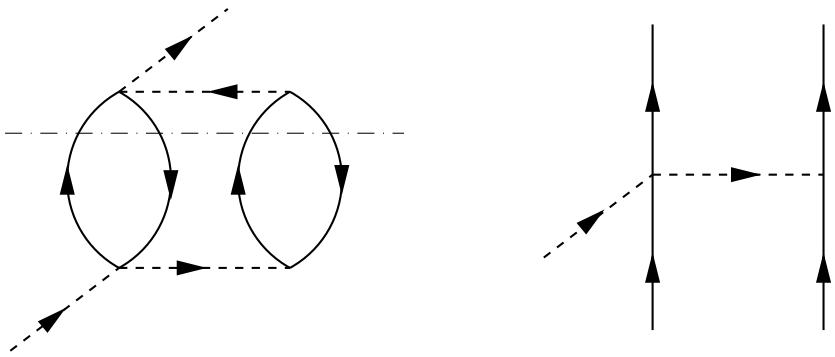

Figure 2.11: Example of a many body diagram (left) regarding a $2p2h$ excitation. To the right the corresponding pion absorption diagram.

2.2 Kaons in nuclear matter

The study of kaon properties in a medium, as a result of their interactions with the nucleons, is a necessary step in the renormalization program of scalar and vector meson resonances in a medium, which is the purpose of this Thesis. For instance, the $\bar{K}K$ channel is responsible for most of the decay width of the ϕ meson in vacuum, and it also appears as a possible intermediate two-meson state in the coupled channel treatment of $\pi\pi$ scattering both in the scalar and vector sectors. The $K\pi$ channel in $I = 1/2$ is also one of the possible channels compatible with the quantum numbers of the controversial κ meson.

We shall work out this problem following closely what is done for the pions. That is, we shall build a kaon selfenergy originating from the interactions with the nucleon inside a Fermi sea, in $S-$ and $P-$waves. However, the nature of the KN and $\bar{K}N$ interactions will establish some conceptual differences with the case of the pion, which will deserve some technical modifications to study the meson propagator and eventually the spectral representations.

Moreover, in the case of in-medium pions we neglected the small contributions from the $S-$wave selfenergy, due to the strong contribution of the $P-$wave (driven by the excitation of Δh pairs) which dominates the medium effects in the physical processes to be discussed later. In the case of the kaons, we have that kind of important contribution even from the $S-$wave inter-

action and it has a noticeable effect, for instance, in the ϕ meson spectrum in the medium, since the emitted kaons stand very close to the production threshold.

We discuss below how the kaon $S-$ and $P-$wave selfenergies arise in the medium. Most of the results presented here are borrowed from several works dealing with the KN interactions in free space and in the medium [27–30]. We present a brief summary here, and some novelties related to kaon loop calculations will be stressed later in Chapter 6.

2.2.1 $S-$wave kaon selfenergy

The interactions of K^+, K^0 and $\bar{K}^0$, K^- with the nucleons of the medium are rather different and it is necessary to treat them separately. We can expect the KN interaction to be smooth at low energies, since there are no $S = 1$ baryonic resonances to be excited, except for the recently found Θ^+ baryon which has been predicted to couple very weakly to KN and would produce a very small effect [31].

To obtain a $S-$wave selfenergy we follow the $t\rho$ approximation of Refs. [27, 30], and a (density dependent) repulsive constant selfenergy is obtained for the K^+ (a similar expression holds for the K^0):

$$\Pi_{K^+} = \frac{1}{2}(t_{K^+p} + t_{K^+n})\rho \simeq 0.13 m_K^2 \frac{\rho}{\rho_0} \ . \tag{2.23}$$

This can be interpreted as an in-medium shift of the kaon mass, $m_K \rightarrow m_K^*(\rho)$, according to

$$m_K^{*\,2}(\rho) = m_K^2 + \Pi_K(\rho) \simeq 1.13 m_K^2 \frac{\rho}{\rho_0} \ , \tag{2.24}$$

what implies a 6% shift at normal nuclear matter density.

The $\bar{K}N$ interaction, however, is dominated at low energies by the excitation of the $\Lambda(1405)$ resonance, which appears just below the $\bar{K}N$ threshold. This resonance is closely related to the interaction of the $\bar{K}N$ system with other meson-baryon channels, and it is indeed successfully generated in a unitary coupled channel approach to the $S-$wave $\bar{K}N$ scattering [29]. In this work, the authors make use of the lowest order chiral Lagrangian to describe the interaction of the $\bar{K}N$ system and its coupling to a set of meson-baryon

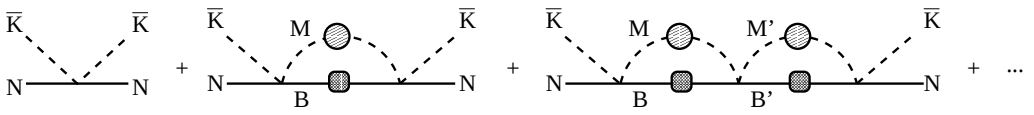

Figure 2.12: Diagrammatic representation of the BS equation in $\bar{K}N$ scattering in the medium. The blobs indicate intermediate meson selfenergies and baryon mean field potentials. The first and last baryon lines in each term correspond to a hole propagator.

channels, namely K^-p, $\bar{K}^0n$, $\pi^0\Lambda$, $\pi^0\Sigma^0$, $\pi^+\Sigma^-$, $\pi^-\Sigma^+$, $\eta\Lambda$, $\eta\Sigma^0$, $K^+\Xi^-$ and $K^0\Xi^0$ for K^-p scattering, and K^-n, $\pi^0\Sigma^-$, $\pi^-\Sigma^0$, $\pi^-\Lambda$, $\eta\Sigma^-$ and $K^0\Xi^-$ for K^-n scattering. The $\Lambda(1405)$ is dynamically generated in this approach from a Bethe-Salpeter (BS) equation which accounts for the rescattering of the meson-baryon system, and it appears as a pole of the T matrix in the complex energy plane. Even though appearing below the KN threshold, the resonance acquires a finite width as a consequence of its strong coupling to some of the coupled channels, namely $\pi\Lambda$ and $\pi\Sigma$, which provide enough phase space for the resonance to decay. The experimental cross sections for K^-p scattering to the different coupled channels are well reproduced.

Starting from this successful scheme in free space, an effective interaction in the medium, $T^{\bar{K}N}_{eff}$, is obtained in Ref. [30] by solving the coupled channel Bethe-Salpeter equation including Pauli blocking on the nucleons, mean-field binding potentials for the baryons involved and the medium modifications of π mesons and $\bar{K}$ mesons themselves. The pion propagators are dressed with the $P-$wave selfenergy discussed in the previous section including a contribution from $2p2h$ excitations. The kaon propagators are dressed with the $S-$wave selfenergy plus a $P-$wave contribution due to hyperon-hole (Yh) excitations, that we discuss below in detail. The $\bar{K}$ selfenergy is obtained by summing the in-medium effective interaction over the nucleons in the Fermi sea. This leads to a selfconsistent calculation, since the antikaon selfenergy is also an input in the calculation of the effective $\bar{K}N$ interaction in the medium, through the in-medium meson-baryon loops in the BS equation.

We refer the reader to Refs. [27–30] for further details of the model.

2.2.2 $P-$wave kaon selfenergy

Kaons can also couple to the nucleons in $P-$wave, what sets up a further contribution to the selfenergy in the medium. In principle, for low energy kaons (e.g. kaons emitted in ϕ decay), one could expect the $S-$wave selfenergy to be dominant. For higher momenta, the $P-$wave selfenergy may become very important and we shall include it as well, so that we have a reliable description of the kaon properties in a wide range of energies and momenta.

The $P-$wave kaon selfenergies arise, in the many-body language that we follow throughout this work, due to the excitation of Yh components. We consider the contribution of Λh, Σh and $\Sigma^* h$ excitations ($\Sigma^* = \Sigma^*(1385)$), which are the first ones allowed by phase space already at low kaon momenta. The corresponding many-body mechanisms are shown in Fig. 2.13. The analytical structure of these diagrams follows closely that of the Δh excitation in the pion selfenergy. We have one baryon propagator and an in-medium nucleon propagator, which can only contribute as a hole. Note, however, that because of strangeness conservation, only direct terms are permitted for the $\bar{K}$ excitations (Fig. 2.13a). Conversely, the K selfenergy arises from the crossed terms (Fig. 2.13b). In a wide range of energy and momentum, the excited hyperon lies far from the pole in the crossed kinematics. Therefore we expect a very small, real and almost energy independent contribution from diagram 2.13b. As a result the K is barely modified by the $P-$wave selfenergy. Thus we can safely neglect it in the kaon selfenergies and loop calculations, and we only discuss in detail the $\bar{K}$ selfenergy from direct terms.

The $\bar{K}NY$ vertices ($Y = \Lambda, \Sigma$) involved are derived from the lowest order chiral Lagrangian coupling the octet of pseudoscalar mesons to the $1/2^+$ baryon octet, as it is done for instance in Ref. [30]. We have included this Lagrangian in Appendix C for reference. The $\bar{K}NY$ vertices can be written as follows,

$$V_{\bar{K}NY} \equiv -it_{\bar{K}NY} = -\widetilde{V}_{\bar{K}NY}\gamma^\mu\gamma_5 q_\mu \simeq \widetilde{V}_{\bar{K}NY}\vec{\sigma}\vec{q} \ , \tag{2.25}$$

for an incoming $\bar{K}$ with momentum q, where the $\widetilde{V}_{\bar{K}NY}$ factors, defined as $\widetilde{V}_{\bar{K}NY} = \alpha\frac{D+F}{2f} + \beta\frac{D-F}{2f}$, contain the required $\bar{K}NY$ couplings and $SU(3)$

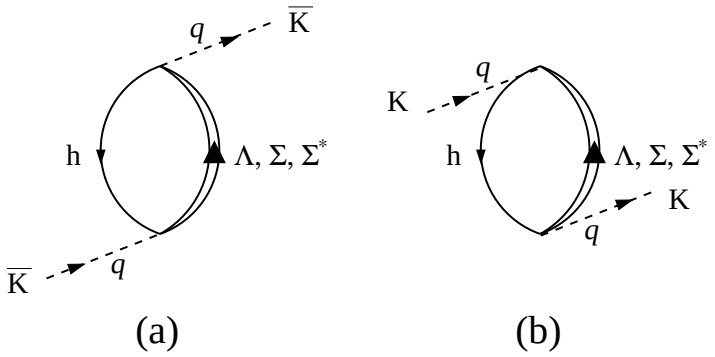

Figure 2.13: Kaon $P-$wave selfenergy diagrams: (a) $\bar{K}$ direct term; (b) K crossed term.

factors. We provide the values of α, β in Table 2.1. In Eq. (2.25) we have performed a non-relativistic reduction of these vertices.

	$K^-p \to \Lambda$	$K^-p \to \Sigma^0$	$K^-n \to \Sigma^-$	$\bar{K}^0n \to \Lambda$	$\bar{K}^0n \to \Sigma^0$	$\bar{K}^0p \to \Sigma^+$
α	$-\frac{2}{\sqrt{3}}$	0	0	$-\frac{2}{\sqrt{3}}$	0	0
β	$\frac{1}{\sqrt{3}}$	1	$\sqrt{2}$	$\frac{1}{\sqrt{3}}$	-1	$\sqrt{2}$

Table 2.1: Coefficients for the $\bar{K}NY$ couplings of Eq. (2.25).

The $\bar{K}N\Sigma^*$ vertex can be written as

$$V_{\bar{K}N\Sigma^*} = \widetilde{V}_{\bar{K}N\Sigma^*}\vec{S}^\dagger\vec{q} = \frac{g_{\Sigma^*}}{2M_N}A\vec{S}^\dagger\vec{q}\ , \tag{2.26}$$

with $\vec{S}^\dagger$ the $1/2 \to 3/2$ spin transition operator and A given in Table 2.2. $\widetilde{V}_{\bar{K}N\Sigma^*}$ cannot be obtained from the Lagrangian since the Σ^*, $J^P = 3/2^+$,

	$K^-p \to \Sigma^{*0}$	$K^-n \to \Sigma^{*-}$	$\bar{K}^0p \to \Sigma^{*+}$	$\bar{K}^0n \to \Sigma^{*0}$
A	$-\frac{1}{\sqrt{2}}$	-1	-1	$\frac{1}{\sqrt{2}}$

Table 2.2: Coefficient for the $\bar{K}N\Sigma^*$ couplings of Eq. (2.26).

does not belong to the $J^P = 1/2^+$ baryon octet. This coupling is estimated in Ref. [116] first by using the $SU(6)$ quark model to relate the πNN coupling to the $\pi N\Delta$, and then using $SU(3)$ symmetry to relate the $\pi N\Delta$ coupling

to the one for $\bar{K}N\Sigma^*$, since the Σ^* belongs to the same decuplet as the Δ. The result is $\frac{g_{\Sigma^*}}{2M_N} = \frac{2\sqrt{6}}{5}\frac{D+F}{2f}$.

For the nucleon propagator in the medium we use the non-relativistic expression obtained in Appendix A, from which only the hole term plays a role in this case, as it happened for the Δh mechanism in the pion self-energy. The hyperon propagators are also considered in a lowest order non-relativistic approximation, namely, $G_Y(p) = [p^0 - E_Y(\vec{p}) + i\epsilon]^{-1}$ with $E_Y(\vec{p}) = \sqrt{M_Y^2 + \vec{p}^{\,2}} \simeq M_Y + \frac{p^2}{2M_Y}$. We shall include, though, relativistic recoil corrections to the $\bar{K}NY$ vertices so that we can safely use the kaon selfenergy on a wider range of energies, and we discuss them below.

The $P-$wave $\bar{K}$ selfenergy reads[4]

$$\begin{aligned}
\Pi_{\bar{K}}^{Pwave}(q^0,\vec{q};\rho) &\equiv \vec{q}^{\,2}\widetilde{\Pi}_{\bar{K}}^{Pwave}(q^0,\vec{q};\rho) \\
&= \frac{1}{2}\widetilde{V}^2_{K^-p\Lambda} f^2_\Lambda(q)\vec{q}^{\,2} U_\Lambda(q^0,\vec{q};\rho) \\
&+ \frac{3}{2}\widetilde{V}^2_{K^-p\Sigma^0} f^2_\Sigma(q)\vec{q}^{\,2} U_\Sigma(q^0,\vec{q};\rho) \\
&+ \frac{1}{2}\widetilde{V}^2_{K^-p\Sigma^{*0}} f^2_{\Sigma^*}(q)\vec{q}^{\,2} U_{\Sigma^*}(q^0,\vec{q};\rho)\ ,
\end{aligned} \tag{2.27}$$

where U_Y ($Y = \Lambda, \Sigma, \Sigma^*$) stands for the Lindhard function including only spin factors and direct kinematics. We provide analytical expressions for these functions in Appendix B.

The f_Y^2 functions in Eq. (2.27) stand for relativistic recoil corrections. At the lowest order, the first corrections to the expressions of the vertices used here read $f_{0Y}(q) = 1 - \frac{q^0}{n_y M_Y}$, with $n_\Lambda = n_\Sigma = 2$ and $n_{\Sigma^*} = 1$.

To account for the off-shell behaviour of the kaon-baryon vertices, Eq. (2.27) also includes a form factor for each kaon-baryon vertex (not shown explicitly). In Refs. [116, 161] a dipolar form factor is used, namely $[\Lambda^2/(\Lambda^2 - q^2)]^2$, with $\Lambda = 1.05$. Some technical difficulties of using such form factors arise in loop calculations, and they are discussed in Chapter 6 for the particular case of ϕ meson decay in a nuclear medium.

Finally, higher order effects in density in the kaon selfenergy, like those induced by the short range correlations in the pion selfenergy have been

[4]The $P-$wave selfenergy for the kaon is easily obtained from Eq. (2.27) by changing the sign of q^0, namely, $\Pi_K^{Pwave}(q^0,\vec{q};\rho) = \Pi_{\bar{K}}^{Pwave}(-q^0,\vec{q};\rho)$.

studied in [32,33]. The effects have been found to be very small at the densities considered throughout this Thesis, and we shall neglect any contribution from this source.

2.2.3 Spectral representation of the kaon propagator

We have built up the irreducible kaon selfenergy from $S-$ and $P-$wave interactions with the nucleons. The in-medium kaon propagator, from summing up the Dyson series, reads

$$D_{\bar{K}(K)}(q^0,\vec{q};\rho) = \frac{1}{q^2 - m_K^2 - \Pi_{\bar{K}(K)}(q^0,\vec{q};\rho)} \ . \tag{2.28}$$

We shall rewrite the kaon propagator in terms of a spectral representation as we did for the pion, which turns to be convenient to simplify both analytical results and numerical calculations. The spectral function for the kaons, $S_{\bar{K}(K)}$, is given by

$$\begin{aligned} S_{\bar{K}}(q^0,\vec{q};\rho) &= -\frac{1}{\pi}\mathrm{Im}D_{\bar{K}}(q^0,\vec{q};\rho) \\ &= -\frac{1}{\pi}\frac{\mathrm{Im}\Pi_{\bar{K}}(q^0,\vec{q};\rho)}{[q^2 - m_K^2 - \mathrm{Re}\Pi_{\bar{K}}(q^0,\vec{q};\rho)]^2 + \mathrm{Im}\Pi^2_{\bar{K}}(q^0,\vec{q};\rho)} \ , \\ S_K(q^0,\vec{q};\rho) &= -\frac{1}{\pi}\mathrm{Im}D_K(q^0,\vec{q};\rho) = \delta[(q^0)^2 - \widetilde{\omega}_K^2(q)] \ , \end{aligned} \tag{2.29}$$

with $\widetilde{\omega}_K^2(q) = \vec{q}^{\,2} + m_K^2 + \Pi_K(\rho)$. In the third line of Eq. (2.29) we explicitly consider an energy independent selfenergy for the kaon.

Note that the kaon propagator in the medium cannot be an even function of q^0, since the kaon selfenergy discussed in the previous sections is not a symmetric function of the energy. Moreover, a proper description of the kaon propagator in a nuclear medium should consider the crossing symmetry relation

$$D_{\bar{K}(K)}(-q^0,\vec{q};\rho) = D_{K(\bar{K})}(q^0,\vec{q};\rho) \ , \tag{2.30}$$

which indeed holds at zero baryonic density. This is an important point in loop calculations, because the q^0 variable runs over all possible values of the energy, and the kaon propagator should contain the information of both the $\bar{K}$ and K poles, as it happens in free space.

We shall use the following spectral representation [161] for the kaon propagators,

$$D_{\bar{K}(K)}(q^0,\vec{q};\rho) = \int_0^\infty d\omega \left(\frac{S_{\bar{K}(K)}(\omega,\vec{q};\rho)}{q^0-\omega+i\eta} - \frac{S_{K(\bar{K})}(\omega,\vec{q};\rho)}{q^0+\omega-i\eta} \right) \quad , \tag{2.31}$$

which considers properly the $\bar{K}$ and K poles and satisfies the crossing relation in Eq. (2.30). Note that the imaginary part of the propagator entirely arises from the first term in Eq. (2.31), for positive q^0, carrying the information of the appropriate spectral function. The second term, far from the pole for positive q^0, gives a small contribution to the real part of $D_{\bar{K}(K)}$. The role of these terms is exchanged under the change of sign in q^0. We depict in Fig. 2.14 the resulting $\bar{K}$ spectral function at several nuclear densities and two different kaon momenta.

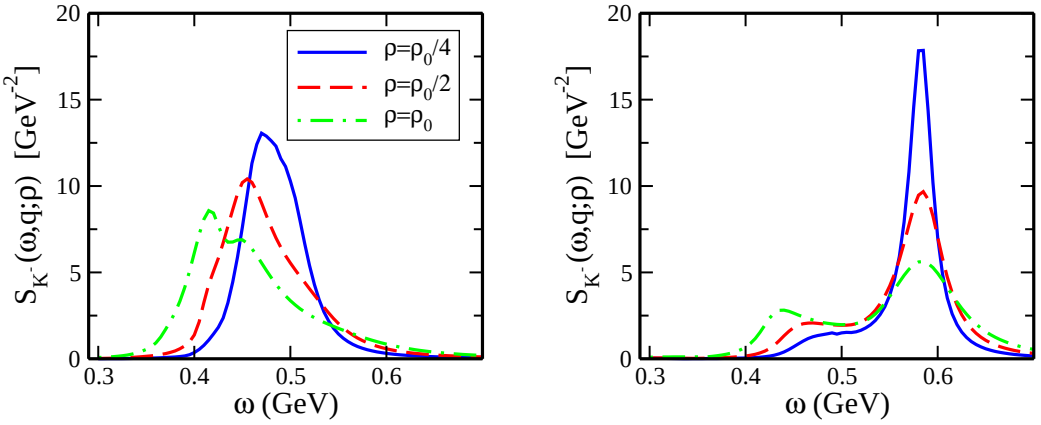

Figure 2.14: $\bar{K}$ spectral function for several nuclear densities. Left: at zero momentum. Right: $|\vec{q}| = 300$ MeV.

If we use Eq. (2.31) for the in-medium pion propagator, and having into account that the pion selfenergy described in this chapter is symmetric in energy (thus $S_{\pi^+} = S_{\pi^-} = S_{\pi^0}$), the pion spectral function can factorize out of the brackets in Eq. (2.31) and one ends up with the ordinary Lehmann representation in Eq. (2.22). The spectral representation in Eq. (2.31) is also useful to describe the pion propagator in asymmetric nuclear matter, where the π^+ and π^- selfenergies are no longer equal.

Chapter 3

Scalar-isoscalar (σ channel) meson-meson scattering in the nuclear medium

The existence of a light scalar isoscalar meson (σ meson) has been a controversial topic in Nuclear Physics. Recently, several results in the literature support this hypothesis [34–37] although, however, the nature of this meson as a genuine QCD state or as a dynamically generated resonance in $\pi\pi$ scattering is still under debate. A review of the current status of the discussion can be found in Ref. [38].

The σ meson is such a broad resonance that its effects are hardly visible in phase shifts or decay plots. This situation could be quite different at finite densities and/or temperatures, since the σ could become lighter and narrow, as discussed in Refs. [39–45]. This topic is of special interest due to the relevance of the $I = J = 0$ channel in the nucleon nucleon interaction. Any substantial change of the σ properties could alter the in-medium nucleon nucleon interaction and therefore our current understanding of the nuclear matter in heavy ion collision, neutron stars or even in normal nuclei if the changes occur at low densities.

The density dependence of the σ properties has been studied in several models. For instance, in Refs. [42,46,47] it has been found a decrease of the σ mass as a function of the nuclear density within a generalized Nambu Jona-Lasinio model, so that the σ mass converges to the mass of the pion, its chiral partner. In the same model, however, the ρ, ω and π meson masses remain almost constant with the density. In Ref. [48], the σ propagator was studied

in the Linear Sigma Model and the results show an enhanced and narrow σ spectral function near the 2π threshold, as a consequence of a partial restoration of chiral symmetry, in which the σ mass would approach m_π. The same conclusions were reached using the non-linear chiral Lagrangian in Ref. [49].

Similar results, with large enhancements in the $\pi\pi$ amplitude around the 2π threshold, have been found in a quite different approach by studying the $S-$wave, $I = 0$ $\pi\pi$ correlations in nuclear matter [50–53]. In these works the medium modifications of the σ channel are induced by the strong $P-$wave coupling of the pion to the particle-hole (ph) and Delta-hole (Δh) nuclear excitations. It was pointed out in [54, 55] that this attractive σ selfenergy induced by the pion renormalization in the nuclear medium could be complementary to the additional $S-$wave renormalization found in [48, 49], thus leading to even larger effects.

On the experimental side, there are also several results showing strong medium effects in the σ channel at low invariant masses in the $A(\pi, 2\pi)$ [56–60] and $A(\gamma, 2\pi)$ [61] reactions. At the moment, the cleanest signal probably corresponds to the $A(\gamma, 2\pi^0)$ reaction, which shows large density effects that have been predicted in Ref. [62], using a model for the $\pi\pi$ final state interaction which we shall describe in the present chapter.

Our aim in this work is to study the σ mass and width at finite nuclear densities in the context of the model developed in [63–68]. These works, which provide a very economical and successful description of a wide range of hadronic phenomenology, use as input the lowest order Lagrangian of Chiral Perturbation Theory (χPT) [69] and calculate the meson meson scattering amplitude in a non-perturbative, coupled channel framework which guarantees unitarity. The σ meson is not a basic degree of freedom in the present models, but it is dynamically generated and appears as a pole of the $\pi\pi$ scattering amplitude in the second Riemann sheet of the energy complex plane.

The nuclear medium effects on the scalar isoscalar channel were implemented in this framework in Refs. [53, 70]. We follow the same lines in this work, and also study the effect of some additional mechanisms which were found to be relevant in Ref. [82], according to a chiral counting scheme. We

include in Section 3.1 a description of the model for the $\pi\pi$ interaction in vacuum and consider the nuclear medium effects in Section 3.2. Next we describe how to extrapolate the $\pi\pi$ scattering amplitude onto the energy complex plane in the present approach, in order to search for the σ pole position at finite nuclear densities. This is done in Section 3.3 and the results from this calculation are discussed in Section 3.4. A set of additional medium effects, not previously considered in the present approach, are studied in Section 3.5. We summarize our conclusions in Section 3.6.

3.1 Chiral unitary model of $L = 0$ meson meson scattering

The theoretical study of meson meson scattering in the last years has experienced a profound development as a result of combining the information contained in the Lagrangians of Chiral Perturbation Theory (χPT) with the use of non-perturbative methods to build the scattering amplitudes. We summarize here a non-perturbative chiral model of meson meson scattering in the scalar sector introduced in Ref. [68], which provides a successful description of many scattering observables with a single parameter and generates, out of the interactions between the pseudoscalar octet mesons, the relevant meson resonances in the isoscalar (σ, f_0) and isovector (a_0) channels in the range of energies of $\sqrt{s} \lesssim 1.2$ GeV. These resonances manifest as singularities in the scattering amplitudes, allocated in the second Riemann sheet (2ndRS) of the energy complex plane.

The starting point in the model is the lowest order Lagrangian of χPT, which contains the most general low energy interactions of the pseudoscalar meson octet, namely

$$\mathcal{L}_2 = \frac{1}{12f^2}\langle(\partial_\mu\Phi\Phi - \Phi\partial_\mu\Phi)^2 + M\Phi^4\rangle \ , \tag{3.1}$$

where the symbol $\langle\,\rangle$ indicates the trace in flavour space, f is the pion decay constant and Φ, M are the pseudoscalar meson field and mass $SU(3)$

matrices,

$$\Phi \equiv \frac{\vec{\lambda}}{\sqrt{2}}\vec{\phi} = \begin{pmatrix} \frac{1}{\sqrt{2}}\pi^0 + \frac{1}{\sqrt{6}}\eta & \pi^+ & K^+ \\ \pi^- & -\frac{1}{\sqrt{2}}\pi^0 + \frac{1}{\sqrt{6}}\eta & K^0 \\ K^- & \bar{K}^0 & -\frac{2}{\sqrt{6}}\eta \end{pmatrix} \quad , \tag{3.2}$$

$$M = \begin{pmatrix} m_\pi^2 & 0 & 0 \\ 0 & m_\pi^2 & 0 \\ 0 & 0 & 2m_K^2 - m_\pi^2 \end{pmatrix} \quad ,$$

with the mass matrix given in the isospin limit. We shall work in a coupled channel framework. The relevant two-meson states for $I = 0$ are given by

$$\begin{aligned} |K\bar{K}\rangle &= -\frac{1}{\sqrt{2}}|K^+(\vec{q})K^-(-\vec{q}) + K^0(\vec{q})\bar{K}^0(-\vec{q})\rangle \\ |\pi\pi\rangle &= -\frac{1}{\sqrt{6}}|\pi^+(\vec{q})\pi^-(-\vec{q}) + \pi^-(\vec{q})\pi^+(-\vec{q}) + \pi^0(\vec{q})\pi^0(-\vec{q})\rangle \ , \end{aligned} \tag{3.3}$$

with $|\pi^+\rangle = -|1\,1\rangle$ and $|K^+\rangle = -|\frac{1}{2}\,\frac{1}{2}\rangle$ in the isospin basis, what fixes the isospin phase convention. We shall ignore in this work the contribution from the $|\eta\eta\rangle$ state since we are mainly interested in $\pi\pi$ scattering in the energy region below $\sqrt{s}$ =1 GeV and, as it has been studied in Ref. [67], the $|\eta\eta\rangle$ state starts to be relevant for energies around 1.2 GeV.

The $S-$wave projected tree level amplitudes from $\mathcal{L}_2$ in the $I = 0$ channel read

$$\begin{aligned} V_{11} &= -\frac{1}{4f^2}\left(3s + 4m_K^2 - \sum_i p_i^2\right) \ , \\ V_{21} &= -\frac{1}{3\sqrt{12}f^2}\left(\frac{9}{2}s + 3m_K^2 + 3m_\pi^2 - \frac{3}{2}\sum_i p_i^2\right) \ , \\ V_{22} &= -\frac{1}{9f^2}\left(9s + \frac{15m_\pi^2}{2} - 3\sum_i p_i^2\right) \ , \end{aligned} \tag{3.4}$$

with s the Mandelstam variable and p_i the momentum of the four mesons involved ($p_1 = k$, $p_2 = p$, $p_3 = k'$, $p_4 = p'$ as in the first diagram of Fig. 3.1). The subindices in V_{ij} correspond to the notation $|1\rangle = |K\bar{K}, I = 0\rangle$

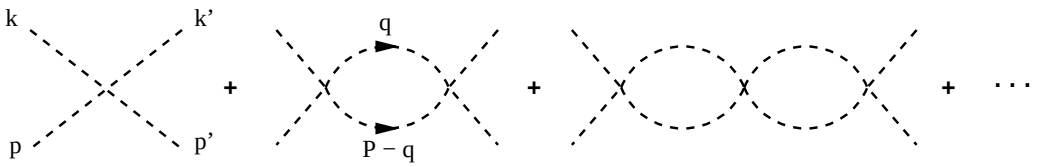

Figure 3.1: Diagrammatic representation of the LS equation.

and $|2>= |\pi\pi, I = 0\rangle$. Note that the on-shell amplitudes are obtained by substituting $p_i^2 \to m_i^2$ in Eq. (3.4).

The range of applicability of χPT is clearly limited by the presence of resonances, which can never be accommodated in a perturbative expansion in powers of the momentum of the particles, since such an expansion would not generate a pole in the scattering amplitude, T. The use of non-perturbative methods help recover the analytical structure of T and implement full unitarity of the amplitude, which in χPT is only satisfied at the perturbative level. We choose the tree level meson meson amplitudes from $\mathcal{L}_2$ as the potential or kernel to be iterated in a set of coupled channel Bethe-Salpeter (BS) equations, namely

$$T_{ij} = V_{ij} + \overline{V_{il} G_{ll} T_{lj}} \ . \tag{3.5}$$

The bar over the second term in Eq. (3.5) indicates the integral character of the BS equation, meaning

$$\overline{V_{il} G_{ll} T_{lj}} = \int \frac{d^4q}{(2\pi)^4} \, V_{il}(k,p;q) \, G_{ll}(P,q) \, T_{lj}(q;k',p') \ , \tag{3.6}$$

where $P = k + p = k' + p'$ is the total momentum of the two-meson system ($s = P^2$) and G_{ii} contains the product of the two meson propagators,

$$G_{ii} = i \frac{1}{q^2 - m_{1i}^2 + i\epsilon} \quad \frac{1}{(P-q)^2 - m_{2i}^2 + i\epsilon} \ . \tag{3.7}$$

We make explicit distinction of masses in the meson propagators, m_{1i} and m_{2i}, since in general we could have the scattering of two different mesons, as for instance $\pi\eta$ scattering in the $I = 1$ channel. For the isoscalar channel we have $m_{1i} = m_{2i} \equiv m_i$ and $m_1 = m_K$, $m_2 = m_\pi$. A diagrammatic representation of the BS equation is depicted in Fig. 3.1. For $I = 0$, each of

the loops can be built from either two pion or kaon propagators, as they are coupled by means of the meson meson amplitudes in Eq. (3.4).

The particular off-shell dependence of the meson meson amplitudes has a practical consequence which converts the set of integral BS equations into ordinary algebraic equations, as it is shown in detail in Ref. [68]. The on-shell values of V_{ij} from Eq. (3.4) are obtained substituting $p_i^2 = m_i^2$. The off-shell extrapolation can be written as follows

$$V = V_{on} + \beta \sum_i (p_i^2 - m_i^2) \ , \tag{3.8}$$

with β depending on the particular channel. The first iteration of the BS equation (set $T_{lj} = V_{lj}$ in the right hand side of Eq. (3.5)) corresponds to the evaluation of the one loop diagram in Fig. 3.1, which involves the squared off-shell amplitude V,

$$V^2 = V_{on}^2 + 2\beta V_{on} \sum_i (p_i^2 - m_i^2) + \beta^2 \sum_{ij} (p_i^2 - m_i^2)(p_j^2 - m_j^2) \ . \tag{3.9}$$

The second and third terms in the previous equation lead to cancellations of the meson propagators in Eq. (3.6), and give rise to divergent contributions with the same structure as the on-shell tree level amplitudes and the mass terms. Thus, we can disregard this contributions in the sense of the renormalization of the theory, since they will be effectively reabsorbed in a renormalization of the coupling constant f and the masses of the particles. The use of the physical value of f and m_i incorporates effectively those terms and they do not have to be considered in the calculation. As a result the tree level amplitudes factorize on-shell outside the loop integral. The procedure can be repeated to higher order iterations and thus the coupled channel BS equations become ordinary algebraic equations given by

$$T_{ik} = V_{ik} + V_{ij} G_{jj} T_{jk} \ , \tag{3.10}$$

where we now change the notation for the G function as follows,

$$G_{jj} = i \int \frac{d^4q}{(2\pi)^4} \frac{1}{q^2 - m_{1j}^2 + i\epsilon} \frac{1}{(P-q)^2 - m_{2j}^2 + i\epsilon} \ . \tag{3.11}$$

The solution of the coupled channel BS equations reads, in matrix notation,

$$T = [1 - VG]^{-1}V \quad . \tag{3.12}$$

The G loop function is divergent and has to be regularized. We choose a cut-off in the momentum of the particles in the loop, q_{max}, and this is the only parameter in the model to be fixed by the experimental data. The best value which gives a good agreement with the data for phase shifts and inelasticities in all the included channels[1] and the decay widths of the generated resonances is $q_{max} \simeq 1.1$ GeV. The dependence of the results on the chosen parameter is moderate, and particularly negligible for $I = 0$ $\pi\pi$ scattering in the energy region below $\sqrt{s} \lesssim 500$ MeV, where we are interested for the study of the influence of the σ pole and its properties in the nuclear medium. The present model generates the σ and $f_0(980)$ resonances which appear as poles of the scattering amplitude in $L = 0$, $I = 0$. The coupling of channels is essential to produce the $f_0(980)$ resonance, while the σ pole is little affected by the coupling of the pions to $K\bar{K}$. We summarize the pole positions found in the energy complex plane in Table 3.1.

	$\mathrm{Re}\sqrt{s}_{pole}$ (MeV)	$\mathrm{Im}\sqrt{s}_{pole}$ (MeV)
σ	469	203
f_0	994	22

Table 3.1: Pole positions in the energy complex plane for the σ and f_0 resonances.

Additional information on this model and other related approaches for different spin isospin channels can be found in Refs. [65, 66, 68, 71]. For a comparison to experimental data for phase shifts and inelasticities we refer to Ref. [68], Figs. 3-9.

3.2 $\pi\pi$ scattering in the nuclear medium

We shall concentrate on the nuclear medium effects on the $\pi\pi$ channel in $L = I = 0$, namely the σ channel. The modification of the $\pi\pi$ scattering

[1] In Ref. [68] the $I = 1$ channel giving rise to the a_0 resonance is also considered to fix the cut-off parameter.

amplitude in the presence of a nuclear medium in the frame of the present model has been studied in [10, 53, 70]. We shall follow closely the ideas developed in those works and include some additional mechanisms which could have some effect on the scattering amplitude and/or the σ pole position.

As we are mainly interested in the low energy region, which is not very sensitive to the kaon channel, we shall only consider the nuclear medium effects on the pions. The effects of the nuclear medium in the $K\bar{K}$ channel, relevant to study the behaviour of the f_0 and a_0 resonances at finite density, have been studied in Ref. [70] by using the kaon selfenergies discussed in Chapter 2. The main changes of the pion propagation in the nuclear medium come from the $P-$wave selfenergy, as stated in Chapter 2, produced basically by the coupling of the pion to ph and Δh excitations. Let as consider the medium correction diagrams at the level of one ph or Δh insertion in the pion propagator (first order in the nuclear density), which appear at the level of one loop terms in the BS equation, as shown in Fig. 3.2. As it was

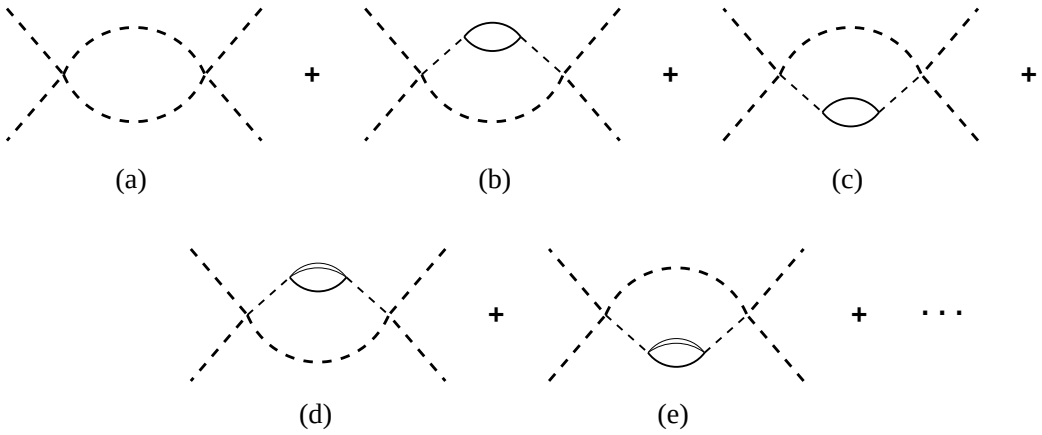

Figure 3.2: One loop diagrams contributing to the $\pi\pi$ scattering amplitude with ph and Δh excitations.

discussed in [53], these mechanisms are related to the $\pi N \to \pi\pi N$ amplitude, as can be seen by doing the analytical cut of diagrams (b-e) in Fig. 3.2. The resulting topology is shown in Fig. 3.3a, which is the pion pole term of the $\pi N \to \pi\pi N$ amplitude. On the basis of chiral symmetry, another term has to be considered at the same order in the chiral expansion, which is the tree-pion nucleon contact term in Fig. 3.3b. The inclusion of this term was found to

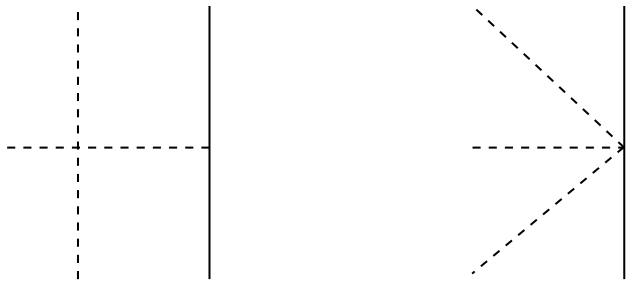

Figure 3.3: Pion pole (a) and contact term (b) topologies contributing to the $\pi N \to \pi\pi N$ amplitude.

be relevant for the $\pi N \to \pi\pi N$ amplitude since it cancels the dependence on unphysical parameters accounting for unitary transformations of the chiral Lagrangians and redefinitions of the fields. Combining the πNN and $3\pi NN$ vertices we can obtain a set of additional diagrams which also contribute to the medium modified $\pi\pi$ scattering amplitude, as shown in Fig. 3.4. The

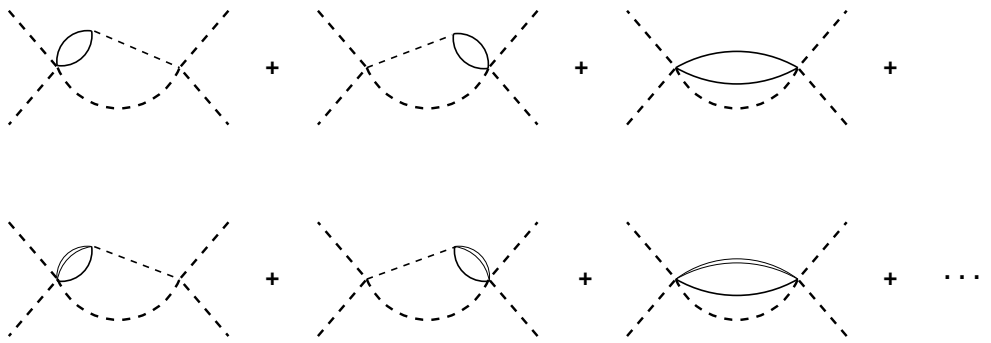

Figure 3.4: One loop diagrams contributing to the $\pi\pi$ scattering amplitude including the $3\pi NN$ contact vertices.

necessary Feynman rules for the vertices involving pions and nucleons can be derived from the general chiral Lagrangian coupling the pseudoscalar meson and $1/2^+$ baryon octet [14], which we include in Appendix C for reference. As discussed in Chapter 2, the Δ couplings are considered in a phenomenological way by the usual substitution

$$\sigma_i \tau^\lambda \to \frac{f^*_\Delta}{f_N} S_i^\dagger \, T^{\dagger\lambda} \tag{3.13}$$

in the pion-nucleon vertices. Eventually, the contribution of diagrams involving Δh excitations can be accounted for by substituting the nuclear Lindhard function, U_N, by the full Lindhard function, $U = U_N + U_\Delta$, according to the definitions given in Chapter 2 and Appendix B, Eqs. (2.15, B.4).

The calculation of the $\pi\pi$ scattering amplitude in the nuclear medium requires to solve the BS equation including the new terms discussed above. In vacuum, the off-shell parts of the $\pi\pi$ tree level amplitudes could be disregarded in the sense of the renormalization of the theory by using the physical values of the coupling f and the meson masses, leading to the on-shell factorization of this amplitudes and an algebraic solution of the BS equation. The new terms to be included have an explicit dependence on the nuclear density, and thus a similar mechanism for on-shell factorization relying on the renormalization program is not possible. In spite of this, a fruitful cancellation of terms was found in [53] which allows for an algebraic solution of the BS equation in the nuclear medium. It turns out that the off-shell contribution from diagram 3.2b, namely, the terms depending on the off-shell extrapolation of V^2 given in Eq. (3.9) cancel exactly with the sum of diagrams in Fig. 3.4, which arise once the $3\pi NN$ contact vertex is taken into account. Further arguments in favour of the cancellation found between the present diagrams were discussed in Ref. [89].

The same operation can be repeated for higher order iterations of the BS equation, with the result that the $\pi\pi$ amplitudes in diagrams like 3.2b can be factorized on-shell and the family of diagrams in Fig. 3.4 do not have to be included. Thus the BS equation becomes algebraic as in the free case, with solution

$$T_{22} = \frac{V_{22} + V_{21} G_{11} T_{12}}{1 - V_{22}\, \widetilde{G}_{22}} \ , \tag{3.14}$$

where $V_{22} = V_{22,\,on}$ here and $\widetilde{G}_{22}$ stands for the two-pion loop function including insertions of ph and Δh excitations in the pion propagators. For T_{12} we take the vacuum solution of the coupled channel BS equation, since we have not included medium effects on the $K\bar{K}$ channel. We can go beyond the first order in density for the pions in the loop by dressing the propagators with the pion selfenergy discussed in Chapter 2, which also accounts for the effect of short range correlations, and the previous argument regarding the

off-shell cancellation of amplitudes is still valid. Hence the $\widetilde{G}_{22}$ function is defined as

$$\widetilde{G}_{22}(P,\rho) = i \int \frac{d^4q}{(2\pi)^4} D(q^0,\vec{q};\rho) D(P^0-q^0,\vec{q};\rho) \ , \tag{3.15}$$

with $D(q,\rho) = [q^2 - m_\pi^2 - \Pi_\pi(q,\rho)]^{-1}$ and the pion selfenergy given in Eq. (2.18). The calculation of $\widetilde{G}_{22}$ can be simplified by using the spectral representation of the pion propagator given in Eq. (2.22). This is discussed in detail in the next section.

In Refs. [10,70], another set of medium corrections were considered within the frame of chiral Lagrangians to connect with several mechanisms proposed in different calculations within the Linear Sigma Model. Since the proposed mechanisms, involving nucleon tadpole terms, either vanish or slightly modify the results of the present calculation, we do not include them here and refer the reader to the quoted works and references therein for further details.

The $\pi\pi$ scattering amplitude obtained using this model exhibits, at finite density, a strong shift of strength towards low energies as compared to the free case. In Fig. 3.5, we show the imaginary part of this amplitude for several densities and the vacuum result for reference. We are mainly interested in the region around the two-pion threshold. For results at higher energies we refer the reader to Ref. [53], Fig. 7, where the f_0 resonance clearly manifests as a dip in the amplitude at energies close to 1 GeV. See also Fig. 11 in Ref. [70], where the medium effects on the $K\bar{K}$ channel were included and as a consequence the f_0 in the medium practically fades away at nuclear densities around ρ_0. Fig. 3.5 shows a reduction of strength below the σ region and an accumulation of strength at low energies around the pion threshold, particularly leading to a non-vanishing contribution in the imaginary part of the amplitude below $E = 2m_\pi$. We shall discuss this issue in detail in Section 3.4.

Quite similar results have been found using different models [52] and it has been suggested that this accumulation of strength, close to the pion threshold, could reflect a shift of the σ pole which would approach the mass of the pion. We investigate such a possibility in the next section.

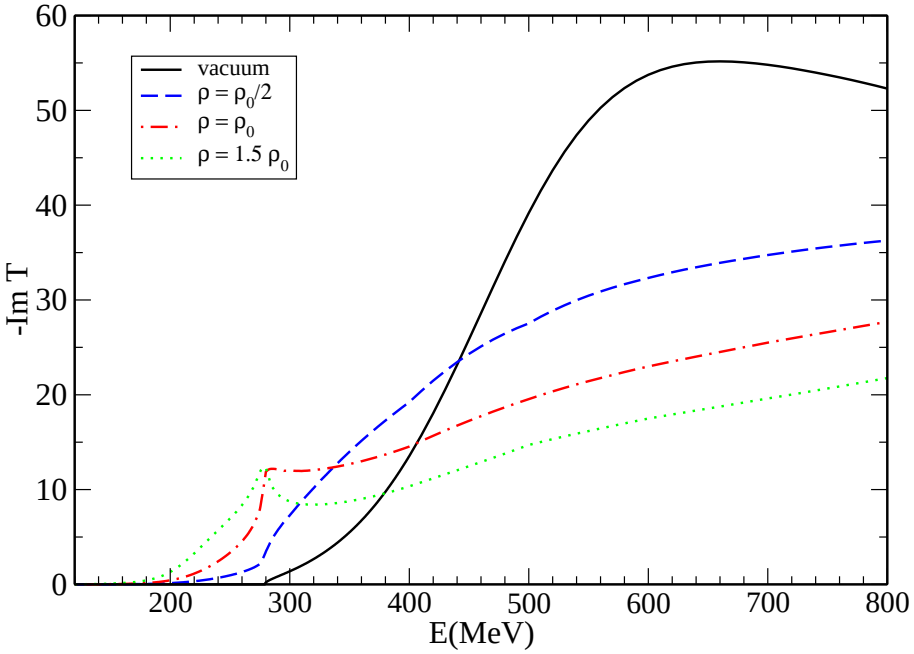

Figure 3.5: Imaginary part of the $\pi\pi$ scattering amplitude at several densities.

3.3 The σ pole in the energy complex plane

In order to simplify the calculation of T_{22} at finite density, and particularly the search of the σ pole, we disconnect the interactions between kaons and pions and work in a single channel (decoupled) calculation. This is equivalent to compute T_{22} as given by Eq. (3.14) with the prescription $T_{12} = T_{21} = 0$. With this prescription, the σ vacuum pole position occurs approximately at $\sqrt{s}_{pole} = 500 - 200\,i$ [MeV]. A compilation of values for this magnitude obtained in several recent analysis can be found in Refs. [35, 78, 79].

To look for the σ pole we have to extrapolate the scattering amplitude, T_{22}, to the 2ndRS in the energy complex plane. Once this is done we evaluate $|T_{22}|^{-1}$ and look for a zero with an appropriate numerical algorithm. The analytical structure of the meson meson scattering amplitudes is driven by the two-meson loop function, given in Eq. (3.15). We can simplify the calcu-

lation of $\widetilde{G}_{22}$ by using the Lehmann representation for the pion propagators,

$$D(q^0,\vec{q}) = \int_0^\infty d\omega\, 2\omega\, \frac{S_\pi(\omega,\vec{q})}{(q^0)^2-\omega^2+i\epsilon} \ . \tag{3.16}$$

An appropriate change of variables lets us rewrite $\widetilde{G}_{22}$ as follows

$$\widetilde{G}_{22} = \int_0^\infty \frac{dW}{2\pi}\Big[\frac{1}{P^0-W+i\epsilon} - \frac{1}{P^0+W-i\epsilon}\Big]\, F(W) \ , \tag{3.17}$$

where $F(W)$ is a positively defined real function, independent of the energy, given by

$$F(W) = \int \frac{d^3q}{(2\pi)^3} \int_{-W}^{W} du\, \pi\, S_\pi(\frac{W-u}{2},\vec{q}\,\rho) S_\pi(\frac{W+u}{2},\vec{q}\,\rho) \ , \tag{3.18}$$

which in vacuum takes the simple form

$$F_{vac}(W) = \frac{p_\pi(W)}{4\pi\, W}\,\Theta(W-2m_\pi) = \frac{1}{4\pi}\sqrt{\frac{1}{4}-\frac{m_\pi^2}{W^2}}\,\Theta(W-2m_\pi) \ . \tag{3.19}$$

The momentum cut-off, used to regularize the loop function, is implicit in Eq. (3.18). From Eq. (3.17) the expression of the two pion loop function in the 2ndRS can be derived as

$$\widetilde{G}_{22}^{2ndRS} = \frac{1}{2\pi}\int_0^\infty dW\Big[\frac{1}{P^0-W+i\epsilon}-\frac{1}{P^0+W}\Big]\, F(W)+i\, F(\mathrm{Re}P^0) \ . \tag{3.20}$$

The ϵ in the pole term of the integral can be neglected for P^0 in the complex plane. We have included a detailed derivation of the previous result in Chapter 4, Section 4.3, where the more general case for two different mesons in the loop is considered.

3.4 Results for the σ mass and width at finite density

The function $F(E)$ includes the phenomenological information on the pion selfenergy in the nuclear medium. The results for several densities are shown in Fig. 3.6. The $F(E)$ strength is related to the imaginary part of the σ propagator or spectral function and therefore it reflects the energy and density dependence of the different σ decay channels. We can classify them

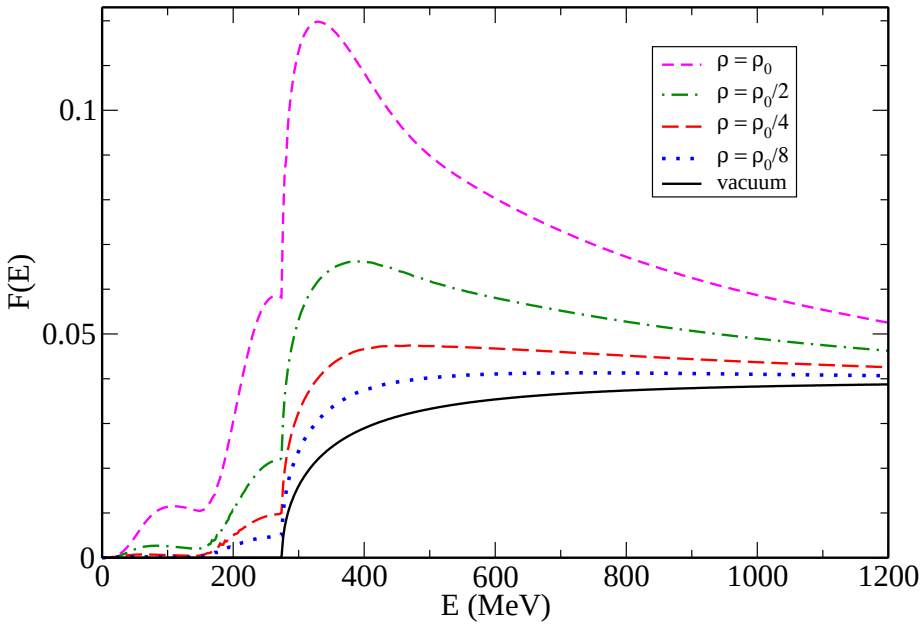

Figure 3.6: $F(E)$ at several densities.

according to their density dependence, as shown diagrammatically in Fig. 3.7.

In vacuum and at low densities, the σ meson can only decay into two pions, $\sigma \to \pi\pi$. Therefore we have a threshold at $E = 2m_\pi$. As the density grows, the $\sigma \to \pi\, ph$ decay channel becomes relevant and we have a new threshold at $E = m_\pi$, which is clearly visible in the curve corresponding to $\rho = \rho_0/8$. Finally, at larger densities, mechanisms such as $\sigma \to ph\, ph$, which go like ρ^2 become more important. They are possible even at very low energies, and because of this the $F(E)$ has a non-vanishing contribution at energies well below the pion threshold. This fact is reflected as well in the imaginary part of the scattering amplitude, Fig. 3.5, at densities of the order of ρ_0.

Using the two meson propagator of Eq. (3.20) we can solve the BS equation, obtain the meson meson scattering amplitude and look for the poles in the energy complex plane. The results for the σ pole position are shown

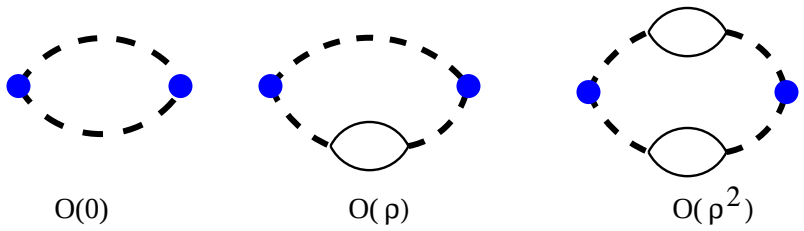

Figure 3.7: σ decay channels classified according to their density dependence.

in Fig. 3.8 for densities up to $1.5\rho_0$. Note, however, that the calculation is more reliable at low densities because some contributions of order ρ^2 or higher are missing. We find that both the σ mass and width from the pole

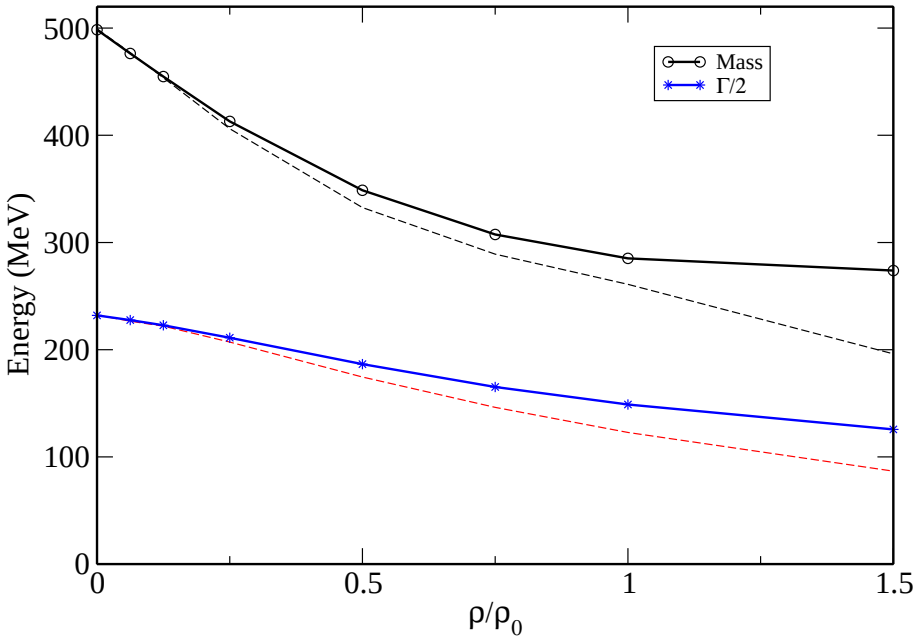

Figure 3.8: σ mass and half width from the pole as a function of the nuclear density. Dashed lines include also the $2ph$ pion selfenergy pieces.

decrease as the density increases, reaching a values of around 250 MeV for

the mass and a similar width at 1.5 times the nuclear density. In Ref. [53] a contribution from two-particle two-hole excitations was also included in a phenomenological way in the pion selfenergy using the information of the optical potentials obtained from pionic atoms data. At large densities this mechanism becomes relevant, as shown in the figure, decreasing further both mass and width. These results are little sensitive to the kaon channel. Its omission affects less than 1 percent the mass and increases the width around 5 percent. The observed changes in the σ mass and width can be cast in terms of an effective potential which can be approximated by

$$\mathcal{V}(\rho) = a\,\frac{\rho}{\rho_0} + b\,\left(\frac{\rho}{\rho_0}\right)^2 \tag{3.21}$$

with $a = -358 - i\,108$ [MeV] and $b = 140 + i\,23.6$ [MeV].

Qualitatively similar results for the mass are found in other models, as in Ref. [80]. Notice however that in that work the medium effects respond to a reduction of the pion decay constant (f), which we keep constant in our formalism. The basic ingredient that drives the mass decrease in our calculation is the $P-$wave interaction of the pion with the baryons in the medium.

Although the σ mass drops significantly, the width stays relatively large, even when the mass is close or below the 2π threshold. This width comes mostly from medium decay channels, namely, the decay into a single pion and a ph excitation or $2ph$ excitations. According to our results, we would not expect a signal of a narrow σ meson in the medium as proposed in Ref. [45] or in other calculations that include only purely mesonic decays. The reduced σ mass found here could modify the long and medium range nucleon nucleon interaction in nuclei or nuclear matter.

3.5 Further mechanisms according to chiral counting scheme

The diagrams accounted for in the former approach do not provide a complete set of diagrams which contribute to a certain order in a chiral expansion. There is an explicit choice of mechanisms which is based on its tested relevance in pion physics reactions. A systematic chiral power counting has

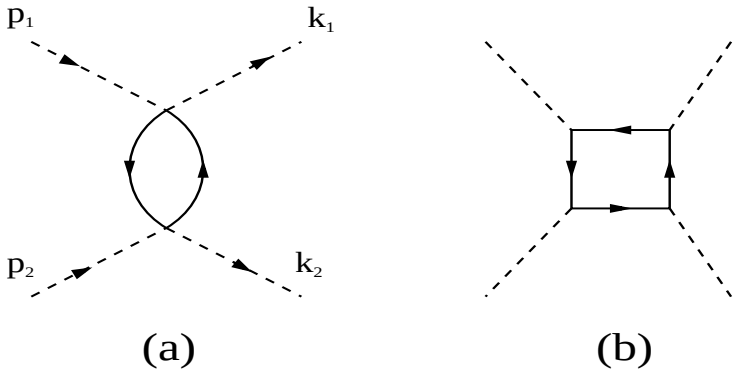

Figure 3.9: (a) *ph* bubble exchange in the t channel; (b) Box diagram.

been done in [82], where different diagrams from the ones included in our approach are considered at the first order in density. We shall study in this section the effect of the mechanisms included in [82] on the $\pi\pi$ scattering amplitude and the σ pole calculation. In this work, however, the $P-$wave pion selfenergy was not considered in the systematic study of the four-point Green's function of the pion. The $P-$wave selfenergy of the pion, considered in this work, is an essential ingredient for the renormalization of the pion in the medium, except at very low energies, where it could be omitted. Therefore we shall estimate the effect of the medium effects in Ref. [82] *together* with the relevant medium effects considered in this work.

The mechanisms considered in [82] which are relevant for $\pi\pi$ scattering in $S-$wave and modify the kernel of the BS, are shown in Fig. 3.9. The $\pi\pi$ isoscalar contribution in the s channel with a *ph* excitation in the t channel, Fig. 3.9(a), is given by

$$-it = -\left(\frac{1}{4f^2}\right)^2 (p_1^0 + k_1^0)(p_2^0 + k_2^0) U_N(q) \equiv -i\,\tilde{t}\; i\, U_N(q) \tag{3.22}$$

with $q = p_1 - k_1$. In Eq. (3.22) we are using the $\pi\pi NN$ vertex from the lowest order chiral Lagrangian in a non-relativistic approximation. We have neglected the isoscalar πN amplitude since it is very small compared with the isovector one [83], and actually it vanishes at the lowest order in the chiral expansion. The magnitude of t was shown in [82] to be comparable to the $s-$wave $\pi\pi$ amplitude from the lowest order chiral Lagrangian, at densities

of the order of the nuclear density, ρ_0. However, the following considerations have to be taken into account:

First, at the pion threshold, the diagram of Fig. 3.9(a) is proportional to $U_N(q^0 = 0, \vec{q} = \vec{0})$. This quantity is evaluated in [82] using the ordinary limit of the Lindhard function at $q^0 = 0$ and $|\vec{q}| \to 0$, which is finite and larger in size than for any finite value of $|\vec{q}|$. This limit is however quite different from the value of the response function in finite nuclei at $\vec{q} = \vec{0}$, which is strictly zero, as already noted in [82]. Indeed, in nuclear matter the Lindhard function reads $U_N(q) = U_d(q) + U_c(q)$, with $U_c(q^0, \vec{q}) = U_d(-q^0, \vec{q})$, and

$$U_d(q^0, \vec{q}) = 4 \int \frac{d^3p}{(2\pi)^3} \frac{n(\vec{p})[1 - n(\vec{p} + \vec{q})]}{q^0 + E_N(\vec{p}) - E_N(\vec{p} + \vec{q}) + i\epsilon} \ . \tag{3.23}$$

The numerator in the integrand of Eq. (3.23) is zero for $\vec{q} = \vec{0}$ since $n(\vec{p})^2 = n(\vec{p})$ with a Fermi distribution. However, the denominator is also zero for $q^0 = 0$, $|\vec{q}| \to 0$ and the limit exists, giving rise to a finite and large value of $U(q^0, \vec{q} \to \vec{0})$. In finite nuclei the numerator would also be zero, as for instance in $N = Z$ and closed shell nuclei, where the transition from the initial to the excited level involves the matrix element $< n|e^{i\vec{q}\vec{r}}|i >$ at $\vec{q} = \vec{0}$, which is exactly zero because of the orthogonality of the wave functions. However, the denominator contains an energy gap, Δ, from the ground state to the first excited state, which makes it finite and hence the response function vanishes. In the Appendix of [85] the nuclear Lindhard function with a gap is given explicitly. We include analytic expressions for U_d and U_c in Appendix B. The consideration of the Lindhard function with a gap weakens somewhat the contribution of Fig. 3.9(a) with respect to the results in Ref. [82], particularly at energies close to threshold. We have depicted both the tree level $\pi\pi$ amplitude from the lowest order chiral Lagrangian and the t-channel ph exchange amplitude, projected onto the $S-$wave, in Fig. 3.10 for comparison. We have also taken into account the fact that the isovector πN amplitude reflects the exchange of a ρ in the t channel [86], and include in Eq. (3.22) the appropriate form factor regarding the two ρ propagators, $F(q) = (M_\rho^2/(M_\rho^2 + \vec{q}^{\,2}))^2$. This factor further reduces, but very weakly, the mechanism of Fig. 3.9(a).

To study the effect of the additional $\pi\pi$ potential given by Eq. (3.22)

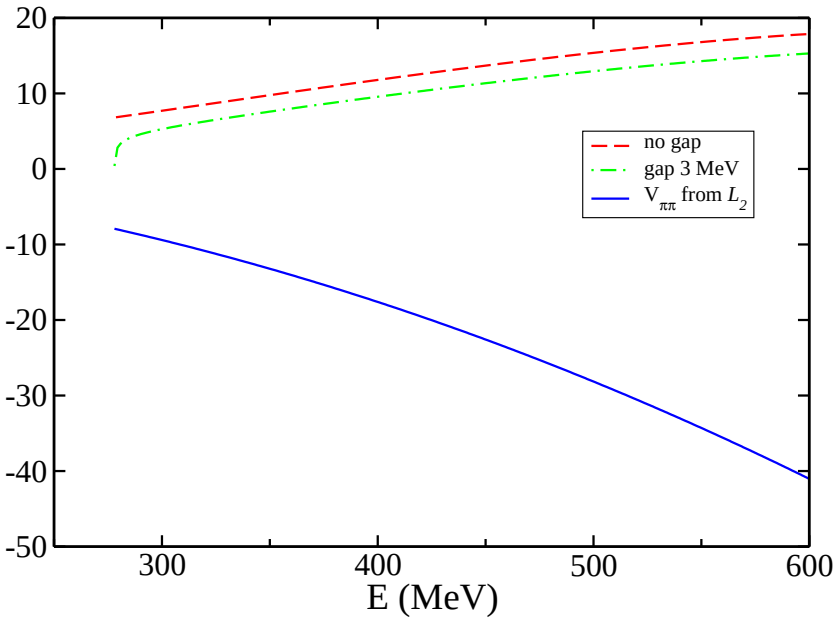

Figure 3.10: Comparison between the tree level $\pi\pi$ amplitude from the lowest order chiral Lagrangian and the t-channel ph exchange of Fig. 3.9(a).

we include the on-shell, $S-$wave projected part of t together with the $\pi\pi$ amplitude, V, as the kernel of the BS equation. We assume the external pion legs in the t amplitude to be on-shell for this calculation, as we do for the $\pi\pi$ vertex. The latter was justified in Ref. [68] and also in Ref. [67] in the framework of the N/D method. However, it is not clear that this could be done with the currently included mechanism and thus the full off-shell BS equation should be solved, which cannot be done analytically. Therefore the present calculation has to be considered as an approach to the problem, and it should provide a sensible test of the influence of the new mechanism on the $\pi\pi$ scattering amplitude and the σ pole, once the full scattering series is considered. With the new kernel we solve again the Bethe Salpeter equation in the medium and search for the poles in the complex energy plane. The results are shown in Fig. 3.11 and we can see that, in spite of the comparable size of the new term with respect to V, the strong nonlinearities in the BS equation make the changes in the in-medium mass and width of the σ moderate as compared to the previous results in Fig. 3.8. Qualitatively we

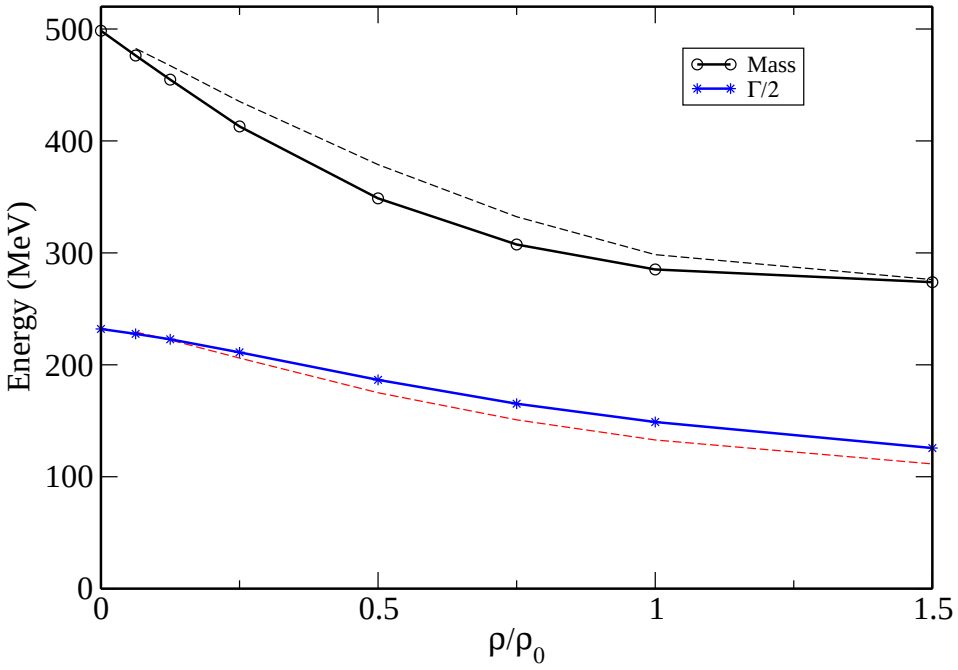

Figure 3.11: σ mass and half width as a function of the density. Solid lines are same as in Fig. 3.8, and dashed lines correspond to the inclusion of the mechanism in Fig. 3.9(a) assuming the four pions to be on shell.

obtain a similar behaviour as a function of the nuclear density.

We shall estimate now the effect of mechanism 3.9(a) when including it with its off-shell dependence in the pion loops implicit in the BS equation. Let us construct the amplitude of diagram 3.12(a), which is the one-loop analogue of diagram 3.12(b) by substituting a $\pi\pi$ vertex by the $t-$channel exchange of a *ph* excitation. The calculation of digram 3.12(a) is given in detail in Appendix D. A comparison between these two terms would show the relative contribution of the new mechanism in the scattering series.

To include the obtained loop function in the BS equation we define an

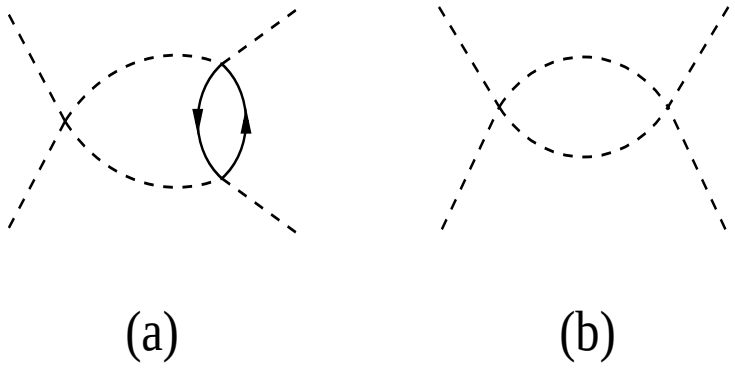

Figure 3.12: Loop contributions to the Bethe Salpeter equation.

effective additional potential, $\delta V(P^0, \rho)$, such that

$$\frac{\delta V(P^0, \rho)}{V} = \frac{\mathcal{T}(P^0, \rho)}{VGV} \ , \tag{3.24}$$

with $\mathcal{T}(P^0, \rho)$ the amplitude of diagram 3.12(a), which guarantees $VG\delta V = \mathcal{T}(P^0, \rho)$. We solve again the Bethe Salpeter equation in the medium, using $V + \delta V$ as the kernel potential, and considering the renormalization of the pion propagators. This approximation takes into account, at first order in density, the pion loop diagrams shown in Fig. 3.13, which let us evaluate the relative weight of the new terms. As before we have assumed that the evaluated loop function, $\mathcal{T}(P^0, \rho)$, can be on-shell factorized and iteratively inserted in the series, leading to the BS equation with the modified kernel as explained above.

The pole search is done as explained in Section 3.3. The results are depicted in Fig. 3.14, which are remarkably similar to those where we neglect this new contribution, also shown in the figure. The consideration of loop effects in our approach for actual reactions involving two-pion production in nuclei has as a consequence a sensible reduction of the contribution of the t channel ph excitation. We can safely neglect it in the BS equation, despite its relevance at tree level, for practical purposes of finding the poles in the T matrix

The box diagram of Fig. 3.9(b) was found to be smaller in size than the $t-$channel ph exchange in Ref. [82], particularly at small energies, where the

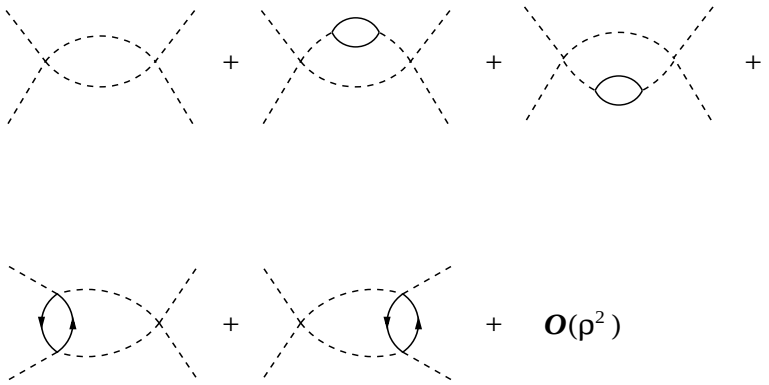

Figure 3.13: One loop terms in the BS equation up to linear order in density.

$P-$wave character of the vertices make the contribution negligible. As before, a detailed analysis of the contribution of this mechanism when inserted in a pion loop function would be advisable. We expect an important suppression of the box diagram for large values of the pion momentum, q, and in addition there could be further cancellation of terms as it was shown in Ref. [10]. The conclusion in that work is that this term can be safely neglected for practical purposes, regarding the modification of the σ pole in the nuclear medium.

3.6 Conclusions

In this work, we have calculated the $\pi\pi$ scalar-isoscalar scattering amplitude in vacuum and in a nuclear medium, starting from the lowest order chiral Lagrangian and using a unitary framework with coupled channels which proves rather successful in describing the meson-meson interaction in the scalar sector. This model generates, out of pseudoscalar meson degrees of freedom, the σ, f_0 and a_0 resonances, which appear as singularities of the scattering amplitudes. The current arguments in favour of a σ meson as rather a $\pi\pi$ resonance of dynamical origin than a genuine QCD state built from $q\bar{q}$ pairs, are thus supported in recent chiral unitary formulations of the $\pi\pi$ interaction as the one we have followed in the present work.

The medium corrections to the isoscalar $\pi\pi$ amplitude have been included, at the first order in density, in terms of ph and Δh insertions in the pion prop-

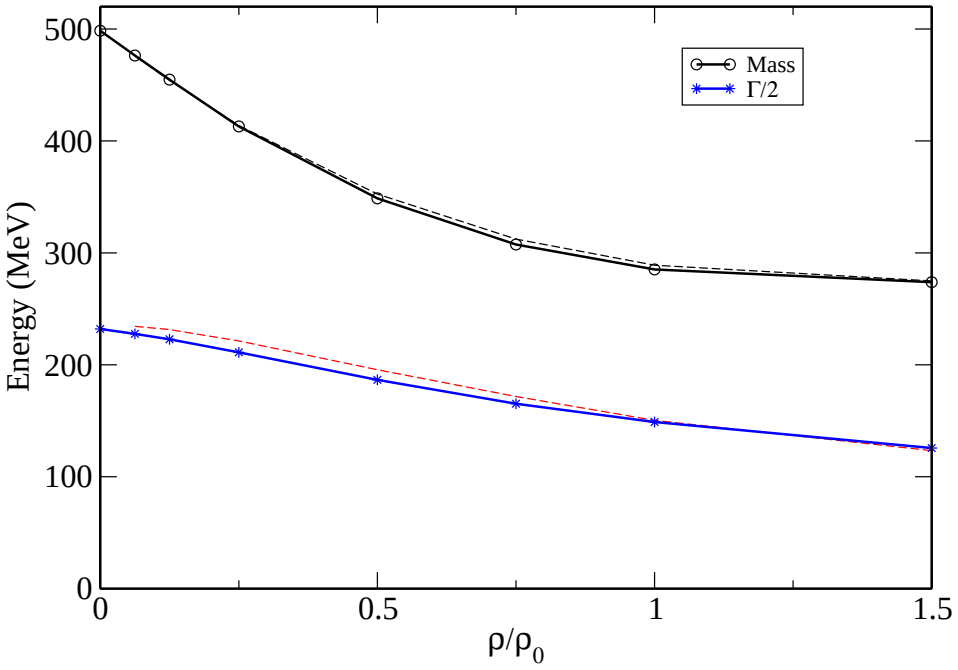

Figure 3.14: σ mass and half width as a function of the density. Solid lines are same as in Fig. 3.8, and dashed lines correspond to the inclusion of the mechanism of Fig. 3.9(a) with two pions off shell as they appear in Fig. 3.12(a).

agator. Other diagrams involving a $3\pi NN$ contact vertex, which was found to be essential in order build the $\pi N \to \pi\pi N$ amplitude, have been considered at the one-loop level. The latter mechanisms provide a useful cancellation with the off-shell extrapolations of the $\mathcal{O}(p^2)$ $\pi\pi$ amplitudes in one-loop diagrams, so that an algebraic solution of the Bethe-Salpeter equation in a nuclear medium is also possible. Our results show a reduction of strength of $\mathrm{Im}T_{22}$ in the σ region and an accumulation of strength close to pion threshold and below, which are features shared by most of the approaches.

We have also searched for the lightest pole of the $\pi\pi$ scattering amplitude, which we identify with the σ meson, in the complex energy plane as a

function of the baryon density. The analytical extrapolation of the scattering amplitude onto the 2ndRS has been done by using the Lehmann representation for the pion propagators.

The results obtained show a dropping of the σ mass as a function of the density, down to values close to two pion masses at normal nuclear density. The width decreases moderately and reaches values around 300 MeV at $\rho = \rho_0$. In the nuclear medium there are more channels for the σ decay, like pion-ph or ph-ph. The presence of these channels partly makes up for the strong reduction of the 2π channel due to the smaller phase space available when the σ mass drops.

We have also taken into account new terms in the kernel of the Bethe Salpeter equation, which have been found to be relevant in a recent study based on a chiral power counting in the many body problem. The most important contribution which applies to our case involves a $t-$channel exchange of a ph excitation between the two interacting pions. We have made an approximate calculation to estimate its contribution in the scattering equation. We have found, in the on-shell approximation, that this mechanism is not as important as one could expect from its comparison, at tree level, with the lowest order chiral $\pi\pi$ amplitude. Furthermore, we have also found that the contribution of this mechanism with its off-shell dependence in pion loops is much suppressed and has little influence in the σ pole behaviour with the nuclear density.

Altogether, the changes in the mass and width of the σ are significantly large, compared to other typical meson or baryon properties in a dense medium. Therefore, we could expect a visible signal in the invariant mass distributions of two pions (or photons) in 2π (2γ) production experiments if the pions (photons) can couple strongly to the scalar isoscalar channel. Some present data seem to support these claims, although further experiments and calculations should be performed to test these findings. Particularly, in a recent calculation of the two-pion photoproduction reaction in nuclei [62], the final state interaction of the produced pions was implemented using the present model for the scalar-isoscalar channel. Two important consequences were found, which we summarize as follows:

1. The inclusion of $\pi\pi$ rescattering with the present model improved con-

siderably the reproduction of experimental data of the total cross section for the photoproduction on the proton, at photon energies in the range $E_\gamma = 400 - 500$ MeV.

2. The $\pi^0\pi^0$ (isoscalar) invariant mass distribution calculated for ^{12}C and ^{208}Pb experienced a visible shift of strength to lower energies when the medium effects on the pions were considered as described in this work.

Posterior experimental results from the TAPS Collaboration [61] seem to agree with the predicted effect, although there is still debate about its origin. For instance, in Ref. [90] it is argued that the same experimental data can be explained without introducing medium effects beyond absorption and quasi-elastic scattering of the final state particles.

Chapter 4

Kaon nuclear optical potentials and the κ meson in the nuclear medium

In Chapter 2 we studied medium effects on the pion and kaon propagators. Particularly the kaon properties in a nuclear medium have received much attention in the last years, both theoretically and experimentally. There is already clear experimental evidence of strong medium effects that deviate from simple low density theorem predictions on the strong enhancement of the K^- production in heavy-ion collisions in the KaoS experiments at GSI [93]. Although this result could imply a very attractive potential it is difficult to extrapolate it to the high density and low temperature relevant for the neutron stars.

Also visible medium effects have been found in kaonic atoms. However, there is a strong controversy on the theoretical interpretation of these data, with widely different potentials available in the literature which provide a reasonable agreement to the data. They could be classified in two basic kinds, some phenomenological potentials, usually deeply attractive, [94–97] and other chirally motivated potentials [27–30, 98–102], which after the need of a selfconsistent treatment of the kaon and the $\Lambda(1405)$ in the medium was shown [28], are clearly less attractive.

Some other observables that could be sensitive to the kaonic nuclear potential have been suggested, like the study of the ϕ mass in nuclear reactions. However, due to the cancellation between attraction and repulsion for the antikaon and kaon respectively little if some effect is expected [6]. In addition,

the considerable ϕ meson mean life makes decaying inside the nucleus improbable, despite the rather strong increase of the ϕ width in the medium typically reported in literature (see Chapter 6 and references therein). To compensate for this experimental handicap, several proposals have been made for reactions in which the ϕ meson is either produced with low momenta or appropriate experimental cuts are proposed to isolate such events [161, 162].

On the other hand some interesting developments have taken place in the study of the light scalar mesons, in particular the σ and the κ. The σ meson now appears to be quite well established both theoretically and experimentally [103] although some discussion on its nature still remains open. In particular, unitarized models consistent with chiral constraints describe the $\pi\pi$ phase shifts and clearly predict a pole at masses of around 470 MeV [37,104]. Some works using this kind of chiral models have also studied the isospin $I = 1/2$ channel and find a very wide κ meson at masses around 800 MeV. A compilation of results both experimental and theoretical can be found in [79, 105, 106].

In the unitarized chiral models, which we follow in this Thesis, the σ and κ mesons can be understood as $\pi\pi$ and πK resonances and this has important consequences for their interaction with the nuclear medium, as their selfenergy will be directly related to that of the π and K mesons. The σ medium properties have been studied using different approaches finding always a strong reduction of its mass and a much narrower width at high baryonic densities [53, 107, 108]. There are some experimental signals that strongly suggest that this is indeed the case. A quite strong enhancement of the $\pi\pi$ invariant mass spectrum at the low masses predicted for the in-medium σ has been found in both $(\pi, \pi\pi)$ [109–112] and $(\gamma, \pi\pi)$ reactions [61, 62, 90]. In the unitarized chiral models the mass reduction of the σ, and its narrowing in the nuclear medium are mainly produced by the well known attractive $P-$wave pion-nucleus optical potential. A similar, although richer in complexity, situation could occur for the κ meson. Given the clearly different interaction of the kaons and antikaons with the medium one could expect a splitting of the masses of κ and anti-κ. The difference would be sensitive to the different optical potential suffered by kaons and antikaons. Furthermore, as for the σ case, the strong attraction over the pion could lead

to a common mass reduction and a narrower width.

Our purpose in this chapter is to investigate this possibility. We start by presenting a simple model of meson meson scattering that predicts a κ pole and is consistent with the meson-meson phenomenology at low and intermediate energies. Next, we incorporate the nuclear medium effects using for that two different kaon potentials in order to study the sensitivity of the observables to these potentials.

4.1 $K\pi$ scattering in a chiral unitary approach

We briefly revise in this section the model of $K\pi$ scattering, which is based on the chiral unitary approach to meson meson scattering developed in [68], and already introduced in Chapter 3. In that work, a good agreement with experimental phase shifts for the $S-$wave meson meson scattering in the $I = 0, 1$ channels was found. We solve the Bethe-Salpeter (BS) equation, namely $T = V + VGT$, in which the kernel V is taken as the $I = 1/2$ $K\pi$ tree level amplitude from the lowest order χPT Lagrangian. After projecting onto the $S-$wave, this amplitude reads

$$V = \frac{1}{4f^2}\left[-\frac{5}{2}s + m_\pi^2 + m_K^2 + \frac{3}{2}\frac{(m_K^2 - m_\pi^2)^2}{s}\right] . \tag{4.1}$$

In Eq. (4.1), s is the Mandelstam variable, m_π and m_K are the pion and kaon masses, respectively, and f is the meson decay constant, which we take to be $f^2 = (100\,\mathrm{MeV})^2 \simeq f_\pi f_K$ as in Ref. [104]. Actually, at lowest order in the chiral expansion the same f constant is kept for each of the meson meson scattering processes. At order p^4, f is renormalized in a different way for the different scattering processes involving only pions ($\pi\pi$, f_π^2), pions and kaons ($K\pi$, $f_K f_\pi$) or only kaons ($\bar{K}K$, f_K^2) [66].

Despite the integral character of the BS equation, it was found in [68] that the V amplitude can be factorized on-shell out of the integral in the VGT term order by order in an iterative solution, and so can T. Thus T can be algebraically solved in terms of the V amplitude and the G function. The latter contains the integral of the two meson propagators,

$$G(\sqrt{s}) = \frac{1}{4\pi^2}\int_0^{q_{max}} dq\, \frac{q^2}{\omega_\pi(q)\omega_K(q)}\, \frac{\omega_\pi(q) + \omega_K(q)}{s - (\omega_\pi(q) + \omega_K(q))^2 + i\epsilon} , \tag{4.2}$$

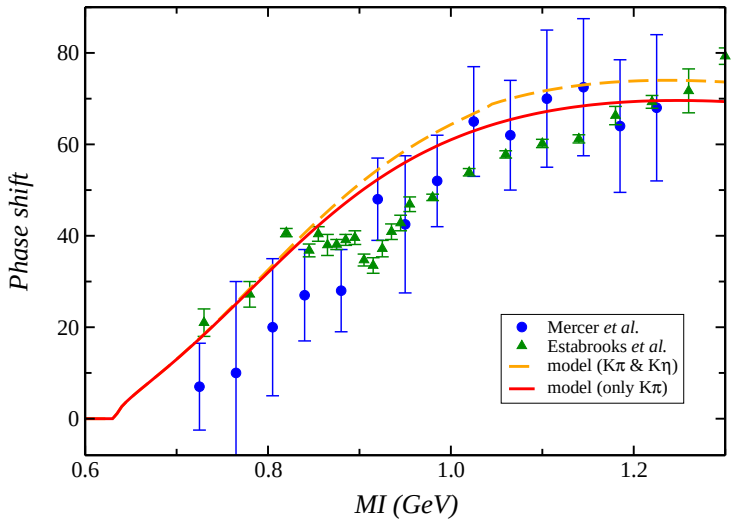

Figure 4.1: $K\pi \to K\pi$ phase shifts in the $I = 1/2$ channel. The solid line is the result of the model described in the text. The dashed line correspond to the coupled channel calculation including $K\eta$ as intermediate state. Data sets are taken from Refs. [114] (dots) and [115] (triangles).

with $\omega_\pi(q) = \sqrt{q^2 + m_\pi^2}$ and $\omega_K(q) = \sqrt{q^2 + m_K^2}$. In Eq. (4.2) we regularize the G function with a cut-off in the momentum of the mesons in the loop. A value of $q_{max} = 850$ MeV is used, what leads to a satisfactory fit to the $I = 1/2$ $K\pi$ phase shifts, as shown in Fig. 4.1. With the same cut-off a good reproduction of data is obtained simultaneously for the $\pi\pi$ channel in $I = 0$ (σ channel) at low and intermediate energies (below 1 GeV), although a higher cut-off of about 1 GeV was used in Chapter 3 and in [53, 68]. This indicates a low sensitivity of the results in the energy region of interest to the regularization parameter used here.

We have not considered in this calculation the contribution of the $K\eta$ intermediate state, which is also compatible with the quantum numbers of the process. Its inclusion leads to a coupled channel calculation, as done in [68] and in Chapter 3 for $\pi\pi$ and $\bar{K}K$ channels. However, it was found in [113] that this channel barely mixes with the $K\pi$ channel. We have also checked that accounting for it barely modifies the phase shifts in the region beyond 1 GeV, and produces no visible effect at lower energies (see Fig. 4.1). Since we are mainly interested in the medium effects on the $K\pi$ channel, we

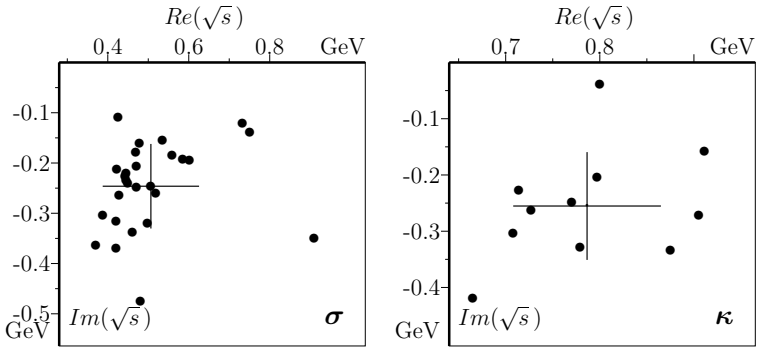

Figure 4.2: Compilation of results for the σ and κ poles in the complex energy plane, from Ref. [79].

shall ignore the $K\eta$ contribution from now on.

The scattering amplitude in this channel exhibits a pole in the second Riemann sheet (2ndRS) of the complex energy plane, which we identify with the κ meson. The pole that we find is located at $M_\kappa + i\,\Gamma_\kappa/2 = 825 + 460\,i$ (MeV). For completeness we show in Fig. 4.2 a compilation of results for the κ pole, which we borrow from [79].

4.2 $K\pi$ scattering in the nuclear medium

We consider medium corrections to the $K\pi$ scattering amplitude by dressing the meson propagators with appropriate self-energies regarding the interactions of the mesons with the surrounding nucleons of the nuclear medium [9]. The pion selfenergy has been discussed in Chapter 2. It is built from the excitation, in $P-$wave, of ph and Δh pairs. Additionally, a resummation of short range correlation terms in terms of the Landau-Migdal parameter g' is done. We recall here the final expression that we stated in Chapter 2,

$$\Pi_\pi(q^0,\vec{q};\rho) = f(\vec{q}^{\,2})^{\,2}\,\vec{q}^{\,2}\frac{(\frac{D+F}{2f})^2\,U(q^0,\vec{q};\rho)}{1-(\frac{D+F}{2f})^2\,g'U(q^0,\vec{q};\rho)}\ , \tag{4.3}$$

where $(D+F)/(2f)$ is the πNN coupling from the lowest order chiral Lagrangian, $U = U_N + U_\Delta$ is the Lindhard function for the ph and Δh excitations and $f(\vec{q}^{\,2})$ is a monopolar form factor.

Regarding the kaon selfenergy, we shall consider here two different models, in order to test the sensitivity of the results to these models and their ability to discriminate between them. The first model is a chirally motivated potential [30] which provides a weak attraction for the antikaons. It was introduced in Chapter 2, and we shall refer to it as 'model A'. The second one is a phenomenological potential described in [94], leading to a very strong attraction for the antikaons. We shall call it 'model B'. We briefly describe the main features of both models below.

The KN interaction is smooth at low energies, and both models use a $t\rho$ approximation. The kaon self-energy is given by

$$\Pi_K(\rho) = C\, m_K^2\, \rho/\rho_0 \ , \tag{4.4}$$

where ρ is the nuclear density, ρ_0 stands for the normal nuclear density and C takes the value 0.13 for model A [116] and 0.114 for model B [94].

The $\bar{K}N$ interaction, however, is much richer at low energies. Model A starts from [29], where the $S-$wave $\bar{K}N$ scattering was studied in a chiral unitary model in coupled channels, leading to a successful description of many scattering observables, namely, threshold ratios of K^-p to several inelastic channels; K^-p and K^-n scattering lengths; and K^-p cross sections in the elastic and inelastic channels ($\bar{K}^0n$, $\pi^0\Lambda$, $\pi^\pm\Sigma^\mp$, $\pi^0\Sigma^0$). Medium effects were considered in [30] to obtain an effective $\bar{K}N$ interaction in nuclear matter, from which the $S-$wave $\bar{K}$ self-energy was obtained in a selfconsistent way. Finally, the $P-$wave contribution to the $\bar{K}$ self-energy, arising from the excitation of Yh pairs ($Y = \Lambda, \Sigma, \Sigma^*(1385)$) was also included. Full details can be found in [6, 30]. Model B, based on a dispersive calculation of the kaon potentials, which uses as input the $K^\pm N$ scattering amplitudes, finds a strong $\bar{K}$ potential that drops to -200 MeV at normal nuclear density and zero momentum, and shows a quite strong momentum dependence. We use the parametrization given in [94],

$$\Pi_{\bar{K}}^B(q,\rho) = -[\,0.233 + 0.563\, \exp(-1.242\, q/m_K)\,]\, m_K^2\, \rho/\rho_0 \ . \tag{4.5}$$

These two potentials have been chosen as representative examples of the kaon-nucleus potentials currently discussed in the literature. Some 'deep'

potentials (around 200 MeV depth at zero $\bar{K}$ momentum) are found in phenomenological analysis like [95, 96] and also in the dispersive calculation of model B [94] after some approximations. However, selfconsistent derivations of the $\bar{K}$ optical potential starting from a good description of $\bar{K}N$ scattering produce 'shallow' potentials ($\simeq$ 40 to 60 MeV depth) like model A [30] and the potential obtained in [28]. Both kinds of potentials produce a good agreement with kaonic atom data, and the depth of the optical potential cannot be resolved by analysing these data as has been shown in [102].

4.3 Search for the κ pole

To look for the κ pole in the medium we follow the procedure described in [10] and also described in Chapter 3 for the σ meson in $\pi\pi$ scattering, conveniently adapted to the present problem. We need to evaluate the $K\pi$ scattering amplitude, T, in the 2ndRS of the complex energy ($\sqrt{s}$) plane. The analytical structure of T is driven by the $G(\sqrt{s})$ function, which has a cut on the positive energy real axis. The rest of the functions in the BS equation are analytical and single-valued. To calculate $G(\sqrt{s})$ at finite baryon density, we use the spectral (Lehmann) representations of the meson propagators introduced in Chapter 2,

$$\begin{aligned} D_\pi(q^0,\vec{q};\rho) &= \int_0^\infty d\omega\, 2\omega\, \frac{S_\pi(\omega,\vec{q};\rho)}{(q^0)^2-\omega^2+i\epsilon} \\ D_{\bar{K}(K)}(q^0,\vec{q};\rho) &= \int_0^\infty d\omega \Big(\frac{S_{\bar{K}(K)}(\omega,\vec{q};\rho)}{q^0-\omega+i\eta} - \frac{S_{K(\bar{K})}(\omega,\vec{q};\rho)}{q^0+\omega-i\eta} \Big) \ , \end{aligned} \quad (4.6)$$

where S_π and $S_{\bar{K}(K)}$ are the spectral functions of the pion and the antikaon (kaon), respectively, that are directly related to the selfenergies. After some basic manipulations, $G(\sqrt{s})$ can be written as

$$G(\sqrt{s}) = \frac{1}{2\pi}\int_0^\infty dW \left[\frac{1}{\sqrt{s}-W+i\eta} F_P(W) - \frac{1}{\sqrt{s}+W} F_{NP}(W) \right] \ , \quad (4.7)$$

and $F_P(W)$, $F_{NP}(W)$ (accompanying the 'pole' and 'non-pole' terms, respectively) are real, positively-defined functions independent of $\sqrt{s}$. For $\bar{K}\pi$ scattering they are given by

$$F_P(W) = \int \frac{d^3q}{(2\pi)^3} \int_{-W}^{W} du\, \pi\, S_\pi(\frac{W-u}{2},\vec{q};\rho)\, S_{\bar{K}}(\frac{W+u}{2},\vec{q};\rho)$$

$$F_{NP}(W) = \int \frac{d^3q}{(2\pi)^3} \int_{-W}^{W} du\, \pi\, S_\pi(\frac{W-u}{2}, \vec{q}; \rho)\, S_K(\frac{W+u}{2}, \vec{q}; \rho)\ . \quad (4.8)$$

For $K\pi$ scattering $S_{\bar{K}}$ in Eq. (4.8) has to be replaced by S_K, and vice versa. The cut-off in the meson momentum is included in these functions (not explicitly shown). As an example, in vacuum $F_P = F_{NP} \equiv F_{K\pi}$ factorizes out of the brackets in Eq. (4.7) and reads

$$F_{K\pi}(W) = \frac{1}{4\pi}\frac{q(W)}{W}\,\Theta(W - (m_\pi + m_K))\ , \quad (4.9)$$

with $q(W) = \lambda^{1/2}(W^2, m_\pi^2, m_K^2)/2W$ and λ the Källen function. If we substitute Eq. (4.9) in Eq. (4.7) then we are lead back to Eq. (4.2) for the two-meson propagator function in vacuum.

Let us go to the complex energy plane and let $P^0 \equiv \sqrt{s} \in \mathbb{C}$. The first term in Eq. (4.7) is responsible for the cut in the real axis, when $P^0 \in \mathbb{R}$. We want to isolate the singularity to obtain the discontinuity of the G function in the cut, when crossing from the first to the second Riemann sheet. The first term in the integrand of Eq. (4.7) can be rewritten as

$$\frac{F_P(W)}{P^0 - W} = \frac{F_P(\mathrm{Re}P^0)}{P^0 - W} + \frac{F_P(W) - F_P(\mathrm{Re}P^0)}{P^0 - W}\ . \quad (4.10)$$

The second term in Eq. (4.10) is pole free and does not generate a cut discontinuity in the G function, as can be easily noticed by Taylor expanding $F_P(W)$ around $W = \mathrm{Re}P^0$. The only part in G responsible for the cut can be written as

$$\widetilde{G}(P^0) = \frac{1}{2\pi}\int_0^\infty dW \frac{F_P(\mathrm{Re}P^0)}{P^0 - W}\ . \quad (4.11)$$

For practical purposes we shall cut the W integral to an upper limit W_{max}, so that that the contribution of the $F_{P(NP)}$ functions is negligible beyond that point. Then we can approximate

$$\widetilde{G}(P^0) \simeq \frac{1}{2\pi}\int_0^{W_{max}} dW \frac{F_P(\mathrm{Re}P^0)}{P^0 - W} = \frac{1}{2\pi}F_P(\mathrm{Re}P^0)\log\left(\frac{P^0}{P^0 - W_{max}}\right)\ . \quad (4.12)$$

As it is depicted in Fig. 4.3, whenever P^0 crosses the cut, we obtain an imaginary part from the logarithm in Eq. (4.12) which accounts for the discontinuity of G in the cut. Therefore the G function in the 2ndRS of the

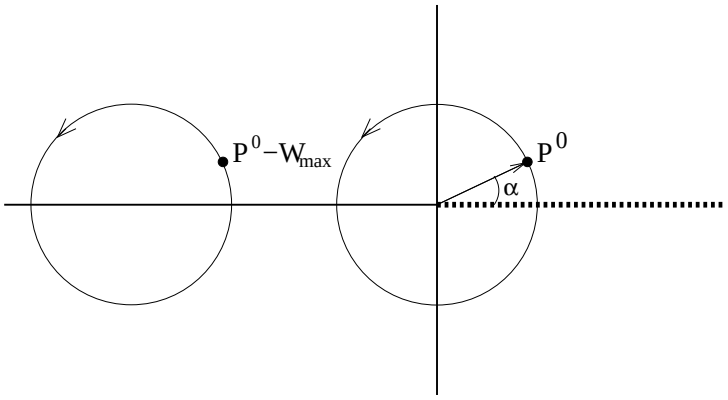

Figure 4.3: Complex energy plane showing the analytical cut on the positive real axis.

complex energy (P^0) plane can be written as

$$G^{2ndRS}(P^0) = \frac{1}{2\pi}\int_0^\infty dW \left[\frac{1}{P^0 - W + i\eta}F_P(W) - \frac{1}{P^0 + W}F_{NP}(W)\right] + i\,F_P(\mathrm{Re}P^0)\ . \quad (4.13)$$

4.4 Results and discussion

We have calculated the $K\pi$ and $\bar{K}\pi$ scattering amplitudes and found the κ pole position for several nuclear densities from $\rho = 0$ to $\rho = 1.5\,\rho_0$. To discuss the results we shall distinguish between the following three cases: (1) free pion, in-medium kaons; (2) in-medium pion, free kaons; and (3) in-medium pions and kaons.

In Fig. 4.4 we show the κ pole position in the complex energy plane, using model A for the kaon self-energies. Every curve departs from a common point, which corresponds to the pole position in the vacuum case, and we increase nuclear density according to the following values: $\rho/\rho_0 = 0, 1/8, 1/4, 1/2, 3/4, 1, 3/2$, which correspond to the successive dots in each trajectory. The curves labeled as '1' correspond to the case of in-medium kaons and free pions. The first interesting fact is that the pole trajectory splits up into two different branches corresponding to $K\pi$ and $\bar{K}\pi$ scattering. This was an expected result since the kaon self-energy is asymmetric for the particle compared to the antiparticle. We can see that, in the $K\pi$ branch,

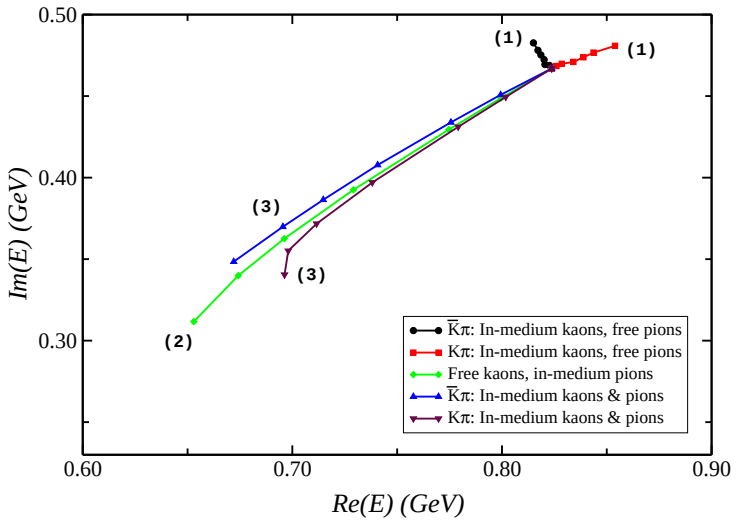

Figure 4.4: κ pole trajectories at finite density. The labels correspond to the three cases discussed in the text.

the κ mass from the pole, $M_\kappa = \mathrm{Re}\sqrt{s}_{pole}$, moves to higher energies. This responds to the repulsion felt by the kaons in the medium. In the $\bar{K}\pi$ branch one finds that the κ pole mass decreases slowly with the nuclear density. However, its decay width increases due to the opening of additional decay channels in the medium, as $\kappa \to \pi M Y h$ and $\kappa \to \pi Y h$. These channels are accounted for in the $\bar{K}$ $S-$ and $P-$wave self-energies.

The next case that we consider corresponds to the curve labeled as '2' in Fig. 4.4, i.e., free kaons and in-medium pions. Since the pion self-energy is the same for the three isospin components (in symmetric nuclear matter), we find a single trajectory for the κ pole. When the nuclear density increases, the pole position rapidly moves to lower energies. This is consistent to what happens for the σ meson and is due to the strong attraction experienced by the pion in the nuclear medium. From this we obtain that M_κ is strongly reduced, from 825 MeV in vacuum down to 650 MeV at $\rho = 1.5\rho_0$, getting very close to the $K\pi$ threshold. Γ_κ also shows a noticeable reduction of 300 MeV at $\rho = 1.5\rho_0$. In fact, one may expect even a stronger reduction in the κ decay width, given the proximity of the pole to the $K\pi$ threshold and the consequent reduction of available phase space for $\kappa \to K\pi$ decays. However, this reduction of phase space is partly compensated by the simultaneous

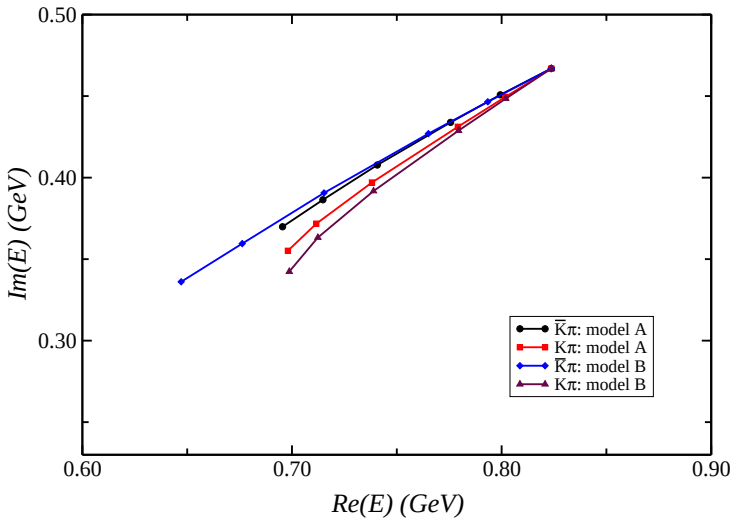

Figure 4.5: κ pole evolution with density. Comparison between two models of anti-kaon self-energy.

opening of pion-related in-medium channels, namely $\kappa \to K\,ph$, $K\,\Delta h$. Such effect was also discussed in [10, 53] for the σ meson in $\pi\pi$ scattering.

Eventually, the two curves labeled as '3' in Fig. 4.4 represent the κ pole evolution with density in the full model A. We find again separate $K\pi$ and $\bar{K}\pi$ branches, whose tendency to lower energies is a clear signal of the strong influence of the attractive pion self-energy. The $K\pi$ branch shows a sudden curvature for densities of and beyond ρ_0. We shall come back to this point later.

In Fig. 4.5 we compare the results on the κ pole position for models A and B and densities up to $\rho = \rho_0$. We observe that the mass splitting between the $K\pi$ and $\bar{K}\pi$ branches is larger in model B, amounting to about 50 MeV at normal nuclear density. The anti-κ pole trajectories, sensitive to the $\bar{K}$ potential, show stronger differences, whereas the κ branches are quite similar since the kaon self-energy only differs at the level of 10 % in the two models. Particularly, the $\bar{K}$ selfenergy in model B does not include an imaginary part, leading to a further decrease of the κ decay width.

We have also calculated the $K\pi$ and $\bar{K}\pi$ scattering amplitudes for several nuclear densities in model A. These amplitudes could be eventually tested

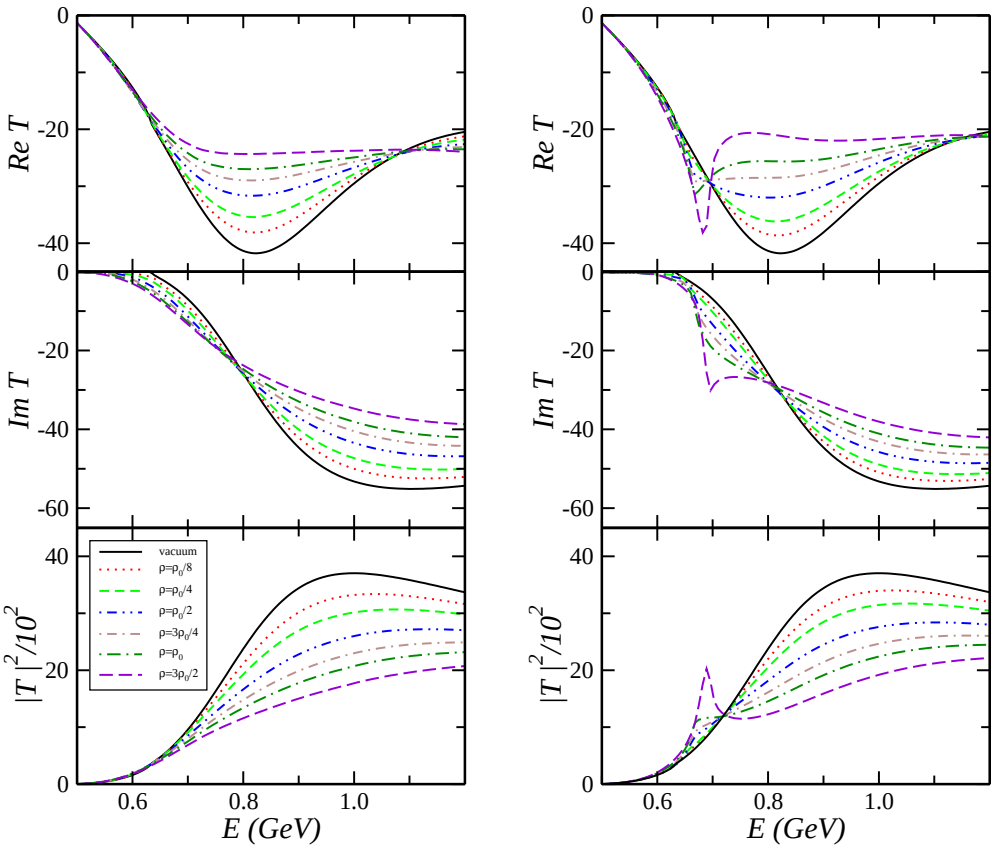

Figure 4.6: Real part, imaginary part and squared modulus of the kaon-pion scattering amplitude at several densities. Left panels correspond to $\bar{K}\pi$ channel, right panels to $K\pi$ channel.

experimentally in reactions with pions and kaons in the final state. The results are shown in Fig. 4.6. The $\bar{K}\pi$ amplitude changes rather smoothly with increasing density. The real part changes little at low energies and flattens at higher energies. The imaginary part displays an increase of strength below 800 MeV as compared to the vacuum case, and the threshold is shifted to lower energies. Beyond 800 MeV, though, we find a progressive decrease of strength. The $K\pi$ channel shows a similar behaviour for $\sqrt{s} \gtrsim 800$ MeV as the $\bar{K}\pi$ channel. However, we observe a greater accumulation of strength below 800 MeV in the imaginary part, which peaks at about 700 MeV at $\rho = 1.5\rho_0$. The real part also reflects a rapidly changing structure in this energy region. This effect was already observed in [53] for the $\pi\pi$ scattering

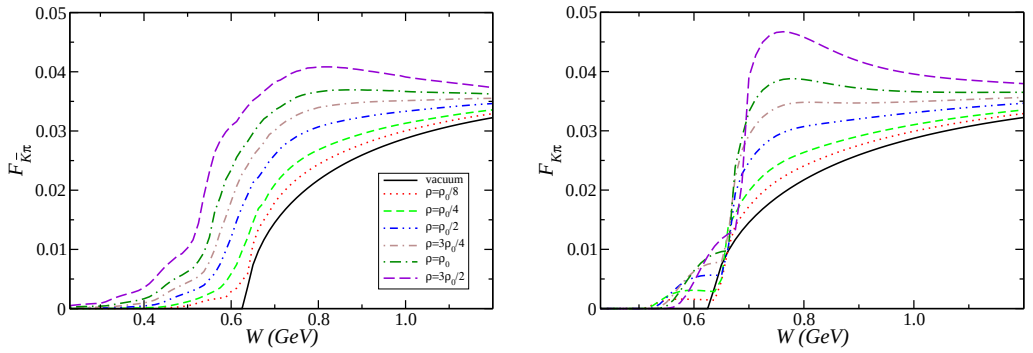

Figure 4.7: $F_{\bar{K}\pi}$ (left) and $F_{K\pi}$ (right) functions for several nuclear densities. The free case is also shown in solid line for reference.

amplitude in the σ channel, and it was found in [10] that this was correlated to a migration of the σ pole to lower energies at finite densities. A similar behavior is found here for the κ meson. In the $\bar{K}\pi$ case some strength of ImT spreads well below the vacuum threshold mainly because of the attraction experienced by the antikaon, that moves the $\bar{K}\pi$ threshold down; and the coupling to in-medium channels with the same quantum numbers occurring at lower energies, for instance meson hyperon - hole excitations. However, for the $K\pi$ case the strength of ImT is strongly accumulated above the in-medium threshold, which is basically determined by the repulsive potential affecting the kaon. The little strength below the vacuum threshold corresponds only to channels in which the pion is absorbed by a particle - hole excitation. We have also included in Fig. 4.6 the squared modulus of the amplitude. In the $\bar{K}\pi$ channel the main visible effect is a strong decrease of strength beyond 700 MeV, whereas in the region around and below threshold little effect can be seen because of the lack of phase space, though it was clearly visible in the imaginary part of the amplitude. The $K\pi$ channel clearly exhibits a prominent structure close to threshold as commented above. These features of the amplitudes as well as the pole trajectories can be better understood by looking at the $F(W)$ functions, which contain the phenomenological information of the pion and kaon self-energies in the medium. They are shown in Fig. 4.7 for $K\pi$ and $\bar{K}\pi$ scattering at several nuclear densities and the vacuum case for reference. As we see, the $\bar{K}\pi$ spectral function

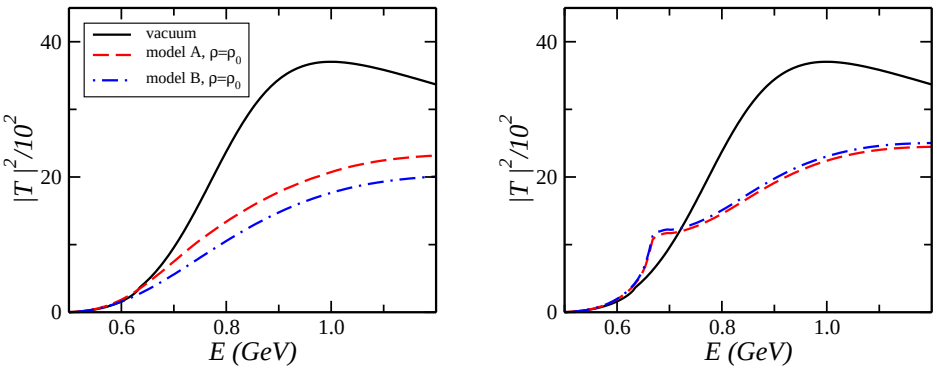

Figure 4.8: Squared modulus of the kaon-pion scattering amplitude, in vacuum and at normal density, for the two models of kaon selfenergy discussed in the text. Left: $\bar{K}\pi$ channel; right: $K\pi$ channel.

is very much spread to lower energies when the density increases, as a result of the $\bar{K}$ attraction in $S-$wave, together with some strength provided by the pion decay channels into a particle-hole pair. On the contrary, $F_{K\pi}$ is far more steep, particularly in the region of the $K\pi$ threshold. Below this point there is some strength, due to the pion decay channels, but most of the strength is concentrated around 700 MeV, after a sudden bump of the function with a huge derivative. This rapid growing of $F_{K\pi}$ corresponds to the opening of the $K\pi$ decay channel, which takes place at energies similar to the free case, except for a small increase of the kaon mass, since the pion selfenergy has a negligible effect close to threshold due to its $P-$wave character.

The resulting scattering amplitudes for model B show a similar trend as for model A but there are some differences. In Fig. 4.8 we show the squared modulus of the amplitudes for model B , at normal nuclear density, together with model A and the free case for reference. The most visible effect, as commented above, corresponds to the $K\pi$ channel where both models are quite similar and there is little theoretical discussion concerning the K potential in the medium. We find very similar results for this channel in the two approaches. A stronger medium effect is observed in the $\bar{K}\pi$ amplitude for model B, as a consequence of the more attractive $\bar{K}$ potential in this model.

In summary, we find a noticeable modification of the $S-$wave $K\pi$ interaction in the κ channel at finite densities. The $\bar{K}\pi$ channel is sensitive to the different $\bar{K}$ potentials used in this work. The most visible medium effect, though, appears in the $K\pi$ channel, where the $\bar{K}$ potential has little influence, and might be observed in $K\pi$ invariant mass distributions around 650 MeV.

4.5 Conclusions

We have studied the κ meson properties in the nuclear medium. We follow a chiral unitary model of $K\pi$ scattering that reproduces the elastic phase shifts in the $I = 1/2$ channel and dynamically generates the κ meson, which appears as a pole in the scattering amplitude. The medium effects have been considered by dressing the pion and kaon propagators with selfenergies that have been calculated elsewhere. When the density is increased, the κ pole moves to lower masses and decay widths. However, it does not become as narrow as to provide a clear signal to be observed experimentally. We have also studied the scattering amplitude at finite densities for the $K\pi$ and $\bar{K}\pi$ channels. We have found that the amplitude is strongly modified in the medium in both channels, and particularly it is sensitive to the differences between models of the anti-kaon potential. The most noticeable effect is the accumulation of strength found at lower invariant masses of the $K\pi$ system. We suggest that this effect could be experimentally observed in reactions where a $S-$wave $K\pi$ pair is produced with low energy in the final state.

Chapter 5

Vector-isovector (ρ channel) meson-meson scattering in the nuclear medium

We start in this chapter the study of the properties of vector mesons in a nuclear medium, particularly the ρ meson. It is difficult to extract information on the mass or width of an in-medium meson from experimental data because in most of the decay channels the final particles undergo a strong distortion before they get out from the dense matter and can reach the detector.

Amongst the possible final state particles from a meson decay in a nuclear medium, electromagnetic decays offer, in principle, a cleaner probe of the high density regions. Neutral vector mesons, like ρ^0, are specially interesting due to its large leptonic width. Any changes in the mass or width of these mesons should be reflected in the invariant mass distributions of the leptonic decay products.

Although there are some problems in the interpretation of data, due to the low statistics and the existence of many additional sources, dilepton spectra such as those measured at CERN [118, 119] and at lower energies at Bevalac [120, 121] may indicate either a lowering of the ρ mass or a large broadening of its width. In the near future, experiments at GSI (HADES Collaboration [122, 123]) and at the Jefferson Lab (CLAS collaboration, G7 experiment) could clarify the situation by providing better statistics and mass resolution.

Many theoretical approaches have been pursued to analyse the ρ meson properties in the medium. A good review of the current situation can be

found in Ref. [124]. Here, we only present a brief description of the main lines of work. Much of the current interest was stimulated by Brown and Rho [125] who by using scale invariance arguments, obtained an approximate in-medium scaling law predicting the ρ mass to decrease as a function of density. Also Hatsuda and Lee [126] found a linear decrease of the masses as a function of density in a QCD sum rules calculation, although recent works [127–129] cast some doubts on these conclusions and find that predictions from QCD sum rules are also consistent with larger ρ masses if the width is broad enough. Several groups have investigated the ρ selfenergy in the nuclear medium studying the decay into two pions, the coupling to nucleons to excite a baryonic resonance, or both. The main effects on the two pion decay channel are produced by the coupling to Δ-hole excitations [130–136]. Whereas the ρ mass is barely changed, quite a large broadening, which provides a considerable strength at low masses, is obtained in these calculations. Another strong source of selfenergy is the excitation of baryonic resonances, mainly the $N^*(1520)$ considered in Refs. [137–140], which further broadens the ρ meson. Finally, we could mention the systematic coupled channel approach to meson-nucleon scattering of Ref. [141] that automatically provides the first order, in a density expansion, of the ρ selfenergy, finding also a large spreading of the strength to states at low energy.

In this Chapter we investigate the ρ meson properties in nuclear matter in a non-perturbative coupled channel chiral model of meson meson scattering. This approach combines constraints from chiral symmetry breaking and unitarity, and has proved very successful in describing mesonic properties in vacuum at low and intermediate energies [66]. The effects of the nuclear medium on the mesons have already been analyzed in this framework, for the scalar isoscalar ($I = J = 0$), "σ" channel [53, 70]. There have been several attempts to translate the nuclear matter results into observable magnitudes, which can be compared with experimental results [62, 112, 142]. However, as mentioned before, it is difficult to disentangle the meson properties at high baryonic densities due to the strong distortion of the decay products. The rho meson studied here is better suited for such a study because of its large leptonic width.

In Section 5.1 we summarize the model of meson meson scattering which

is based on a coupled channel chiral unitary calculation of the T matrix, and we present some results of the model together with existing experimental data on the electromagnetic vector form factor of the pion. In Section 5.2 we discuss how the $\pi\pi$ scattering amplitude in the chiral unitary model can be interpreted in the frame of ρ meson dominance in the $\pi\pi$ interaction, and we rewrite the scattering T matrix in terms of a dressed ρ propagator with a selfenergy coming from the two-pion coupling. We also compare the present model with the gauge vector formulation of the ρ meson. In this formalism it is also possible to obtain the $\pi\pi$ scattering matrix in terms of a dressed propagating ρ meson, and we find both formalisms to provide equivalent results for the T matrix at the level of one-loop renormalization. We devote Section 5.3 to a detailed calculation of the mechanisms contributing to modify the ρ meson selfenergy in a nuclear medium. The gauge vector formalism, which provides interaction Lagrangians for the ρ coupling to pions, nucleons and Δ's, turns out to be an appropriate framework to calculate these mechanisms. The medium effects involve the renormalization of pion propagator as the essential input, as well as several vertex correction diagrams necessary to fulfill gauge invariance. In the last part of this section we consider the ρ couping to other baryonic resonances such as the $N^*(1520)$, which have a remarkable influence in the ρ spectral function at finite density.

5.1 $L = 1$ meson-meson scattering in a chiral unitary approach

Our procedure in this work to study the propagation of the ρ meson is to obtain the $\pi\pi \to \pi\pi$ scattering amplitude in the $(I, J) = (1, 1)$ channel, which is known to be essentially driven by the ρ meson because of vector meson dominance (VMD) [11]. We first give a brief description of the model for meson-meson scattering in vacuum, and then discuss in detail modifications arising in the presence of nuclear matter. In this section we do not try to be comprehensive but just establish the basis of meson-meson scattering in the frame of the Unitarized Chiral Perturbation Theory. In writing this sections we have followed the work by E. Oset, J. A. Oller and J. E. Palomar [143] as well as J. E. Palomar [144]. Further information and detailed calculations

can be found in these references.

A coupled channel chiral unitary approach is developed in these works, based on the tree level contributions from the lowest order χPT Lagrangians [146] including explicit resonance fields [147]. Low energy chiral constraints are satisfied by a matching of expressions with one-loop χPT and unitarity is imposed following the N/D method. The model successfully describes several scattering observables such as the $\pi\pi$ $P-$wave phase shifts and the π, K electromagnetic vector form factors up to $\sqrt{s} \lesssim 1.2$ GeV.

5.1.1 Tree level and unitarization

We start from the $(I = 1)$ $\pi\pi$, $K\bar{K}$ states in the isospin basis:

$$\begin{aligned} |\pi\pi\rangle &= \frac{1}{2}|\pi^+\pi^- - \pi^-\pi^+\rangle \\ |K\bar{K}\rangle &= \frac{1}{\sqrt{2}}|K^+K^- - K^0\bar{K}^0\rangle \ , \end{aligned} \tag{5.1}$$

which include an extra $\frac{1}{\sqrt{2}}$ factor in the normalization of the $\pi\pi$ $I = 1$ state vector (unitary normalization).

The tree level amplitudes, collected in a symmetric 2×2 K matrix, read

$$\begin{aligned} K_{11}(s) &= \frac{1}{3}\frac{p_1^2}{f^2}\left[1 + \frac{2\,G_V^2}{f^2}\frac{s}{M_\rho^2 - s}\right] \\ K_{12}(s) &= \frac{\sqrt{2}}{3}\frac{p_1\,p_2}{f^2}\left[1 + \frac{2\,G_V^2}{f^2}\frac{s}{M_\rho^2 - s}\right] \\ K_{21}(s) &= K_{12}(s) \\ K_{22}(s) &= \frac{2}{3}\frac{p_2^2}{f^2}\left[1 + \frac{2\,G_V^2}{f^2}\frac{s}{M_\rho^2 - s}\right] \ , \end{aligned} \tag{5.2}$$

with the labels 1 for $K\bar{K}$ and 2 for $\pi\pi$ states in the isospin basis. In equation (5.2) G_V is the strength of the pseudoscalar-vector resonance vertex, f the pion decay constant in the chiral limit, s the squared invariant mass, M_ρ the bare mass of the ρ meson and $p_i = \sqrt{s/4 - m_i^2}$. In any of these amplitudes the first term comes from the $\mathcal{O}(p^2)$ chiral Lagrangian, while the second term is the contribution of the resonance Lagrangian [143]. Note also that in the previous equation we are quoting $P-$wave projected partial wave amplitudes,

so that they differ from the full scattering amplitudes by a $(2L+1)P_L(cos\theta)$ factor, with $P_L(cos\theta)$ the L_{th} degree Legendre polynomial and $L = 1$ in this case.

The final expression of the (dimensionless) T matrix is obtained by unitarizing the tree level scattering amplitudes in Eq. (5.2)[1] . To this end we follow the N/D method, which was adapted to the context of chiral theory in Ref. [148]. We get

$$T(s) = [I + K(s) \cdot G(s)]^{-1} \cdot K(s), \tag{5.3}$$

where $G(s)$ is a diagonal matrix given by the loop integral of two meson propagators. In dimensional regularization its diagonal elements are given by

$$G_i^D(s) = \frac{1}{16\,\pi^2}\left[-2 + d_i + \sigma_i(s)\,\log\frac{\sigma_i(s)+1}{\sigma_i(s)-1}\right], \tag{5.4}$$

where the subindex i refers to the corresponding two meson state and $\sigma_i(s) = \sqrt{1-4m_i^2/s}$ with m_i the mass of the particles in the state i.

In Fig. 5.1 we show a diagrammatic representation of the three matrices involved, $K(s)$, $G(s)$ and $T(s)$. The last one represents the resummation performed in Eq. (5.3) with the unitarization procedure (N/D method).

The d_i constants in Eq. (5.4) are chosen to obey the low energy chiral constraints [143],

$$\begin{aligned} d_K &= \frac{-2\,m_\pi^2}{m_K^2 - m_\pi^2}\left(\log\frac{m_\pi^2}{\mu^2} + \frac{1}{2}\log\frac{m_K^2}{\mu^2} + \frac{1}{2}\right) \\ d_\pi &= \frac{m_K^2}{m_K^2 - m_\pi^2}\left(\log\frac{m_\pi^2}{\mu^2} + \frac{1}{2}\log\frac{m_K^2}{\mu^2} + \frac{1}{2}\right), \end{aligned} \tag{5.5}$$

and they are obtained by matching the expressions of the form factors calculated in this approach with those of one loop χPT. In Eq. (5.5) $\mu = 770$ MeV and we have substituted the index values $i = 1, 2$ by their actual meaning.

The regularization can also be carried out following a cut-off scheme. The loop functions with a cut-off in the three-momentum of the particles in the

[1]Details of how the T matrix relates to the S matrix of the scattering can be found in [144], Chapter 4.

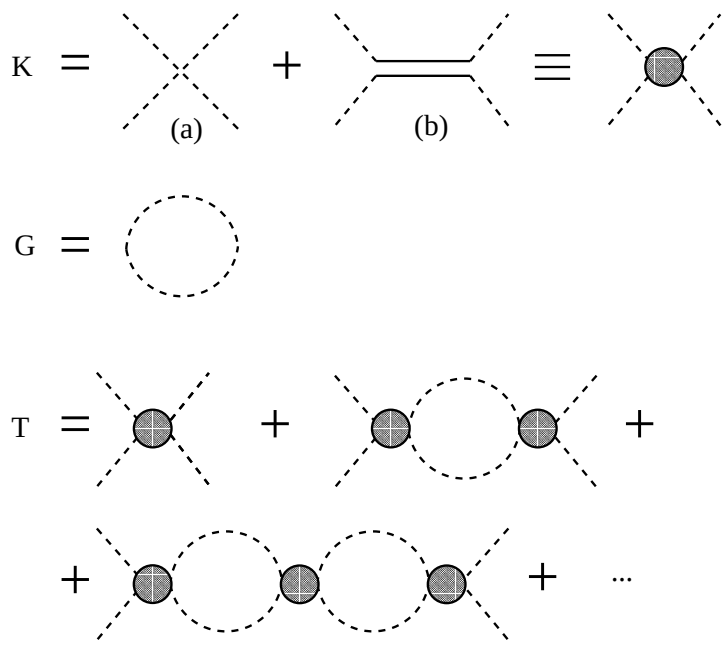

Figure 5.1: Diagrammatic representation of the matrices described in the text. (a) and (b) correspond to the amplitudes derived from the $\mathcal{O}(p^2)$ and resonance chiral Lagrangians respectively. The filled circle represents the effective scattering amplitude. Dashed lines are π, K mesons.

loop can be found in the appendix of Ref. [66], and up to order $\frac{m_i}{q_i^{max}}$ they read

$$G_i^C(s) = \frac{1}{16\,\pi^2}\left[-2\,\log\frac{2\,q_i^{max}}{m_i} + \sigma_i(s)\,\log\frac{\sigma_i(s)+1}{\sigma_i(s)-1}\right], \qquad (5.6)$$

where q_i^{max} is the cut-off mentioned above. By comparing the expressions of the $G_i(s)$ functions in both schemes we can get the equivalent q_i^{max} in order to keep the information of the low energy d_i constants, and therefore one can use equivalently any of the two procedures. In Table 5.1.1 we show the obtained values of the cut-off parameters for both pion and kaon loop functions. The low value of q^{max} for the $\bar{K}K$ loop function indicates that the approximation of Eq. (5.6) is not appropriate and one should use the full expression of $G_K(s)$.

Two meson state	q_i^{max} (GeV)
$\pi\pi$	1.18
$K\bar{K}$	0.50

Table 5.1: Cut-off momenta for the $\pi\pi$, $K\bar{K}$ loop functions in order to reproduce low energy chiral constraints.

5.1.2 Results for meson-meson scattering in vacuum

We summarize here the results for meson-meson scattering in vacuum, focusing on the $\pi\pi$ $I = 1$ channel. The model has no free parameters apart from the bare ρ mass, M_ρ, which is obtained by requiring that the modulus of the $\pi\pi$ $I = 1$ $P-$wave amplitude has a maximum at $\sqrt{s} = M_\rho^{Phys} = 770$ MeV. In table 5.1.2 we collect the final values used in the calculation[2]. For details see [144].

G_V (MeV)	f (MeV)	M_ρ MeV
53	87.4	829.8

Table 5.2: Coupling constants and bare ρ mass. The number of decimals in the latter corresponds to the experimental precision in which the physical mass is given.

In Figs. 5.2 and 5.3 we show the $\pi^+\pi^-$ vector form factor and the $\pi\pi$ $P-$wave phase shifts, respectively. Both observables are very well described from negative values of s up to about 1.44 GeV^2. For higher energies, although the qualitative behaviour of data is reproduced, new structures appear and the model cannot accommodate and give a fair description in that range. These new effects include the presence of more massive resonances like ρ' and ω' in this channel. Moreover, additional multiparticle channels are open (4π, $\omega\pi$) which cannot be simulated since the widths of the resonances in the model are generated dynamically in terms of the included channels. For our purpose we have a nice description of the $\pi\pi \to \pi\pi$ scattering in a wide range of energies around the resonance position, and this settles the

[2]The coupling G_V is obtained from its experimental value, while the pion decay constant f is taken from Ref. [146].

basis for the study of the medium corrections when considering the scattering in nuclear matter.

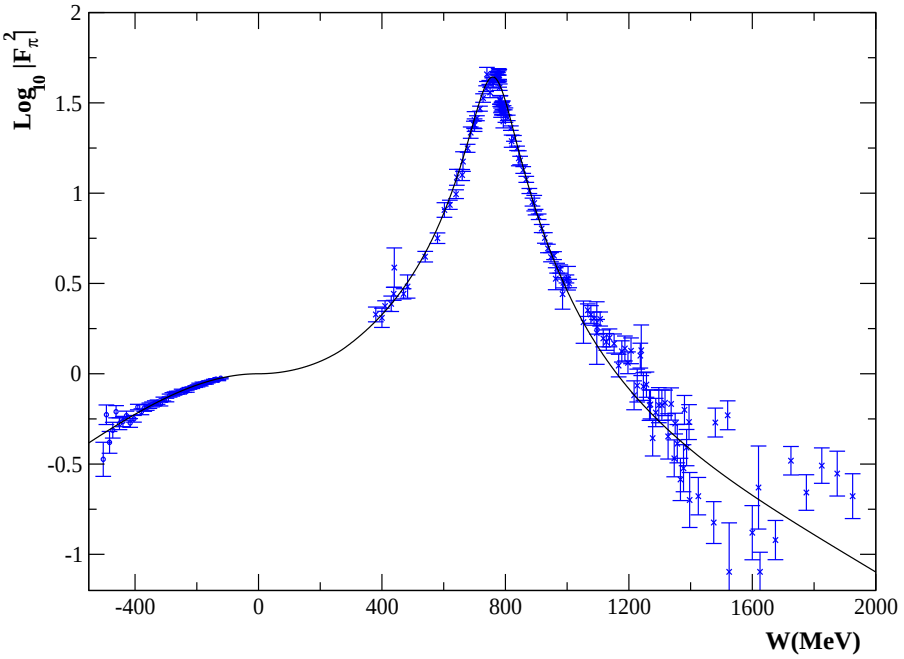

Figure 5.2: $\pi^+\pi^-$ vector form factor. W is defined as $\sqrt{s}$ for $s > 0$ and as $-\sqrt{-s}$ for $s < 0$. Borrowed from [144].

In Fig. 5.4 we show the T_{22} matrix element vs invariant mass. To check how important is the inclusion of the $K\bar{K}$ channel we have performed the calculation in both coupled and decoupled cases. By decoupled case we mean turning off the $K\bar{K} \to \pi\pi$ interaction, what is easily done by setting $K_{12} = 0$ in Eqs. (5.2) and (5.3). The conclusion is that kaon loops produce very small changes in the results and therefore they can be ignored and we can work in the decoupled description for the $\pi\pi \to \pi\pi$ scattering amplitude.

5.2 The ρ selfenergy in a gauge vector model

A very convenient framework to study the ρ meson properties in vacuum and in the medium is the gauge formulation of the ρ as a vector field [132–134]. The gauge principle provides a very simple scheme to obtain the interaction

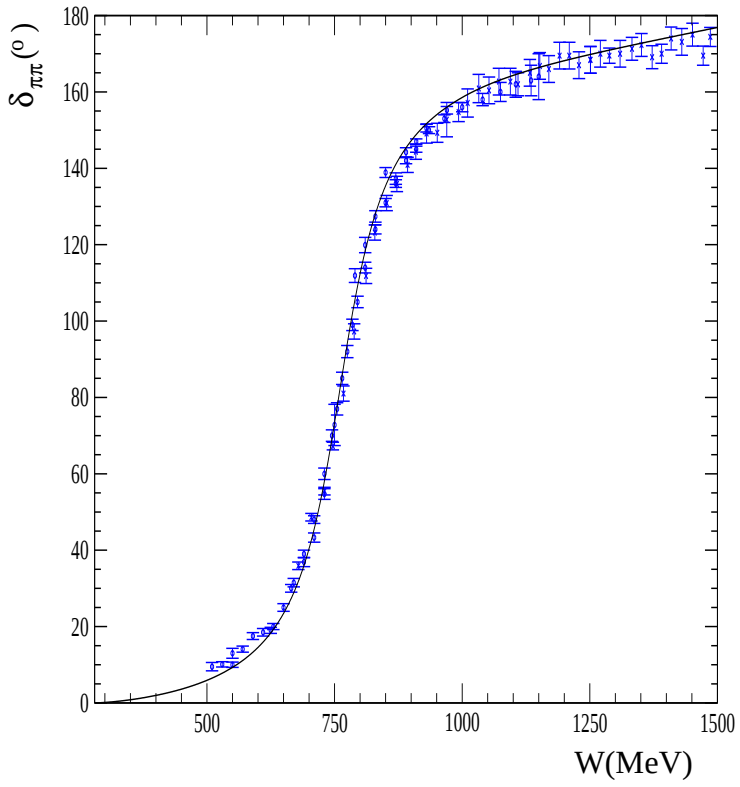

Figure 5.3: $\pi\pi$ $P-$wave phase shifts. W is defined as $\sqrt{s}$ for $s > 0$ and as $-\sqrt{-s}$ for $s < 0$. Borrowed from [144].

Lagrangian involving ρ's, pions and baryons. We would like to make use of this theoretical scheme to calculate the medium effects of the $\pi\pi$ scattering amplitude in the ρ channel. The idea is to study the changes in the ρ meson selfenergy tensor and this issue can be conveniently addressed in the gauge vector formalism, as we shall see below.

First, we want to establish a connection between the description of the $\pi\pi$ scattering amplitude in terms of ρ exchange in the frame of the gauge vector Lagrangian formulation, and the chiral unitary model described in Section 5.1. The tree level $\pi\pi$ amplitude from the χPT Lagrangian is given by the K_{22} matrix element in Eq. 5.2, and is built from the four-pion interaction vertex and the resonance exchange diagram, Fig. 5.1 (a) and (b). In the gauge vector formulation, the tree level $\pi\pi$ amplitude is driven by the

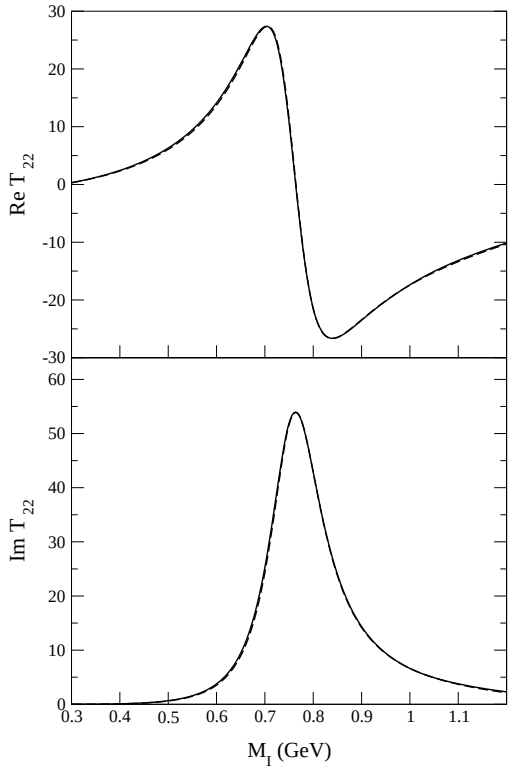

Figure 5.4: Real and imaginary parts of the $\pi\pi \to \pi\pi$ scattering amplitude (T_{22} matrix element). The solid line curve is obtained with the coupled channel formalism including kaons, while the dashed curve is the result of the decoupled calculation.

exchange of a bare ρ, and is given by

$$t_{\pi\pi} = -\frac{4}{3} g_\rho^2 p_\pi^2 \frac{1}{s - M_\rho^2} \ , \tag{5.7}$$

as it can be derived from the Lagrangian terms [134]

$$\mathcal{L}_{\pi\rho} = \mathcal{L}_{\rho\pi\pi} + \mathcal{L}_{\rho\rho\pi\pi} = \frac{1}{2} i g_\rho \rho_\mu (T_3 \vec{\phi} \partial^\mu \vec{\phi} + \partial^\mu \vec{\phi} T_3 \vec{\phi}) - \frac{1}{2} g_\rho^2 \rho_\mu \rho^\mu T_3 \vec{\phi} T_3 \vec{\phi} \ . \tag{5.8}$$

If we assume that $2G_V^2/f^2 = 1$ (as a consequence of VMD), then K_{22} coincides with the amplitude from the vector formulation.

At one loop level in the vector formulation, one can calculate the ρ selfenergy due to the coupling to pions. The bare ρ propagator is then renormalized

and acquires a selfenergy by summing the Dyson series. This selfenergy is built from the two-pion loop and the tadpole diagrams, depicted in Fig. 5.5, and is given by

$$\Pi_\rho^{\mu\nu} = ig_\rho^2 \int \frac{d^4q}{(2\pi)^4} 4q^\mu q^\nu D_0(P-q)D_0(q) - ig_\rho^2 \int \frac{d^4q}{(2\pi)^4} 2g^{\mu\nu} D_0(q). \quad (5.9)$$

On the other hand, the unitarized chiral amplitude for $\pi\pi$ scattering is also performing a resummation of diagrams, as explained in the former section, in which the tree level $\pi\pi$ amplitude factorizes on-shell out of the two-pion loop function, $G(s)$, and no tadpole terms are included.

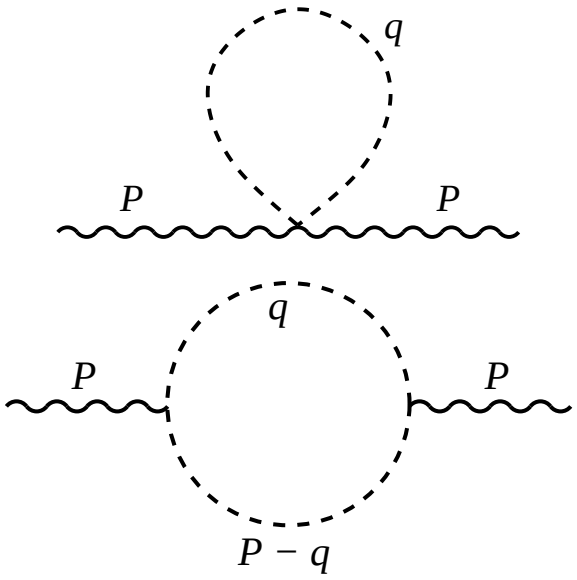

Figure 5.5: Tadpole and two-pion loop diagrams contributing to the ρ meson selfenergy. Wavy lines represent the ρ meson in the gauge vector field formalism and dashed lines are pions.

We can connect both formulations as follows [2]. By using dimensional regularization techniques [145] it is possible to prove that

$$\int \frac{d^4q}{(2\pi)^4} \frac{4q^\mu q^\nu}{(q^2+s+i\epsilon)^2} = \int \frac{d^4q}{(2\pi)^4} \frac{2g^{\mu\nu}}{q^2+s+i\epsilon}. \quad (5.10)$$

Using the former identity, Eq. (5.9) can be written, for a ρ meson at rest, as

$$\Pi_\rho^{ij} = ig_\rho^2 \int \frac{d^4q}{(2\pi)^4} 4q^i q^j [D_0(P-q)D_0(q) - D_0(q)^2]$$

$$
\begin{aligned}
&= ig_\rho^2 \frac{4}{3}\delta^{ij} \int \frac{d^3q}{(2\pi)^3} \int \frac{dq^0}{2\pi} \vec{q}^{\,2} [D_0(P-q)D_0(q) - D_0(q)^2] \\
&= ig_\rho^2 \frac{4}{3}\delta^{ij} \int \frac{d^3q}{(2\pi)^3} \int \frac{dq^0}{2\pi} \vec{q}^{\,2} [D_0(P-q)D_0(q) - \frac{\partial}{\partial m_\pi^2} D_0(q)]. \quad (5.11)
\end{aligned}
$$

In the last equality of Eq. (5.11) we have used a parametric derivative with respect to m_π^2 to rewrite the squared pion propagator. The q^0 integration can be performed analytically and we obtain

$$
\Pi_\rho^{ij} = \frac{4}{3}\delta^{ij} g_\rho^2 \int \frac{d^3q}{(2\pi)^3} \Big[\frac{\vec{q}^{\,2}}{\omega(q)} \frac{1}{(P^0)^2 - 4\omega(q)^2 + i\epsilon} + \frac{\vec{q}^{\,2}}{\omega(q)} \frac{1}{4\omega(q)^2} \Big], \quad (5.12)
$$

where $\omega(q)^2 = m_\pi^2 + \vec{q}^{\,2}$. Now, if we separate in the first term of Eq. (5.12) the on shell and off shell contribution of the factor $\vec{q}^{\,2}$ in the numerator, which comes from the $\rho\pi\pi$ vertices, we have $\vec{q}^{\,2} = \vec{q}^{\,2}_{on} + \vec{q}^{\,2}_{off}$ with $\vec{q}^{\,2}_{on} = (\frac{P^0}{2})^2 - m_\pi^2$. Since $(P^0)^2 - 4\,\omega(q)^2 = -4(\vec{q}^{\,2} - \vec{q}^{\,2}_{on})$, the contribution of the tadpole plus the off-shell part of the two-pion loop diagram is given by

$$
\tilde{\Pi}_\rho^{ij} = -g_\rho^2 \frac{m_\pi^2}{3}\delta^{ij} \int \frac{d^3q}{(2\pi)^3} \frac{1}{\omega(q)^3} \ , \quad (5.13)
$$

which is a logarithmically divergent term independent of P^0 and hence can be absorbed in a renormalization of the ρ bare mass by a proper counter term in the Lagrangian.

The former derivation proves that the formalism keeping tadpoles and full off-shell dependence in the $\rho\pi\pi$ vertex is equivalent to the one discussed in Section 5.1, where only the on-shell part of the $\pi\pi$ tree level amplitude is kept and no tadpole terms are included. In the medium, however, the pion propagator in the tadpole term changes, and the contribution of this diagram becomes density dependent, as we will see in the next section. This means that the tadpole contribution is no longer canceled by a density independent counter term, and it must be considered in the calculation to preserve isospin current conservation [128, 133, 134]. We come back to this issue in the next section, where we calculate the ρ selfenergy in the medium in the framework of the gauge vector field formalism.

To obtain the modified $\pi\pi$ interaction in the $(I, J) = (1, 1)$ channel from the calculated ρ selfenergy we proceed as follows. First we rewrite Eq. (5.3)

in terms of the ρ propagator,

$$D_\rho(s) = \frac{1}{s - M_\rho^2 - \Pi_\rho} \ , \tag{5.14}$$

with Π_ρ the ρ meson selfenergy. For the sake of simplicity, and having in mind the results of Section 5.1, we turn off the interaction between $\pi\pi$ and $K\bar{K}$ systems and work in a decoupled channel approach ($K_{12} = 0$ in Eqs. (5.2) and (5.3)). Then the $\pi\pi \to \pi\pi$ T-matrix element takes the simple form

$$T_{22} = \frac{1}{1 + K_{22}G} K_{22} \ . \tag{5.15}$$

Let us first assume that $\frac{2G_V^2}{f^2} = 1$, as it is indeed the case if VMD holds exactly. Then the K_{22} matrix element reads

$$K_{22} = -\frac{2}{3}\frac{p_\pi^2 M_\rho^2}{f^2}\frac{1}{s - M_\rho^2} \ , \tag{5.16}$$

where one can identify the $P-$wave structure of the $\pi\pi \to \pi\pi$ scattering amplitude mediated by the exchange of a bare ρ meson. Hence the factor $(1 + K_{22}G)^{-1}$ in Eq. (5.15) is accounting for a selfenergy of the ρ meson arising from the coupling with $\pi\pi$ pairs We can therefore write Eq. (5.15) as

$$\begin{aligned} T_{22} &= -\frac{2}{3}\frac{p_\pi^2 M_\rho^2}{f^2}\frac{1}{s - M_\rho^2 - \Pi_\rho^{\pi-loop}} \ , \\ \Pi_\rho^{\pi-loop} &= -K_{22}G(s)\,(s - M_\rho^2) = \frac{2}{3}\frac{p_\pi^2 M_\rho^2}{f^2}G(s) \ , \end{aligned} \tag{5.17}$$

where $\Pi_\rho^{\pi-loop}$ is the selfenergy associated to the two-pion loop.

Now we consider the case $\frac{2G_V^2}{f^2} \neq 1$. Let $a \equiv \frac{2G_V^2}{f^2}$ and proceed as above. The K_{22} matrix element can be easily cast in the form

$$K_{22} = -\frac{2}{3}\frac{p_\pi^2 M_\rho^2}{f^2}B(s)\frac{1}{s - M_\rho^2} \ , \tag{5.18}$$

where $B(s) \equiv 1 + (a-1)\frac{s}{M_\rho^2}$. Eq. (5.18) reduces to Eq. (5.16) if $a = 1$, because in that case $B = 1$ independently of s. For the values of G_V and f of Ref. [143] we find $a \approx 0.7$. For instance, at $s = (M_\rho^{Phys})^2$ we have $B \approx 0.8$,

therefore a 20 % of deviation from VMD is observed. The T matrix element for $\pi\pi \to \pi\pi$ scattering now reads

$$\begin{aligned} T_{22} &= -\frac{2}{3}\frac{p_\pi^2 M_\rho^2}{f^2} B(s) \frac{1}{s - M_\rho^2 - \Pi_\rho^{\pi-loop}} = -\tilde{g}^2 \frac{4}{3} p_\pi^2 D_\rho(s) \\ \Pi_\rho^{\pi-loop} &= \frac{2}{3}\frac{p_\pi^2 M_\rho^2}{f^2} B(s) G(s) \, = \, \tilde{g}^2 \frac{4}{3} p_\pi^2 G(s) \ , \end{aligned} \tag{5.19}$$

where $\tilde{g}^2 = \frac{1}{2}\frac{M_\rho^2}{f^2} B(s)$ defines a coupling with a smooth dependence on the energy. At $s = (M_\rho^{Phys})^2$ we find $\tilde{g} = 5.9$ to be compared, for instance, with a similar value of the coupling constant obtained in Ref. [134] by fitting the electromagnetic vector form factor of the pion (a bare ρ mass of 853 MeV is obtained from the fit in that work).

We have written the $\pi\pi$ amplitude in the chiral unitary model in terms of a dressed ρ meson exchange, which will be sensitive to the medium modifications through the changes in the ρ meson selfenergy.

5.3 Calculation of the ρ selfenergy in the medium

We now address the calculation of the ρ meson selfenergy in the presence of nuclear matter. As already mentioned, the ρ meson strongly couples to intermediate two-pion states. Medium corrections are incorporated in a first step by a proper renormalization of the pion propagator. The pion, when it scatters with the surrounding nucleons, acquires a selfenergy built from ph and Δh excitations as discussed in Chapter 2. The short distance repulsive behaviour of the NN and $N\Delta$ interaction is included to some extent with the short range correlations that correct the pion selfenergy. We shall recall here all these essential inputs.

In addition to the πNN, $\pi N\Delta$ vertices involved in the calculation of the pion selfenergy, gauge invariance demands the presence of $\rho\pi NN$, $\rho\pi N\Delta$ contact vertices. This terms of the Lagrangian generate an additional set of diagrams which participate in important cancellations together with those diagrams coming from the insertion of the pion selfenergy in the two-meson loop component of the ρ selfenergy.

From the discussion in the preceding section we concluded that a tadpole term in nuclear matter must be present in the model. The reason was twofold:

First, this term cannot be reabsorbed in the renormalization of the ρ bare mass (as it can be done in vacuum) because of density dependence; and second, omitting it implies a violation of the isospin current conservation, as it has been discussed in Refs. [128, 133, 134]. The effect of including the medium modified tadpole term is noticeable. It restores the ρ meson mass back to high energies opposing the attraction originated from the coupling to renormalized two-pion loop.

Sticking to the gauge vector field formalism has another consequence. In a minimal coupling scheme [134] the ρ meson also couples to the baryons in the ph or Δh excitations, giving rise to additional contributions. We will describe the most relevant in detail, focusing on the difficulties that arise when dealing with an energy dependent Δ width. Concerning the gauge invariance of the model, we shall discuss about possible sources of small violations in our calculation.

In addition to the interactions with pions, nucleons and Δ's, we improve our calculation by including a direct coupling of the ρ meson to baryonic resonances, giving rise to N^*h excitation pairs. We focus on the $N^*(1520)\,D_{13}$, which in the range of energies under study produces a relevant effect.

5.3.1 Pion selfenergy in nuclear matter (revisited)

The pion selfenergy is the essential ingredient to start with in a description of the propagation properties of the ρ meson in nuclear matter. The coupling of the pion to ph and Δh excitations opens new ρ decay channels such as $\rho \to \pi Nh$, $\rho \to \pi\Delta h \to \pi\pi Nh$, in which a pion is absorbed by the surrounding medium [3]. The processes are depicted in Fig. 5.6. Because of this, it is expectable that the width of the ρ resonance is enlarged for finite densities and that some strength appears at low energies. Notice that the decay threshold is no longer located at energies of two pion masses since the excitation of a ph requires a small amount of energy. In addition, because of the attraction that the pion experiences in nuclear matter (see Fig. 2.9) one

[3] These in medium mechanisms are also considered in other approaches like [128] in which the ρ meson selfenergy is built by means of the *Low Density Theorem* and an accurate description of the vector-meson nucleon scattering amplitudes.

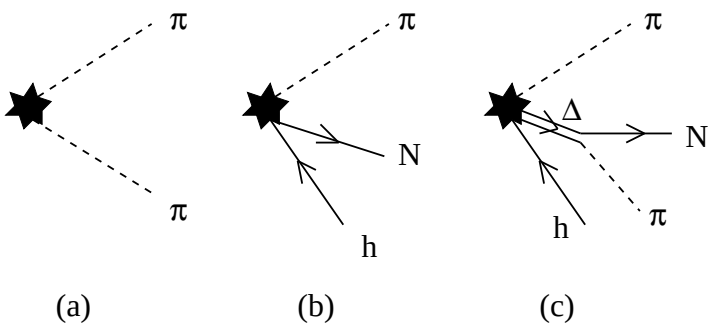

Figure 5.6: Rho decay channels involving pions: (a) Standard two-pion mode; (b) one pion and a ph excitation; (c) one pion and a Δh excitation. The Δ in addition decays into πN. The black box indicates the model dependence.

could expect the ρ mass to decrease as density is increased. However, this point is not obvious a priori because, as we shall see in the next sections, gauge invariance and other requirements of the underlying theory provide additional mechanisms that prevent a strong attraction and the mass shift could eventually occur in the opposite direction. Concerning this aspect there is no agreement in the literature.

Apart from being the most important input of the model, the pion self-energy is also a source of uncertainties in the calculation. First, it depends on the phenomenological parameter g', which has a strong influence on the pion spectral properties. Moreover, the universality condition of a single g' for interactions between $ph-ph$, $ph-\Delta h$ and $\Delta h-\Delta h$ is just a choice in this work and there are other approaches that use different values of the g' parameter to couple these excitations and mix channels [134].

Second, a precise treatment of the Δ decay width has proved to be problematic. It is possible to find in the literature different choices such as simply considering the Δ as a stable particle ($\Gamma_\Delta = 0$) [132], using a non-vanishing but constant decay width (typically the on-shell value, $\Gamma_\Delta(s_\Delta = M_\Delta) = 120$ MeV) [134] or taking into account the full energy dependence, that is the case in the present work. The key point relies on the fact that whenever a fully energy dependent Δ width is used, the Ward-Takahashi identities of the theory are not fulfilled and gauge invariance is violated to some extent. In this work we choose to keep the full Δ width because it plays an important role and the results rather differ from other approaches in which it is

considered as a constant or simply omitted.

The pion selfenergy in the nuclear medium originates from ph and Δh excitations, corresponding to diagrams in Fig. 5.7. We describe the selfenergy as usual in terms of the Lindhard function, as discussed in Chapter 2, which automatically accounts for forward and backward propagating bubbles, hence including both diagrams of Fig. 5.7. Short range correlations are also considered with the Landau-Migdal parameter g' set to 0.7. The final expression reads

$$\Pi_\pi(q,\rho) = f(\vec{q}^{\,2})^2 \vec{q}^{\,2} \frac{C\,U(q,\rho)}{1 - C\,g' U(q,\rho)}, \tag{5.20}$$

where $C = (\frac{D+F}{2f})^2$. We use a monopole form factor, $f(\vec{q}^{\,2}) = \frac{\Lambda^2}{\Lambda^2+\vec{q}^{\,2}}$ in Eq. (5.20), for the πNN and $\pi N\Delta$ vertices with the cut-off parameter set to $\Lambda = 1$ GeV. We will check the sensitivity of our results to variations of both the Λ and g' parameters.

An improvement with respect the result of Chapter 2 is introduced here. For the $\pi N\Delta$ vertex we include a recoil factor $M_N/\sqrt{s_\Delta}$ to account for the fact that the pion momentum $\vec{q}$ in the $\pi N\Delta$ vertex should be considered in Δ center of mass frame, thus a boost from the nuclear matter rest frame is required. This factor reduces to some extent the strength of the pion coupling to Δh, which is the most important source of pion attraction in the medium, and therefore it will be reflected in the eventual results for the ρ meson.

5.3.2 The two-pion loop: propagator modifications and vertex corrections

We start by studying the two-pion loop selfenergy. We perform a non-relativistic approximation of baryon propagators and vertices involving baryons, which simplifies substantially the calculation and allows to use the analytical expressions of the pion selfenergy obtained in Section 2.1 (see also Appendix B). Thanks to this, the analytical structure of the loop function is very clear, and this helps simplify the calculation of loop integrals by using complex analysis methods.

In Fig. 5.8 we show a set of diagrams which contribute at first order in density to the two-pion loop function. We included in this set the leading

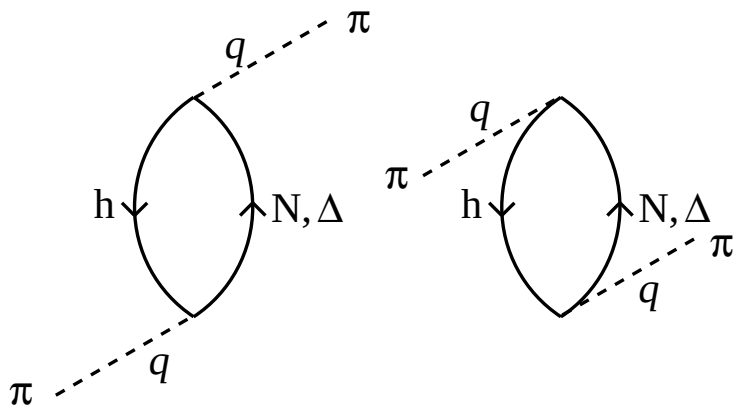

Figure 5.7: Direct and crossed ph, Δh excitation terms giving rise to the pion selfenergy in the nuclear medium, expressed in terms of the Lindhard function as described in the text.

diagrams according to the current non-relativistic approximation. Together with the insertion of the pion selfenergy in the pion propagator (Fig. 5.8a), we have to consider several vertex correction diagrams prescribed by the gauge invariance of the theory [128, 132, 133], Figs. 5.8b to 5.8d. These diagrams can be obtained from (a) by contracting one (b, c) or two (d) pion propagator lines. The contact vertices involved, $\rho\pi NN$ and $\rho\pi N\Delta$, can be derived from the following Lagrangian terms,

$$\begin{aligned} \mathcal{L}_{\rho\pi NN} &= ig_\rho \frac{f_N}{m_\pi} \bar{\psi}\gamma^5 \not{\rho}\vec{\tau}\psi T_3\vec{\phi} \\ \mathcal{L}_{\rho\pi N\Delta} &= -ig_\rho \frac{f^*_\Delta}{m_\pi} \bar{\psi}\vec{T}^\dagger\psi_\mu \rho^\mu T_3\vec{\phi} \quad + \quad \text{h.c.} \end{aligned} \tag{5.21}$$

The required Feynman rules for the contact vertices can be also obtained by requesting the tree level amplitude $\pi N \to \rho N$ to fulfill its associated Ward identity. Let us study the set of diagrams depicted in Fig. 5.9 for the case of an incoming π^+ [4], which constitute a set of gauge invariant diagrams. The amplitude corresponding to the graph 5.9a is given by

$$-it_{(a)} = -ig_\rho \epsilon_\mu (Q+2K)^\mu \frac{i}{(Q+K)^2 - m_\pi^2} \sqrt{2}\left(\frac{D+F}{2f}\right)\vec{\sigma}(\vec{K}+\vec{Q}) \ , \tag{5.22}$$

where K and Q are the momenta of the pion and the ρ meson respectively, ϵ_μ is the polarization vector of the ρ and we are using the chiral notation for

[4] Analogously we get the corresponding amplitude for the $\rho\pi N\Delta$ contact vertex, performing the substitution of Eq. (2.10).

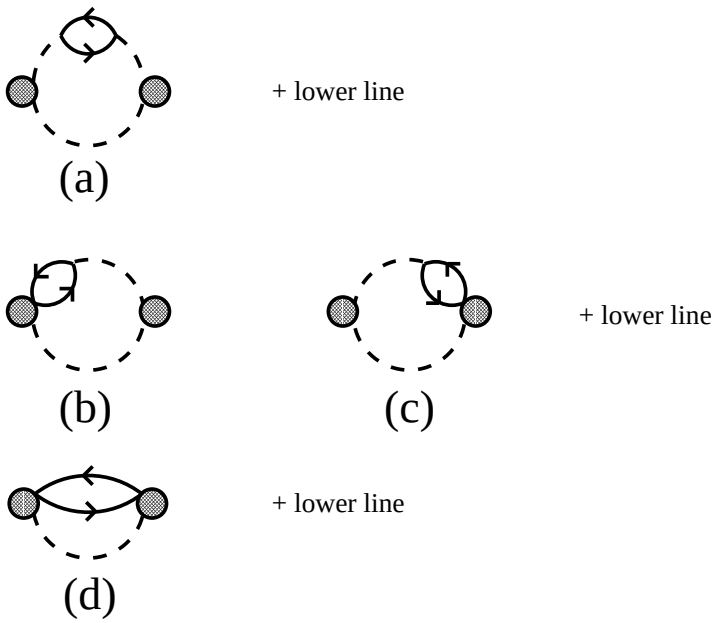

Figure 5.8: Medium correction graphs: single solid lines are reserved for particle-hole excitations.

the πNN coupling. The contact term, represented by Fig. 5.9b, must have the structure

$$-it_{(b)} = \epsilon_\mu B^\mu, \tag{5.23}$$

and gauge invariance requires that if we replace ϵ_μ by Q_μ then the sum of all the terms in Fig. 5.9 vanishes.

To find out the strength of the coupling at the lowest order in the non-relativistic approximation we can neglect the contribution from diagrams 5.9c and 5.9d, since the ρ coupling to baryons is suppressed by a M_B^{-1} factor for the spatial components of the ρNN vertex. Requiring $t^\mu_{\pi^+ n\to p\rho^0} Q_\mu \simeq [t_{(a)} + t_{(b)}]_{(\epsilon\to Q)} = 0$, the following equations hold

$$\begin{aligned} B^0 &= 0 \ , \\ g_\rho\sqrt{2}(\frac{D+F}{2f})\vec{\sigma}\vec{Q} - \vec{B}\vec{Q} &= 0 \ . \end{aligned} \tag{5.24}$$

Solving for B^μ, the amplitude corresponding to diagram 5.9b reads

$$-it_{(b)} = -g_\rho\sqrt{2}(\frac{D+F}{2f})\vec{\sigma}\vec{\epsilon} \ , \tag{5.25}$$

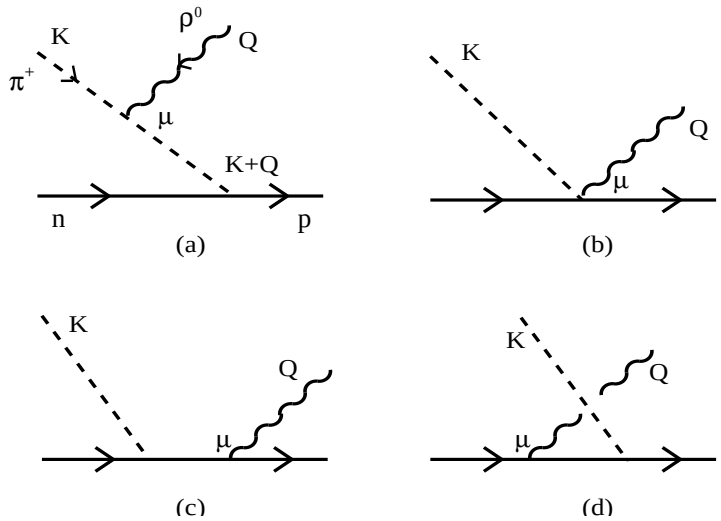

Figure 5.9: Gauge invariant set of diagrams used to calculate the ρ-meson-baryon contact term as explained in the text. The wavy lines represent here the vector meson, the dashed ones pions and the solid lines are reserved for nucleons.

and opposite sign for an incoming π^-. Since we have included a form factor in every πNN, $\pi N\Delta$ vertex, we must account for it consistently in the contact vertex (not shown explicitly in Eq. (5.25)).

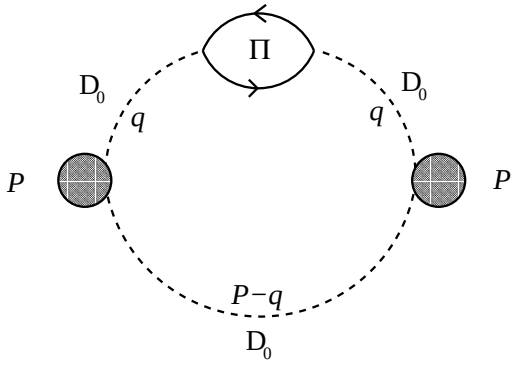

Figure 5.10: Momentum labels for the in-medium correction diagrams. D_0 indicates a pion propagator and Π refers to the pion selfenergy due to ph excitation.

The resulting ρ selfenergy contributions, at the level of a single baryon

loop insertion in the upper pion line of each diagram, are given by

$$\begin{aligned}
\Pi_\rho^{(a)} &= ig_\rho^2 \frac{4}{3}\int \frac{d^4q}{(2\pi)^4}\vec{q}^{\,2} D_0^2(q) D_0(P-q) \overbrace{\Big(\frac{D+F}{2f}\Big)^2 \vec{q}^{\,2} U(q,\rho)}^{\Pi_0(q,\rho)} \\
\Pi_\rho^{(b)} &= ig_\rho^2 \frac{2}{3}\int \frac{d^4q}{(2\pi)^4}\vec{q}^{\,2} D_0(q) D_0(P-q) \Big(\frac{D+F}{2f}\Big)^2 U(q,\rho) \\
\Pi_\rho^{(c)} &= \Pi_\rho^{(b)} \\
\Pi_\rho^{(d)} &= ig_\rho^2 \int \frac{d^4q}{(2\pi)^4} D_0(P-q) \Big(\frac{D+F}{2f}\Big)^2 U(q,\rho) \ . \qquad (5.26)
\end{aligned}$$

The momentum labels are shown in Fig. 5.10 for the first diagram, D_0 stands for the bare propagator of a pion and U includes the contributions from the ph and Δh excitations. We have explicitly indicated the pion selfenergy insertion, Π_0 (see Chapter 2, Eq. (2.15)), in the first line of Eq. (5.26). The contribution from the vertex correction diagrams (b-d) can be accounted for in the calculation of diagram (a) performing the following substitution in Π_0,

$$\vec{q}^{\,2} \to \vec{q}^{\,2} + D_0^{-1}(q) + \frac{3}{4}\frac{D_0^{-2}(q)}{\vec{q}^{\,2}} \ . \qquad (5.27)$$

Finally, we can go beyond the first order in density by using the fully dressed propagator of Eq. (2.21), which performs the Dyson summation of the irreducible pion selfenergy components, including both ph and Δh excitation as well as short range correlations,

$$\Pi_\rho^{\pi-loop}(P^0;\rho) = ig_\rho^2 \frac{4}{3}\int \frac{d^4q}{(2\pi)^4}\vec{q}^{\,2} D(q,\rho) D(P-q,\rho) \ . \qquad (5.28)$$

For the pion selfenergy, we use Eq. (5.20) with the substitution of Eq. (5.27) and this accounts exactly for the vertex correction diagrams in Fig. 5.8 at first order in density.

Eq. (5.28) also includes the contribution for the free two-pion loop selfenergy ($\rho \to 0$), which is already included in the chiral unitary model of the $\pi\pi$ T matrix, see Eq. (5.19). Thus we have to remove the vacuum contribution from Eq. (5.28) and therefore we shall replace $G(s)$ in Eq. (5.19) as follows

$$G(s) \to G(s) + \frac{1}{\vec{q}^{\,2}_{on}}[I_{med}(s) - I_{free}(s)], \qquad (5.29)$$

where

$$\begin{aligned} I_{med}(s) &= i\int \frac{d^4q}{(2\pi)^4}\vec{q}^{\,2}D(q,\rho)D(P-q,\rho) \\ I_{free}(s) &= i\int \frac{d^4q}{(2\pi)^4}\vec{q}^{\,2}D_0(q)D_0(P-q)\ , \end{aligned} \tag{5.30}$$

with the appropriate substitution of Eq. (5.27) in the pion selfenergy of Eq. (5.20).

Each of the integrals in Eq. (5.30) are quadratically divergent. The subtraction $I_{med}-I_{free}$ cancels these quadratic divergences and still a logarithmic divergence remains which in principle has to be regularized with a cut off in the pion loop momentum. However, since $D(q)D(P-q)-D_0(q)D_0(P-q)$ is proportional to the pion selfenergy, the form factors in the πNN and $\pi N\Delta$ vertices make the subtraction convergent.

5.3.3 The pion tadpole diagram in the medium

We have seen in Section 5.2 that, in free space, keeping the full off shell dependence of the $\rho\pi\pi$ vertex and explicitly considering the tadpole term in the calculation of the ρ meson selfenergy is equivalent to calculating with the on shell part of the $\rho\pi\pi$ vertex and describing the pion loop contributions with the $G(s)$ function defined in Section 5.1. This freedom allows us to include the contribution from tadpole diagram in nuclear matter by performing a subtraction of tadpole term in free space and adding the result to the ρ selfenergy of Eqs. (5.14, 5.19). The tadpole selfenergy is given by

$$-i\Pi_\rho^{tad\ \mu\nu} = -2g_\rho^2 g^{\mu\nu}\int \frac{d^4q}{(2\pi)^4}D_0(q)\ , \tag{5.31}$$

which for the spatial components of the selfenergy reads

$$\Pi_\rho^{tad\ ij} = \delta^{ij}\Pi_\rho^{tad} = \delta^{ij}2ig_\rho^2\int \frac{d^4q}{(2\pi)^4}D_0(q). \tag{5.32}$$

The vacuum subtracted tadpole contribution to the ρ meson selfenergy in the medium is

$$\tilde{\Pi}_\rho^{tad}(\rho) = 2ig_\rho^2\int \frac{d^4q}{(2\pi)^4}[D(q,\rho)-D_0(q)]. \tag{5.33}$$

Given the analytical structure of $D(q)$ and $D_0(q)$, by performing a Wick rotation one can see that $\tilde{\Pi}_\rho^{tad}$ is real, and Eq. (5.33) can be rewritten as

$$\tilde{\Pi}^{tad}(\rho) = -2g_\rho^2 \int \frac{d^4q}{(2\pi)^4}[\mathrm{Im}D(q,\rho) - \mathrm{Im}D_0(q)] \ . \tag{5.34}$$

Taking into account that both $D_0(q)$ and $D(q)$ are even functions of q^0, the integration in q^0 can be replaced by twice the integration from 0 to ∞. This integration can be performed analytically for the second term of Eq. (5.34) and we obtain

$$\tilde{\Pi}^{tad}(\rho) = -4g_\rho^2 \int \frac{d^3q}{(2\pi)^3}\Big[\int_0^\infty \frac{dq^0}{2\pi}\mathrm{Im}D(q,\rho) + \frac{1}{4\omega(q)}\Big] \ . \tag{5.35}$$

Eq. (5.35) is free from quadratic divergences. The form factors present in the pion selfenergy make it convergent and a cut off in the pion loop momentum is not required.

5.3.4 Selfenergy diagrams involving the ρ coupling to N, Δ

We discuss here additional ρ selfenergy topologies in which the ρ meson couples directly to the nucleon (Δ) in a ph (Δh) bubble. The required vertices can be derived from the following Lagrangian terms,

$$\begin{aligned}
\mathcal{L}_{\rho NN} &= -\frac{g_\rho}{2}\bar{\psi}\not{\rho}\tau_3\psi \\
\mathcal{L}_{\rho\Delta\Delta} &= g_\rho\bar{\psi}_\mu\not{\rho}T_3^{(\frac{3}{2})}\psi^\mu - \frac{g_\rho}{3}\bar{\psi}_\mu(\gamma^\mu\rho_\nu + \gamma_\nu\rho^\mu)T_3^{(\frac{3}{2})}\psi^\nu \\
&+ \frac{g_\rho}{3}\bar{\psi}_\mu\gamma^\mu\not{\rho}T_3^{(\frac{3}{2})}\gamma_\nu\psi^\nu \ .
\end{aligned} \tag{5.36}$$

The spatial components of these vertices do not contribute at the lowest order of the current non-relativistic approach, and thus we expect the associated ρ selfenergy contributions to be smaller than the ones in Fig. 5.8. Diagrams including one or two ρBB couplings ($B \equiv N, \Delta$) will be suppressed by a M_B^{-1} or M_B^{-2} factors, respectively.

The first additional medium correction that we consider here is the one shown in Fig. 5.11, with the ρ meson attached to a particle line. The

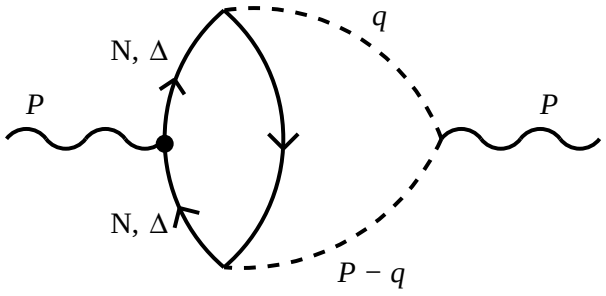

Figure 5.11: Vertex correction involving ρNN, $\rho\Delta\Delta$ vertices.

contribution from this diagram, at first order in density, reads

$$\Pi^{ij}_{1,\,\rho NN}(P^0;\rho) = i\delta^{ij} g_\rho^2 \frac{4}{3}\frac{1}{M_N P^0}\Big(\frac{D+F}{2f}\Big)^2 \int \frac{d^4q}{(2\pi)^4}(\vec{q}^{\,2})^2 D_0(q) D_0(P-q) \frac{1}{2}[\bar{U}_N(q^0-P^0,\vec{q}) - \bar{U}_N(q^0,\vec{q}) + \bar{U}_N(-q^0,\vec{q}) - \bar{U}_N(-q^0+P^0,\vec{q})] \,, \tag{5.37}$$

where the $\bar{U}_N$ functions account for the direct contribution of a nucleon-hole excitation (Fig. 5.7, left) and sum over spin but not over isospin degrees of freedom,

$$\bar{U}_N(q) = -2i \int \frac{d^4p}{(2\pi)^4} G_h(p) G_p(p+q) \,. \tag{5.38}$$

They relate to the nuclear Lindhard function introduced in Chapter 2 by

$$2\,[\bar{U}_N(q^0,\vec{q}) + \bar{U}_N(-q^0,\vec{q})] = U_N(q^0,\vec{q}) \,. \tag{5.39}$$

In Eq. (5.37) the ρNN and $\rho\pi\pi$ vertices bring a factor $(\vec{p}+\vec{q})_i\, q_j$ which survives as a $\delta^{ij}\vec{q}^{\,2}/3$ factor, since the term linear in p_i is odd and vanishes in the baryon loop integration. For the ρ line attached to the hole line the factor is $p_i q_j$ and the whole diagram vanishes.

In the case of a ρ meson coupling to a Δ line, the contribution of the diagram would be similar to Eq. (5.37) expression, with the appropriate spin/isospin factors and Δh Lindhard functions, if a constant Δ width were considered. In the nucleon case one is allowed to express the product of two particle propagators as the difference of such propagators times a global

factor, and the integral over the baryon loop leads to linear combinations of the $\bar{U}_N$ functions. However, the energy dependent Δ width does not allow to rewrite the baryon loop in that way, and we apply an approximation by taking the Fermi average over the two Δ propagators.

Given the two-pion topology of this correction it is convenient to incorporate it by proper substitution in the pion selfenergy, namely

$$\vec{q}^{\,2}U(q^0,\vec{q}) \to \vec{q}^{\,2}U(q^0,\vec{q}) + (\alpha_N+\alpha_\Delta)D_0^{-1}(q^0,\vec{q}) \ , \tag{5.40}$$

with

$$\begin{aligned}
\alpha_N &= \frac{\vec{q}^{\,2}}{2M_N P^0}[\bar{U}_N(q^0-P^0,\vec{q}) - \bar{U}_N(q^0,\vec{q}) + \bar{U}_N(-q^0,\vec{q}) - \bar{U}_N(-q^0+P^0,\vec{q})] \ , \\
\alpha_\Delta &= \frac{\vec{q}^{\,2}}{2M_\Delta}\frac{10}{9}\Big(\frac{f^*_\Delta}{f_N}\Big)^2\frac{\rho}{2}\Big\{\widetilde{G}_\Delta(q^0-P^0,\vec{q})\,\widetilde{G}_\Delta(q^0,\vec{q}) + \\
&\quad \widetilde{G}_\Delta(-q^0,\vec{q})\,\widetilde{G}_\Delta(-q^0+P^0,\vec{q})\Big\} \ ,
\end{aligned} \tag{5.41}$$

and

$$\begin{aligned}
\widetilde{G}_\Delta(q^0,\vec{q}) &= \frac{1}{\sqrt{s_\Delta} - M_\Delta + \frac{i}{2}\Gamma_\Delta(s_\Delta)} \ , \\
s_\Delta &= M_N^2 + (q^0)^2 - \vec{q}^{\,2} + 2q^0\sqrt{M_N^2 + \frac{3}{5}k_F^2} \ ,
\end{aligned} \tag{5.42}$$

to be performed together with the substitution of Eq. (5.27). Eq. (5.40) already accounts for the two possible time orderings in Fig. 5.11: incoming ρ meson coupled to the baryon loop, outgoing ρ meson closing the two pion loop, and vice versa.

We study now a set of diagrams (Fig. 5.12) containing ρNN, $\rho\Delta\Delta$ vertices which are generated from those in Fig. 5.11 by contracting one pion line, in analogy to the way the vertex corrections in Figs. 5.8b, 5.8c where generated from Fig. 5.8a. The selfenergy corresponding to the diagrams in Fig. 5.12 for the ρ absorbed or emitted by a nucleon line reads, at first order in density,

$$\begin{aligned}
\Pi^{ij}_{2,\,\rho NN}(P^0;\rho) &= i\frac{4}{3}\frac{g_\rho^2}{M_N P^0}\Big(\frac{D+F}{2f}\Big)^2\delta^{ij} \times \\
&\quad \times \int \frac{d^4q}{(2\pi)^4}\vec{q}^{\,2}D_0(q)[\bar{U}_N(q^0-P^0,\vec{q}) - \bar{U}_N(q^0+P^0,\vec{q})] \ ,
\end{aligned} \tag{5.43}$$

Figure 5.12: Additional medium corrections. The pion line represent either a π^+ or a π^-. The partners with the outgoing ρ attached to the nucleon (or Δ) line are not displayed.

where the factor four indicates that the contributions of protons or neutrons over the Fermi sea are identical. As before, the ρNN coupling attached to a particle or Δ line contributes with a $(\vec{p}+\vec{q})_i$ factor from which only q_i survives for symmetry reasons. If the ρ is coupled to a hole line, the diagram vanishes.

For the case of the baryon loop involving a Δ the result cannot be expressed in terms of Lindhard functions because of the energy dependence of the Δ width. Instead, we use the same approximation as before for the integration of the fermionic loop and we get

$$\begin{aligned}\Pi^{ij}_{2,\rho\Delta\Delta}(P^0;\rho) &= i\frac{4}{3}\frac{g_\rho^2}{M_\Delta}\frac{10}{9}\Big(\frac{D+F}{2f}\Big)^2\Big(\frac{f^*_\Delta}{f_N}\Big)^2\delta^{ij}\int\frac{d^4q}{(2\pi)^4}\vec{q}^{\,2}D_0(q)\\ &\quad\frac{\rho}{2}\Big\{\widetilde{G}_\Delta(q^0+P^0,\vec{q})\,\widetilde{G}_\Delta(q^0,\vec{q})+\widetilde{G}_\Delta(q^0,\vec{q})\,\widetilde{G}_\Delta(q^0-P^0,\vec{q})\Big\}\,.\end{aligned} \tag{5.44}$$

Finally, some other selfenergy topologies involving two ρBB couplings are considered in detail in Appendix E. These either vanish or are very small (M_B^{-2} suppression factor) and we can safely neglect them. In spite of a detailed consideration of every possible topology for the ρ selfenergy at the first order in density, which in principle would fulfill the Ward identities of the theory, we expect to have small violations of gauge invariance due to the non-relativistic treatment of baryon-meson vertices and baryon propagators, the use of an energy dependent Δ decay width and the momentum dependence of the pion-nucleon form factor. A possible solution for the latter is proposed in [134]. However, the inclusion of the Δ decay width without an explicit violation of the Ward identities is still an open problem in the literature.

5.3.5 $N^*(1520)\,h$ contribution to the ρ meson selfenergy

We study in this section the ρ meson coupling to baryonic resonances, particularly the case of $N^*(1520)$ $I(J^P) = \frac{1}{2}(\frac{3}{2}^-)$[5]. The effect of resonance excitation in the medium has been thoroughly studied elsewhere [138, 139].

The medium effect (excitation of a N^*h pair) can be included an extra selfenergy term in the ρ propagator. The basic vertex involved in this effect is shown in Fig. 5.13a, and the Lagrangian describing the interaction reads, in a non-relativistic approximation [151],

$$\mathcal{L}_{N^*N\rho} = -g_{N^*N\rho}\bar{\psi}_N S_i \vec{\rho}_i \vec{\tau} \psi_{N^*} + h.c., \tag{5.45}$$

where $\psi_{N^*}$is the $N^*(1520)$ field and $g_{N^*N\rho}$ stands for the ρNN^* coupling constant that we take from [151] to be $g_{N^*N\rho} = 7.73/\sqrt{3}$. The Feynman

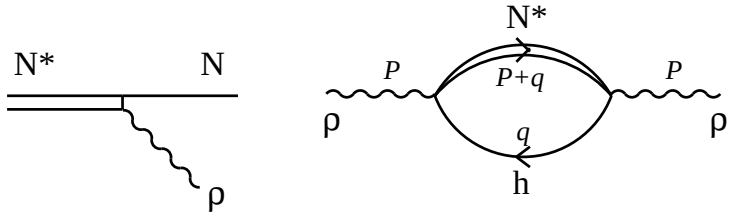

Figure 5.13: (a) ρNN^* vertex. (b) N^*h bubble contributing to the selfenergy of the ρ meson.

rules from the Lagrangian in Eq. (5.45) lead to the following result for the graph 5.13b, including both direct and crossed terms,

$$\begin{aligned} -i\Pi_\rho^{N^*h}(P^0,\vec{P};\rho) &= -(IF)(SF)\, g^2_{N^*N\rho} \int \frac{d^4q}{(2\pi)^4} \\ &\Big[\frac{1}{P^0+q^0-E_{N^*}(\vec{P}+\vec{q})+i\epsilon}\frac{n(\vec{q})}{q^0-E_N(\vec{q})-i\epsilon} \\ &+ \frac{1}{-P^0+q^0-E_{N^*}(\vec{P}+\vec{q})+i\epsilon}\frac{n(\vec{q})}{q^0-E_N(\vec{q})-i\epsilon}\Big] \end{aligned} \tag{5.46}$$

[5]Note that since we are studying the particular case of a ρ meson at rest with respect to the nuclear medium, the contribution of resonances which couple to the ρ in $P-$wave vanishes. The coupling to $N^*(1520)$ is $S-$wave and therefore its contribution to the ρ selfenergy survives even at zero ρ three-momentum.

In Eq. (5.46), $(IF) = 2$ and $(SF) = \frac{4}{3}$ are isospin and spin factors respectively, $n(\vec{q})$ stands for the occupation number of the nucleon hole and $E_B(\vec{q})$ is the energy of the baryon B involved, $E_B(\vec{q}) = \sqrt{M_B^2 + \vec{q}^{\,2}} \simeq M_B + \frac{\vec{q}^{\,2}}{2M_B}$. The q^0 integration can be performed analytically, and we are left with

$$\begin{aligned} \Pi_\rho^{N^*h}(P^0;\rho) &= \frac{2}{3} g_{N^*N\rho}^2 \, U_{N^*}(P^0,\vec{0};\rho) \ , \\ U_{N^*}(P^0,\vec{P};\rho) &= 4\int \frac{d^3q}{(2\pi)^3}\Big[\frac{n(\vec{q})}{P^0 + E_N(\vec{q}) - E_{N^*}(\vec{P}+\vec{q}) + i\epsilon} \\ &+ \frac{n(\vec{q})}{-P^0 + E_N(\vec{q}) - E_{N^*}(\vec{P}+\vec{q}) + i\epsilon}\Big] \ , \end{aligned} \tag{5.47}$$

where we have defined the Lindhard function for the N^*h excitation, U_{N^*}. In both Eqs. (5.46) and (5.47) we have omitted the N^* decay width in the N^* propagator, although it is included in the calculation (see Appendix B for analytical expressions).

5.4 Results and discussion

First of all we show the dependence of our results on parameters that enter the calculation of the pion selfenergy, one of the essential ingredients in the renormalization of the ρ up to this point. In Fig. 5.14 we show the $\pi\pi \to \pi\pi$ scattering amplitude vs invariant mass. The calculation has been performed neglecting the N^*h excitation. The g' parameter in the pion selfenergy is set to 0.7. In the figure we plot the real and imaginary parts for the free case and at normal nuclear matter density. Compared to the free case, the imaginary part shows a clear broadening which is expected since there are new decay channels. At the same time one can observe a shift of the peak of the ρ distribution to higher energies. The resonance shape of the distribution remains at $\rho = \rho_0$ and the zero of the real part of the amplitude also moves to higher energies. At normal nuclear density, the shift amounts to about $30 - 40$ MeV and the width at half maximum is somewhat more than 200 MeV to be compared to the free value of 150 MeV. We have changed the πNN, $\pi N\Delta$ form factor parameter Λ between 900 MeV and 1100 MeV. The differences found are small and this can give an idea of the uncertainties in the present results which we can expect from uncertainties in the pion

selfenergy. Other uncertainties coming from details on the treatment of the Δ resonance will be discussed later.

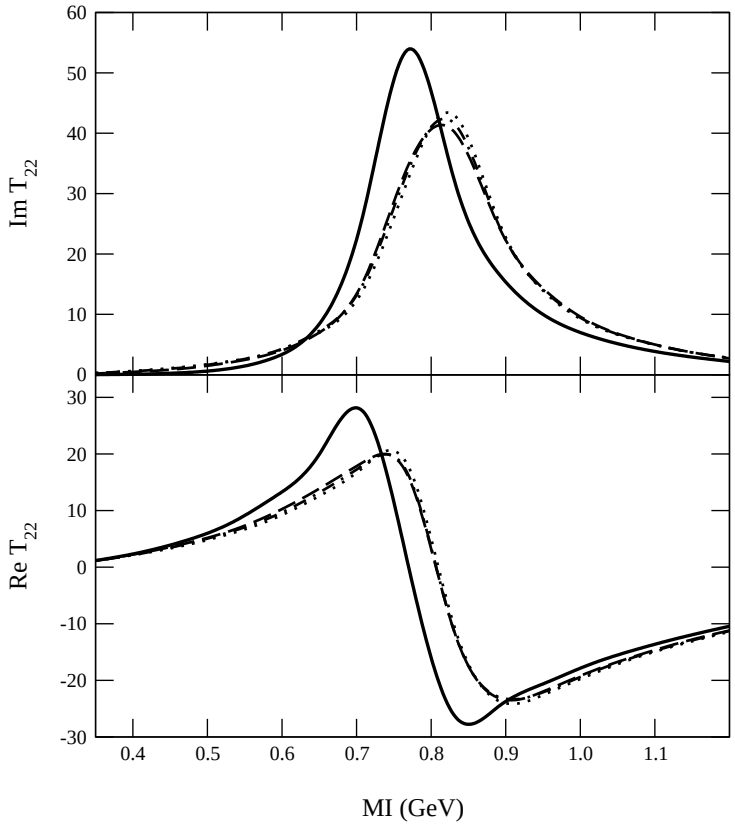

Figure 5.14: Real and imaginary parts of the $\pi\pi \to \pi\pi$ scattering amplitude vs invariant mass. Solid lines stand for the free case. The others correspond to the calculation at $\rho = \rho_0$: dashed-dotted lines for $\Lambda = 1$ GeV, long dashed and dotted lines for $\Lambda = 0.9, 1.1$ GeV respectively.

We have also checked the dependence of the calculation on the g' Landau-Migdal parameter appearing in Eq. (5.20). The results of this check are presented in Fig. 5.15, in which we show the real and imaginary parts of the scattering amplitude at $\rho = \rho_0$. The free case is also displayed for reference. The effects of a varying g' are noticeable in the resonance region whereas the results are insensitive for lower and higher energies. Neither the position of the resonance nor its width are much changed with variations of g' in the standard range of values $[0.6, 0.8]$. We find a fluctuation of the peak

position of around 3 % of the total mass at $\rho = \rho_0$. The results on the mass shift presented so far are in qualitative agreement with other works which find a moderate shift of the ρ meson mass to higher energies at finite densities by using different approaches [132, 134]. Let us recall that in

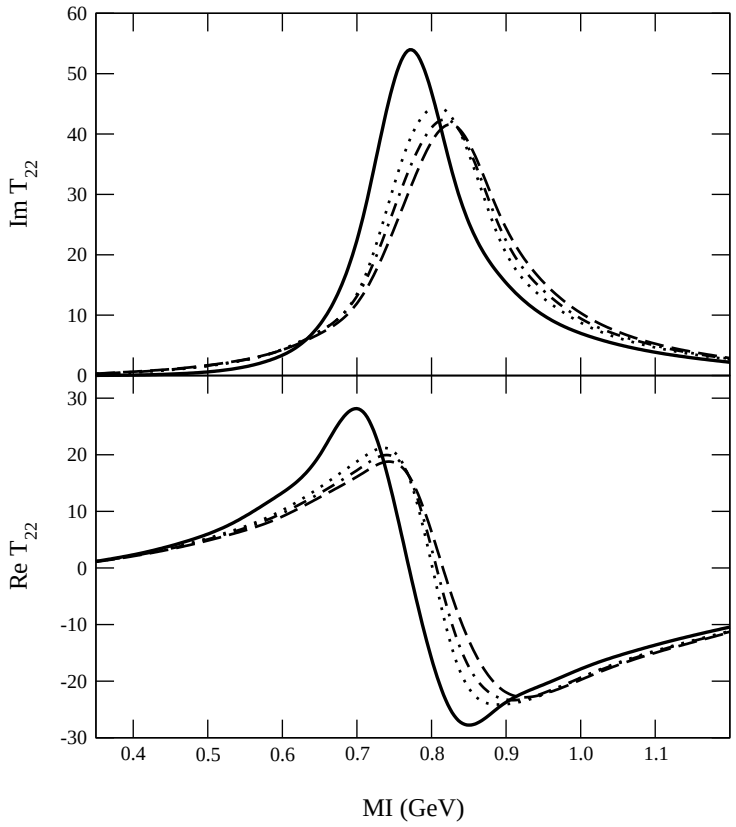

Figure 5.15: The same as in Fig. 5.14 for $\rho = \rho_0$ and several values of g'. Dashed-doted lines stand for $g' = 0.7$, long dashed and dotted lines being for $g' = 0.6, 0.8$ respectively.

our model we choose a universal coupling for the $Nh - Nh$, $Nh - \Delta h$ and $\Delta h - \Delta h$ contact vertices, leading to Eq. (5.20). We saw in Chapter 2 that short range correlations quench the interaction of the pion with the surrounding nucleons. Then we expect the effects of the nuclear medium to be softer as g' is increased. As mentioned, changes of g' in the commented range lead to uncertainties in the position of the resonance of about $20 - 25$ MeV, whereas the width is barely modified. The magnitude of the shift in the mass decreases for increasing g', which is the expected behaviour.

Other authors have explored the feasibility of introducing different values of g' for each channel of the nucleon-delta contact interaction. In [134], for example, rather smaller values of these parameters are chosen ($g'_{Nh-Nh} = 0.6$, $g'_{Nh-\Delta h} = g'_{\Delta h-\Delta h} = 0.2$) for the vertices involving *Delta*'s. Together with a value of Λ below 500 MeV in that work, the remarkable fact is that their results are comparable to ours: a significant broadening of the ρ distribution of about 55 MeV at ρ_0 and an upward shift in the mass are reported. We suggest that the choice of such small values for $g'_{\Delta N^{-1}NN^{-1}}$ and $g'_{\Delta N^{-1}\Delta N^{-1}}$ compensates up to some extent the use of πNN, $\pi N\Delta$ form factors much softer than ours, and the resulting medium effects are of comparable size.

The treatment of the $\Delta(1232)$ resonance is another issue with remarkable impact on the spectral behaviour of the ρ meson. The works of Refs. [132, 134], where the main ingredient is the medium pion selfenergy mostly driven by the coupling to Δh excitations, find also a broadening of the ρ meson. We have found that the shape of the ρ spectral distribution at low energies depends significantly on the Δ resonance properties specially its decay width. For instance, a simplified treatment in which a constant width is assumed gives a bump at around 500 MeV for $\rho \gtrsim \rho_0$. This bump disappears when an energy dependent width is used (see also [124], Fig. 3.13). Nonetheless, in some calculations having explicit energy dependence on the Δ width the bump appearing at low energies in the ρ spectral function, although weakened, still remains. The choice of a constant Δ width is used in [133, 134] to avoid the violation of the Ward-Takahashi identities of the three- and four-point Green's functions involving the ρ meson. However, we believe that energy dependence of the Δ width is a significant piece of phenomenological information as it is observed in the ρ spectral function and we include it in our calculation of the pion selfenergy.

Next we include in the calculation the $N^*(1520)$ contribution to the ρ meson selfenergy in nuclear matter. Our model does not try to be complete since many other resonances should be included. A much detailed work along these lines can be found in Ref. [138]. Our aim is simply to estimate the effect of these type of decay channels on our previous results. The $\pi\pi$ amplitude is plotted in Fig. 5.16 for $\rho = \rho_0$ with and without the N^*h contribution, together with the free case for reference. The possibility of exciting a N^*h

pair is reflected in the structure arising in the amplitude around 550 MeV. As a consequence a sizable amount of strength appears at energies below the ρ meson mass. Our results agree qualitatively with other works in which the ρ meson is allowed to couple to baryonic resonances [138, 141].

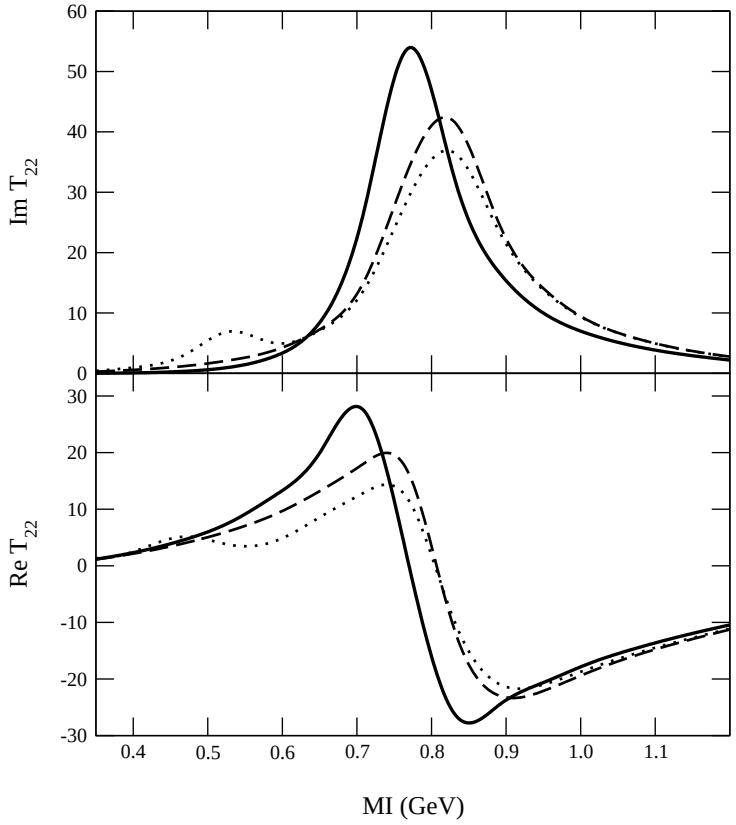

Figure 5.16: Real and imaginary parts of the $\pi\pi \to \pi\pi$ scattering amplitude. Long dashed (dotted) lines correspond to the results without (with) the effects of the coupling ρNN^* at $\rho = \rho_0$, and solid lines stand for the free case.

The same behaviour is reflected in the ρ spectral function $S_\rho = -\frac{1}{\pi}\mathrm{Im}D_\rho$, which we show in Fig. 5.17 for the free case and several values of nuclear matter density. The first effect to be commented is that the peak of the ρ distribution broadens substantially as the density is increased, its width being about 200 MeV for $\rho = \rho_0$. This is accompanied by a clear shift of the position of the resonance to higher energies (in agreement with many other works, see [124] for reference) that amounts, as reported before, to about $30 - 40$

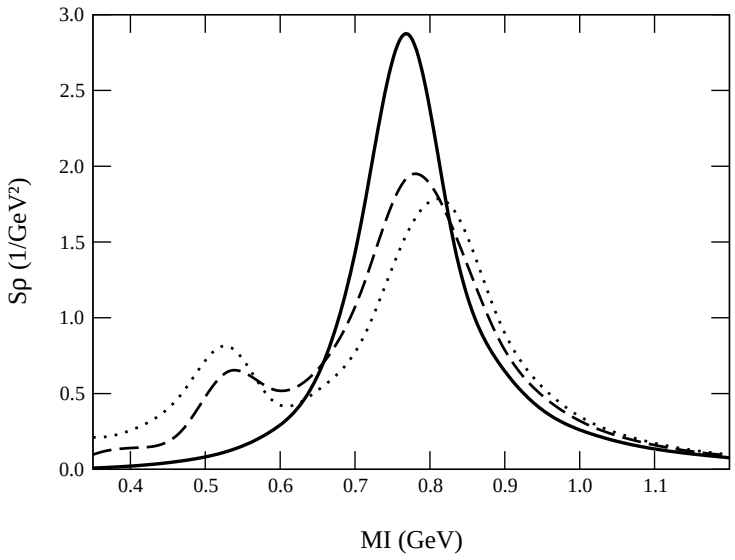

Figure 5.17: Spectral function of the ρ meson for several values of nuclear matter density. Lines are as follows: solid, dashed and dotted stand respectively for $\rho = 0$, $\rho_0/2$ and ρ_0.

MeV for normal nuclear matter density. Together with the ρ peak we can observe a resonant structure corresponding to the excitation of the $N^*(1520)$ appearing around 500-550 MeV. The N^* peak shows more prominent since the spectral function is not suppressed at low energies by the kinematical factor $p_\pi^2 = \frac{s}{4} - m_\pi^2$, present in the scattering amplitude. The coupling to N^*h increases noticeably the amount of strength towards low energies, which goes in the right direction as required by the dilepton radiation spectra in that energy region [124]. The strength of the $N^*(1520)$ peak increases with density, which is expected since this is an effect linear in density in our model. It is also noticeable that the position of this structure is slightly pushed downwards in energy with increasing density, as a consequence of the interference with the other contributions to the ρ selfenergy. In this respect we agree with Refs. [140, 141] where it was pointed out that because of the coupling to baryon resonances, the in medium vector meson strength is split into a meson like mode, which is pushed up in energy and a resonance-hole like mode, which is pushed down in energy.

These results would change if one takes into account that the properties of baryonic resonances depend themselves on the ρ meson medium spectral

function, as it is indeed the case for the $N^*(1520)$ since it decays, for instance, into $N\rho[\pi\pi]$. Therefore a selfconsistent treatment is advisable, particularly for densities higher that ρ_0. This has been done in [138], where a melting of both N^* and ρ meson structures is found at high densities so that none of them are distinguishable any longer. As a consequence, much strength is spread to lower invariant masses. Note however that this result cannot be extrapolated directly to our case since we obtain a weaker contribution of the N^*h excitation and our in-medium ρ is also narrower than in [138].

Our results reflect the most important characteristics of the medium corrections and these are shared qualitatively by many other works in which different approaches to the problem have been used [128, 132–134, 138, 141].

5.5 Summary and outlook

We have analyzed the problem of the ρ properties in a nuclear medium from a new perspective, using a chiral unitary framework to describe the isovector $\pi\pi$ scattering amplitude in free space.

The approach starts from the lowest order chiral Lagrangian involving the pseudoscalar mesons interactions and the coupling of vector mesons to pseudoscalar mesons. The unitarization for meson-meson scattering is done following closely the idea of the N/D method in coupled channels and leads to an iteration of the tree level diagrams obtained from the chiral Lagrangians plus the exchange of bare vector mesons. The free parameters of the theory are obtained by matching the results to those of chiral perturbation theory for the π and K form factors plus the position of the ρ peak. Once this is done the theory reproduces the experimental form factors and the scattering amplitudes in the vector sector with high accuracy up to 1.2 GeV.

The treatment of the ρ in the medium has led us to modify the previous approach, which relies upon the meson-meson on-shell amplitudes, in order to incorporate pion selfenergies and other many-body mechanisms in a gauge invariant way. Whereas in vacuum the formalism keeping tadpole diagrams and full off-shell dependence of the $\rho\pi\pi$ vertex is equivalent to the one followed in Ref. [143], where only the on shell part of the $\rho\pi\pi$ vertex is kept and no tadpole diagrams are considered, in the medium one should explicitly

include tadpole terms in order to preserve gauge invariance. A convenient way to proceed is to rewrite the $\pi\pi$ scattering amplitude in terms of the ρ meson propagator and calculate the medium effects on the ρ selfenergy in the frame of a gauge vector formulation, which provides the required interaction Lagrangians for the ρ coupling to pions, nucleons and Δ's.

The inclusion of medium effects proceeds by dressing the pion propagators with a proper selfenergy and including vertex corrections. In this way the main ρ decay channel into $\pi\pi$ is modified and new decay channels are opened. The main visible effect of the nuclear medium is a broadening of the ρ width as the nuclear density increases. Simultaneously we observe that there is a small shift of the peak to higher energies moderately dependent on the uncertainties of the pion selfenergy.

We have also added another source of medium effects including the coupling of the ρ to the $N^*(1520)\,h$ component. This part is not novel and has been studied elsewhere, but we include it for completeness in order to show how our previous results are affected by this channel. We observe that an important source of strength appears in the ρ spectral function at low energies and that the previous peak of the ρ distribution is slightly pushed to higher energies. Yet the global effect is still a shift of the ρ spectral function peak to higher energies of about $30 - 40$ MeV at $\rho = \rho_0$. Our results would thus agree with those where there is not much shift of the ρ peak but however produce an extra strength in the isovector-vector channel at lower energies than the free ρ mass, although there are quantitative differences.

A selfconsistent treatment of the medium effects has been shown to be advisable elsewhere, particularly for nuclear densities beyond ρ_0. It could be of special interest for the $N^*(1520)$, which gives a visible contribution at energies below the ρ peak and decays into $N\rho \to N\pi\pi$. Also a proper modification of other important N^* decay channels could be relevant, as for instance the $\Delta\pi$ channel. In a recent work [157] the $S-$wave interactions of the baryon decuplet with the pseudoscalar meson octet have been studied in a non-perturbative calculation starting from the lowest order chiral Lagrangian and implementing exact unitarity in coupled channels. For $(S, I) = (0, 1/2)$ the interaction amongst the $\Delta\pi$ and $\Sigma^* K$ coupled channels is included. A pole in the scattering amplitude is found at energies about

1450 MeV once the Δ and Σ^* decay widths are considered. This pole is identified as the $N^*(1520)$, with the consideration that the coupling to the ρN channel, missing in the calculation, could provide the necessary repulsion to allocate the mass from the pole closer to its experimental value. The calculation of Ref. [157] provides a very simple scheme to implement medium effects, as we have discussed in Chapters 2, 3 and 4 for different channels in meson meson and meson baryon interactions. This, together with a suitable modification of the ρN decay channel, would lead to a better determination of the ρ spectral function in the nuclear medium. Work along this line is in progress.

Chapter 6

ϕ meson mass and decay width in nuclear matter

The ϕ meson stands as a a unique probe to study the in-medium properties of vector meson resonances as well as the possibility of finding a partial restoration of chiral symmetry in hadronic matter, since it does not overlap with other light resonances in the mass spectrum. In addition, the changes of some of the ϕ properties are comparatively larger than those of the ρ meson, what would make its experimental observation in principle easier. At the same time, the modification of the ϕ properties in the medium is strongly related to the renormalization of the kaon properties in the medium, a topic which has also received much attention because of notable deviations from the low density theorem needed to reproduce kaonic atoms data [100,101,158,159] and the possibility of formation of kaon condensates in neutron stars [91].

Concerning the change of the ϕ properties in the medium, much of the work done has been partly stimulated by the idea that partial restoration of chiral symmetry may modify the masses of mesons at finite temperature and/or density. The ϕ mass change has been studied in several approaches like using effective Lagrangians [128, 161, 163–165], QCD sum rules [166, 167] or the Nambu-Jona-Lasinio model [168]. The ϕ width modification in matter has also been subject of study in a dropping meson mass scenario [165, 169–173], as a result of collisional broadening through ϕ-baryon [174] or ϕ-meson [175] scattering processes and as a consequence of modifications of the main ϕ decay channels in vacuum [116, 161]. The majority of these works point at

a sizable renormalization of the ϕ width and a small mass shift.

Several proposals to test the ϕ properties in a nuclear medium have been done, for instance, regarding the detection of its decay products in $A-A$ and $p-A$ collisions [160, 176, 177]. Having into account that some calculations have been done for a ϕ at rest in the nucleus [6, 116, 128, 161], it has been suggested to determine its in-medium width using reactions like $\pi^- p \to \phi n$ in nuclei [161] and ϕ photoproduction in nuclei [162], selecting those events in which the ϕ emerges with a small momentum. The latter proposal is possible by means of the elementary reaction $\gamma N \to \phi N$, with the ϕ going in the backward direction and the help of the Fermi motion of the nucleons. Another possibility to investigate the changes of the ϕ width, considered in Ref. [8], is to look for ϕ loss of flux in ϕ nuclear photoproduction. The A dependence in this loss can be related to the ϕ width in the medium. The drawback is that in this experiment a large fraction of the produced ϕ mesons comes out with a sizable momentum, for instance, of the order of 1500 MeV/c in the ongoing experiment at *SPring8/Osaka* [180]. The combination of data and theoretical models could make the experiment useful to learn about ϕ nuclear properties, provided that a suitable extrapolation of the properties of a ϕ at rest to a ϕ with a finite momentum can be done.

The purpose of this Chapter is to obtain the ϕ meson selfenergy in cold symmetric nuclear matter from which we shall study how the mass and decay width are modified in the medium. We follow the lines of Ref. [116] in which the main input to the calculation of the ϕ selfenergy in nuclear matter is the kaon selfenergy of [30], arising from $S-$ and $P-$wave interactions with the nucleons, as introduced in Chapter 2.

Although we adhere to this approach for the kaon selfenergy, we introduce some technical novelties in this chapter. Whereas the work in [116] is devoted to the calculation of the in-medium ϕ width and thus only the imaginary part of the ϕ selfenergy is obtained, we also focus on the real part to look for the shift in the ϕ mass. This leads us to improve the model of [116] by including additional mechanisms required by gauge invariance as well as performing a finer study of the relativistic recoil corrections considered in the $P-$wave kaon selfenergy.

In Section 6.1 we detail our model of the ϕ selfenergy for which we use the

vector field representation of Ref. [161]. $S-$ and $P-$wave kaon selfenergies are quoted as the major input of the calculation in nuclear matter and a set of vertex corrections involving contact ϕ-meson-baryon vertices are considered as requested by gauge invariance. Special attention is devoted to study the transversality of the selfenergy by looking at the Ward identities of the model. We also explain in this section the regularization procedure which we base on a subtraction of the vacuum selfenergy. In Section 6.2 we present our results for the selfenergy of a ϕ meson at rest, and the consequent findings for the mass and width in a nuclear medium. Attending to the current experimental proposals, we extend our results for the ϕ width in a medium to account for finite momentum, and apply our results to study inclusive nuclear ϕ photoproduction. This is done in Section 6.3. Finally, we summarize our conclusions in Section 6.4.

6.1 ϕ meson selfenergy in vacuum and in nuclear matter

In this work we shall deal with the coupling of the ϕ to $K\bar{K}$ channels, which in vacuum accounts for 85 % of the total decay width. It was found in [116,161] that the in medium $\bar{K}K$ related channels give rise to a ϕ width several times larger than in free space. Here we shall focus in the medium modifications of the ϕ meson selfenergy (both real and imaginary parts) arising from $\bar{K}K$ related channels, and we shall ignore further renormalization coming from other contributing channels in free space as the 3π channel[1].

To describe the interactions of the ϕ meson with pseudoscalar mesons and baryons, we follow the model developed in [128, 178]. The Lagrangian describing the coupling of the ϕ meson to kaons reads

$$\mathcal{L}_{\phi,kaons} = -ig_\phi \phi_\mu (K^- \partial^\mu K^+ - K^+ \partial^\mu K^- + \bar{K}^0 \partial^\mu K^0 - K^0 \partial^\mu \bar{K}^0) + g_\phi^2 \phi_\mu \phi^\mu (K^- K^+ + \bar{K}^0 K^0) \ , \quad (6.1)$$

and it provides, at $\mathcal{O}(g_\phi^2)$, a ϕ meson selfenergy Π_ϕ^{free} consisting of two-kaon loop contributions and kaon tadpole terms (see Fig. 6.1). The free width to

[1]In Refs. [128, 161] the 3π channel contribution to the ϕ selfenergy is evaluated in vacuum. The real part, related to the ϕ mass renormalization, is found to be negligible.

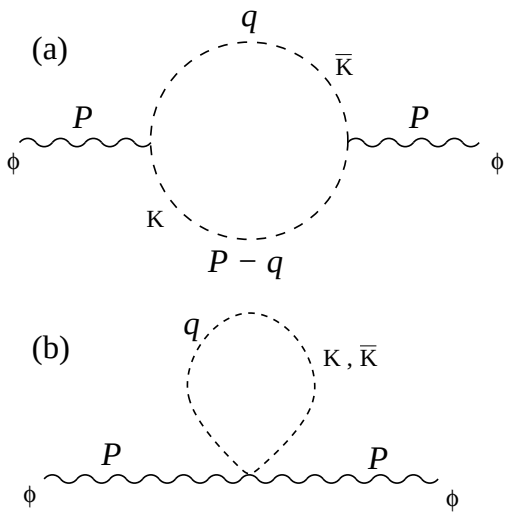

Figure 6.1: Diagrams contributing to the $\mathcal{O}(g_\phi^2)$ ϕ selfenergy in free space: (a) two-kaon loop, (b) kaon tadpole.

the $K\bar{K}$ channel can be readily calculated from the imaginary part of Π_ϕ^{free} and, by comparing to the experimental value of $\Gamma_{\phi\to K^+K^-}$, the coupling is determined as $g_\phi = 4.57$.

The calculation of the ϕ meson selfenergy in nuclear matter, Π_ϕ^{med}, proceeds by a dressing of the kaon propagators including both $S-$ and $P-$wave selfenergies, as well as vertex corrections demanded by gauge invariance. Since we are interested in both the real and imaginary parts of the ϕ selfenergy, the tadpole terms have to be explicitly included in the calculation and properly modified in the medium. The first step that we follow to include the effects of the medium consists of a modification of the kaon propagator with a proper selfenergy $\Pi_K(q^0, \vec{q}; \rho)$. A diagrammatic representation is shown in Fig. 6.2.

We shall use the renormalized kaon propagators given in spectral (Lehman) representation [161], as introduced in Chapter 2, which we recall here

$$D_{\bar{K}(K)}(q^0, \vec{q}; \rho) = \int_0^\infty d\omega \Big(\frac{S_{\bar{K}(K)}(\omega, \vec{q}; \rho)}{q^0 - \omega + i\eta} - \frac{S_{K(\bar{K})}(\omega, \vec{q}; \rho)}{q^0 + \omega - i\eta} \Big), \tag{6.2}$$

where $S_{\bar{K}(K)}$ is the spectral function of the $\bar{K}(K)$ meson,

$$S_{\bar{K}(K)}(q^0, \vec{q}; \rho) = -\frac{1}{\pi} \frac{\mathrm{Im}\,\Pi_{\bar{K}(K)}(q^0, \vec{q}; \rho)}{|(q^0)^2 - \vec{q}^{\,2} - m_K^2 - \Pi_{\bar{K}(K)}(q^0, \vec{q}; \rho)|^2} \ , \tag{6.3}$$

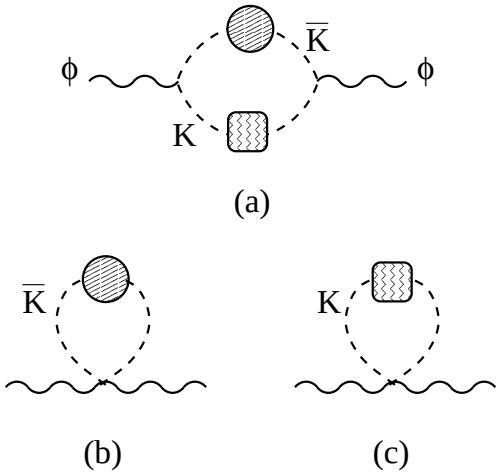

Figure 6.2: Medium modified diagrams contributing to the ϕ meson selfenergy in nuclear matter after including kaon selfenergies. The dressing of $\bar{K}(K)$ propagator is indicated by a round (squared) box.

and $\Pi_{\bar{K}(K)}$ is the $\bar{K}(K)$ selfenergy in nuclear matter. The in-medium ϕ selfenergy arising from dressing the kaon propagators, for a ϕ meson at rest, reads

$$\Pi_\phi^{ij}(P^0;\rho) = \delta^{ij} i 2 g_\phi^2 \frac{4}{3} \int \frac{d^4q}{(2\pi)^4} \vec{q}^{\,2} D_K(P-q;\rho) D_{\bar{K}}(q;\rho)$$
$$+\delta^{ij} i 2 g_\phi^2 \Big\{ \int \frac{d^4q}{(2\pi)^4} D_{\bar{K}}(q;\rho) + \int \frac{d^4q}{(2\pi)^4} D_K(q;\rho) \Big\} \equiv \delta^{ij} \Pi_\phi(P^0;\rho) \ . \quad (6.4)$$

Note that because of transversality, for a ϕ meson at rest only the (diagonal) spatial components of the selfenergy tensor are non-vanishing.

Eq. (6.4) can be further simplified by using the spectral representation of the kaon propagators and substituting explicitly the spectral function of the K^+, K^0, Eq. (2.29). The dq^0 and $d\Omega_q$ integrations can be readily evaluated and the ϕ selfenergy takes the simple form

$$\begin{aligned} \Pi_\phi(P^0;\rho) &= 2 g_\phi^2 \frac{1}{2\pi^2} \frac{4}{3} \int_0^\infty dq\, \vec{q}^{\,2} \Big\{ \frac{\vec{q}^{\,2}}{\widetilde{\omega}(q)} \int_0^\infty d\omega \frac{S_{\bar{K}}(\omega, |\vec{q}|;\rho)\,(\omega + \widetilde{\omega}(q))}{(P^0)^2 - (\omega + \widetilde{\omega}(q))^2 + i\epsilon} \\ &+ \frac{3}{4} \Big[\int_0^\infty d\omega S_{\bar{K}}(\omega, |\vec{q}|;\rho) + \frac{1}{2\widetilde{\omega}(q)} \Big] \Big\}, \end{aligned} \quad (6.5)$$

where $\widetilde{\omega}(q)^2 = \vec{q}^{\,2} + m_K^2 + \Pi_K(\rho)$.

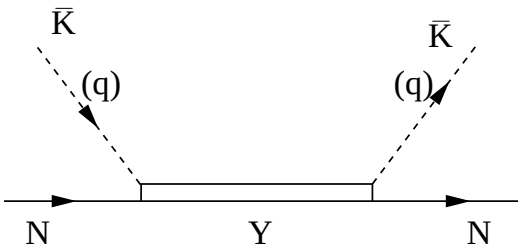

Figure 6.3: Open diagram corresponding to a kaon Yh excitation.

6.1.1 Kaon selfenergies (revisited)

In the model of Ref. [116] a non-relativistic treatment of the $\bar{K}NY$ vertices is used, including relativistic recoil corrections of $\mathcal{O}(1/M_Y)$, to deal with the imaginary part of the ϕ selfenergy. However, in this work, we are also concerned with the calculation of $\mathrm{Re}\,\Pi_\phi^{med}$ and larger energies and momenta are involved in the loop contributions. Note that the relativistic correction factors in Eq. (2.27), Chapter 2, quoted as $f_Y^2(q)$, are in principle valid for a low range of (positive) energies below M_Y, and actually fail at $q^0 = n_Y M_Y$ where the factor vanishes, killing the selfenergy contribution. We have improved the model of [116] in the treatment of the relativistic recoil corrections as we explain below. We derive the fully relativistic $\bar{K}N \to Y \to \bar{K}N$ (Fig. 6.3 amplitude for an in-medium nucleon at rest and keep only the positive energy part of the intermediate hyperon propagator. Then, the $P-$wave kaon selfenergy can be written as in Eq. (2.27), with the following relativistic correction factors,

$$f_Y^2(q) = 1 + \frac{(E_Y - M_Y)^2 - (q^0)^2}{4E_Y M_Y} \ , \tag{6.6}$$

where $E_Y = \sqrt{M_Y^2 + \vec{q}^{\,2}}$ and q^0 is the kaon energy.

Additionally, to account for the off-shell behaviour of the kaon-baryon vertices we have included static dipolar form factors. In [116,161] relativistic dipolar form factors where used, each $\bar{K}NY$ vertex carrying a $(\Lambda^2/(\Lambda^2 - (q^0)^2 + \vec{q}^{\,2}))^2$ factor with $\Lambda = 1.05$ GeV. In this work, the use of such form factors is not a proper approach because it generates fictitious poles in the real parts of the loop contributions to the ϕ selfenergy. Instead, we choose to use a static version, namely $(\Lambda/(\Lambda + \vec{q}^{\,2}))^2$ at each $\bar{K}NY$ vertex.

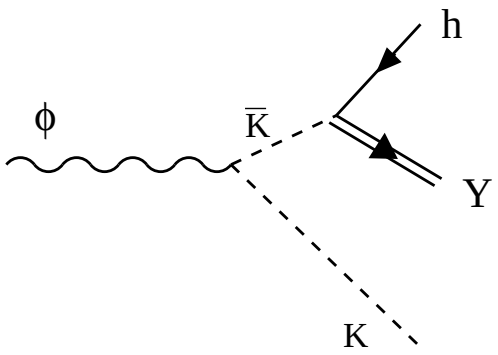

Figure 6.4: ϕ meson decay into a K meson and a $Y-h$ excitation.

We want to keep consistency with the vertices used in [116, 161]. Thus, to compensate for both changes, we properly rescale the $\bar{K}NY$ form factors by we multiplying each $\bar{K}NY$ vertex by $C\,(\Lambda/(\Lambda+\vec{q}^{\,2}))^2$ and fixing the C constant by performing a matching to the expressions in [116,161] for energies in which the kaon excites an on-shell Yh pair. The process is depicted in Fig. 6.4 in which a ϕ meson decays into a kaon and $Y-h$ excitation. It corresponds to the unitary cut of the selfenergy diagram in Fig. 6.6a and relates to the ϕ-nucleon scattering process $\phi N \to KY$. In the situation of a ϕ at rest respect to the nuclear medium the energies and momenta carried by the on-shell K and the off-shell $\bar{K}$ are given by

$$\begin{aligned} E_K &= \frac{(M_N+M_\phi)^2+m_K^2-M_Y^2}{2(M_N+M_\phi)} \ , \\ E_{\bar{K}} &= M_\phi - E_K \ , \\ |\vec{q}|_K &= |\vec{q}|_{\bar{K}} = \sqrt{E_{\bar{K}}^2-m_K^2} \ . \end{aligned} \tag{6.7}$$

The matching proceeds by demanding the following equality to be satisfied,

$$C^2\Big(\frac{\Lambda^2}{\Lambda^2+|\vec{q}|_K^2}\Big)^4 f_Y^2(E_{\bar{K}},|\vec{q}|_{\bar{K}}) = \Big(\frac{\Lambda^2}{\Lambda^2-E_{\bar{K}}^2+|\vec{q}|_K^2}\Big)^4 f_{0\,Y}^2(E_{\bar{K}}) \ , \tag{6.8}$$

what fixes the value of the scaling constant C in terms of the chosen cut-off parameter $\Lambda = 1.05$ GeV [116, 161]. We set M_Y to an average value of 1200 MeV, f_Y^2 is given in Eq. (6.6) and $f_{0\,Y}^2 = (1-E_{\bar{K}}/(2M_Y))^2$ is the recoil factor of Ref. [116]. We get a scaling constant value of $C = 1.04$.

6.1.2 Vertex corrections and gauge invariance

The introduction of the ϕ coupling to kaons and the kaon nucleon interaction in a gauge vector description of the ϕ meson demands to consider additional $\phi\bar{K}NY$ contact interaction vertices. These vertices can be evaluated systematically from the Lagrangian as done in Ref. [128]. Alternatively, one can also obtain the Feynman rules for these vertices by requiring the $\phi N \to KY$ amplitude to vanish when replacing the vector meson polarization by its four-momentum, as explicitly done for the $\rho\pi NN$, $\rho\pi N\Delta$ couplings in Chapter 5. In other words, we shall impose the Ward-Takahashi identities of the theory at the vertex level. Let us consider the set of diagrams depicted in Fig. 6.5. Note that, differently from the case of the ρ meson (see Fig. 5.9(d)), the diagram in which the ϕ is coupled to the nucleon line is missing, since the ϕNN coupling is OZI forbidden and actually is not present in the Lagrangian. The amplitude for the $\phi N\bar{K}Y$ vertex ($Y = \Lambda, \Sigma$) is given, in the non-relativistic approximation, by

$$\begin{aligned} -it_{\phi\bar{K}NY} &\equiv -it^{\mu}_{\phi\bar{K}NY}\epsilon_{\mu} \\ &= [ig_{\phi}(2k+q)^{\mu}\frac{i}{(k+q)^2 - m_K^2 + i\epsilon}\widetilde{V}_{\bar{K}NY}\vec{\sigma}(\vec{k}+\vec{q}) + B^{\mu}_{\phi\bar{K}NY}]\epsilon_{\mu} \ , \end{aligned} \tag{6.9}$$

where ϵ_μ is the ϕ polarization vector, the $\widetilde{V}_{\bar{K}NY}$ coefficients are given in Eq. (2.25) and Table 2.1, and the momentum labels correspond to those in Fig. 6.5. Note that the contribution from diagram 6.5(c) is order p/M_Y and we neglect it consistently with our non-relativistic expansion of vertices and baryon propagators. The amplitude for the contact vertex in Fig. 6.5(b) reads $-it^{cont}_{\phi\bar{K}NY} = B^{\mu}_{\phi\bar{K}NY}\epsilon_\mu$ and we want to solve for $B^{\mu}_{\phi\bar{K}NY}$. Now we replace ϵ_μ by q_μ and gauge invariance demands $-it^{\mu}_{\phi\bar{K}NY}q_\mu = 0$. Note that the kaon propagator in Eq. (6.9) is canceled by a $(2k+q)q$ factor in the numerator. Thus, we find the following equations for $B^{\mu}_{\phi\bar{K}NY}$

$$\begin{aligned} B^{0}_{\phi\bar{K}NY} &= 0 \\ -\vec{B}_{\phi\bar{K}NY} - g_{\phi}\widetilde{V}_{\bar{K}NY}\vec{\sigma} &= 0 \ . \end{aligned} \tag{6.10}$$

Eventually the amplitude for the contact vertex reads

$$-it^{cont}_{\phi\bar{K}NY} = -\vec{B}_{\phi\bar{K}NY}\vec{\epsilon} = g_{\phi}\widetilde{V}_{\bar{K}NY}\vec{\sigma}\vec{\epsilon} \ . \tag{6.11}$$

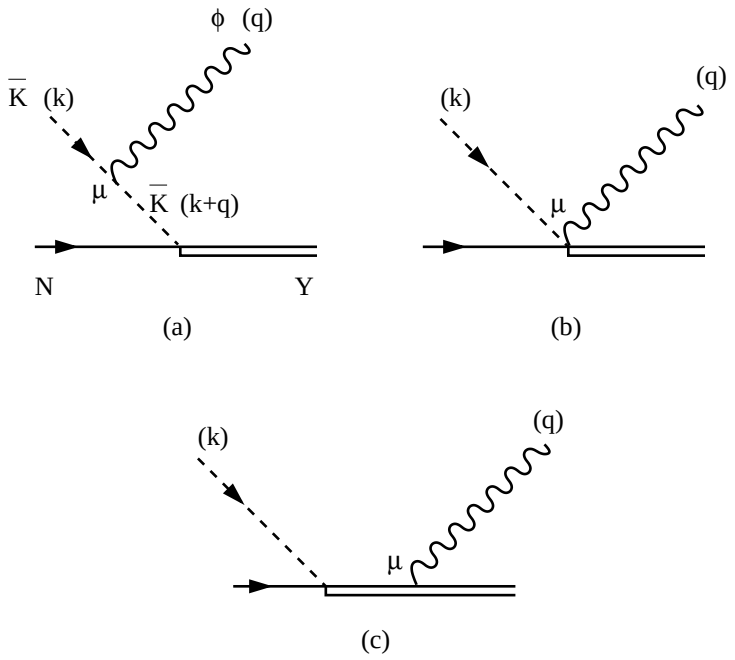

Figure 6.5: Set of diagrams satisfying the Ward identity on the vertex, involving the $P-$wave $\bar{K}NY$ coupling and its associated contact vertex.

The presented method allows us to obtain in a similar way the contact vertex for the $\Sigma^*(1385)$, which can not be derived from the Lagrangian since it does not belong to the $J^P = \frac{1}{2}^+$ baryon octet. The $\bar{K}N\Sigma^*$ vertex was introduced in a phenomenological way in Chapter 2 and, following the same steps as above we obtain, for the $\phi\bar{K}N\Sigma^*$ contact vertex,

$$-it^{cont}_{\phi\bar{K}N\Sigma^*} = g_\phi \widetilde{V}_{\bar{K}N\Sigma^*} \vec{S}^\dagger \vec{\epsilon} \ , \tag{6.12}$$

and $\widetilde{V}_{\bar{K}N\Sigma^*}$ is given also in Chapter 2, see Eq. (2.26) and Table 2.2.

At the lowest order in the nuclear density, the $P-$wave kaon selfenergy insertions plus the associated vertex corrections discussed above are considered in the ϕ selfenergy diagrams depicted in Fig. 6.6. The contribution of diagram (a) in Fig. 6.6 has already been considered in Eqs. (6.4, 6.5) since it corresponds to a single bubble insertion in the $\bar{K}$ propagator and it is accounted for by using the fully dressed kaon propagators in the calculation of the ϕ meson selfenergy. Diagrams (b-d), however, cannot be cast as medium modifications of the meson propagators but as genuine vertex

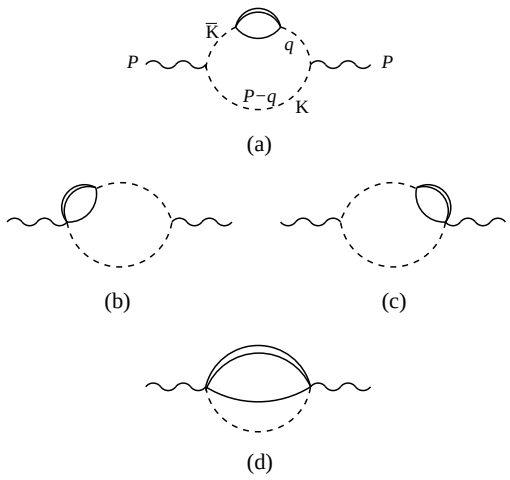

Figure 6.6: $\mathcal{O}(\rho)$ contributions to the ϕ selfenergy from $P-$wave kaon selfenergy insertions and related vertex corrections.

corrections. Let us call Π_ϕ^{VC1} and Π_ϕ^{VC2} to the selfenergy contributions associated to diagrams (b)+(c) and (d), respectively. Using the Feynman rules derived in [116] and introduced in Chapter 2, together with the ones derived in this section one finds, at first order in density,

$$\begin{aligned}\Pi_\phi^{VC1}(P^0;\rho) &= i2g_\phi^2\frac{4}{3}\int\frac{d^4q}{(2\pi)^4}\,\vec{q}^{\,2}\,\widetilde{\Pi}_{\bar{K}}^{Pwave}(q;\rho) \\ &\qquad \frac{1}{(P^0-q^0)^2-\omega^2(q)+i\epsilon}\;\frac{1}{(q^0)^2-\omega^2(q)+i\epsilon}\;, \qquad (6.13)\end{aligned}$$

$$\Pi_\phi^{VC2}(P^0;\rho) = i2g_\phi^2\int\frac{d^4q}{(2\pi)^4}\,\widetilde{\Pi}_{\bar{K}}^{Pwave}(q;\rho)\,\frac{1}{(P^0-q^0)^2-\omega^2(q)+i\epsilon}\;, \quad (6.14)$$

with $\omega^2(q)=\vec{q}^{\,2}+m_K^2$. In Eqs. (6.13, 6.14) we have used bare kaon propagators. These results can be improved to account for higher orders in density by considering additional selfenergy insertions in the kaon propagators. Actually we can substitute the bare kaon propagators in Eqs. (6.13, 6.14) by the fully dressed propagators. Using the spectral (Lehmann) representation for the kaon propagators we obtain

$$\begin{aligned}\Pi_\phi^{VC1} &= 2g_\phi^2\frac{4}{3}\int\frac{d^3q}{(2\pi)^3}\,\vec{q}^{\,2} \\ &\qquad \Big[\int_0^\infty d\omega'\Big\{\frac{1}{2\widetilde{\omega}(q)}\,\frac{S_{\bar{K}}(\omega',\vec{q};\rho)}{P^0-(\omega'+\widetilde{\omega}(q))+i\eta}\,\widetilde{\Pi}_{\bar{K}}^{Pwave}(P^0-\widetilde{\omega}(q),\vec{q};\rho)\end{aligned}$$

$$
\begin{aligned}
&- \frac{1}{2\widetilde{\omega}(q)} \frac{S_{\bar{K}}(\omega', \vec{q}; \rho)}{P^0 + \omega' + \widetilde{\omega}(q)} \widetilde{\Pi}_{\bar{K}}^{Pwave}(-\widetilde{\omega}(q), \vec{q}; \rho) \Big\} \\
&+ \frac{1}{4\widetilde{\omega}(q)^2} \frac{1}{P^0} [\widetilde{\Pi}_{\bar{K}}^{Pwave}(-\widetilde{\omega}(q), \vec{q}; \rho) - \widetilde{\Pi}_{\bar{K}}^{Pwave}(P^0 - \widetilde{\omega}(q), \vec{q}; \rho)] \Big] \ ,
\end{aligned} \tag{6.15}
$$

$$
\Pi_\phi^{VC2}(P^0; \rho) = 2g_\phi^2 \int \frac{d^3q}{(2\pi)^3} \frac{1}{2\widetilde{\omega}(q)} \widetilde{\Pi}_{\bar{K}}^{Pwave}(P^0 - \widetilde{\omega}(q), \vec{q}; \rho) \ . \tag{6.16}
$$

Both contributions Π_ϕ^{VC1}, Π_ϕ^{VC2} are finite provided that suitable form factors are used in the $P-$wave $\bar{K}NY$ vertices.

In the same line as done for the kaon-nucleon $P-$wave interaction, gauge invariance prescribes a coupling of the ϕ meson to the $S-$wave $\bar{K}NMY$ vertices. This coupling is obtained by substituting the ordinary derivative in the meson-baryon chiral Lagrangian of Ref. [29] (see Eq. (5) therein) by a covariant derivative which includes the $SU(3)$ vector meson field matrix V^μ and reads

$$
\partial^\mu \Phi \to D^\mu \Phi = \partial^\mu \Phi - i \frac{g}{2} [V^\mu, \Phi] \ , \tag{6.17}
$$

where Φ represents the pseudoscalar meson field matrix (we follow the notation of [128] and therefore $g_\phi = g/\sqrt{2}$). It is also possible to obtain the actual Feynman rules calculating the amplitude $t_{MY \to \bar{K}N\phi} \equiv t^\mu_{MY \to \bar{K}N\phi} \epsilon_\mu(\phi)$, and requiring $t^\mu_{MY \to \bar{K}N\phi} q_\mu = 0$ with q the four-momentum carried by the ϕ meson field. The involved diagrams are shown in Fig. 6.7.

The ϕ selfenergy diagrams involving the $S-$wave kaon selfenergy insertions plus the related vertex corrections are shown in Fig. 6.8. As in the case of the $P-$wave gauging, the contribution of the first diagram in Fig. 6.8 is already included in Eqs. (6.4, 6.5) by using the renormalized kaon propagators dressed with the $S-$wave selfenergy of Ref. [30]. We expect the other three terms, Fig. 6.8(b-d), to give a small contribution to the imaginary part of the ϕ selfenergy because of the reduced phase space of the intermediate states.

The necessary Feynman rules for the vertices involved (Fig. 6.9) are given by

$$
\begin{aligned}
-it_{\bar{K}NMY} &= i \frac{1}{4f^2} C_{\mathrm{i,f}} \gamma^\mu (q+k)_\mu \\
-it_{\bar{K}NMY\phi} &= i g_\phi \frac{1}{4f^2} C_{\mathrm{i,f}} \gamma^\mu \epsilon_\mu(\phi) \ ,
\end{aligned} \tag{6.18}
$$

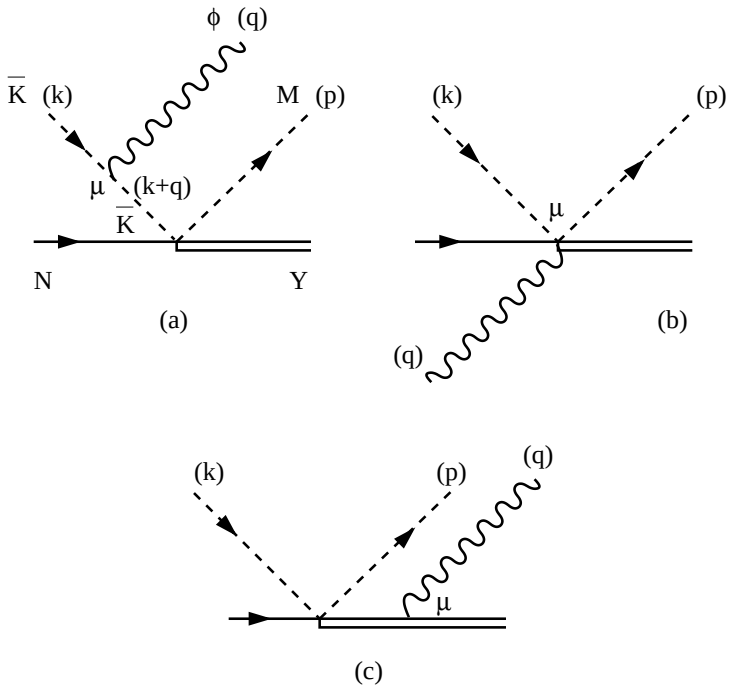

Figure 6.7: Set of diagrams satisfying the Ward identity on the vertex, involving the $S-$wave $\bar{K}NY$ coupling and its associated contact vertex.

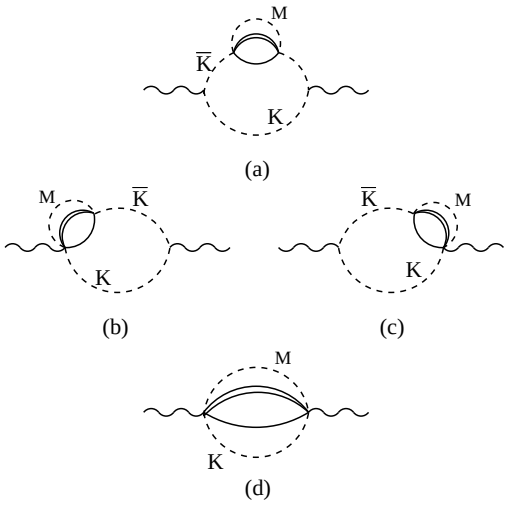

Figure 6.8: $\mathcal{O}(\rho)$ contributions to the ϕ selfenergy from $S-$wave kaon selfenergy insertions and related vertex corrections.

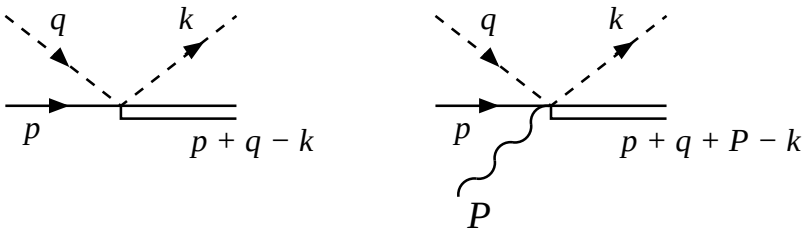

Figure 6.9: $S-$wave kaon-nucleon vertex (left) and the corresponding ϕ contact coupling (right).

where the $C_{\rm i,f}$ coefficients, related to the initial and final states, can be found in [29]. We use a non-relativistic reduction of these vertices and only keep the γ^0 terms in in $t_{\bar{K}NMY}$. The $\bar{K}NMY\phi$ vertices contribute directly to the $\mathcal{O}(1/M_B)$ order, but we shall keep them to check explicitly that these diagrams contribute little to the ϕ selfenergy. To simplify the calculation, we also neglect terms linear in the nucleon hole momentum, an approximation that we used already to calculate some ρ selfenergy diagrams in Chapter 5. We select the case of an intermediate $\pi^0\Lambda$ state, which is the one less disfavored in phase space and, under these assumptions, we find

$$\begin{aligned}\Pi_\phi^{VC1'}(P^0,\rho) &= -ig_\phi^2\frac{1}{128f^4M_\Lambda\pi^2}\frac{1}{P^0}\Big\{\mathcal{P}\int_0^\infty dq\frac{\vec{q}^{\,2}}{\omega_K(q)}\Big[\frac{I(-P^0-\omega_K(q),|\vec{q}|)}{P^0+2\omega_K(q)} \\ &+ \frac{I(-\omega_K(q),|\vec{q}|)}{P^0-2\omega_K(q)}\Big] - i\pi\frac{|\vec{q}_{on}|}{2}\,I(-P^0/2,|\vec{q}_{on}|)\,\Theta(P^0-2m_k)\Big\}\ ,\end{aligned} \tag{6.19}$$

for diagrams (b) and (c), where the $I(q^0,|\vec{q}|)$ function is defined as

$$\begin{aligned}I(q^0,|\vec{q}|) &= \frac{-i}{(2\pi)^2}\int_0^\infty dk\,\vec{k}^{\,2}\,\frac{q^0+P^0-\omega_\pi(k)}{2\omega_\pi(k)} \\ &\int_{-1}^{+1} du\,(\vec{q}^{\,2}-\vec{q}\cdot\vec{k})\,U_\Lambda(q^0+P^0+\omega_\pi(k),\vec{q}-\vec{k};\rho/2)\ ,\end{aligned} \tag{6.20}$$

with $\sigma(P^0)=\sqrt{1-4m_K^2/(P^0)^2}$, $|\vec{q}_{on}|=\sigma(P^0)\,P^0/2$, $\omega_K(q)=\sqrt{\vec{q}^{\,2}+m_K^2}$, $\omega_\pi(k)=\sqrt{\vec{k}^{\,2}+m_\pi^2}$, and $u\equiv\frac{\vec{q}\cdot\vec{k}}{|\vec{q}|\cdot|\vec{k}|}$; and

$$\Pi_\phi^{VC2'}(P^0,\rho)=ig_\phi^2\frac{3}{256f^4M_\Lambda^2}\frac{1}{2\pi^2}\int_0^\infty dq\frac{\vec{q}^{\,2}}{2\omega_K(q)}\widetilde{I}(-\omega_K(q),|\vec{q}|)\ , \tag{6.21}$$

for diagram (d), with

$$\widetilde{I}(q^0,|\vec{q}|) = \frac{-i}{(2\pi)^2}\int_0^\infty dk\,\frac{\vec{k}^{\,2}}{2\omega_\pi(k)}\int_{-1}^{+1} du\,(\vec{q}-\vec{k})^2\,U_\Lambda(q^0+P^0+\omega_\pi(k),\vec{q}-\vec{k};\rho/2)\ . \tag{6.22}$$

The imaginary parts of $\Pi_\phi^{VC1'}$ and $\Pi_\phi^{VC2'}$ are finite and very small compared to the contributions of the kaon selfenergy insertion diagrams and the $P-$wave vertex corrections discussed above. The real parts are divergent and one has to regularize both the $\pi - Yh$ loop and the external kaon loop. Under reasonable momentum cut-offs ($1-2$ GeV) we find that the real parts are of the same order as the imaginary parts and thus negligible compared to the leading contributions.

The introduction of the contact vertices, following a minimal coupling scheme as in Refs. [116, 128], guarantees gauge invariance and therefore the ϕ selfenergy is transverse. In our approach, there are small violations of gauge invariance due to some omitted diagrams which we discuss below, the non-fully relativistic treatment of the vertices involving baryons, which keep only the lowest orders in a (p/M) expansion [30]; and also to the fact that only the positive energy part of the hyperon propagators has been included in the calculation. In particular, for the ϕ at rest which is the case under study, transversality of the selfenergy tensor means that Π_ϕ^{00}, Π_ϕ^{i0} and Π_ϕ^{0j} should vanish at the lowest order that contributes to Π_ϕ^{ij} in a (p/M) expansion, where p is the kaon momentum. To accomplish with this, one has to consider all the possible ϕ selfenergy diagrams at order g_ϕ^2 which include the ones in Figs. 6.6 and 6.8, plus their partners with the Yh bubble inserted in the kaon line, plus those in which the ϕ meson is coupled to any hyperon line, which we did not comment so far. We have explicitly checked that transversality of the ϕ selfenergy is achieved at the lowest order in a (p/M) expansion, and we have included in Appendix F a justification of the transversality of $\Pi_\phi^{\mu\nu}$ under the current approximations. For instance we show there that, in our non-relativistic approximation, certain classes of diagrams only contribute to Π_ϕ^{ij} whereas others only relate to $\Pi_\phi^{i0(0j)}$ or Π_ϕ^{00}. This classification further justifies our choice of diagrams for the present calculation of the ϕ selfenergy.

6.1.3 Regularization and vacuum subtraction

The ϕ meson selfenergy, as introduced in the previous sections, is a quadratically divergent object either in the medium or in free space, and therefore a regularization procedure is required to remove divergences. Actually, since we are interested in the medium modifications of the ϕ meson, we calculate a subtracted in-medium selfenergy, which we shall call $\Delta\Pi_\phi^{med}$, defined as

$$\Delta\Pi_\phi^{med}(P^0;\rho) = \Pi_\phi(P^0;\rho) - \Pi_\phi(P^0;\rho=0) \ . \tag{6.23}$$

As we explain below this subtraction of the vacuum selfenergy cancels all divergences leading to a finite result both for the real and imaginary parts of $\Delta\Pi_\phi^{med}$. We calculate Π_ϕ^{free} and Π_ϕ^{med} in a cut-off scheme, so that each of them depends on a regularization parameter q_{max}, and the subtraction gives a finite result in the limit $q_{max} \to \infty$.

Diagrammatically, once the vacuum ϕ selfenergy is subtracted one is left, at first order in density, with single meson selfenergy insertion diagrams in the propagators and vertex correction involving one baryonic loop. Those diagrams involving $P-$wave couplings and related vertex corrections are convergent once the form factors are considered, as can be seen from power counting. For the $S-$wave selfenergy insertion diagrams convergence is not as immediate to show because we are using a complex model for the kaon selfenergy which provides the energy and momentum dependence of the kaon spectral function in a particular range of energies. It can be shown that these diagrams including $S-$wave selfenergy insertions are also convergent provided that for high energy and momentum, out of the range of validity of the model, the $S-$wave kaon selfenergy behaves as a constant or as a decreasing function. We have chosen to set the kaon selfenergy to a constant out of the range of applicability of the model (beyond to 1.5 GeV). We take for this constant the value of the kaon selfenergy at the boundary energy of 1.5 GeV and zero momentum. Then the subtracted ϕ selfenergy is free from divergences and depends only on P^0, the nuclear density ρ and the choice of this constant. In fact the dependence of the results on the boundary value of the $S-$wave kaon selfenergy is very small as we have checked numerically.

6.2 The ϕ mass and width at finite density

In Fig. 6.10 we show the imaginary part of the subtracted ϕ selfenergy for different densities from $\rho_0/4$ to ρ_0. The resulting width of the ϕ meson grows as a function of the density, and after adding the free width it reaches the value of around 30 MeV at the vacuum ϕ mass for normal nuclear density. Most of the ϕ decay channels contributing to the in-medium width have a smooth behaviour at the energies under consideration, except for the $\phi \rightarrow K\Sigma^* h$ channel which, neglecting the Σ^* width, has a threshold at 940 MeV. This threshold moves to higher energies as density grows because of the repulsive potential felt by the kaons. The position of this threshold could be used to constrain the kaon and Σ^* optical potentials. The results are

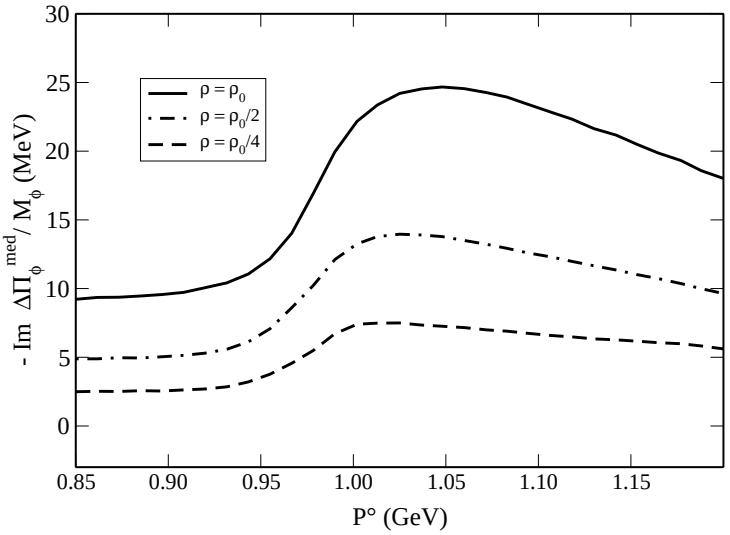

Figure 6.10: Imaginary part of the subtracted ϕ meson selfenergy in nuclear matter for several densities.

quite similar in size and shape to those of Ref. [116], except for the more visible bump related to the Σ^* channels. The shape of the imaginary part of the subtracted selfenergy also agrees quite well with the results of [161] although a larger width of around 45 MeV is obtained in that work. The possible reasons of this difference are related to the different approaches in the calculation of the kaon selfenergies [116] and the consideration of the recoil factors here.

In Fig. 6.11, we show the ϕ subtracted width at normal nuclear density obtained by successively considering different choices of antikaon selfenergy and the inclusion of vertex corrections. In all cases we use the full $S-$wave repulsive kaon selfenergy in the calculation. The lowest curve corresponds to the ϕ subtracted medium width when the $\bar{K}$ propagator incorporates only the $S-$wave $\bar{K}$ selfenergy. This selfenergy is mildly attractive, compensating in part the repulsion felt by the kaon. Its imaginary part comes from the kaon decaying into $\pi\Lambda h$ and $\pi\Sigma h$ and therefore this corresponds to the ϕ decay channels $\phi \to K\pi\Lambda h$ and $\phi \to K\pi\Sigma h$.

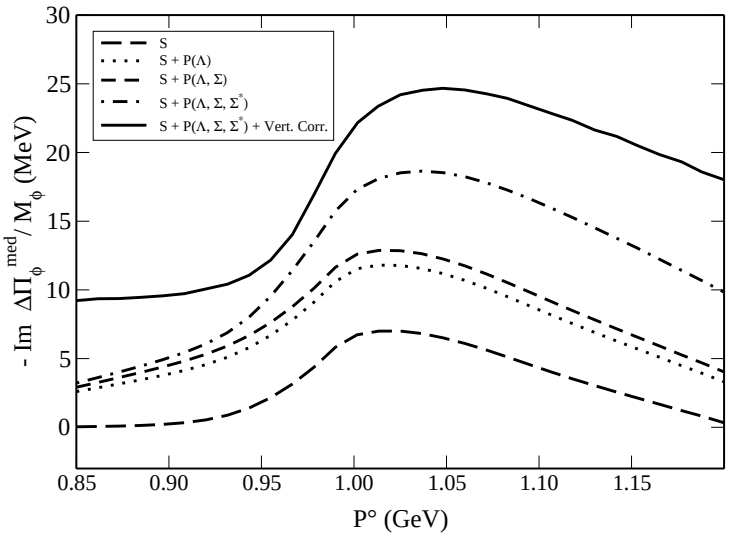

Figure 6.11: Contributions to the imaginary part of the subtracted ϕ meson selfenergy in nuclear matter at $\rho = \rho_0$.

In the next curves, we consider additionally the $P-$wave $\bar{K}$ selfenergy due to the kaon coupling to a Λh, $\Lambda h + \Sigma h$ and $\Lambda h + \Sigma h + \Sigma^* h$ excitations. We find a quite small contribution from the Σ and sizable contributions from the $\phi N \to K\Lambda$ and $\phi N \to K\Sigma^*$ processes. As commented above, the Σ^* channel has its threshold around 940 MeV and therefore only contributes strongly above this energy. The small contribution below the threshold, visible in the figure, is due to the approximation of using a constant Σ^* width in the calculation. The $\phi N \to K\Lambda$ channel has a much lower threshold and thus its contribution depends little on energy. Finally, the solid line also incorporates the vertex corrections leading to a further enhancement of the total width.

In Fig. 6.12 we show the real part of $\Delta\Pi_\phi^{med}$ which we find mildly attractive up to energies around 1.1 GeV. The change in the ϕ mass at $\sqrt{s} = M_\phi$ is approximately 8 MeV to lower energies at $\rho = \rho_0$. This small correction is in agreement with previous works [161,163], although disagrees with naive scaling expectations. There are recent experimental results at $T = 0$ [179] which do not observe any signature of in-medium modification of the ϕ mass in the reaction $pA \to K^+K^-X$. However, one should be careful in the interpretation of the results without a detailed theoretical calculation. On the one hand, the distortion of the final kaons and the initial protons could force the reaction to occur at the nuclear surface and therefore at low densities. On the other hand, due to the long ϕ lifetime and the large average ϕ momentum a good part of the events could correspond to ϕ decays in vacuum. Furthermore, for those events with a fast ϕ meson, the use of a selfenergy obtained for a ϕ at rest is not justified.

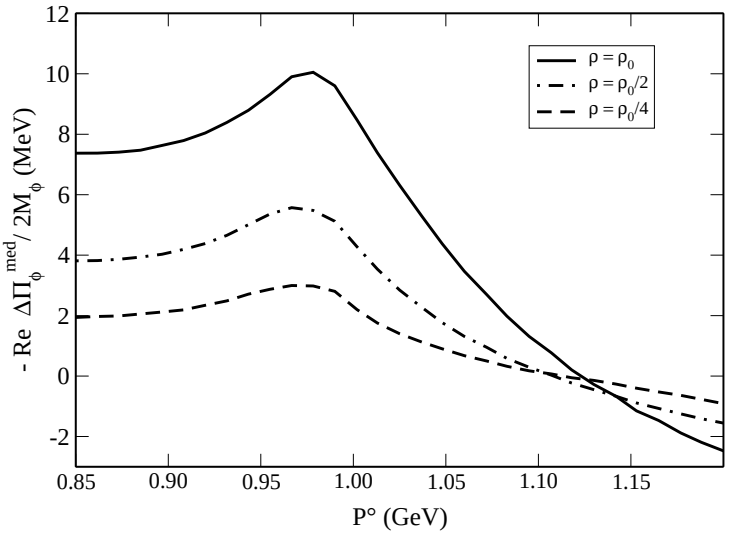

Figure 6.12: Real part of the subtracted ϕ meson selfenergy in nuclear matter for several densities.

6.3 Application to inclusive nuclear ϕ photoproduction

As commented at the beginning of this chapter, there have been several proposed experiments to observe the ϕ properties in a nuclear medium, as for instance the ϕ production in nuclei by using pions and photons. The handicap in these experiments is the long ϕ lifetime, which makes most of the ϕ decay events to take place outside the target nucleus, unless appropriate kinematical conditions are required to isolate those events in which the ϕ is produced with a small momentum. The consequence of such constraints is a considerable reduction of the production cross section, what turns eventually into a poor statistics for the mass and width observables, usually reconstructed from the invariant mass distribution of K^+K^- pairs resulting from ϕ decay. Another problematic issue, pointed in [181], is the effect of the Coulomb interaction on the observed kaon pairs, which could remove the changes in the K^+K^- mass distribution coming from the modified ϕ decay width at finite density, mainly as a consequence of K^- binding in the nucleus.

We propose here a different method to study possible medium effects in inclusive ϕ photoproduction in nuclei [8]. We look at the ϕ flux reduction in the nuclear reaction with respect to the elementary production reaction on the nucleon. As we shall discuss below, the ϕ loss of flux - particularly its dependence with the mass number, A - can be related to the changes in the ϕ width at finite nuclear density. We shall focus on the experimental setup of the ongoing experiment at *Spring8/Osaka*, in which ϕ mesons with a momentum of the order of 1.5 GeV are photoproduced in several nuclei. The drawback in this experiment is that the largest fraction of the produced ϕ's comes out with such a large momentum, what could make calculations for ϕ mesons at rest with respect to the nuclear medium inaccurate. To overcome this problem we extend our ϕ selfenergy model to account for finite momentum.

6.3.1 ϕ photoproduction cross section

We start by defining an observable sensitive to the loss of ϕ flux because of nuclear effects. Let $\Pi_\phi(P^0, \vec{P}; \rho)$ be the ϕ selfenergy in a nuclear medium as a function of its momentum, P, and the nuclear density, ρ. We have

$$\frac{\Pi_\phi}{2\omega} \equiv V_{opt} = \ \mathrm{Re}V_{opt} \ + \ i\,\mathrm{Im}V_{opt} \ , \tag{6.24}$$

and hence

$$\frac{\Gamma_\phi}{2} = -\mathrm{Im}V_{opt} = -\mathrm{Im}\frac{\Pi_\phi}{2\omega} \quad ; \qquad \Gamma_\phi = -\frac{\mathrm{Im}\Pi_\phi}{\omega} \equiv \frac{d\mathcal{P}}{dt} \ , \tag{6.25}$$

where V_{opt} is the ϕ optical potential, ω is the ϕ energy and $\mathcal{P}$ is the ϕ decay probability, including nuclear quasielastic and absorption channels. Hence, we have for the probability of loss of flux per unit length

$$\frac{d\mathcal{P}}{dl} = \frac{d\mathcal{P}}{v\,dt} = \frac{d\mathcal{P}}{\frac{P}{\omega}dt} = -\frac{\mathrm{Im}\Pi_\phi}{P} \ , \tag{6.26}$$

with $P \equiv |\vec{P}|$. The nuclear cross section for inclusive ϕ photoproduction can be written as follows

$$\frac{d\sigma_A}{d\Omega} = \int d^3\vec{r}\rho(r)\frac{d\sigma}{d\Omega}\ e^{-\int_0^\infty dl \frac{-1}{P}\mathrm{Im}\Pi_\phi(P^0,P;\rho(r'))} \ , \tag{6.27}$$

where $\frac{d\sigma}{d\Omega}$ and $\frac{d\sigma_A}{d\Omega}$ are the elementary and nuclear differential cross section and $\vec{r}\,' = \vec{r} + l\frac{\vec{P}}{|\vec{P}|}$ with $\vec{r}$ the ϕ production point inside the nucleus. The exponential factor in Eq. (6.27) represents the survival probability of the ϕ meson in its way out of the nucleus. If the ϕ did not get absorbed inside the nucleus then we would get the typical result for an electromagnetic reaction $\frac{d\sigma_A}{d\Omega} = A\frac{d\sigma}{d\Omega}$. Eq. (6.27) relies in the eikonal approximation which is accurate for the large ϕ momentum involved in the process. In practice one might expect small corrections to the formula, even if the ϕ did not decay, from two sources:

i) Distortion of the ϕ trajectory because of the real part of the potential

ii) Change of direction and energy of the ϕ in quasielastic collisions $\phi N \to \phi' N'$.

The first effect should be negligible since the real part of the potential is so weak that only modifies the mass of the ϕ in a few MeV, as shown in Section

6.2. The second effect should be very weak too, since the ϕNN coupling is forbidden because of the OZI rule. On the other hand, the effect from this source would simply lead to a slight change in the ϕ direction but not to the disappearance of the ϕ. This simply means that collecting the ϕ in a narrow cone along the forward direction, where practically all the ϕ go, both because of the kinematics in the Lab frame and the extremely forward direction of the $\gamma N \to \phi N$ cross section [182], would guarantee that the ϕ's undergoing quasielastic collisions in the nucleus are accounted for in the nuclear cross section. In order to adjust to this experiment we should not remove theoretically the events in which ϕ undergoes quasielastic collisions. This will be done by including in $\mathrm{Im}\Pi_\phi$ only the ϕ absorption events, included in our ϕ selfenergy model.

The integral in Eq. (6.27) does not depend on the direction of the ϕ momentum and thus we have

$$\mathcal{P}_{out} \equiv \frac{\sigma_A}{A\sigma} = \frac{1}{A}\int d^3\vec{r}\rho(r)\ e^{\int_0^\infty dl\,\frac{1}{P}\mathrm{Im}\Pi_\phi(P^0,P;\rho(r'))}\ , \tag{6.28}$$

and this is the magnitude which we evaluate as a function of P and A, which can be interpreted as the probability for a ϕ to escape from the nucleus. The density profiles for the different nuclei, $\rho(r)$, have been taken from [185].

6.3.2 Extension of the model for finite momentum

The ϕ selfenergy from the $\bar{K}K$ loop diagram, which is given in Eq. (6.4) for a ϕ at rest, has to be evaluated for the general case of a ϕ with finite momentum. The result reads

$$\Pi_\phi(P^0,\vec{P};\rho) = 2ig_\phi^2\frac{4}{3}\int\frac{d^4q}{(2\pi)^4}\Big[\frac{(P\cdot q)^2}{m_\phi^2}-q^2\Big]D_K(P^0-q^0,\vec{P}-\vec{q};\rho)D_{\bar{K}}(q^0,\vec{q};\rho) \tag{6.29}$$

for a ϕ meson with a momentum P. We do not include the tadpole terms in the present calculation since we are only interested in the imaginary part of the ϕ selfenergy which relates to the ϕ decay width.

By using the spectral representation of the kaon propagators, which sums up to all orders the insertion of irreducible kaon selfenergy terms, the imag-

inary part of Π_ϕ can be written as

$$\begin{aligned}\mathrm{Im}\Pi_\phi(P^0,\vec{P};\rho) &= -\frac{1}{4\pi}g_\phi^2\frac{4}{3}\int_0^\infty dq\,\vec{q}^{\,2}\int_{-1}^{1}du\,\frac{1}{\widetilde{\omega}_{P-q}} \\ &\Big[\frac{(P\cdot q)^2}{m_\phi^2}-q^2\Big]_{q^0=P^0-\widetilde{\omega}_{P-q}} S_{\bar{K}}(P^0-\widetilde{\omega}_{P-q},\vec{q};\rho)\,\Theta(P^0-\widetilde{\omega}_{P-q})\ ,\end{aligned} \tag{6.30}$$

where $u=\vec{P}\cdot\vec{q}/|\vec{P}|\,|\vec{q}|$ and $\widetilde{\omega}_{P-q}=\sqrt{(\vec{P}-\vec{q})^2+m_K^2+\Pi_K(\rho)}$. The kaon spectral function includes both the kaon $S-$ and $P-$wave selfenergy contributions.

The evaluation of the vertex correction diagrams at a finite ϕ momentum is done in a similar way. We restrict to the diagrams in Figs. 6.5, 6.6, related to the kaon $P-$wave selfenergy, which were find to contribute most to the ϕ selfenergy, together with the $\bar{K}K$ loop. The result for these mechanisms, quoted in Eqs. (6.13, 6.14) for zero momentum, read now

$$\begin{aligned}\Pi_\phi^{VC1}(P^0,\vec{P};\rho) &= i2g_\phi^2\frac{4}{3}\int\frac{d^4q}{(2\pi)^4}[\vec{q}^{\,2}-\frac{1}{M_\phi^2}(\vec{P}\vec{q})(P\cdot q)] \\ &\widetilde{\Pi}_{\bar{K}}^{Pwave}(q;\rho)D_{\bar{K}}(q;\rho)D_K(P-q;\rho)\ ,\end{aligned} \tag{6.31}$$

$$\Pi_\phi^{VC2}(P^0,\vec{P};\rho)=i\frac{2}{3}g_\phi^2\left(3+\frac{\vec{P}^{\,2}}{M_\phi^2}\right)\int\frac{d^4q}{(2\pi)^4}\widetilde{\Pi}_{\bar{K}}^{Pwave}(q;\rho)D_K(P-q;\rho)\ . \tag{6.32}$$

6.3.3 Results and discussion

In Fig. 6.13 we show the imaginary part of the ϕ selfenergy as a function of the ϕ momentum for different nuclear densities. The contribution to $\mathrm{Im}\Pi_\phi$ coming from the free ϕ decay into $\bar{K}K$, non density dependent, has been subtracted from the full $\mathrm{Im}\Pi_\phi$ since the $\bar{K}K$ pairs coming from the free decay would be detected and counted as a ϕ event, and hence they do not contribute to the loss of flux required in the argument of the exponential in Eq. (6.28). The imaginary part of the ϕ selfenergy behaves softly with the ϕ momentum, increasing moderately in absolute value for higher values of P.

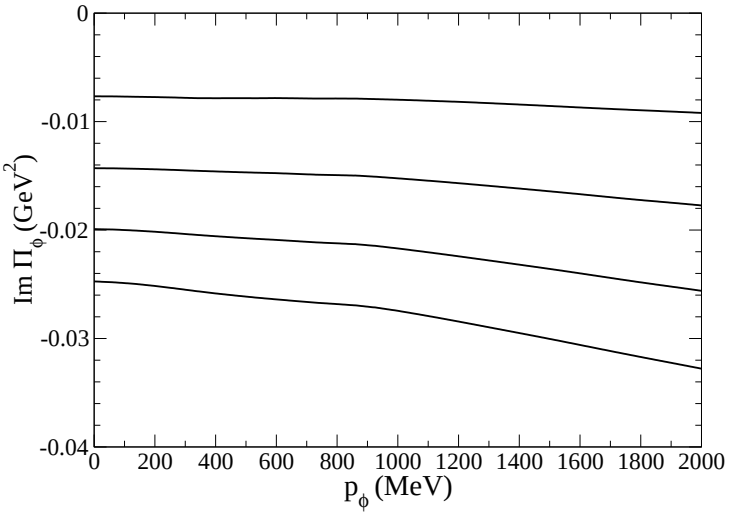

Figure 6.13: Imaginary part of the in medium ϕ selfenergy, without the inclusion of the free part, as a function of the ϕ momentum and the density.

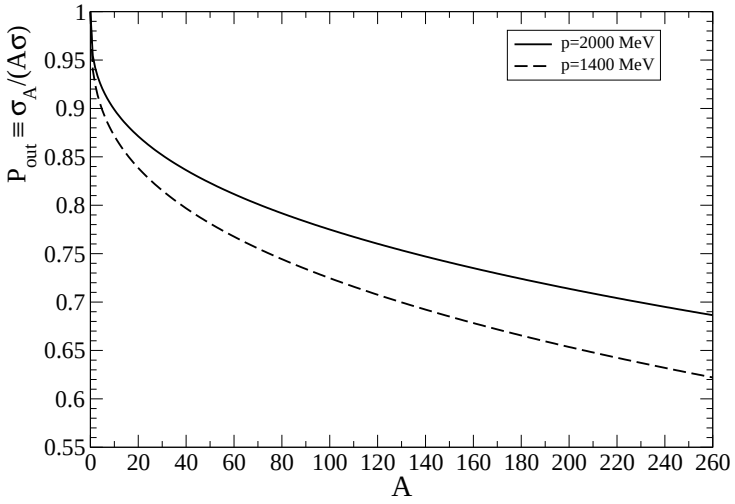

Figure 6.14: $\sigma_A/(A\sigma)$ as a function of the nuclear mass number for two different momentum of the ϕ calculated with the model described in the text.

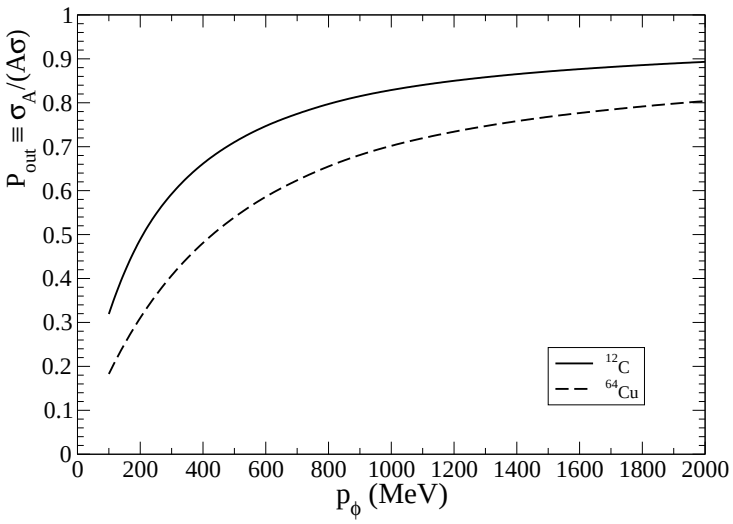

Figure 6.15: $\sigma_A/(A\sigma)$ as a function of the momentum of the ϕ for two different nuclei calculated with the two models described in the text.

In Fig. 6.14 we show the ratio $\sigma_A/(A\sigma)$, which represents the probability of a photoproduced ϕ to go out the nucleus, calculated theoretically as a function of A and for two different momenta. We observe that for $p =$ 1400 MeV and heavy nuclei this ratio can be of the order of 0.65, indicating a clear ϕ loss of flux which should be identifiable experimentally.

In Fig. 6.15 we show instead the results for $\sigma_A/(A\sigma)$ as a function of the ϕ momentum for two nuclei, ^{12}C and ^{64}Cu. In this figure we observe that the amount of ϕ flux lost is larger for smaller ϕ momentum. This is logical to expect since the probability of ϕ decay per unit length is given by $-\mathrm{Im}\Pi_\phi/P$, which is larger for small momenta because of the factor $1/P$. This occurs in spite of the fact that $-\mathrm{Im}\Pi_\phi$ decreases with P, as can be seen in Fig. 6.13, because this P dependence is weaker than that of the $1/P$ factor. The set up of the experiment at *SPring8/Osaka* [180] is such that it produces ϕ momenta around 1500 MeV, using photons from 1.4 to 2.4 GeV, coming from ϕ production in the CM frame forward direction. A possibility to enhance the ϕ flux reduction is to use photons of lower energy. For instance, for photon momentum around 1.6 GeV, not far from the production threshold, the ϕ momentum is around 100 MeV in the CM frame and around 1000 MeV in the Lab frame. As one can see in Fig. 6.15, in a nucleus like ^{64}Cu the

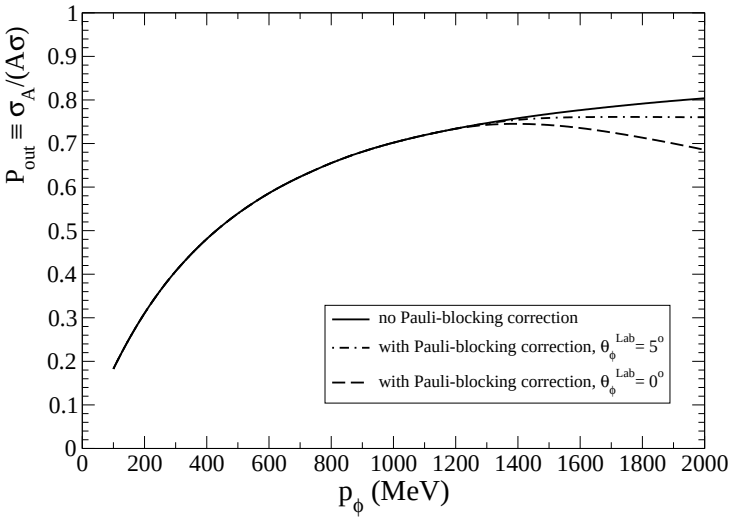

Figure 6.16: Effect of the Pauli-blocking correction in $\sigma_A/(A\sigma)$ as a function of the momentum of the ϕ for ^{64}Cu.

depletion factor goes from 0.8 at $P = 2000$ MeV to 0.7 at $P = 1000$ MeV. This factor would be 0.57 for $A \simeq 240$.

So far the only nuclear effects considered have been the ones related to the absorption of the ϕ meson. At this point it is worth mentioning that other nuclear effects regarding the production mechanism may lead to a further ϕ loss of flux or change in the ϕ distribution. These other nuclear effects are mainly the Pauli blocking of the final nucleon and the Fermi motion of the initial one. The first one may lead to a reduction of the ϕ flux in comparison to the free case because a certain amount of events are forbidden due to the Pauli blocking of the final nucleon. On the other hand the initial Fermi motion can distort the distribution of the final ϕ mesons. In order to estimate the possible flux reduction due to these sources, we have included in the integrand of Eq. (6.28) a factor $G(Q, \rho)$, borrowed from [183], which considers a Fermi average of these effects:

$$G(Q,\rho) = 1 - \Theta(2 - \widetilde{Q}) \left(1 - \frac{3}{4}\widetilde{Q} + \frac{1}{16}\widetilde{Q}^{\,3}\right) , \tag{6.33}$$

where $\widetilde{Q} = |\vec{Q}|/k_F$ with $\vec{Q}$ the momentum transfer of the nucleon and $k_F = (\frac{3}{2}\pi^2\rho(r))^{1/3}$ is the Fermi momentum of the nucleons.

In Fig. 6.16 we show $\sigma_A/(A\sigma)$ as a function of the ϕ momentum for

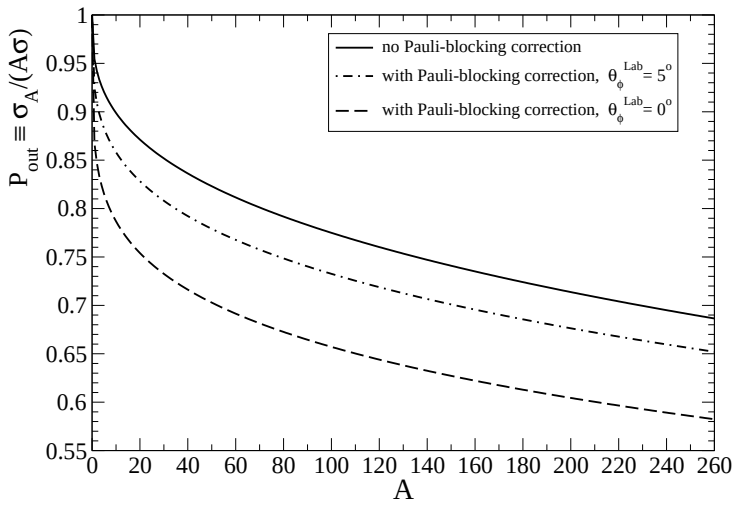

Figure 6.17: Effect of the Pauli-blocking correction in $\sigma_A/(A\sigma)$ as a function of the nuclear mass number for $P_\phi = 2000$ MeV.

^{64}Cu. In solid line we show the result without considering the effect of Eq. (6.33), (i.e., the same as in Fig. 6.15). The other lines represent the results considering the Pauli effect estimation, using Eq. (6.33). Note that the Q dependence of the G factor introduces another kinematical variable in the $\mathcal{P}_{out}$ observable. We have chosen this extra variable to be the zenithal angle of the ϕ meson in the Lab frame (θ_ϕ^{Lab}). The dashed and dot-dashed curves represent the results considering the Pauli effect for $\theta_\phi^{Lab} = 0^o$ and 5^o respectively. We can see that significant effects are obtained for large ϕ momenta, what is expectable since large ϕ momenta imply small final nucleon momenta, which are strongly Pauli blocked. The Pauli effect also decreases with the ϕ meson angle because the momentum transfer strongly increases with this angle, and therefore the largest effect is obtained for the ϕ forward direction. Since the ϕ photoproduction is strongly forward peaked, one can expect $\mathcal{P}_{out}$ to be actually somewhere between the dashed and dot-dashed lines in a real experiment.

In Fig. 6.17 we show the A dependence of $\mathcal{P}_{out}$ without including the Pauli correction (solid line) and including it for $\theta_\phi^{Lab} = 0^o$ and 5^o (dashed and dot-dashed lines respectively), all for $P_\phi = 2000$ MeV where the effect is maximum. We observe that the loss of flux due to the Pauli correction is nearly constant in a wide range of the mass number, resulting in a reduction

of around 0.1 in $\mathcal{P}_{out}$ for the forward direction. Nonetheless this effect is relatively smaller for heavier nuclei compared to the ϕ absorption.

The cross sections calculated in this work are inclusive, summing over all possible final nuclear excited states. The coherent cross section, where the final nucleus is the original one, is not included in the calculation. Its evaluation requires a complete knowledge of the spin and isospin dependence of the elementary $\gamma N \to \phi N$ amplitude and a different treatment than the one done here. The coherent and incoherent cross sections can in principle be separated experimentally, as done in the case of pions around the delta energy region [184]. However, this might be difficult at higher energies where one usually has a poorer energy resolution. An alternative to this separation, concerning the present work, is to look for ϕ production at finite angles where the momentum transfer to the nucleus is large and the coherent process can be neglected.

Our argument is as follows. In general, the amplitude for the $\gamma N \to \phi N$ elementary process will have a non-spin-flip (nsf) part and a spin-flip (sf) part, $T_{\gamma N\to\phi N} \approx T_{nsf} + T_{sf}$. The evaluation of the coherent photoproduction cross section involves an average of the amplitude over spin and isospin degrees of freedom - and over the nucleons - and then the spin-flip part of the amplitude vanishes when summing over spin,

$$\sigma_{A,\,coher} \approx \Big| \sum_{m_s, m_t,\, nucleons} T_{\gamma N\to\phi N} \Big|^2 \approx |T_{sf}|^2 \,. \tag{6.34}$$

On the contrary, in the incoherent process, the nsf and the sf parts of the amplitude contribute incoherently to the cross section, namely,

$$\sigma_{A,\,incoher} \approx \sum_{m_s, m_t,\, nucleons} \Big| T_{\gamma N\to\phi N} \Big|^2 \approx |T_{nsf}|^2 + |T_{sf}|^2 \,. \tag{6.35}$$

Therefore, the ratio between the cross sections for coherent and the incoherent processes is

$$\mathcal{R} \equiv \frac{(d\sigma_A/d\Omega)_{coher}}{(d\sigma_A/d\Omega)_{incoher}} \simeq \frac{(d\sigma_A/d\Omega)_{coher}}{A\,(d\sigma/d\Omega)} \simeq \frac{|A\,\mathcal{F}(Q)|^2}{A}\,\frac{|T_{nsf}|^2}{|T_{nsf}|^2 + |T_{sf}|^2} \lesssim |A\,\mathcal{F}(Q)|^2 \,, \tag{6.36}$$

where $Q \equiv |\vec{Q}|$ is the momentum transfer of the nucleon and $\mathcal{F}(Q)$ is the nuclear form factor. Thus $|A\,\mathcal{F}(Q)|^2$ stands for an upper bound of, $\mathcal{R}$, the

ratio of coherent to incoherent nuclear cross sections. If we consider the Pauli-blocking effects on the production mechanism as estimated above, the upper bound for $\mathcal{R}$ is modified as follows,

$$\mathcal{R} \lesssim \frac{|A\,\mathcal{F}(Q)|^2}{A\,G(Q)} \ . \tag{6.37}$$

The nuclear form factor is obtained as the Fourier transform of the density distribution,

$$A\,\mathcal{F}(Q) = \int d^3r\, e^{i\vec{Q}\vec{r}}\rho(\vec{r}) = \frac{4\pi}{Q}\int_0^\infty dr\, r\, \rho(r)\, \sin(Qr) \ . \tag{6.38}$$

We use the 3-parameter-Fermi nuclear density profiles from Ref. [185].

We have studied the obtained upper bound to $\mathcal{R}$ as a function of the photon energy and the ϕ meson angle θ_ϕ^{Lab} for several nuclei. The results are depicted in Fig. 6.18 as contour plots. We did not include in this figure the effect of the Pauli-blocking factor of Eq. (6.33). The result for ^6Li indicates that the upper bound is smaller than 10% for ϕ angles beyond 4.5 degrees or photon energies below 1950 MeV. However it is quite larger for ϕ angles close to the forward direction and higher energies. For ^{12}C the results are similar, although the region where the upper bound is considerable is now smaller. The situation becomes more favorable for heavier nuclei, as *Aluminium* and *Copper*, for which we obtain an upper bound always lower than 10% in the present kinematical conditions.

The inclusion of the estimated Pauli-blocking effect, Eq. (6.37), leads to an enhancement of the predicted upper bound for the coherent to incoherent ratio of around a 20% at most (forward direction and normal nuclear density).

In practical terms, from the experimental point of view, we can say that in nuclei around ^{16}O or heavier and photon energies smaller than 2000 MeV, the coherent contribution is negligible. This discussion may serve to select an experimental setup in which the coherent contribution can be neglected, hence facilitating the interpretation of the data.

6.4 Summary and conclusions

In summary, we have studied the ϕ selfenergy in a cold symmetric nuclear medium, by considering the medium effects over the tadpole and $K\bar{K}$ decay

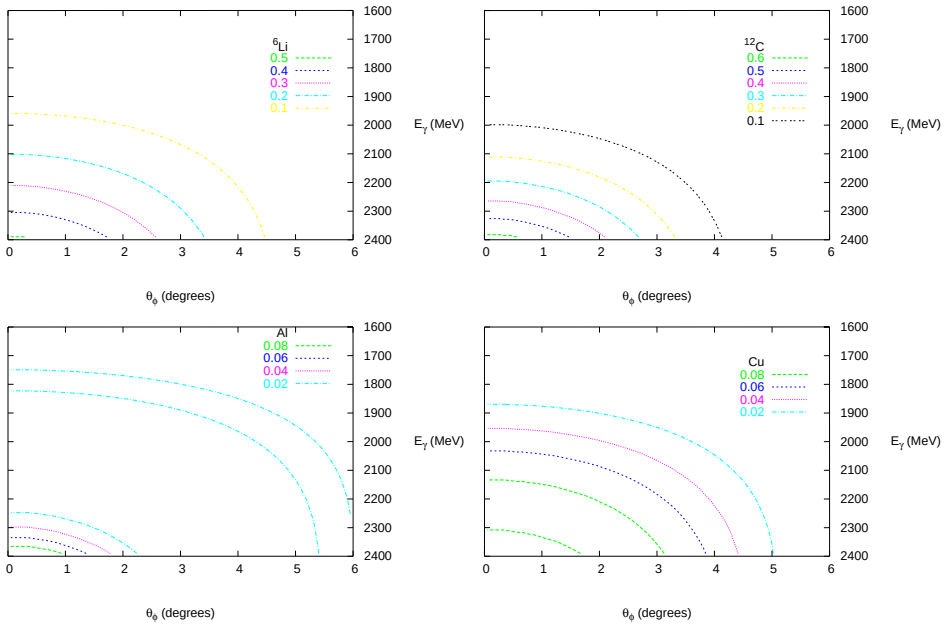

Figure 6.18: Contour plot for the upper bound of $\mathcal{R}$, as a function of the photon energy and the ϕ Lab angle, for several nuclei.

diagrams which dominate the ϕ vacuum selfenergy. This has been done by dressing the kaons with $S-$ and $P-$wave selfenergies. The $S-$wave antikaon selfenergy was obtained in a selfconsistent coupled channel unitary calculation based on effective chiral Lagrangians in which Pauli blocking, pion selfenergy and mean field potentials of the baryons are taken into account. The $P-$ wave is driven by the coupling to hyperon-hole excitations. In addition to these selfenergy insertions we have calculated a set of vertex corrections required by gauge invariance, and we have studied in detail possible violations of transversality in our model due to non-relativistic approximations, which we find to be small. For a ϕ meson at rest with respect to the nuclear medium, we obtain a small mass shift of around 8 MeV and a width of around 30 MeV at normal nuclear density. Thus, the main medium effect on the ϕ meson is the growth of its width by almost one order of magnitude at normal nuclear density. Nevertheless, the ϕ stays narrow enough to be visible as an isolated resonance and it could give a clear signal in possible experiments measuring dilepton or $\bar{K}K$ spectra.

As an application of our results, conveniently extrapolated to finite ϕ momentum, we have studied the survival rate of ϕ's produced in nuclear ϕ photoproduction, and how this survival rate is tied to the ϕ width in the medium and the momentum of the ϕ. The survival rates for ϕ mesons coming from photons in the range of 1.6 to 2.4 GeV are of the order of 0.7, a significant deviation from unity, which in principle should be measurable experimentally. We have shown the A dependence of the expected $\sigma_A/(A\sigma)$ ratio as well as its dependence on the ϕ momentum. Comparison of the results with experimental numbers of the incoming experiments would help determine the accuracy of the present models for the ϕ width in a dense medium. These models could then be used to extrapolate results at other ϕ momenta and one could then get a fair idea of how the ϕ properties are modified in nuclear matter for ϕ's at any finite momenta below those studied in the present work.

Chapter 7

Concluding remarks

The present work illustrates the complexity of the many body physics involved in the renormalization of meson resonances in a nuclear medium. We have studied the most relevant mechanisms, at low nuclear densities, responsible for the modified properties of the low lying meson resonances in the scalar (σ, κ) and vector (ρ, ϕ) sectors. A guiding principle throughout this work has been followed. Namely, the properties of meson resonances in a nuclear medium depend strongly on the light pseudoscalar mesons to which they decay (π, K). An appropriate many body calculation of the pseudoscalar meson selfenergies in the medium is the essential ingredient in the models presented here.

In Chapter 2 we have discussed in some detail the pion and kaon selfenergies in a nuclear medium. In the many body language, the pion selfenergy is mostly driven by the excitation of ph and Δh components due to the πN interaction in $P-$wave. Nuclear short range correlations have been also considered by a suitable resummation of second order diagrams involving the interaction between ph and Δh components, which is described in terms of the Landau-Migdal parameter g'. A Dyson resummation of irreducible selfenergy terms leads to the renormalized pion propagator in the nuclear medium, which we have rewritten in terms of the Lehmann representation relying on the pion spectral function. This spectral representation has been very useful to simplify many calculations in the following chapters, since it clearly exhibits the analytical structure of the pion propagator. As a result of the considered in-medium mechanisms, the pion experiences a strongly at-

tractive potential already at densities of the order of ρ_0. Its spectral function exhibits a very rich structure, widely spread in energy, in which the contribution from ph and Δh modes can be identified. We have also discussed for completeness other contributions to the pion selfenergy which are not relevant in the present work at the energies and small nuclear densities considered. These include the $S-$wave pion selfenergy, the excitation of other nucleon resonances with πN decay modes and higher order mechanisms in the density expansion as the two particle two hole selfenergy.

Concerning the kaon selfenergy, the manifest differences between the KN and $\bar{K}N$ interaction lead to a dramatically different treatment of the nuclear medium effects on the kaon and the antikaon. Whereas a $t\rho$ approximation is usually enough to describe the K selfenergy, due to the soft behaviour of the KN interaction at low energies, the $\bar{K}N$ system is strongly influenced by the $\Lambda(1405)$ resonance, thus a non-perturbative calculation is advisable. We have discussed a recent model of $\bar{K}N$ interaction based on a unitary extension of χPT in coupled channels which, after a selfconsistent treatment of nuclear medium effects, leads to an energy dependent $S-$wave $\bar{K}$ selfenergy consistent with the experimental data from kaonic atoms. The $P-$wave KN interaction also leads to relevant medium effects on the kaon properties. A $P-$wave selfenergy has been discussed from the coupling to Yh excitations, providing sizable corrections to the $\bar{K}$ selfenergy and almost negligible effects in the case of the K. The meson baryon chiral Lagrangian has been used to obtain the interaction vertices. In this case, a unitarization of the tree level KN amplitudes does not improve the calculation, since the $P-$wave interaction does not provide the necessary strength to generate a resonance state, as it has been shown elsewhere. As we did for the pion, we have stated the spectral representation of the kaon propagator in terms of the spectral functions for the kaon and the antikaon.

In Chapters 3 and 4 we have studied the scalar ($L = 0$) mesons σ and κ propagating in a nuclear medium. These resonances couple to the $\pi\pi$ and $K\pi$ meson systems in the isospin 0 and 1/2 channels, respectively. We have started from a common description of the meson meson scattering amplitudes in the scalar sector by means of a coupled channel chiral unitary model. This model is based on the solution of a Bethe Salpeter equation which iterates

the lowest order meson meson interaction from the chiral Lagrangian. The scalar resonances are dynamically generated in the present approach, out of the pseudoscalar degrees of freedom, and appear as poles in the scattering amplitudes on the unphysical Riemann sheet. After considering the medium effects for the pion, which eventually amount to using the renormalized pion propagator in the two-meson loop function of the scattering amplitude, we find a strongly modified $\pi\pi$ amplitude which accumulates a sizable amount of strength at energies around and below the two pion threshold, as the nuclear density is increased. We have investigated if this behaviour could be reflecting a migration of the σ pole towards lower energies. To search for this, the $\pi\pi$ amplitude has been continued onto the second Riemann sheet of the complex energy plane. This is possible in a quite simple way, since the analytical structure of the scattering amplitude is provided by the two-meson loop function. This function can be evaluated for complex values of the energy on the unphysical sheet once the discontinuity on the analytical cut (real positive energy axis) is obtained. The σ pole has been found to move to lower energies and approach the real energy axis as the nuclear density increases, what indicates not only a mass reduction but also a decrease of the σ width. At normal nuclear density, the mass from the pole reaches a value of around 250 MeV and a similar value for the decay width is obtained, as compared to the values in free space $M_\sigma = 500$ MeV and $\Gamma_\sigma = 400$ MeV. This behaviour is a consequence of the strongly attractive potential felt by the pion in the nuclear medium. Actually one would expect even a stronger reduction of the σ width at finite densities, given the smaller phase space available for 2π decay as a consequence of the σ mass reduction. However, the open in-medium σ decay channels, as for instance $\sigma \to \pi\, ph$ and $\sigma \to \pi\, \Delta h$, prevent a more drastic reduction in the σ width and the eventual effect is moderate.

We have also taken into account some new in-medium mechanisms not previously considered in the present approach, which according to a chiral counting scheme could be relevant for the $\pi\pi$ interaction in the nuclear medium. We have found, in an approximate calculation of the scattering equation, that these mechanisms have little influence on the position of the σ pole as a function of the nuclear density, leading to similar results as previously found.

We suggest that the observed density effects on the σ properties and particularly on the $\pi\pi$ scattering amplitude could provide a visible signal in experiments producing two pions in the final state which couple in the $I = 0$ channel. A recent calculation of the two-pion photoproduction reaction in nuclei, in which the two-pion final state interactions have been implemented following the model presented here, predicts sizable effects on the two-pion isoscalar invariant mass distribution for several nuclei. Posterior experimental data from the TAPS Collaboration seem to support this prediction, although the theoretical interpretation of the measured effects is still under debate.

The study of the κ meson in Chapter 4 follows the same scheme as done for the σ meson. A novelty with respect to Chapter 3 arises here, namely, the kaon propagator enters the calculation of the $K\pi$ scattering amplitude. In the nuclear medium, the K and the $\bar{K}$ propagators behave rather differently, as discussed in Chapter 2. This implies that the κ properties, which we obtain from the $K\pi$ amplitude, will differ from the ones of the anti-κ, which is generated in $\bar{K}\pi$ scattering. The strong attraction experienced by the pion in the nuclear medium suggests that similar sizable effects of mass and decay width reduction, as obtained for the σ meson, could take place for the κ meson at finite densities. If this happens, given the fact that the anti-kaon is also attracted in the medium, one could expect a dramatic decrease of the κ mass which could lead to a very narrow κ resonance if the mass is reduced below the $K\pi$ threshold for increasing nuclear densities. We also suggest that the differences between the κ and anti-κ properties in the medium could be useful to test the widely different existing models for the antikaon nucleus potential, which however lead to a consistent reproduction of the data from kaonic atoms.

The medium effects have been introduced within the pion and kaon propagators, as discussed in Chapter 2. To look for the κ pole at finite nuclear densities, we have extended the scattering amplitude onto the second Riemann sheet, following a similar procedure as done for the σ meson, by means of the spectral (Lehmann) representation of the pion and kaon propagators. As the density is increased, the κ pole is found to move to lower energies, strongly dominated by the effect of the pion selfenergy, as can be seen by

comparing the pole trajectories for the κ and the anti-κ. Yet, the global differences between the two branches are moderate. Particularly, for the anti-κ mode we find a sizable width reduction, although not enough to provide a clear signal to be observed experimentally. As it happened for the σ in $\pi\pi$ scattering, the available open decay channels in the nuclear medium make up for the mass reduction and the κ width is not drastically reduced. The $K\pi$ scattering amplitudes exhibit sizable modifications reflecting the medium effects on the pseudoscalars and the κ pole behaviour. For instance, the imaginary part of the $\bar{K}\pi$ amplitude is increased below and around the $K\pi$ threshold, as a consequence of the in-medium channels which are open at energies much below $m_K + m_\pi$. Particularly, for the $K\pi$ mode, where the $\bar{K}$ potential has little influence, we have found an accumulation of strength at energies above the $K\pi$ threshold, similar to what is observed for the σ meson in $\pi\pi$ scattering. Experimental efforts to investigate these effects in the $K\pi$ amplitude in reactions leading to a correlated $K\pi$ pair in the final state would be most welcome.

In Chapters 5 and 6 we have carried out the renormalization of the vector meson resonances ρ and ϕ in a nuclear medium. These mesons are considered as suitable tools to explore nuclear matter at high densities. Both ϕ and ρ mesons couple strongly to dilepton pairs, which are barely distorted in their way out of the high density regions taking place in heavy ion collisions or even ordinary nuclei. This offers a cleaner probe of the in-medium properties of the ρ and ϕ, since the dilepton mass spectrum should reflect the spectral shape of the vector mesons decaying in a nuclear medium. On the other hand, the study of ϕ meson decays could provide visible signals of medium effects on the vector mesons, since it does not overlap with other light resonances in the mass spectrum. In addition, as stated in some theoretical calculations, the changes in some of the properties of the ϕ at finite densities are comparatively larger than those of the ρ. Thus, the experimental observation of these properties could be in principle easier, as for instance measuring the K^+K^- spectrum from ϕ decay in nuclei. The study of the ϕ properties in the nuclear medium is also useful to test the kaon nuclear potentials currently discussed in the literature. Unfortunately, the present experiments are not precise enough to provide a clear interpretation of data in terms of changes in the mass

and/or width of vector mesons. Forthcoming experiments (HADES @ GSI) exploring vector meson decays in a nuclear medium from heavy ion collisions could provide better statistics and mass resolution. Alternative methods to evaluate possible signals of in-medium effects in nuclear production reactions of vector mesons have also been recently proposed (Spring8/Osaka, CLAS @ Jefferson Lab).

The ρ meson is studied in Chapter 5 starting from a chiral unitary model of $\pi\pi$ scattering in $L = 1$. The basic meson meson interaction potentials are provided by the lowest order chiral Lagrangian with explicit coupling of bare resonances. The unitarization of the tree level amplitudes is accomplished following the N/D method in coupled channels, which determines the scattering amplitudes in terms of the on-shell tree level amplitudes and the two-meson loop function already used in Chapter 3. The model is parameter free once low energy chiral constraints are imposed, except for a regularization parameter which is set to optimize the physical position of the resonance peak in the scattering amplitudes, and it has been tested versus experimental data for pion and kaon electromagnetic form factors and phase shifts from meson meson scattering with a very accurate reproduction of data in a wide range of energies. We have explored the $\pi\pi$ channel in $I = 1$, where the ρ meson shows up. From former theoretical studies of the ρ in a nuclear medium, we find that a very convenient way to describe the medium modifications of the vector meson is to obtain the ρ selfenergy in a gauge vector field representation. We have shown that both formalisms lead to similar results for the $\pi\pi$ amplitude in vacuum, which can be written in terms of a ρ propagator 'dressed' with a selfenergy term accounting for the ρ coupling to the pions. This selfenergy, responsible for the decay properties of the ρ in vacuum, is found to be equivalent in both formalisms at the one loop level. Our study of medium effects in the ρ meson and the isovector $\pi\pi$ scattering amplitude leads us to evaluate all the possible mechanisms contributing to the ρ selfenergy at finite densities. The essential ingredient is again the $P-$wave pion selfenergy from Chapter 2. However, the gauge principle provides for the present problem additional ρ couplings to the pions, nucleons and Δ's which generate many other selfenergy topologies which have to be considered to fulfill gauge invariance and obtain a transverse ρ selfenergy tensor. We have

discussed most of these topologies in detail. Some of the calculations have been included in the appendixes.

As the nuclear density is increased, the ρ distribution is sizably broadened as new decay channels in the medium open, from the pion excitation of ph and Δh components. In spite of the strongly attractive pion potential, the ρ mass stands barely modified, exhibiting a small shift to higher energies, moderately dependent on the model uncertainties in the pion selfenergy. Amongst other contributions, the consideration of the Δ decay width has important consequences in the ρ spectral function, particularly at low energies. Including explicitly the Δ decay width introduces small violations of gauge invariance, which is an open problem in the literature.

The contribution of N^*h excitations has been found to enhance considerably the spectral strength of the ρ at low energies. At normal nuclear densities the ρ spectral function shows two clear structures, one corresponding to the in-medium broadened ρ, with a width of around 200 MeV, and a second one at lower energies from the N^*h mode. We have discussed about the necessity of a selfconsistent treatment of medium effects, which could be important to explore higher densities than the ones studied in this work. An appropriate calculation of medium effects on the N^* decay modes into $\pi\Delta$ and ρN would lead to a selfconsistent evaluation of the ρ selfenergy and a better determination of the ρ spectral function.

In Chapter 6, the ϕ meson selfenergy in a nuclear medium has been calculated, following a similar scheme as for the ρ selfenergy in Chapter 5. We could have also started from the meson meson scattering amplitude in a chiral unitary approach for the $(L = 1, I = 0)$ channel, where the ϕ shows up. Here we have chosen to obtain the ϕ mass and decay width in the medium directly from the ϕ selfenergy, following a gauge vector Lagrangian approach. This model had been previously used to obtain the ϕ width in a nuclear medium. We have improved the model to account for both the ϕ mass and width at finite densities. The renormalization of the kaon propagators in the nuclear medium is the most important input of the calculation. The spectral representation of the kaon propagators have proved to be very useful to simplify many analytical calculations, leading to eventual easier numerical evaluations. We have payed special attention to estimate possible sources of

small violations of gauge invariance coming from standard non-relativistic approximations in the model, justifying the choice of a certain family of diagrams and neglecting other contributions in the ϕ selfenergy. For a ϕ meson at rest with respect to the nuclear medium, we have obtained sizable contributions to the ϕ decay width from the open medium decay channels $\phi \to K\pi\Lambda h$ and $\phi \to K\pi\Sigma h$, related to the $S-$wave kaon selfenergy, and $\phi \to K\Lambda h$ and $\phi \to K\Sigma^* h$ related to the $P-$wave kaon selfenergy. The final ϕ width at normal nuclear density is about 7 times the free decay width. In spite of such a sizable effect, the ϕ still remains as a narrow resonance. The real part of the ϕ potential leads to a negligibly small mass shift of a few MeV at densities of the order of ρ_0. Recent experimental data from the K^+K^- spectrum in the pA reaction seem to be consistent with this result although a reliable interpretation of these data would require a detailed theoretical study of this reaction.

We have also extended our model for finite ϕ momentum to accommodate a recent experimental proposal to study the ϕ renormalization in a nuclear medium, by means of the ϕ photoproduction reaction in nuclei (Spring8/Osaka). We have studied the survival rate of the emitted ϕ's, which directly depends on the imaginary part of the ϕ selfenergy, and exhibits a particular dependence on the nuclear mass number. We have found survival rates which significantly deviate from unity for several nuclei, which in principle could be measurable experimentally. We have also studied possible experimental setups to avoid the contribution of the coherent ϕ photoproduction, which is not included in our calculation. We have provided estimated upper bounds for the coherent to incoherent cross section ratio, based on a study of the spin structure of the elementary production amplitude and a calculation of the nuclear form factor.

In this work, it has been extensively shown that the renormalization of meson resonances in a nuclear medium is not a trivial task, and a detailed analysis of possible interaction mechanisms with the nuclear medium has to be considered to provide a reliable description of the meson properties at finite nuclear densities. Moreover, the coupling of meson resonances to the light pseudoscalar mesons cannot be ignored, since substantial in-medium changes arise as a consequence of the sizable potentials which these mesons

experience in the medium. We have shown that the use of χPT to impose low energy constraints on the scattering amplitudes together with non-perturbative coupled channel dynamical models which generate the considered meson resonances stands as a suitable framework to study the renormalization of meson resonances in the nuclear medium, which we have carried out with standard techniques of many body Quantum Field Theory.

Appendix A

Nucleon propagator in nuclear matter

We devote this appendix to quote some results of Many Body Theory of use throughout of this work. In writing the following sections we have made extensive use of [11–13, 17].

A.1 Many body fermion systems

A very convenient starting point for the study of a fermion many body system is the non-interacting Fermi sea or Fermi gas. It corresponds to an homogeneous and isotropic ensemble of non-interacting, point-like fermions occupying a continuum of momentum states under the restrictions of the Pauli principle. A Fermi gas is therefore an infinitely extense medium and hence it has no realization in Nature, but it is very appropriate to perform transparent calculations which would become very difficult in finite systems.

Homogeneity implies energy and momentum conservation as a consequence of translational invariance. On the other hand, relativistic covariance is manifestly lost since the Fermi sea establishes a particular reference frame.

Because of Pauli blocking there should be only one fermion in each available state, that is, one fermion in each elementary cell of volume $(2\pi\hbar)^3$ in the configuration space. In the ground state (zero temperature is assumed), all momentum 'levels' or orbitals are filled up to the Fermi momentum k_F, so that the occupation number for a single particle state with momentum $\vec{k}$

is

$$n(\vec{k}) = \begin{cases} 1 & |\vec{k}| \leq k_F \\ 0 & |\vec{k}| > k_F \end{cases} \tag{A.1}$$

In this work we consider nuclear matter to behave as a Fermi gas of nucleons with equal number of protons and neutrons (symmetric nuclear matter), thus the total isospin is null. Each momentum state has additional degeneracies because of the two (equally) possible nucleon spin and isospin orientations. Thus the number N of nucleons in a certain volume V is ($\hbar = 1$)

$$N = 4V \int_{k_F} \frac{d^3k}{(2\pi)^3} = 4V \int \frac{d^3k}{(2\pi)^3} n(\vec{k}) = 4V \frac{4\pi}{3} \frac{k_F^3}{(2\pi)^3} \ , \tag{A.2}$$

and hence the nucleon density is given by [1]

$$\rho \equiv \frac{N}{V} = \frac{2}{3\pi^2} k_F^3 \ . \tag{A.5}$$

In Table A.1 we show characteristic values of the Fermi momentum, density and Fermi energy (defined as $\epsilon_F = \frac{k_F^2}{2M_N}$) for normal nuclear matter.

A.2 The fermion Green's function in the medium

Let $|\phi_0\rangle$ be the ground state of a non-interacting many body fermion system, i.e., a Fermi gas. The spectrum of states of the system can be built up

[1] To account for the number of allowed states we use a large cubical box with sides of length L, so that the volume is $V = L^3$. The boundary conditions on the walls determine the possible eigenvalues for the momentum,

$$k_i = \frac{2\pi}{L} n_i \ , \tag{A.3}$$

with $i = x, y, z$ and $n_i \in \mathbb{Z}$. Proceeding from a finite box to an infinitely extense system means that the momentum takes eigenvalues in the continuum and the sum over momentum states turns into an integral,

$$\sum_{\vec{k}} \equiv \sum_{n_i} \longrightarrow \left(\frac{L}{2\pi}\right)^3 \int d^3k = V \int \frac{d^3k}{(2\pi)^3} \ . \tag{A.4}$$

To obtain the nucleon density, the limit $L \to \infty$ ($V \to \infty$), $N \to \infty$ with N/V finite is performed.

k_F (MeV)	ρ_0 (fm^{-3})	ϵ_F (MeV)
269	0.17	38

Table A.1: Characteristic values defining normal nuclear matter.

from the vacuum by defining the corresponding creation and annihilation operators. Denoting them by $a_k^\dagger$, a_k we have

$$a_{k_i}|(N_1,...,N_{i-1},N_i,N_{i+1},...)\rangle = \begin{cases} (-1)^{\nu_i}|(N_1,...,N_{i-1},0,N_{i+1},...)\rangle & N_i = 1 \\ 0 & \text{otherwise} \end{cases}$$
$$a_{k_i}^\dagger|(N_1,...,N_{i-1},N_i,N_{i+1},...)\rangle = \begin{cases} (-1)^{\nu_i}|(N_1,...,N_{i-1},1,N_{i+1},...)\rangle & N_i = 0 \\ 0 & \text{otherwise} \end{cases} \tag{A.6}$$

where ν_i is the number of states occupied before the state i. These operators satisfy the usual anticommutation relations for fermions

$$\begin{aligned} \{a_k, a_{k'}^\dagger\} &= \delta_{\vec{k},\vec{k'}} \\ \{a_k, a_{k'}\} &= 0 \\ \{a_k^\dagger, a_{k'}^\dagger\} &= 0 \ . \end{aligned} \tag{A.7}$$

In the previous equations we have used the notation N_1, N_2,... for the occupation number of the orbitals labeled as $1, 2$,... We are considering these orbitals to be ordered by increasing energy, being E_i the monoparticular solution for the energy eigenvalue problem, and $E_1 < E_2 < ... < E_n$ with $E_n = \epsilon_F$ the Fermi energy associated to the state with momentum k_F. For simplicity we adopted here a notation of discrete momentum, as if working in a box of arbitrary volume V (the limit to the continuum is straightforward).

In Many Body Theory it is customary to make a distinction between the occupied and unoccupied states. In this way it is very convenient to introduce the creation and annihilation operators of the type a, b, defined such that

$$\left.\begin{aligned} a_k &\equiv a_k(\text{generic}) \\ a_k^\dagger &\equiv a_k^\dagger(\text{generic}) \end{aligned}\right\} |\vec{k}| > k_F$$
$$\left.\begin{aligned} b_k &\equiv a_k^\dagger(\text{generic}) \\ b_k^\dagger &\equiv a_k(\text{generic}) \end{aligned}\right\} |\vec{k}| \leq k_F \ . \tag{A.8}$$

Hence $b_k^\dagger$ destroys a particle below the Fermi sea or equivalently creates a hole in the Fermi sea. On the contrary b_k creates a particle below the Fermi sea or equivalently destroys a hole in the Fermi sea. In terms of these a, b operators the anticommutation relations read

$$\begin{aligned} \{a_k^\dagger, b_{k'}\} = \{a_k, b_{k'}^\dagger\} = \{a_k^\dagger, b_{k'}^\dagger\} &= 0 \\ \{a_k, a_{k'}^\dagger\} &= \delta_{\vec{k},\vec{k'}} \\ \{b_k, b_{k'}^\dagger\} &= \delta_{\vec{k},\vec{k'}} \ , \end{aligned} \tag{A.9}$$

so non-vanishing relations involve only either particle-like or hole-like operators.

The fermion field operators $\Psi(x)$, $\overline{\Psi}(x)$ are given by (λ labels spin)

$$\begin{aligned} \Psi(x) &= \sum_{\lambda,\, k} \mathcal{N}\{a_{\lambda\, k} u_\lambda(\vec{k}) e^{-ikx} + d_{\lambda\, k}^\dagger v_\lambda(\vec{k}) e^{ikx}\} \\ \overline{\Psi}(x) &= \sum_{\lambda,\, k} \mathcal{N}\{a_{\lambda\, k}^\dagger \overline{u}_\lambda(\vec{k}) e^{ikx} + d_{\lambda\, k} \overline{v}_\lambda(\vec{k}) e^{-ikx}\} \end{aligned} \tag{A.10}$$

where $\mathcal{N}$ is the appropriate normalization constant in the box, d, $d^\dagger$ are the antifermion creation and annihilation operators, respectively, and u_λ, v_λ are the Dirac spinors,

$$u_\lambda(\vec{k}) = \sqrt{E_k + M_N} \begin{pmatrix} \chi_\lambda \\ \frac{\vec{\sigma}\vec{k}}{E_k + M_N}\, \chi_\lambda \end{pmatrix} \quad , \quad v_\lambda(\vec{k}) = \sqrt{E_k + M_N} \begin{pmatrix} \frac{\vec{\sigma}\vec{k}}{E_k + M_N}\, \chi_\lambda \\ \chi_\lambda \end{pmatrix} \tag{A.11}$$

with $E_k = \sqrt{\vec{k}^{\,2} + M_N^2}$ and M_N the nucleon mass, and $\{\chi_\lambda\}$ a spin basis. The pieces containing the fermion operators a, $a^\dagger$ in Eq. (A.10), which we denote by $\Psi^{(+)}$ and $\overline{\Psi}^{(-)}$ respectively, can be rewritten in terms of the a, b operators introduced above and they read

$$\begin{aligned} \Psi(x)^{(+)} &= \sum_{\lambda,\, |\vec{k}| > k_F} \mathcal{N}\, a_{\lambda\, k} u_\lambda(\vec{k}) e^{-ikx} + \sum_{\lambda,\, |\vec{k}| \le k_F} \mathcal{N}\, b_{\lambda\, k}^\dagger u_\lambda(\vec{k}) e^{-ikx} \\ \overline{\Psi}(x)^{(-)} &= \sum_{\lambda,\, |\vec{k}| > k_F} \mathcal{N}\, a_{\lambda\, k}^\dagger \overline{u}_\lambda(\vec{k}) e^{ikx} + \sum_{\lambda,\, |\vec{k}| \le k_F} \mathcal{N}\, b_{\lambda\, k} \overline{u}_\lambda(\vec{k}) e^{ikx} \ . \end{aligned} \tag{A.12}$$

Although we have expanded the fermion field operators in a base of free solutions of the Dirac equation, this expansion could be performed in a certain

orthonormal basis of wave functions in general different from the plane wave basis. The use of the plane wave basis does not mean a loss of generality even in the presence of interactions, since one can always work in the Interaction picture and then the fermion field operators keep on satisfying the free Dirac equation.

The introduction of the a, b operators has some advantages as we explain below. Recall that we defined $|\phi_0\rangle$ as the ground state of the non-interacting Fermi sea, with all the orbitals filled up to the Fermi momentum k_F. The a, b operators satisfy the property

$$\begin{aligned} a_k|\phi_0\rangle &= 0 \\ b_k|\phi_0\rangle &= 0, \end{aligned} \tag{A.13}$$

which reflects the fact that $|\phi_0\rangle$ contains no occupied states for $|\vec{k}| > k_F$ to be destroyed by a_k, and contains no hole states ($|\vec{k}| \leq k_F$) to be destroyed by b_k, since all these states are occupied in $|\phi_0\rangle$. Thus all annihilation operators of the type a, b acting on the uncorrelated Fermi sea vanish. This is extremely advantageous for perturbative calculations in many body fermion systems. The idea is to shift the vacuum state $|0\rangle$ and elaborate a perturbation theory around the $|\phi_0\rangle$ state. Having into account the property in Eq. (A.13), the only non-vanishing contributions to any perturbative calculation involving a $\langle\phi_0|...|\phi_0\rangle$ matrix element (e.g. Green function, one-body operator expectation values, spectrum of excited states of the system) come from fully contracted terms in the Wick expansion.

We introduce the Green's function of the system as follows:

$$iG(x,x') = \frac{\langle\Psi_0|T\{\Psi_H(x)\,\overline{\Psi}_H(x)\}|\Psi_0\rangle}{\langle\Psi_0|\Psi_0\rangle} \ . \tag{A.14}$$

Here $|\Psi_0\rangle$ represents the ground state of the fully interacting many body fermion system, and $\Psi_H(x)$ is the fermion field operator in the Heisenberg picture, H the Hamiltonian of the system, and $T\{...\}$ stands for the standard time ordered product operator.

The evaluation of the fermion Green's function or propagator for a non-interacting Fermi sea is very instructive and provides the lowest order approximation to the full Green's function of the many body system. In this

case $|\Psi_0\rangle = |\phi_0\rangle$ and $H = H_0$, therefore the Heisenberg and Interaction pictures coincide. Translational invariance implies that $G(x,x') = G(x-x')$, and this suggests to work with the Fourier transform into the momentum space, leading to (the limit to infinitely extense medium is implicit)

$$iG(x,x') \equiv iG(x-x') = \int \frac{d^4k}{(2\pi)^4} e^{-ik(x-x')} iG(k) \ . \tag{A.15}$$

The result of the calculation in momentum space for the non-interacting Fermi sea is

$$\begin{aligned} G^0(k) &= \frac{\Theta(|\vec{k}|-k_f)}{\not{k}-m+i\epsilon} + \frac{\Theta(k_f-|\vec{k}|)}{\not{k}-m-i\epsilon} \\ &= \frac{1-n(\vec{k})}{\not{k}-m+i\epsilon} + \frac{n(\vec{k})}{\not{k}-m-i\epsilon} \ , \end{aligned} \tag{A.16}$$

according to Eq. (A.1). This result can be rewritten as follows:

$$\begin{aligned} G^0(k) &= (\not{k}+m)\left[\frac{1}{k^2-m^2+i\epsilon} + 2\pi i\, n(\vec{k})\,\delta(k^2-m^2)\Theta(k^0)\right] \\ &= (\not{k}+m)\left[\frac{1}{(k^0)^2-\omega_k^2+i\epsilon} + 2\pi i\,\frac{n(\vec{k})}{2\omega_k}\,\delta(k^0-\omega_k)\Theta(k^0)\right] \ , \end{aligned} \tag{A.17}$$

by means of the complex variable result $\frac{1}{f(x)\pm i\epsilon} = \mathcal{P}\left(\frac{1}{f(x)}\right) \mp i\pi\delta(f(x))$. In the previous expression ω_k is the energy corresponding to the single particle state of momentum $\vec{k}$ for the H_0 Hamiltonian.

We can perform a nonrelativistic approximation to Eq. (A.17) for a Fermi sea of nucleons. To do this we first separate the contributions of the positive and negative energy parts of the propagator, by means of the following identity:

$$\frac{1}{\not{k}-M_N+i\epsilon} = \frac{1}{2E_k}\,\frac{\sum_\lambda u_\lambda(\vec{k})\overline{u}_\lambda(\vec{k})}{k^0-E_k+i\epsilon} + \frac{1}{2E_k}\,\frac{\sum_\lambda v_\lambda(-\vec{k})\overline{v}_\lambda(-\vec{k})}{k^0+E_k-i\epsilon} \ , \tag{A.18}$$

with $E_k = \sqrt{\vec{k}^{\,2}+M_N^2}$ and $\not{k}+M_N = \sum_\lambda u_\lambda(\vec{k})\overline{u}_\lambda(\vec{k})$, according to the normalization in Eq. (A.11). Using Eqs. (A.17) and (A.18) we find

$$G^0(k) = \frac{1-n(\vec{k})}{2E_k}\,\frac{\sum_\lambda u_\lambda(\vec{k})\overline{u}_\lambda(\vec{k})}{k^0-E_k+i\epsilon} + \frac{n(\vec{k})}{2E_k}\,\frac{\sum_\lambda u_\lambda(\vec{k})\overline{u}_\lambda(\vec{k})}{k^0-E_k-i\epsilon}$$

$$+\frac{1}{2E_k}\,\frac{\sum_\lambda v_\lambda(-\vec{k})\overline{v}_\lambda(-\vec{k})}{k^0+E_k-i\epsilon}\ . \qquad \text{(A.19)}$$

The corresponding nonrelativistic reduction in the Lab frame consists of neglecting the negative energy term in Eq. (A.19). In addition we take $E_k \simeq M_N$ everywhere but in the pole terms, where we use $E_k \simeq M_N + \vec{k}^{\,2}/2M_N$. Omitting the spin-isospin structure, we are lead to

$$\begin{aligned} G^0(\omega,\vec{k}) &= \frac{1-n(\vec{k})}{\omega-\omega_k+i\epsilon}+\frac{n(\vec{k})}{\omega-\omega_k-i\epsilon} \\ &= \frac{1}{\omega-\omega_k+i\epsilon}+2\pi i\, n(\vec{k})\,\delta(\omega-\omega_k)\ . \end{aligned} \qquad \text{(A.20)}$$

Note that in the first line of Eq. (A.20), the first piece of G^0 corresponds to a particle propagating above the Fermi surface, while the second term corresponds to a hole propagating inside the Fermi sea. In the second line we observe that G^0 separates into a free fermion propagator plus a genuine many body correction (the term with the delta function) which only contributes for momenta below k_F. For virtual nucleons ($k^0 \neq \omega_k$) G^0 coincides with the free propagator, and the same occurs for complex k^0.

The hole propagator behaves like the antiparticle propagator in the vacuum space, and indeed it shares its analytical properties. One can think in terms of the Dirac sea and apply this image to our case. Now we do not have positive and negative energy states but states above or below the Fermi surface, and we deal with particle-hole excitations instead of particle-antiparticle pairs. To take into account both phenomena one has to extend the Dirac sea so that all the states are filled up to the Fermi energy. A pictorial description is shown in Fig. A.1.

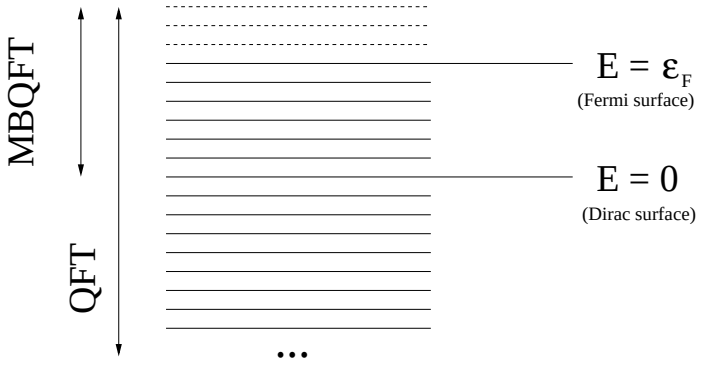

Figure A.1: Pictorial view of the Dirac and Fermi seas.

Appendix B

Lindhard functions

We quote in this appendix analytical expressions for the different Lindhard functions used in this work. The following results hold for a symmetric nuclear medium.

The nuclear Lindhard function (Eq. (2.7)) reads, after performing the integrals over the nucleon loop momentum, as follows

$$U_N(q^0,\vec{q};\rho)=\frac{3}{2}\rho\frac{M_N}{qk_F}\Big[z+\frac{1}{2}(1-z^2)\log\frac{z+1}{z-1}+z'+\frac{1}{2}(1-z'^2)\log\frac{z'+1}{z'-1}\Big]\,, \tag{B.1}$$

with

$$z=\frac{M_N}{qk_F}\left[q^0-\frac{q^2}{2M_N}\right]\ ,\ z'=\frac{M_N}{qk_F}\left[-q^0-\frac{q^2}{2M_N}\right]\ , \tag{B.2}$$

q stands for $|\vec{q}|$ here, and $\rho=\frac{2}{3\pi^2}k_F^3$. The valuation of the logarithm has to be chosen appropriately to provide the correct sign for the imaginary part of U_N. The real part of U_N is provided by Eq. (B.1) taking the modulus of the argument in the logarithms. The imaginary part of U_N is given by

$$\mathrm{Im}\,U_N(q^0,\vec{q};\rho)=-\frac{3}{4}\pi\rho\frac{M_N}{qk_F}\Big[(1-z^2)\Theta(1-|z|)-(1-z'^2)\Theta(1-|z'|)\Big]\frac{q^0}{|q^0|}\,. \tag{B.3}$$

The Δh Lindhard function, which can be also derived from Chapter 2, is given after some approximations [13] by

$$U_\Delta(q^0,\vec{q};\rho)=\frac{2}{3}\left(\frac{f^*_\Delta}{f_N}\right)^2\rho\frac{M_\Delta}{qk_F}\Big[z_\Delta+\frac{1}{2}(1-z_\Delta^2)\log\frac{z_\Delta+1}{z_\Delta-1}+z'_\Delta+\frac{1}{2}(1-z'^2_\Delta)\log\frac{z'_\Delta+1}{z'_\Delta-1}\Big]\,, \tag{B.4}$$

with

$$\begin{aligned} z_\Delta &= \frac{M_\Delta}{qk_F}\left[q^0 - \frac{q^2}{2M_\Delta} - \omega_R + \frac{i}{2}\Gamma_\Delta(q^0,\vec{q})\right] \ , \\ z'_\Delta &= \frac{M_\Delta}{qk_F}\left[-q^0 - \frac{q^2}{2M_\Delta} - \omega_R + \frac{i}{2}\Gamma_\Delta(-q^0,\vec{q})\right] \ , \end{aligned} \tag{B.5}$$

where $\omega_R = M_\Delta - M_N$ and the Δ width is given by

$$\begin{aligned} \Gamma_\Delta(q) &= \frac{1}{3}\frac{1}{4\pi}\left(\frac{f^*_\Delta}{m_\pi}\right)^2 \frac{q^3_{cm}}{\sqrt{s_\Delta}}(M_N + \sqrt{M_N^2 + q^2_{cm}})\Theta(\sqrt{s_\Delta} - M_N - m_\pi) \ , \\ s_\Delta &= M_N^2 + (q^0)^2 - \vec{q}^{\,2} + 2q^0\sqrt{M_N^2 + \frac{3}{5}k_F^2} \ , \\ q_{cm} &= \lambda^{1/2}(s_\Delta, M_N^2, m_\pi^2)/2\sqrt{s_\Delta} \ . \end{aligned} \tag{B.6}$$

The previous expressions of Lindhard functions hold, for q^0 in the complex plane, for U_N and also for U_Δ in the case of $\Gamma_\Delta(q) = 0$.

We also quote in this appendix the nuclear Lindhard function with an energy gap Δ, explicitly separated into the direct and crossed contributions, $U_N = U_d + U_c$. From [85] we have

$$U_d(q^0,\vec{q},\Delta;\rho) = 4\int \frac{d^3p}{(2\pi)^3}\frac{n(\vec{p})[1-n(\vec{p}+\vec{q})]}{q^0 + \varepsilon(\vec{p}) - \varepsilon(\vec{p}+\vec{q}) - \Delta + i\epsilon} \tag{B.7}$$

and $U_c(q^0,\vec{q},\Delta;\rho) \equiv U_d(-q^0,\vec{q},\Delta;\rho)$. We use the same notation U_N for the nuclear Lindhard with a gap, and explicitly include the energy gap Δ in the arguments of the function to distinguish between them. We shall use the definitions

$$x = \frac{q}{k_F} \ , \ \ \nu = \frac{2M_N q^0}{k_F^2} \ , \ \ \delta = \frac{2M_N\Delta}{k_F^2} \ . \tag{B.8}$$

Once the integration in Eq. (B.7) is done, the real part of U_d reads, for $x \leq 2$,

$$\begin{aligned} \mathrm{Re}\, U_d(q^0,\vec{q},\Delta;\rho) &= -\frac{2M_N k_F}{\pi^2}\frac{1}{2x}\Big\{\frac{x}{2} - \frac{\nu-\delta}{4} + \frac{\nu-\delta}{2}\ln\Big|\frac{\nu-\delta+x^2-2x}{\nu-\delta}\Big| \\ &+ \frac{1}{2}\left[1 - \frac{1}{4}\left(\frac{\nu-\delta}{x} - x\right)^2\right]\ln\Big|\frac{\nu-\delta-x^2-2x}{\nu-\delta+x^2-2x}\Big|\Big\} \end{aligned} \tag{B.9}$$

and, for $x > 2$,

$$\begin{aligned} \mathrm{Re}\, U_d(q^0,\vec{q},\Delta;\rho) &= -\frac{2M_N k_F}{\pi^2}\frac{1}{2x}\Big\{\frac{-\nu+\delta+x^2}{2x} \\ &+ \frac{1}{2}\left[1 - \frac{1}{4}\left(\frac{\nu-\delta}{x} - x\right)^2\right]\ln\Big|\frac{\nu-\delta-x^2-2x}{\nu-\delta-x^2+2x}\Big|\Big\} \end{aligned} \tag{B.10}$$

The imaginary part of U_d is given by $\mathrm{Im}\, U_d(q^0,\vec{q},\Delta;\rho) = \mathrm{Im}\, \tilde{U}(q^0-\Delta,\vec{q};\rho) \times \Theta(q^0-\Delta)$, with

$$\mathrm{Im}\, \tilde{U}(q^0,\vec{q};\rho) = -\frac{3}{4}\pi\rho\frac{M_N}{qk_F}\Big[(1-z^2)\Theta(1-|z|) - (1-z'^{\,2})\Theta(1-|z'|)\Big]\frac{q^0}{|q^0|} \ , \tag{B.11}$$

where the z, z' variables are defined in Eq. (B.2).

The Yh Lindhard function, U_Y, only contains the contribution from direct terms, associated to the $\bar{K}$ $P-$wave selfenergy. The crossed terms are associated to the K, and can be obtained from the following expressions by changing $q^0 \to -q^0$. We provide here the real and imaginary parts separately, although a compact expression in terms of complex logarithms can be used, provided that a suitable prescription for the imaginary part is given. The real part of U_Y reads

$$\mathrm{Re}\, U_Y(q^0,\vec{q};\rho) = \frac{3}{2}\rho\frac{M_Y}{qk_F}\Big[z_Y + \frac{1}{2}(1-z_Y^2)\log\Big|\frac{z_Y+1}{z_Y-1}\Big|\Big] \ , \tag{B.12}$$

with z_Y given by

$$z_Y = \frac{M_Y}{qk_F}\left[q^0 - \frac{q^2}{2M_Y} - (M_Y - M_N)\right] \ , \tag{B.13}$$

and for the imaginary part we have

$$\mathrm{Im}\, U_Y(q^0,\vec{q};\rho) = -\pi\frac{3}{4}\rho\frac{M_Y}{qk_F}\left[(1-z_Y^2)\Theta(1-|z_Y|)\right] \ . \tag{B.14}$$

We provide now the analytic expression for the Lindhard function corresponding to the $N^*(1520)h$ excitation by a ρ meson, quoted in Eq. (5.47), after some approximations:

$$U_{N^*}(q^0,\vec{q};\rho) = \frac{3}{2}\rho\frac{M_{N^*}}{qk_F}\Big[z_{N^*} + \frac{1}{2}(1-z_{N^*}^2)\log\frac{z_{N^*}+1}{z_{N^*}-1} + z'_{N^*} + \frac{1}{2}(1-z'^2_{N^*})\log\frac{z'_{N^*}+1}{z'_{N^*}-1}\Big], \tag{B.15}$$

with the z_{N^*} and z'_{N^*} functions defined as

$$\begin{aligned} z_{N^*} &= \frac{M_{N^*}}{qk_F}\left[q^0 - \frac{q^2}{2M_{N^*}} - (M_{N^*}-M_N) + \frac{i}{2}\Gamma_{N^*}(q^0,\vec{q})\right] \ , \\ z'_{N^*} &= \frac{M_{N^*}}{qk_F}\left[-q^0 - \frac{q^2}{2M_{N^*}} - (M_{N^*}-M_N) + \frac{i}{2}\Gamma_{N^*}(-q^0,\vec{q})\right] \ . \end{aligned} \tag{B.16}$$

Eq. (B.16) includes the information of the N^* decay width, which can be found in [151]. The limit of Eq. (B.15) when $\vec{q} \to \vec{0}$, which is required in Chapter 5, is given by

$$U_{N^*}(q^0, \vec{0}; \rho) = \rho \left[\frac{1}{q^0 - (M_{N^*} - M_N) + \frac{i}{2}\Gamma(q^0, \vec{0})} + \frac{1}{-q^0 - (M_{N^*} - M_N)} \right] . \tag{B.17}$$

Appendix C

Chiral Lagrangians

The lowest order chiral Lagrangian for the pseudoscalar meson octet interactions is given by

$$\mathcal{L}_2 = \frac{f^2}{4}\langle \partial_\mu U^\dagger \partial^\mu U + M(U + U^\dagger)\rangle \ , \tag{C.1}$$

where $\langle\rangle$ stands for the trace in flavour space, f is the pion decay constant, and U reads

$$U(\Phi) = \exp(i\sqrt{2}\Phi/f) \ . \tag{C.2}$$

Φ and M are the $SU(3)$ matrices for the pseudoscalar meson fields and the meson masses in the isospin limit, respectively,

$$\begin{aligned} \Phi \equiv \frac{\vec{\lambda}}{\sqrt{2}}\vec{\phi} &= \begin{pmatrix} \frac{1}{\sqrt{2}}\pi^0 + \frac{1}{\sqrt{6}}\eta & \pi^+ & K^+ \\ \pi^- & -\frac{1}{\sqrt{2}}\pi^0 + \frac{1}{\sqrt{6}}\eta & K^0 \\ K^- & \bar{K}^0 & -\frac{2}{\sqrt{6}}\eta \end{pmatrix} \ , \\ M &= \begin{pmatrix} m_\pi^2 & 0 & 0 \\ 0 & m_\pi^2 & 0 \\ 0 & 0 & 2m_K^2 - m_\pi^2 \end{pmatrix} \ . \end{aligned} \tag{C.3}$$

If we expand for the minimal number of meson fields we obtain for $\mathcal{L}_2$

$$\mathcal{L}_2 = \frac{1}{12f^2}\langle (\partial_\mu \Phi\Phi - \Phi\partial_\mu\Phi)^2 + M\Phi^4 \rangle \ . \tag{C.4}$$

The general chiral Lagrangian containing the interactions between the pseudoscalar meson octet and the $1/2^+$ baryon octet reads

$$\begin{aligned}
\mathcal{L}_1^{(B)} &= \langle \bar{B} i\gamma^\mu \nabla_\mu B\rangle - M_B\langle \bar{B}B\rangle \\
&+ \frac{D+F}{2}\langle \bar{B}\gamma^\mu\gamma_5 u_\mu B\rangle + \frac{D-F}{2}\langle \bar{B}\gamma^\mu\gamma_5 B u_\mu\,\rangle \\
&= \langle \bar{B} i\gamma^\mu \nabla_\mu B\rangle - M_B\langle \bar{B}B\rangle \\
&+ \frac{1}{2}D\langle \bar{B}\gamma^\mu\gamma_5\,\{u_\mu, B\}\rangle + \frac{1}{2}F\langle \bar{B}\gamma^\mu\gamma_5[u_\mu, B]\rangle \ , \qquad \text{(C.5)}
\end{aligned}$$

according to the following notation,

$$\begin{aligned}
\nabla_\mu B &= \partial_\mu B + [\Gamma_\mu, B] \\
\Gamma_\mu &= \frac{1}{2}(u^+\partial_\mu u + u\partial_\mu u^+) \\
U &= u^2 = \exp(i\sqrt{2}\Phi/f) \\
u_\mu &= iu^+\partial_\mu U u^+ \ , \qquad \text{(C.6)}
\end{aligned}$$

with the baryon field matrix given by

$$B = \begin{pmatrix} \frac{1}{\sqrt{2}}\Sigma^0 + \frac{1}{\sqrt{6}}\Lambda & \Sigma^+ & p \\ \Sigma^- & -\frac{1}{\sqrt{2}}\Sigma^0 + \frac{1}{\sqrt{6}}\Lambda & n \\ \Xi^- & \Xi^0 & -\frac{2}{\sqrt{6}}\Lambda \end{pmatrix} \ . \qquad \text{(C.7)}$$

At lowest order in momentum, the meson baryon $S-$wave interaction Lagrangian ($MMBB$ vertices) comes from the Γ_μ term in the covariant derivative, namely

$$\mathcal{L}_1^{(B)} = \langle \bar{B} i\gamma^\mu \frac{1}{4f^2}[(\Phi\partial_\mu\Phi - \partial_\mu\Phi\Phi)B - B(\Phi\partial_\mu\Phi - \partial_\mu\Phi\Phi)]\rangle \ . \qquad \text{(C.8)}$$

The $P-$wave interactions (MBB vertices) arise from the terms tied to the D and F couplings. Particularly, restricting to nucleon degrees of freedom, the baryon field matrix reads

$$B = \begin{pmatrix} 0 & 0 & p \\ 0 & 0 & n \\ 0 & 0 & 0 \end{pmatrix} \ , \qquad \text{(C.9)}$$

and the Lagrangian term is given by

$$\begin{aligned}\mathcal{L}_1^{(B)} &= \frac{D+F}{2}(\bar{p}\gamma^\mu\gamma_5 u_\mu^{11} p + \bar{n}\gamma^\mu\gamma_5 u_\mu^{22} n + \bar{n}\gamma^\mu\gamma_5 u_\mu^{21} p + \bar{p}\gamma^\mu\gamma_5 u_\mu^{12} n) \\ &+ \frac{D-F}{2}(\bar{p}\gamma^\mu\gamma_5 u_\mu^{33} + \bar{n}\gamma^\mu\gamma_5 u_\mu^{33} n)\,, \end{aligned} \tag{C.10}$$

where u_μ^{ij} denotes the ij element of the u_μ matrix, given as

$$u_\mu = -\frac{\sqrt{2}}{f}\partial_\mu\Phi + \frac{\sqrt{2}}{12f^3}(\partial_\mu\Phi\Phi^2 - 2\Phi\partial_\mu\Phi\Phi + \Phi^2\partial_\mu\Phi) + O(\Phi^5)\,. \tag{C.11}$$

In the previous equation we have explicitly expanded u_μ up to three meson fields as required in Chapter 3.

Appendix D

Calculation of some diagrams in $(I, J) = (0, 0)$ scattering

The amplitude corresponding to the diagram in Fig. D.1 is given by

$$-i\mathcal{T}(P^0, \rho) = \int \frac{d^4q}{(2\pi)^4}(-i\tilde{t})\frac{i}{(q+p)^2 - m_\pi^2 + i\epsilon}\frac{i}{(q-p')^2 - m_\pi^2 + i\epsilon}(-iV)\, iU_N(q) \ , \tag{D.1}$$

with the momentum labels as shown in the figure and $P^0 = 2p^0$ according to the notation in Chapter 3. In the previous equation $\tilde{t}$ corresponds to the amplitude of the $t-$channel ph exchange between two pions, as defined in Eq. (3.22), and V is the $\pi\pi$ amplitude from the lowest order chiral Lagrangian. In order to perform the integral it is useful to separate $U_N(q)$ into the direct and crossed parts, $U_N(q) = U_d(q) + U_c(q)$, given their different analytical structure.

In Fig. D.2 we depict the pole and cut structure for the different terms

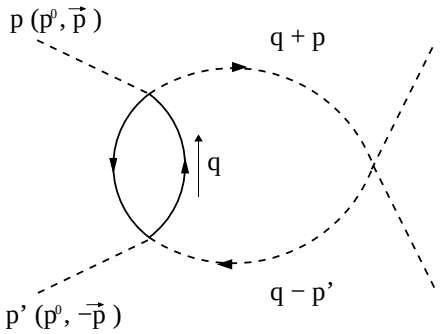

Figure D.1: Loop contribution of the ph exchange in the t channel.

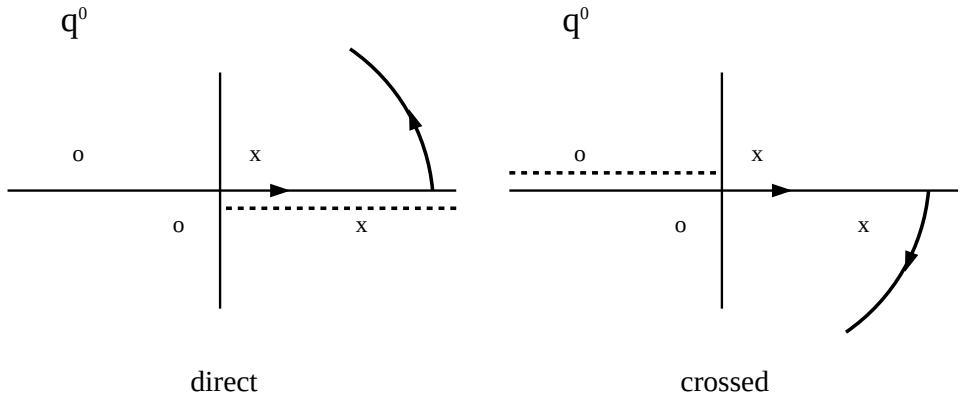

Figure D.2: Analytical structure of the integrand in Eq. D.1. The poles of the pion propagators are represented by 'x' and 'o' symbols, and the dotted lines correspond to the analytical cuts of the Lindhard function. The arrows indicate the circuit used for the integration of each term.

and the selected path for the integration in the complex plane. The poles are located at

$$\begin{aligned} q^0 &= -p^0 + \omega(\vec{p}+\vec{q}) - i\epsilon \ , \ \ q^0 = -p^0 - \omega(\vec{p}+\vec{q}) + i\epsilon \\ q^0 &= p^0 + \omega(\vec{p}+\vec{q}) - i\epsilon \ , \ \ q^0 = p^0 - \omega(\vec{p}+\vec{q}) + i\epsilon \ . \end{aligned} \tag{D.2}$$

The integration over the q^0 variable is done by closing the contour on the upper half plane for the U_d part and on the lower half plane for the U_c part. The result of the integration is

$$\begin{aligned} \mathcal{T}(P^0,\rho) = -\left(\frac{1}{4f^2}\right)^2 (2p^0)^2\, V(P^0) \int \frac{d^3q}{(2\pi)^3}\, \frac{1}{4\omega^2} \Big\{ \frac{U_c(p^0+\omega,\vec{q})}{p^0+\omega} \\ -\frac{U_d(p^0-\omega,\vec{q})}{p^0-\omega+i\epsilon} + \frac{U_d(p^0-\omega,\vec{q}) - U_c(p^0+\omega,\vec{q})}{p^0} \Big\} \Big(\frac{M_\rho^2}{M_\rho^2+\vec{q}^{\,2}}\Big)^2 \ , \end{aligned} \tag{D.3}$$

where $\omega \equiv \omega(\vec{p}+\vec{q}) = \sqrt{(\vec{p}+\vec{q})^2 + m_\pi^2}$ and we have explicitly written the ρ meson exchange form factor arising from each $\pi\pi NN$ vertex.

Note that we have factorized both the $\pi N \to \pi N$ and the $\pi\pi \to \pi\pi$ vertices on shell. This is done in analogy to the on-shell factorization of meson-meson amplitudes in Ref. [29], where it is shown that the off-shell part

of the amplitudes in loop functions contribute to a renormalization of the tree level diagrams (no meson loop). An alternative justification using dispersion relations, which require only the on-shell information, is given in [88]. It is not clear that the same factorization can be done for the present mechanism, and this calculation has to be considered as an on-shell approximation to the full contribution of this diagram.

Appendix E

Calculation of some ρ selfenergy diagrams

We include in this section a set of diagrams which either give a small contribution to the ρ selfenergy or vanish because of symmetry reasons for the particular case of a ρ meson at rest. We have classified the graphs in two sets, depending on the number of pion propagators (zero or one pionic lines), as it is shown in Fig. E.1.

No pion lines

The first vanishing contribution corresponds to the diagram labeled as E.1a, in which a ρ meson directly couples to a ph excitation. This mechanism does not contribute for a ρ meson at rest, since both the particle and the hole have the same momentum. The ρ could be also attached to a Δh excitation. This diagram involves a $\rho N\Delta$ coupling which cannot be derived from the gauge principle by a minimal substitution, since in this case the ρ does not couple to the isospin current (this vertex accounts for an *isovector magnetic transition* [11,133]). In a non-relativistic approximation, the $\rho N\Delta$ vertex has the structure $(\vec{S}\times\vec{P})\,\vec{T}$, with $\vec{P}$ the ρ momentum, and therefore it vanishes for a ρ meson at rest. A similar diagram with a ρ meson coupled to a $\Delta\Delta$ baryon loop could be in principle built in the present model, but this contribution is not existent at zero temperature since we only have a Fermi sea of nucleons and no possibility of Δ thermal excitation.

The previous mechanism, which involves two ρ's coupled to a nucleon bubble, takes into account ρN scattering over all the nucleons of the Fermi

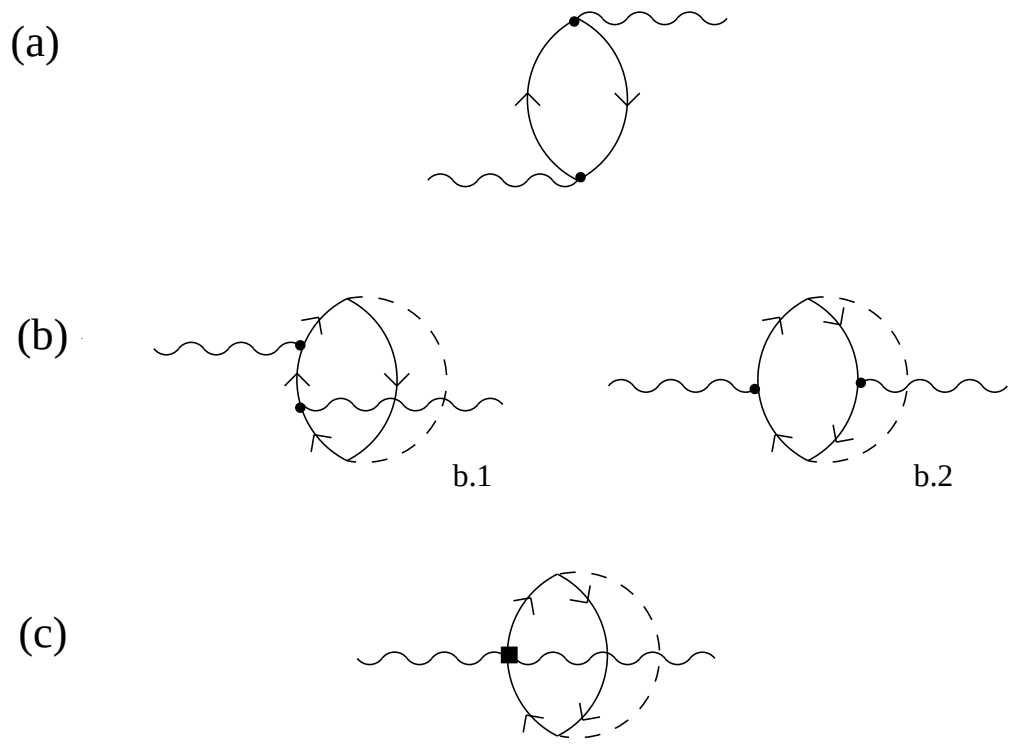

Figure E.1: Medium correction graphs not included in the calculation: sets (a) and (b) involving zero and one pion lines. ρNN, $\rho\Delta\Delta$ vertices are displayed as dots.

sea, as indicated diagrammatically in Fig. E.2a by opening the hole line. If we calculate a non-relativistic approximation of the $\rho N \to \rho N$ amplitude in powers of p/M_N, starting from the relativistic Lagrangian of Eq. (5.36), we obtain the direct and crossed nucleon pole terms with non-relativistic nucleon propagator and ρNN vertices, plus a contact term of order M_N^{-1} which is represented diagrammatically as a $\rho\rho NN$ contact vertex, Fig. E.2b. This was shown in Ref. [133] where this vertex is generated by a minimal substitution in a non-relativistic treatment of the ρNN Lagrangian. If the nucleon lines of this diagram are closed for a many-body calculation, one obtains a nucleon tadpole diagram (Fig. E.3b) which contributes as an additional linear-in-density term of the ρ meson selfenergy, of order M_N^{-1}. The Feynman rule for the $\rho\rho NN$ vertex (Fig. E.3a) can be derived from the $\rho N \to \rho N$ amplitude

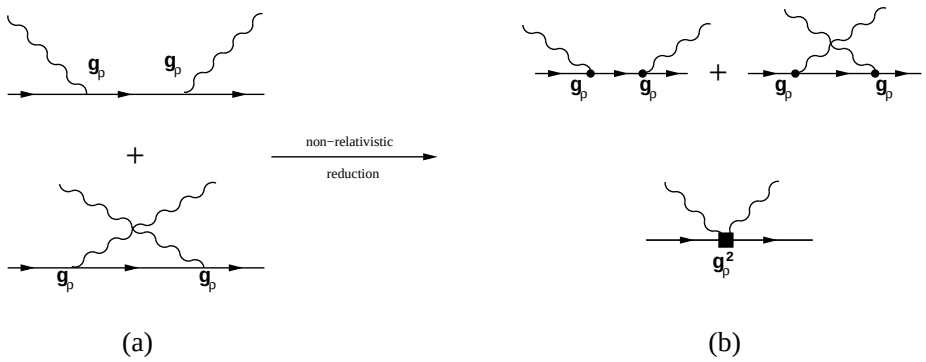

Figure E.2: Diagrammatic representation of the non-relativistic reduction of the $\rho N \to \rho N$ amplitude.

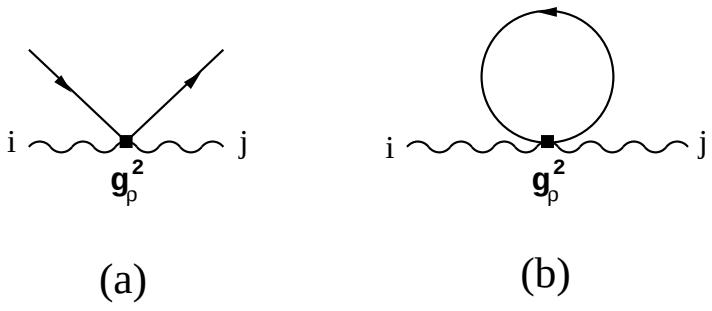

Figure E.3: (a) $\rho\rho NN$ vertex. (b) Nucleon tadpole term.

and it reads, for its spatial components,

$$-it^{ij}_{\rho\rho NN} = -ig_\rho^2 \frac{1}{4}\frac{1}{M_N}\,\delta^{ij}\ . \tag{E.1}$$

The nucleon tadpole term is easily evaluated as

$$\begin{aligned}\Pi^{ij}_{\rho\rho NN}(\rho) &= -i\delta^{ij} g_\rho^2 \frac{1}{M_N}\int \frac{d^4p}{(2\pi)^4}\,\frac{n(\vec{p})}{p^0 - E_N(\vec{p}) - i\epsilon} \\ &= \delta^{ij} g_\rho^2 \frac{1}{M_N}\int \frac{d^3p}{(2\pi)^3}\,n(\vec{p}) = \delta^{ij} g_\rho^2 \frac{1}{4}\frac{1}{M_N}\,\rho\ .\end{aligned} \tag{E.2}$$

The result is an energy independent real selfenergy proportional to the nuclear matter density. Its inclusion as a selfenergy term in the ρ meson propagator leads to a small repulsive shift of a few MeV at normal nuclear density.

One pion line

Here we distribute the graphs in two subsets: both ρ mesons coupled to either a particle or a hole line, Fig. E.1(b.1), and one ρ meson line attached to the particle line and the other one to the hole line, Fig. E.1(b.2).

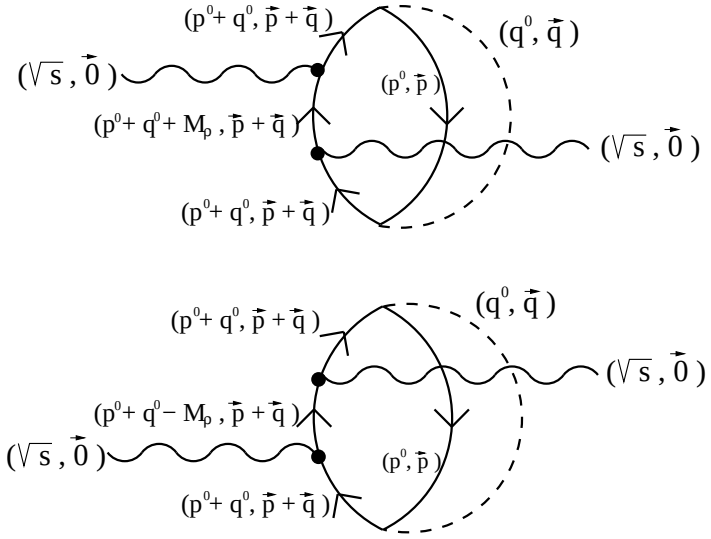

Figure E.4: Momentum labeling of the diagram with two ρ mesons coupled to the particle line.

Let us calculate the contribution of diagrams E.1(b.1) to the ρ meson selfenergy. We focus on the case in which both incoming and outgoing ρ mesons are coupled to the particle line (in Fig. E.4 the momentum labels are shown). We get the following expression:

$$\begin{aligned} -i\Pi^{ij}_{\rho\,(b.1)}(P^0;\rho) &= -i\delta^{ij}\Big(\frac{D+F}{2f}\Big)^2 g_\rho^2 \frac{1}{M_N^2}\int \frac{d^4q}{(2\pi)^4}(\vec{q}^{\,2})^2 D(q) \\ &\quad \int \frac{d^4p}{(2\pi)^4}\Big\{ G_h(p)\, G_p^2(p+q)\, G_p(p^0+q^0+P^0,\vec{p}+\vec{q}) + \\ &\quad G_h(p)\, G_p^2(p+q)\, G_p(p^0+q^0-P^0,\vec{p}+\vec{q})\Big\} \end{aligned} \tag{E.3}$$

where G_p (G_h) stands for the propagator of a particle (hole). The ρNN vertices provide a $(\vec{p}+\vec{q})_i(\vec{p}+\vec{q})_j$ factor. The terms linear and quadratic in $\vec{p}$, when performing the integration over the momentum in the baryonic

loop, give rise to contributions of order $\rho^{\frac{4}{3}}$ and higher powers in the nuclear density. We neglect those contributions and then Eq. (E.3) follows. This result can be expressed in terms of Lindhard functions. The product of nucleon propagators in Eq. (E.3) can be rewritten as

$$\begin{aligned}
&G_h(p)\,G_p^2(p+q)\,G_p(p^0+q^0+P^0,\vec{p}+\vec{q}) = \\
&\quad\frac{\partial}{\partial\alpha}\Big\{\frac{1}{P^0+\alpha}\Big[G_h(p)\,G_p(p^0+q^0-\alpha,\vec{p}+\vec{q})-G_h(p)\,G_p(p^0+q^0+P^0,\vec{p}+\vec{q})\Big]\Big\} \\
&G_h(p)\,G_p^2(p+q)\,G_p(p^0+q^0-P^0,\vec{p}+\vec{q}) = \\
&\quad\frac{\partial}{\partial\alpha}\Big\{\frac{-1}{P^0-\alpha}\Big[G_h(p)\,G_p(p^0+q^0-\alpha,\vec{p}+\vec{q})-G_h(p)\,G_p(p^0+q^0-P^0,\vec{p}+\vec{q})\Big]\Big\}
\end{aligned} \tag{E.4}$$

where the limit $\alpha \to 0$ is assumed. Commutation of the ∂_α derivative with the integration over the baryonic loop momentum allows us to write

$$\begin{aligned}
\Pi^{ij}_{\rho\,(b.1)}(P^0;\rho) = i\delta^{ij}\frac{1}{2}\Big(\frac{D+F}{2f}\Big)^2 g_\rho^2\frac{1}{M_N^2}\int\frac{d^4q}{(2\pi)^4}\,(\vec{q}^{\,2})^2\,D(q) \\
\frac{1}{(P^0)^2}\Big[\bar{U}_N(q^0+P^0,\vec{q})+\bar{U}_N(q^0-P^0,\vec{q})-2\,\bar{U}_N(q)\Big]\,,
\end{aligned} \tag{E.5}$$

where the $\bar{U}_N$ function, the Lindhard function for a forward propagating ph bubble, stands for

$$\bar{U}_N(q) = -2i\int\frac{d^4p}{(2\pi)^4}\,G_h(p)\,G_p(p+q) \tag{E.6}$$

and satisfies

$$2\,[\bar{U}_N(q^0,\vec{q})+\bar{U}_N(-q^0,\vec{q})] = U_N(q^0,\vec{q})\,. \tag{E.7}$$

We have compared numerically the size of this contribution to any of those included in Fig. 5.8 and we find that it is around two orders of magnitude smaller in the range of energy under study. Including this contribution in the calculation has no visible effect and therefore we neglect it, and so we do with the terms in which the ρ is coupled to a Δ line. In this derivation we have neglected all terms linear or quadratic in the hole momentum, since they

generate contributions of higher order in density. Following this criterium, we can discard other contributions from diagrams with a ρ meson coupled to a hole line. In particular this is the case of the partners of the graphs shown of Fig. E.4, with both ρ mesons coupled to the hole line. The same happens to the diagrams of the type of the one shown in Fig. E.1(b.2).

We are left with the evaluation of diagram in Fig. E.1c, which appears at the level of one pion loop from the $\rho\rho NN$ contact vertex discussed above. The momentum labels are similar as in Fig. E.4. Using the Feynman rule for the $\rho\rho NN$ vertex in Eq. (E.1) we find

$$\begin{aligned} -i\Pi^{ij}_{\rho\,(c)}(P^0;\rho) &= -ig_\rho^2 \frac{3}{M_N}\Big(\frac{D+F}{2f}\Big)^2 \delta^{ij} \\ &\int \frac{d^4q}{(2\pi)^4}\,\vec{q}^{\,2}\,D(q)\int \frac{d^4p}{(2\pi)^4} G(p)\,G(p+q)^2 \ , \end{aligned} \tag{E.8}$$

where $G(p)$ denotes the whole nucleon propagator with both the particle and the hole pieces. It is possible to rewrite $G(p+q)^2$ as

$$G(p+q)^2 = \partial_\alpha G(p^0+q^0-\alpha,\vec{p}+\vec{q}) \ , \tag{E.9}$$

with $\alpha \to 0$. The integration of the baryonic loop is then given by

$$\begin{aligned} \int \frac{d^4p}{(2\pi)^4}\,G(p)\,G(p+q)^2 = \partial_\alpha \int \frac{d^4p}{(2\pi)^4}\,G(p)\,G(p^0+q^0-\alpha,\vec{p}+\vec{q}) = \\ \frac{i}{4}\partial_\alpha U_N(q^0-\alpha,\vec{q})\Big|_{\alpha\to 0} \ , \end{aligned} \tag{E.10}$$

which is an odd function of q^0 since the nuclear Lindhard function is even in q^0. As a consequence the dq^0 integration vanishes and the contribution of these terms is null. Similar arguments for the case of a Δ in the particle line also lead to a null contribution.

Appendix F

Transversality of the ϕ meson selfenergy tensor

We provide here an explicit calculation of the ϕ selfenergy tensor for a ϕ meson at rest with respect to the nuclear medium, with the aim to show that transversality is preserved under the current approximations used in Chapter 6. The ϕ selfenergy in vacuum, including two-kaon loop diagrams and kaon tadpole diagrams, is transverse as can be easily shown using standard techniques of QFT. We focus on the in-medium diagrams contributing at the level of one Yh loop bubble insertion (first order in density). We shall perform the study for the set of diagrams involving $P-$wave KN couplings and related vertex corrections. A similar derivation following the same steps as here can be done for the set of diagrams involving $S-$wave KN couplings.

We start by stating the Ward identities for on-shell tree level amplitudes involving $\bar{K}$, ϕ, N and Y external lines, both in the fully relativistic theory and after some non-relativistic approximations. This is very illustrative to see how cancellations between diagrams take place, and will help classifying ϕ selfenergy diagrams for the study of $\Pi_\phi^{\mu\nu}$.

The amplitude corresponding to the sum of diagrams in Fig. 6.5, contracted with the ϕ momentum, is given by

$$\begin{aligned} -it^{\mu}_{\phi\bar{K}NY}q_\mu = {} & ig_\phi(2k+q)\,q\,\frac{i}{(k+q)^2-m_K^2}(-1)D_{\bar{K}NY}(\not{k}+\not{q})\gamma_5 \\ & +(-1)g_\phi D_{\bar{K}NY}\not{q}\gamma_5 + ig_\phi\not{q}\,\frac{i}{\not{p}+\not{k}-M_Y}(-1)D_{\bar{K}NY}\not{k}\gamma_5 \ , \end{aligned} \tag{F.1}$$

where p is the momentum of the nucleon and we have omitted the Dirac spinors for simplicity ($\bar{u}_Y ... u_N$). In Eq. (F.1) we use $(k+q)^2-m_K^2 = 2kq+q^2$

($k^2 = m_K^2$ for an external on-shell kaon) in the first term of the right hand side (r.h.s), and apply the Dirac equation on the third term of the r.h.s, $\bar{u}_r \not{q} = \bar{u}_r \left[\not{p} + \not{k} + \not{q} - M_Y - (\not{p} + \not{k} - M_Y)\right] = \bar{u}_r \left[-(\not{p} + \not{k} - M_Y)\right]$. Then we are lead to

$$-it^{\mu}_{\phi\bar{K}NY} q_\mu = g_\phi D_{\bar{K}NY} \Big\{ (\not{k} + \not{q})\gamma_5 - \not{q}\gamma_5 - \not{k}\gamma_5 (\not{p} + \not{k} - M_Y) \frac{1}{\not{p} + \not{k} - M_Y} \Big\} = 0 \ . \tag{F.2}$$

For the non-relativistic approximation we keep the lowest order in the vertices involving the coupling of mesons and baryons and the positive energy part of the baryon propagators. Thus we substitute, for these vertices and propagators,

$$\begin{aligned} \gamma^\mu q_\mu &\rightarrow q^0 \\ \gamma^\mu \gamma_5 q_\mu &\rightarrow -\vec{\sigma}\vec{q} \\ \frac{1}{\not{p} - M_B + i\epsilon} &\rightarrow \frac{1}{p^0 - E_B(\vec{p}) + i\epsilon} \end{aligned} \tag{F.3}$$

where B stands for baryon ($B = N, Y$). The Ward identity reads now

$$-it^{\mu}_{\phi\bar{K}NY} q_\mu = g_\phi D_{\bar{K}NY} \Big\{ -\vec{\sigma}(\vec{k} + \vec{q}) + \vec{\sigma}\vec{q} - \vec{\sigma}\vec{k} \, \frac{q^0}{p^0 + k^0 - E_Y(\vec{p} + \vec{k})} \Big\} \ , \tag{F.4}$$

where we have omitted the spin structure ($\chi^\dagger_{r'} ... \chi_r$). In the third term of the r.h.s we can replace $p^0 + k^0 = -q^0 + E_Y(\vec{p} + \vec{k} + \vec{q})$ for an external on-shell hyperon, and then the second plus the third terms cancel the first term except for terms of the order of $|\vec{p} + \vec{k}|/M_Y$. These terms are proportional to $|\vec{q}|$, thus for the case of a ϕ meson at rest the corrections are even smaller. The Ward identity in Eq. (F.4) is then satisfied exactly within our approximation scheme.

We have seen through this exercise that the third diagram in Fig. 6.5 is relevant to respect the Ward identities, what means that the diagrams in which the ϕ meson couples to the hyperon lines are important to keep transversality of the ϕ selfenergy. However, according to our non-relativistic expansion, the ϕYY vertex contributes at lowest order for the time component ($\mu = 0$) and thus has to be considered in the calculation of Π^{00}_ϕ and $\Pi^{i0(0j)}_\phi$, whereas leads to higher order corrections in Π^{ij}_ϕ, which we explicitly

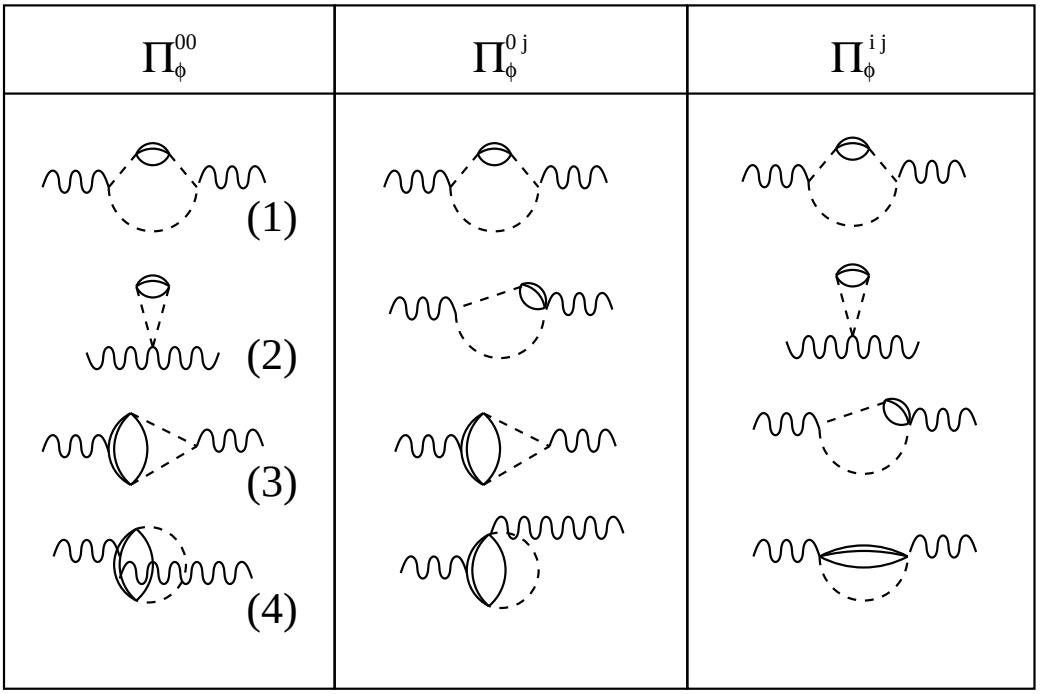

Figure F.1: Classification of diagrams according to their leading contribution to the phi selfenergy in the non-relativistic approximation.

neglect. To prove transversality of the selfenergy tensor we have to show that $q_\mu \Pi_\phi^{\mu\nu} = 0$, which for a ϕ meson at rest is equivalent to

$$\begin{aligned} q^0\,\Pi_\phi^{00} = 0 \leftrightarrow \Pi_\phi^{00} = 0 \ , \\ q^0\,\Pi_\phi^{0j} = 0 \leftrightarrow \Pi_\phi^{0j} = 0 \ . \end{aligned} \tag{F.5}$$

We show in Fig. F.1 a classification of ϕ selfenergy topologies attending to which components of the selfenergy tensor they contribute to at the lowest order in the non-relativistic expansion.

Let us evaluate $q^0\,\Pi_\phi^{00}$. For this we have to calculate all the diagrams with the topologies shown in the left box of Fig. F.1. The final expression reads

$$q^0\,\Pi_\phi^{00} = 2 g_\phi^2 D_{\bar{K}NY}^2 \int \frac{d^4k}{(2\pi)^4}\, D(k^0,\vec{k})\,\vec{k}^{\,2} \int \frac{d^4p}{(2\pi)^4}\, G_h(p)$$

$$\begin{aligned} (1) \quad & \Big\{ q^0(q^0-2k^0)(q^0-2k^0)\, D(k^0,\vec{k})\, D(q^0-k^0,\vec{k})\, G_Y(p^0+k^0,\vec{p}+\vec{k}) \\ (1') \quad & +q^0(q^0-2k^0)(q^0-2k^0)\, D(q^0-k^0,\vec{k})\, D(q^0-k^0,\vec{k})\, G_Y(p^0+k^0-q^0,\vec{p}+\vec{k}) \\ (2) \quad & -2q^0\, D(k^0,\vec{k})\, G_Y(p^0+k^0,\vec{p}+\vec{k}) \end{aligned}$$

$$
\begin{aligned}
(3)\quad & -2q^0(q^0-2k^0)\,D(q^0-k^0,\vec{k})\,G_Y(p^0+k^0-q^0,\vec{p}+\vec{k})\,G_Y(p^0+k^0,\vec{p}+\vec{k}) \\
(4)\quad & +q^0\,G_Y(p^0+k^0,\vec{p}+\vec{k})\,G_Y(p^0+k^0-q^0,\vec{p}+\vec{k})\,G_Y(p^0+k^0,\vec{p}+\vec{k}) \\
(4')\quad & +q^0\,G_Y(p^0+k^0,\vec{p}+\vec{k})\,G_Y(p^0+k^0+q^0,\vec{p}+\vec{k})\,G_Y(p^0+k^0,\vec{p}+\vec{k})\Big\}\ . \qquad \text{(F.6)}
\end{aligned}
$$

The numbers between brackets at the beginning of each line indicate which topology in Fig. F.1 gives rise to the corresponding terms. To find cancellations in Eq. (F.6) we proceed as we did for the Ward identity on the vertices. We take profit of available factors to cancel meson and baryon propagators, what diagrammatically corresponds to shrinking meson and baryon lines to a point. To proceed we note that the following identities are satisfied,

$$
\begin{aligned}
q^0(q^0-2k^0) &= D^{-1}(q-k)-D^{-1}(k) \\
q^0 &= -G_Y^{-1}(p^0+k^0,\vec{p}+\vec{k})+G_Y^{-1}(p^0+k^0+q^0,\vec{p}+\vec{k}) \\
&= G_Y^{-1}(p^0+k^0,\vec{p}+\vec{k})-G_Y^{-1}(p^0+k^0-q^0,\vec{p}+\vec{k})\ . \qquad \text{(F.7)}
\end{aligned}
$$

Using $q^0(q^0-2k^0)$ to remove one meson propagator in lines $(1,1')$ and q^0 to remove one baryon propagator in line (3) we find some cancellations and we are lead to

$$
\begin{aligned}
& q^0\,\Pi_\phi^{00}=2g_\phi^2 D^2_{\bar{K}NY}\int\frac{d^4k}{(2\pi)^4}\,\vec{k}^{\,2}\int\frac{d^4p}{(2\pi)^4}\,G_h(p) \\
(1)\quad & \Big\{(q^0-2k^0)\,D(k^0,\vec{k})\,D(k^0,\vec{k})\,G_Y(p^0+k^0,\vec{p}+\vec{k}) \\
(1')\quad & -(q^0-2k^0)\,D(q^0-k^0,\vec{k})\,D(q^0-k^0,\vec{k})\,G_Y(p^0+k^0-q^0,\vec{p}+\vec{k}) \\
(2)\quad & -2q^0\,D(k^0,\vec{k})\,D(k^0,\vec{k})\,G_Y(p^0+k^0,\vec{p}+\vec{k}) \\
(3)\quad & -(q^0-2k^0)\,D(k^0,\vec{k})\,D(q^0-k^0,\vec{k})\,[G_Y(p^0+k^0-q^0,\vec{p}+\vec{k})-G_Y(p^0+k^0,\vec{p}+\vec{k})] \\
(4)\quad & +q^0\,D(k^0,\vec{k})\,G_Y(p^0+k^0,\vec{p}+\vec{k})\,G_Y(p^0+k^0-q^0,\vec{p}+\vec{k})\,G_Y(p^0+k^0,\vec{p}+\vec{k}) \\
(4')\quad & +q^0\,D(k^0,\vec{k})\,G_Y(p^0+k^0,\vec{p}+\vec{k})\,G_Y(p^0+k^0+q^0,\vec{p}+\vec{k})\,G_Y(p^0+k^0,\vec{p}+\vec{k})\Big\}\ . \\
& \qquad\qquad\qquad\qquad\qquad\qquad\qquad\qquad\qquad\qquad\qquad\qquad\qquad\qquad\qquad\qquad \text{(F.8)}
\end{aligned}
$$

It is straightforward to note that, after this rearrangement of terms and with a suitable change of variables ($q^0-k^0\to k'^0$ and then $k'^0\to-\tilde{k}^0$ in line $(1')$), lines $(1,1')$ and (2) cancel exactly between them. We are left with the following expression,

$$
\begin{aligned}
& q^0\,\Pi_\phi^{00} = 2g_\phi^2 D_{\bar{K}NY}^2 \int \frac{d^4k}{(2\pi)^4}\,\vec{k}^{\,2} \int \frac{d^4p}{(2\pi)^4}\,G_h(p) \\
(3)\quad & \Big\{ -(q^0-2k^0)\,D(k^0,\vec{k})\,D(q^0-k^0,\vec{k})\,[G_Y(p^0+k^0-q^0,\vec{p}+\vec{k}) - G_Y(p^0+k^0,\vec{p}+\vec{k})] \\
(4)\quad & +q^0\,D(k^0,\vec{k})\,G_Y(p^0+k^0,\vec{p}+\vec{k})\,G_Y(p^0+k^0-q^0,\vec{p}+\vec{k})\,G_Y(p^0+k^0,\vec{p}+\vec{k}) \\
(4')\quad & +q^0\,D(k^0,\vec{k})\,G_Y(p^0+k^0,\vec{p}+\vec{k})\,G_Y(p^0+k^0+q^0,\vec{p}+\vec{k})\,G_Y(p^0+k^0,\vec{p}+\vec{k})\Big\}\ .
\end{aligned}
\tag{F.9}
$$

By using the remaining q^0 and (q^0-2k^0) factors and the relations in Eq. (F.7) we can cancel a meson propagator in line (3) and two baryon propagators out of three in lines $(4,4')$. In the following we only quote, for simplicity, the terms in the braces of Eq. (F.9). The sum of lines $(4,4')$ leads to

$$
\begin{aligned}
& \frac{1}{q^0}\,D(k^0,\vec{k})\,[G_Y(p^0+k^0-q^0,\vec{p}+\vec{k}) - G_Y(p^0+k^0,\vec{p}+\vec{k})] \\
- \quad & \frac{1}{q^0}\,D(k^0,\vec{k})\,[G_Y(p^0+k^0,\vec{p}+\vec{k}) - G_Y(p^0+k^0+q^0,\vec{p}+\vec{k})]\ ,
\end{aligned}
\tag{F.10}
$$

and line (3) reads

$$
\begin{aligned}
- \quad & \frac{1}{q^0}\,D(k^0,\vec{k})\,[G_Y(p^0+k^0-q^0,\vec{p}+\vec{k}) - G_Y(p^0+k^0,\vec{p}+\vec{k})] \\
+ \quad & \frac{1}{q^0}\,D(q^0-k^0,\vec{k})\,[G_Y(p^0+k^0-q^0,\vec{p}+\vec{k}) - G_Y(p^0+k^0,\vec{p}+\vec{k})]\ .
\end{aligned}
\tag{F.11}
$$

The first lines of Eqs. (F.10, F.11) cancel exactly and, with the change of variables used above, the second line of Eq. (F.11) can be rewritten as the second line of Eq. (F.10) with an opposite global sign, thus leading to an exact cancellation of all the terms.

Next we have to show that $q^0\,\Pi_\phi^{i0(0j)}$ vanishes, what requires to evaluate all the diagrams in the center box of Fig. F.1. It is found that all the contributions from these diagrams are odd in $\vec{k}$ and thus the integration over the three-momentum space vanishes for each of them independently.

Bibliography

[1] D. Cabrera, E. Oset and M. J. Vicente-Vacas, Acta Phys. Polon. B **31** (2000) 2167 [arXiv:nucl-th/0006029].

[2] D. Cabrera, E. Oset and M. J. Vicente Vacas, Nucl. Phys. A **705** (2002) 90 [arXiv:nucl-th/0011037].

[3] E. Oset *et al.*, Pramana **57** (2001) 417 [arXiv:nucl-th/0101032].

[4] D. Cabrera, AIP Conf. Proc. **603** (2001) 237 [arXiv:nucl-th/0107046].

[5] D. Cabrera, Nucl. Phys. A **721** (2003) 759.

[6] D. Cabrera and M. J. Vicente Vacas, Phys. Rev. C **67** (2003) 045203 [arXiv:nucl-th/0205075].

[7] D. Cabrera, Prog. Theor. Phys. Suppl. **149** (2003) 67.

[8] D. Cabrera, L. Roca, E. Oset, H. Toki and M. J. V. Vacas, Nucl. Phys. A **733** (2004) 130 [arXiv:nucl-th/0310054].

[9] D. Cabrera and M. J. Vicente Vacas, Phys. Rev. C **69** (2004) 065204 [arXiv:nucl-th/0403017].

[10] D. Cabrera, M. J. Vicente Vacas and E. Oset. In preparation.

[11] T. E. O. Ericson and W. Weise, *OXFORD, UK: CLARENDON (1988) 479 P. (THE INTERNATIONAL SERIES OF MONOGRAPHS ON PHYSICS, 74).*

[12] E. Oset, *In *Motril 1982, Proceedings, Quarks, Mesons and Isobars In Nuclei*, 1-60.*

[13] L. L. Salcedo, P.D. Thesis, Valladolid, March 1985.

[14] A. Pich, Rept. Prog. Phys. **58** (1995) 563 [arXiv:hep-ph/9502366].

[15] E. Oset, P. Fernandez de Cordoba, L. L. Salcedo and R. Brockmann, Phys. Rept. **188** (1990) 79.

[16] E. Jenkins and A. V. Manohar, Phys. Lett. B **259** (1991) 353.

[17] A. L. Fetter and J. D. Walecka, *NEW YORK, USA: Mc GRAW-HILL (1971) 601 P. (INTERNATIONAL SERIES IN PURE AND APPLIED PHYSICS, Quantum Theory of Many-Particle Systems).*

[18] E. Oset, H. Toki and W. Weise, Phys. Rept. **83** (1982) 281.

[19] A. Gomez Nicola, J. Nieves, J. R. Pelaez and E. Ruiz Arriola, Phys. Lett. B **486** (2000) 77 [arXiv:hep-ph/0006043].

[20] N. Fettes, U. G. Meissner and S. Steininger, Nucl. Phys. A **640** (1998) 199 [arXiv:hep-ph/9803266].

[21] N. Fettes and U. G. Meissner, Nucl. Phys. A **676** (2000) 311 [arXiv:hep-ph/0002162].

[22] L. Alvarez-Ruso, Phys. Lett. B **452** (1999) 207 [arXiv:nucl-th/9811058].

[23] T. Inoue, E. Oset and M. J. Vicente Vacas, Phys. Rev. C **65** (2002) 035204 [arXiv:hep-ph/0110333].

[24] T. Inoue and E. Oset, Nucl. Phys. A **710** (2002) 354 [arXiv:hep-ph/0205028].

[25] J. Nieves, E. Oset and C. Garcia-Recio, Nucl. Phys. A **554** (1993) 554.

[26] E. Oset and L. L. Salcedo, Nucl. Phys. A **468** (1987) 631.

[27] N. Kaiser, P. B. Siegel and W. Weise, Nucl. Phys. A **594** (1995) 325 [arXiv:nucl-th/9505043].

[28] M. Lutz, Phys. Lett. B **426** (1998) 12 [arXiv:nucl-th/9709073].

[29] E. Oset and A. Ramos, Nucl. Phys. A **635** (1998) 99 [arXiv:nucl-th/9711022].

[30] A. Ramos and E. Oset, Nucl. Phys. A **671** (2000) 481 [arXiv:nucl-th/9906016].

[31] W. R. Gibbs, arXiv:nucl-th/0405024.

[32] T. Waas, M. Rho and W. Weise, Nucl. Phys. A **617** (1997) 449 [arXiv:nucl-th/9610031].

[33] E. E. Kolomeitsev and D. N. Voskresensky, Phys. Rev. C **68** (2003) 015803 [arXiv:nucl-th/0211052].

[34] D. E. Groom *et al.* [Particle Data Group Collaboration], Eur. Phys. J. C **15** (2000) 1.

[35] N. A. Tornqvist, arXiv:hep-ph/0008135.

[36] E. M. Aitala *et al.* [E791 Collaboration], Phys. Rev. Lett. **86** (2001) 770 [arXiv:hep-ex/0007028].

[37] G. Colangelo, J. Gasser and H. Leutwyler, Nucl. Phys. B **603** (2001) 125 [arXiv:hep-ph/0103088].

[38] S. . Ishida *et al.*, "Possible existence of the sigma-meson and its implications to hadron physics". KEK-Proceedings 2000-4, 1 (December 2000); Soryushiron Kenkyu (Kyoto) 102 (2001), E1. http://amaterasu.kek.jp/YITPws/

[39] T. Hatsuda and T. Kunihiro, Phys. Rev. Lett. **55** (1985) 158.

[40] T. Hatsuda and T. Kunihiro, Prog. Theor. Phys. **74** (1985) 765.

[41] T. Hatsuda and T. Kunihiro, Phys. Lett. B **185** (1987) 304.

[42] V. Bernard, U. G. Meissner and I. Zahed, Phys. Rev. Lett. **59** (1987) 966.

[43] V. Bernard, U. G. Meissner and I. Zahed, Phys. Rev. D **36** (1987) 819.

[44] G. E. Brown and M. Rho, Phys. Rept. **269** (1996) 333 [arXiv:hep-ph/9504250].

[45] T. Hatsuda, Nucl. Phys. A **698** (2002) 243 [arXiv:hep-ph/0104139].

[46] V. Bernard and U. G. Meissner, Phys. Rev. D **38** (1988) 1551.

[47] V. Bernard and U. G. Meissner, Nucl. Phys. A **489** (1988) 647.

[48] T. Hatsuda, T. Kunihiro and H. Shimizu, Phys. Rev. Lett. **82** (1999) 2840.

[49] D. Jido, T. Hatsuda and T. Kunihiro, Phys. Rev. D **63** (2001) 011901 [arXiv:hep-ph/0008076].

[50] P. Schuck, W. Norenberg and G. Chanfray, Z. Phys. A **330** (1988) 119 .

[51] R. Rapp, J. W. Durso and J. Wambach, Nucl. Phys. A **596** (1996) 436 [arXiv:nucl-th/9508026].

[52] Z. Aouissat, R. Rapp, G. Chanfray, P. Schuck and J. Wambach, Nucl. Phys. A **581** (1995) 471 [arXiv:nucl-th/9406010].

[53] H. C. Chiang, E. Oset and M. J. Vicente-Vacas, Nucl. Phys. A **644** (1998) 77 [arXiv:nucl-th/9712047].

[54] Z. Aouissat, G. Chanfray, P. Schuck and J. Wambach, Phys. Rev. C **61** (2000) 012202.

[55] D. Davesne, Y. J. Zhang and G. Chanfray, Phys. Rev. C **62** (2000) 024604 [arXiv:nucl-th/9909032].

[56] F. Bonutti *et al.* [CHAOS Collaboration], Phys. Rev. Lett. **77** (1996) 603.

[57] F. Bonutti *et al.* [CHAOS Collaboration], Nucl. Phys. A **638** (1998) 729.

[58] P. Camerini, N. Grion, R. Rui and D. Vetterli, Nucl. Phys. A **552** (1993) 451 [Erratum-ibid. A **572** (1993) 791].

[59] F. Bonutti *et al.* [CHAOS Collaboration], Phys. Rev. **C60** (1999) 018201.

[60] A. Starostin *et al.* [Crystal Ball Collaboration], Phys. Rev. Lett. **85** (2000) 5539.

[61] J. G. Messchendorp *et al.*, Phys. Rev. Lett. **89** (2002) 222302 [arXiv:nucl-ex/0205009].

[62] L. Roca, E. Oset and M. J. Vicente Vacas, Phys. Lett. B **541** (2002) 77 [arXiv:nucl-th/0201054].

[63] A. Dobado, M. J. Herrero and T. N. Truong, Phys. Lett. B **235** (1990) 134.

[64] A. Dobado and J. R. Pelaez, Phys. Rev. D **47** (1993) 4883 [arXiv:hep-ph/9301276].

[65] J. A. Oller, E. Oset and J. R. Pelaez, Phys. Rev. Lett. **80** (1998) 3452 [arXiv:hep-ph/9803242].

[66] J. A. Oller, E. Oset and J. R. Pelaez, Phys. Rev. D **59** (1999) 074001 [Erratum-ibid. D **60** (1999) 099906] [arXiv:hep-ph/9804209].

[67] J. A. Oller and E. Oset, Phys. Rev. D **60** (1999) 074023 [arXiv:hep-ph/9809337].

[68] J. A. Oller and E. Oset, Nucl. Phys. A **620** (1997) 438 [Erratum-ibid. A **652** (1997) 407] [arXiv:hep-ph/9702314].

[69] J. Gasser and H. Leutwyler, Nucl. Phys. B **250** (1985) 517.

[70] E. Oset and M. J. Vicente Vacas, Nucl. Phys. A **678** (2000) 424 [arXiv:nucl-th/0004030].

[71] J. Nieves and E. Ruiz Arriola, Nucl. Phys. A **679** (2000) 57 [arXiv:hep-ph/9907469].

[72] J. Nieves and E. Ruiz Arriola, Phys. Lett. B **455** (1999) 30 [arXiv:nucl-th/9807035].

[73] G. Chanfray and D. Davesne, Nucl. Phys. A **646** (1999) 125.

[74] T. Kunihiro, arXiv:hep-ph/9905262.

[75] U. G. Meissner, Rept. Prog. Phys. **56** (1993) 903 [arXiv:hep-ph/9302247].

[76] V. Bernard, N. Kaiser and U. G. Meissner, Int. J. Mod. Phys. E **4** (1995) 193 [arXiv:hep-ph/9501384].

[77] G. Ecker, Prog. Part. Nucl. Phys. **35** (1995) 1 [arXiv:hep-ph/9501357].

[78] V. E. Markushin, Z. Xiao and H. Q. Zheng, Nucl. Phys. A **695** (2001) 273 [arXiv:hep-ph/0011260].

[79] E. van Beveren and G. Rupp, arXiv:hep-ph/0201006.

[80] T. Hatsuda and T. Kunihiro, arXiv:nucl-th/0112027.

[81] W. Weise, Nucl. Phys. A **690** (2001) 98.

[82] U. G. Meissner, J. A. Oller and A. Wirzba, Annals Phys. **297** (2002) 27 [arXiv:nucl-th/0109026].

[83] H. C. Schroder *et al.*, Phys. Lett. B **469** (1999) 25.

[84] E. Oset and D. Strottman, Phys. Rev. Lett. **70** (1993) 146.

[85] E. Oset, D. Strottman, H. Toki and J. Navarro, Phys. Rev. C **48** (1993) 2395.

[86] T. E. Ericson and W. Weise, *OXFORD, UK: CLARENDON (1988) 479 P. (THE INTERNATIONAL SERIES OF MONOGRAPHS ON PHYSICS, 74).*

[87] R. A. Arndt, I. I. Strakovsky, R. L. Workman and M. M. Pavan, Phys. Rev. C **52** (1995) 2120 [arXiv:nucl-th/9505040].

[88] J. A. Oller and U. G. Meissner, Phys. Lett. B **500** (2001) 263 [arXiv:hep-ph/0011146].

[89] G. Chanfray and D. Davesne, arXiv:nucl-th/9806086.

[90] P. Muhlich, L. Alvarez-Ruso, O. Buss and U. Mosel, Phys. Lett. B **595** (2004) 216 [arXiv:nucl-th/0401042].

[91] D. B. Kaplan and A. E. Nelson, Phys. Lett. B **175** (1986) 57.

[92] A. Ramos, J. Schaffner-Bielich and J. Wambach, Lect. Notes Phys. **578** (2001) 175 [arXiv:nucl-th/0011003].

[93] F. Laue *et al.* [KaoS Collaboration], Phys. Rev. Lett. **82** (1999) 1640 [arXiv:nucl-ex/9901005].

[94] A. Sibirtsev and W. Cassing, Nucl. Phys. A **641** (1998) 476 [arXiv:nucl-th/9805021].

[95] E. Friedman, A. Gal and C. J. Batty, Phys. Lett. B **308** (1993) 6.

[96] E. Friedman, A. Gal and C. J. Batty, Nucl. Phys. A **579** (1994) 518.

[97] E. Friedman, A. Gal and J. Mares, Phys. Rev. C **60** (1999) 024314 [arXiv:nucl-th/9804072].

[98] T. Waas, N. Kaiser and W. Weise, Phys. Lett. B **365** (1996) 12.

[99] T. Waas, N. Kaiser and W. Weise, Phys. Lett. B **379** (1996) 34.

[100] S. Hirenzaki, Y. Okumura, H. Toki, E. Oset and A. Ramos, Phys. Rev. C **61** (2000) 055205.

[101] A. Baca, C. Garcia-Recio and J. Nieves, Nucl. Phys. A **673** (2000) 335 [arXiv:nucl-th/0001060].

[102] A. Cieply, E. Friedman, A. Gal and J. Mares, Nucl. Phys. A **696** (2001) 173 [arXiv:nucl-th/0104087].

[103] K. Hagiwara *et al.* [Particle Data Group Collaboration], Phys. Rev. D **66** (2002) 010001.

[104] J. A. Oller and E. Oset, Phys. Rev. D **60** (1999) 074023 [arXiv:hep-ph/9809337].

[105] W. Ochs, arXiv:hep-ph/0311144.

[106] D. V. Bugg, Phys. Lett. B **572** (2003) 1.

[107] R. Rapp, J. W. Durso and J. Wambach, Nucl. Phys. A **596** (1996) 436 [arXiv:nucl-th/9508026].

[108] T. Hatsuda, T. Kunihiro and H. Shimizu, Phys. Rev. Lett. **82** (1999) 2840.

[109] F. Bonutti *et al.* [CHAOS Collaboration], Nucl. Phys. A **638** (1998) 729.

[110] F. Bonutti *et al.* [CHAOS Collaboration], Phys. Rev. Lett. **77** (1996) 603.

[111] R. Rapp *et al.*, Phys. Rev. C **59** (1999) 1237 [arXiv:nucl-th/9810007].

[112] M. J. Vicente Vacas and E. Oset, Phys. Rev. C **60** (1999) 064621 [arXiv:nucl-th/9907008].

[113] J. A. Oller, E. Oset and J. R. Pelaez, Phys. Rev. D **59** (1999) 074001 [Erratum-ibid. D **60** (1999) 099906] [arXiv:hep-ph/9804209].

[114] R. Mercer *et al.*, Nucl. Phys. **32B** (1971) 381.

[115] P. Estabrooks, R. K. Carnegie, A. D. Martin, W. M. Dunwoodie, T. A. Lasinski and D. W. G. Leith, Nucl. Phys. B **133** (1978) 490.

[116] E. Oset and A. Ramos, Nucl. Phys. A **679** (2001) 616 [arXiv:nucl-th/0005046].

[117] D. E. Groom *et al.* [Particle Data Group Collaboration], Eur. Phys. J. C **15**, 1 (2000).

[118] G. Agakishiev *et al.* [CERES Collaboration], Phys. Rev. Lett. **75** (1995) 1272.

[119] B. Lenkeit *et al.* [CERES-Collaboration], Nucl. Phys. **A661** (1999) 23 [nucl-ex/9910015].

[120] R. J. Porter *et al.* [DLS Collaboration], Phys. Rev. Lett. **79** (1997) 1229 [nucl-ex/9703001].

[121] K. Ozawa *et al.* [E325 Collaboration], Phys. Rev. Lett. **86** (2001) 5019 [nucl-ex/0011013].

[122] J. Friese [HADES Collaboration], Prog. Part. Nucl. Phys. **42** (1999) 235.

[123] E. L. Bratkovskaya, W. Cassing and U. Mosel, Nucl. Phys. A **686** (2001) 568 [nucl-th/0008037].

[124] R. Rapp and J. Wambach, Adv. Nucl. Phys. **25** (2000) 1 [hep-ph/9909229].

[125] G. E. Brown and M. Rho, Phys. Rev. Lett. **66** (1991) 2720.

[126] T. Hatsuda and S. H. Lee, Phys. Rev. **C46** (1992) 34.

[127] S. Leupold, W. Peters and U. Mosel, Nucl. Phys. **A628** (1998) 311 [nucl-th/9708016].

[128] F. Klingl, N. Kaiser and W. Weise, Nucl. Phys. **A624** (1997) 527 [hep-ph/9704398].

[129] S. Mallik and A. Nyffeler, Phys. Rev. C **63** (2001) 065204 [hep-ph/0102062].

[130] M. Asakawa, C. M. Ko, P. Levai and X. J. Qiu, Phys. Rev. **C46** (1992) 1159.

[131] M. Asakawa and C. M. Ko, Phys. Rev. **C48** (1993) 526.

[132] G. Chanfray and P. Schuck, Nucl. Phys. **A555** (1993) 329.

[133] M. Herrmann, B. L. Friman and W. Norenberg, Nucl. Phys. **A560** (1993) 411.

[134] M. Urban, M. Buballa, R. Rapp and J. Wambach, Nucl. Phys. **A641** (1998) 433 [nucl-th/9806030].

[135] M. Urban, M. Buballa and J. Wambach, Nucl. Phys. **A673** (2000) 357 [nucl-th/9910004].

[136] W. Broniowski, W. Florkowski and B. Hiller, nucl-th/0103027.

[137] R. Rapp, G. Chanfray and J. Wambach, Nucl. Phys. **A617** (1997) 472 [hep-ph/9702210].

[138] W. Peters, M. Post, H. Lenske, S. Leupold and U. Mosel, Nucl. Phys. **A632** (1998) 109 [nucl-th/9708004].

[139] M. Post, S. Leupold and U. Mosel, Nucl. Phys. A **689** (2001) 753 [nucl-th/0008027].

[140] B. Friman, Acta Phys. Polon. B **29** (1998) 3195 [nucl-th/9808071].

[141] M. Lutz, B. Friman and G. Wolf, Nucl. Phys. **A661** (1999) 526.

[142] R. Rapp *et al.*, Phys. Rev. **C59** (1999) R1237 [nucl-th/9810007].

[143] J. A. Oller, E. Oset and J. E. Palomar, Phys. Rev. D **63** (2001) 114009 [hep-ph/0011096].

[144] J. E. Palomar, 'Descripción Quiral Unitaria de los Factores de Forma Vectoriales de Piones y Kaones y sus Aplicaciones', Trabajo de Investigación, Junio 2001.

[145] F. Mandl and G. Shaw, *Chichester, Uk: Wiley (1984) 354 P. (A Wiley-interscience Publication).*

[146] J. Gasser and H. Leutwyer, Nucl. Phys. **B250** (1985) 465, 517, 539.

[147] G. Ecker, J. Gasser, H. Leutwyler, A. Pich and E. de Rafael, Phys. Lett. **B223** (1989) 425; G. Ecker, J. Gasser, A. Pich and E. de Rafael, Nucl. Phys. **B321** (1989) 311.

[148] J. A. Oller and E. Oset, Phys. Rev. **D60** (1999) 074023.

[149] A. Ramos and E. Oset, Nucl. Phys. A **663** (2000) 525.

[150] C. Garcia-Recio, E. Oset and L. L. Salcedo, Phys. Rev. C **37** (1988) 194.

[151] J. A. Gomez Tejedor, F. Cano and E. Oset, Phys. Lett. B **379** (1996) 39 [arXiv:nucl-th/9510007].

[152] Y. Koike and A. Hayashigaki, Prog. Theor. Phys. **98** (1997) 631 [nucl-th/9609001].

[153] K. Saito, K. Tsushima and A. W. Thomas, Phys. Rev. **C56** (1997) 566 [nucl-th/9703011].

[154] P. Maris, C. D. Roberts and S. M. Schmidt, Phys. Rev. **C57** (1998) 2821 [nucl-th/9801059].

[155] K. Sakamoto, M. Nakai, H. Kouno, A. Hasegawa and M. Nakano, Int. J. Mod. Phys. **E9** (2000) 169 [nucl-th/9909054].

[156] E. Oset, L. Roca and M. J. Vicente-Vacas, private communication.

[157] S. Sarkar, E. Oset and M. J. Vicente Vacas, arXiv:nucl-th/0407025.

[158] C. J. Batty, E. Friedman and A. Gal, Phys. Rept. **287** (1997) 385.

[159] A. Gal, Nucl. Phys. A **691** (2001) 268 [arXiv:nucl-th/0101010].

[160] S. Pal, C. M. Ko and Z. w. Lin, Nucl. Phys. A **707** (2002) 525 [arXiv:nucl-th/0202086].

[161] F. Klingl, T. Waas and W. Weise, Phys. Lett. B **431** (1998) 254 [arXiv:hep-ph/9709210].

[162] E. Oset, M. J. Vicente Vacas, H. Toki and A. Ramos, Phys. Lett. B **508** (2001) 237 [arXiv:nucl-th/0011019].

[163] H. Kuwabara and T. Hatsuda, Prog. Theor. Phys. **94** (1995) 1163 [arXiv:nucl-th/9507017].

[164] C. Song, Phys. Lett. B **388** (1996) 141 [arXiv:hep-ph/9603259].

[165] A. Bhattacharyya, S. K. Ghosh, S. C. Phatak and S. Raha, Phys. Rev. C **55** (1997) 1463 [arXiv:nucl-th/9602042].

[166] M. Asakawa and C. M. Ko, Nucl. Phys. A **572** (1994) 732.

[167] S. Zschocke, O. P. Pavlenko and B. Kampfer, arXiv:nucl-th/0205057.

[168] J. P. Blaizot and R. Mendez Galain, Phys. Lett. B **271** (1991) 32.

[169] C. M. Ko, P. Levai, X. J. Qiu and C. T. Li, Phys. Rev. C **45** (1992) 1400.

[170] E. V. Shuryak and V. Thorsson, Nucl. Phys. A **536** (1992) 739.

[171] D. Lissauer and E. V. Shuryak, Phys. Lett. B **253** (1991) 15.

[172] A. R. Panda and K. C. Roy, Mod. Phys. Lett. A **8** (1993) 2851.

[173] C. M. Ko and D. Seibert, Phys. Rev. C **49** (1994) 2198 [arXiv:nucl-th/9312010].

[174] W. Smith and K. L. Haglin, Phys. Rev. C **57** (1998) 1449 [arXiv:nucl-th/9710026].

[175] L. Alvarez-Ruso and V. Koch, Phys. Rev. C **65** (2002) 054901 [arXiv:nucl-th/0201011].

[176] B. Kampfer, O. P. Pavlenko and S. Zschocke, Eur. Phys. J. A **17** (2003) 83 [arXiv:nucl-th/0211067].

[177] R. S. Bhalerao and S. K. Gupta, Mod. Phys. Lett. A **12** (1997) 127 [arXiv:hep-ph/9701315].

[178] F. Klingl, N. Kaiser and W. Weise, Z. Phys. A **356** (1996) 193 [arXiv:hep-ph/9607431].

[179] K. Ozawa *et al.*, Nucl. Phys. A **698** (2002) 535.

[180] T. Ishikawa et al., Private communication.

[181] P. Muhlich, T. Falter, C. Greiner, J. Lehr, M. Post and U. Mosel, Phys. Rev. C **67** (2003) 024605 [arXiv:nucl-th/0210079].

[182] E. Anciant *et al.* [CLAS Collaboration], Phys. Rev. Lett. **85** (2000) 4682 [arXiv:hep-ex/0006022].

[183] C. Garcia-Recio, E. Oset and L. L. Salcedo, Phys. Rev. C **37** (1988) 194.

[184] J. Arends, N. Floss, A. Hegerath, B. Mecking, G. Noldeke and R. Stenz, Z. Phys. A **311** (1983) 367.

[185] C. W. De Jager, H. De Vries and C. De Vries, Atom. Data Nucl. Data Tabl. **14**, 479 (1974).